

Hemodynamics of ageing, ventricular-arterial coupling and noninvasive assessment of key hemodynamical and cardiac quantities

Présentée le 30 octobre 2020

à la Faculté des sciences et techniques de l'ingénieur
Laboratoire d'hémodynamique et de technologie cardiovasculaire
Programme doctoral en biotechnologie et génie biologique

pour l'obtention du grade de Docteur ès Sciences

par

Stamatia Zoi PAGOULATOU

Acceptée sur proposition du jury

Prof. H. Altug, présidente du jury
Prof. N. Stergiopoulos, directeur de thèse
Prof. P. Segers, rapporteur
Dr D. Adamopoulos, rapporteur
Prof. D. Pioletti, rapporteur

Acknowledgements

As I am arriving towards the end of my PhD studies, I would like to take this opportunity to thank a number of people who supported me throughout this journey. I want to start by expressing my deepest and most sincere gratitude towards my professor and mentor, Professor Nikos Stergiopoulos, who gave me the opportunity to work in his laboratory and took me under his wings during the past four years. Professor Stergiopoulos is not only an accomplished academic with excellent expertise on the field, but also – and most importantly – is a genuinely nice and decent person. I cannot possibly thank him enough for the opportunities that he gave me as well as for the amazing paths that opened in my life thanks to him.

A heartfelt thank you goes to our collaboration team in the University Hospitals in Geneva, and more specifically to the cardiologist Dr. Dionysios Adamopoulos and the MRI group led by Professor Jean-Paul Vallée, who were implicated in several projects that I undertook in my PhD. I would like to thank each and one of them personally for the fruitful collaboration, interesting discussions and valuable support in every step of this thesis – be it setting up measuring protocols, providing clinical data, or simply explaining to me how the clinical world works. My gratitude is extended to the entire team of the cardiology and medical imaging departments of the Hospital, especially to Dr. Lindsey Crowe for her valuable assistance in obtaining MRI data.

At this point, I would like to thank all the members of my laboratory, the LHTC group that I met and interacted with in the course of the past four years. I want to start by thanking Dr. Bram Trachet who made a significant contribution to my work, both in terms of helping me find the vision as well as practically assisting me with whatever I needed. Bram is one of the most talented people I had the chance to meet; he was always there for me, and for that I will always be grateful. I deeply hope that our pathways will cross again. A big thanks goes to all lab members: Mauro for assisting me with the computational projects, Lydia for her inexhaustible good mood, George for his sharp thinking and laughs, Vicky for the prolific collaboration, Quentin for his amazing work and help, Mike for his genuine kindness, Maïia for the laughs, Augusto, Rodrigo, Fabiana, Natalia, Allancer, Pedro for bringing the Brazilian vibe into the lab and for being incredibly nice people, François for his good mood and positivity, Adan for his academic assistance, Stéphane for being an inspirational role model, Valeria for her strong Argentinian temperament, Stef for being the most amazing friend, Seb for being Seb, Michel and Olympia for their good mood. Finally, I want to particularly acknowledge the immense help I received from Sylvia Widmer throughout my PhD; thank you so much, Sylvia. My gratitude and wishes are also extended to the members of the two other labs of our floor, the LBO and Microbs groups, for maintaining a fun working ambience.

During these past four years I had the opportunity to work with many talented Bachelor and Masters students. I would like to thank them for their valuable help and collaboration, thank you, Karim, David, Camilla, Aurélie, Antoine, Sami, Matthieu, Lore, Nathan, and Yanan. I would also like to acknowledge the assistance of the entire group in the administration of the EDBB program who was always available to help me with anything I needed, particularly the incredible Sonja Bodmer and Sandra Roux.

When I first arrived to Lausanne four years ago I was a different person than I am today and for that I want to thank all the amazing friends that made my life here so much fun: Oriane, Raquel, Elena, Mr. Lorenz, Stef, Simo (and Anna), Yasmine, Bharath and Sandra, George, Seb, Ece, Jens, Matina, Vasilina and Christos, Ted, Rania, Lili, Isaac the magician, Eftychia, and Eirini. My deepest thank you goes to Ms. Soula for her warm personality and for taking care of me all these years. And of course, I want to thank Constantinos for being the most positive person I know, for walking this journey alongside with me and for filling my life with so much love. *Με την ελπίδα ότι θα κάνουμε ριζες.*

Finally, the greatest support in my life comes from my family. Pursuing this PhD was not easy, neither physically nor psychologically, but I always had my people by my side. This thesis is, therefore, devoted to my beloved parents, Dionysis and Kalliopi, for always guiding my way, and my beautiful sister, Katerina, for always being my dearest friend. *Με πολλή αγάπη.*

Matina Pagoulatou
Lausanne, 28 September 2020

Abstract

Ageing is a natural process that affects both the anatomical and functional properties of the cardiovascular system and alters the coupling characteristics between the heart and the aorta. These alterations may predispose the cardiovascular system in the development and progression of cardiovascular diseases (CVD), such as hypertension and left ventricular (LV) hypertrophy. CVDs are currently the leading cause of morbidity and mortality globally, and with the population of elderly steadily increasing, they are expected to become socio-economic burden in the near future. Therefore, it is of outmost importance that we achieve profound understanding of the effects of ageing on the performance of the cardiovascular system in order to decipher the link between old age and pathology. Additionally, the clinical community is in need of accurate, noninvasive tools for monitoring relevant hemodynamic parameters and assess cardiovascular health.

Accordingly, the presented body of research aimed at providing novel insights into the evolution of hemodynamics with ageing (Part I) and the physiology of the ventricular-arterial interaction (Part II) by leveraging the potential of a state-of-the-art one-dimensional (1D) model of the systemic circulation. A major goal of this dissertation was also the development, implementation and validation of novel noninvasive tools for monitoring biomarkers of importance (Part III), as well as the evaluation of existing or novel techniques to derive aortic biomechanical properties (Part IV).

In Part I, we presented a validated 1D model of the systemic circulation that was adjusted to account for the effects of ageing, as reported by previous literature. The ageing model was found highly consistent with published data from large-scale studies in terms of pressure evolution, aortic wave shape and wave reflection indices. Examination of the wave reflection profile revealed an increase in the forward wave amplitude over time, which constitutes the principal determinant of the age-induced increase in systolic pressure. Additionally, we highlighted the importance of considering the heterogeneous effects of ageing on the arterial distensibility when adapting the properties of the arterial tree model, so as to predict correctly central hemodynamics. A method for personalizing the parameters of the arterial tree according to measurement of aortic flow and peripheral pressure was, subsequently, proposed and validated.

In Part II, we demonstrated the importance of the cardiac systolic function on central and peripheral hemodynamics under physiological and pathological conditions. By means of our computational 1D model, we showed that a physiological increase in cardiac contractility leads to a steeper forward pressure wave pumped by the heart, which, subsequently, drastically alters central and peripheral pressure and flow waves, and augments the pressure amplification from the aorta to the periphery. A major finding was that characteristic pressure phenotypes (*Type A* and *Type C*), which are commonly associated with arterial stiffness, are also highly dependent on LV contractility. These computational results were in good agreement with our subsequent *in vivo* study, conducted in a group of aortic valve stenosis patients subjected to Transcatheter Aortic Valve Replacement (TAVR). Removal of the aortic valve stenosis led to the immediate enhancement of the forward wave, which was linked with a change in the shape of the aortic waveforms and the development of post-TAVR systolic hypertension.

Part III of this thesis was devoted to the design, development, testing and validation of a method to achieve cardiac and hemodynamic monitoring based on simple, readily available, noninvasive measurements. The concept is based on the personalization of the parameters of the mathematical model of the cardiovascular system according to patient data from sphygmomanometry and routine echocardiography, and the subsequent derivation of cardiovascular properties in a reverse-engineering approach. Particular attention was given to the derivation of the end-systolic elastance (E_{es}), commonly used as an index of LV systolic function or ventricular contractility. The proposed method for deriving E_{es} was tested *in vivo* and was validated against invasive measurements, demonstrating high accuracy and robustness.

Finally, in Part IV, we evaluated existing and novel methods for the assessment of the biomechanical properties of the aorta. We first investigated whether local aortic area compliance, measured as lumen area changes over pulse pressure, is an appropriate index of volume compliance or distensibility when applied to the proximal aorta. We found both *in silico* and *in vivo* that neglecting the longitudinal strain of the proximal aorta during contraction might lead to severe underestimation of distensibility. Importantly, this

underestimation could be inconsistent among different populations and patient groups. In a second analysis, we focused our attention on measures of regional aortic compliance. More specifically, we examined the potential of using compressed-sensing (CS) 4D Flow MRI to reliably estimate aortic pulse wave velocity (PWV). After employing various algorithms to calculate the time delay between flow signals, we demonstrated that high correlation and good agreement between the CS-4D and high-resolution 2D phase contrast (PC) PWV estimates can be achieved for both the proximal and distal aorta. CS-4D MRI was also able to capture the anticipated increase in proximal aortic PWV with age.

Key words : Ageing • Cardiovascular modeling • Noninvasive monitoring • Inverse methods • Ventricular-arterial interaction • 4D Flow MRI

Résumé

Le vieillissement est un processus naturel qui affecte les propriétés anatomiques et fonctionnelles du système cardiovasculaire et modifie les caractéristiques de couplage entre le cœur et l'aorte. Ces altérations peuvent prédisposer le système cardiovasculaire dans le développement et la progression de maladies cardiovasculaires (MCV), telles que l'hypertension et l'hypertrophie ventriculaire gauche (VG). Les maladies cardiovasculaires sont actuellement la principale cause de morbidité et de mortalité dans le monde, et vue que la population de personnes âgées augmente constamment, elles devraient devenir un fardeau socio-économique dans un avenir proche. Par conséquent, il est d'haute importance que nous parvenions à une compréhension approfondie des effets du vieillissement sur la performance du système cardiovasculaire afin de déchiffrer le lien entre la vieillesse et ces pathologies. De plus, la communauté clinique a besoin d'outils précis et non invasifs pour surveiller des paramètres hémodynamiques pertinents et évaluer la santé cardiovasculaire.

Dans cette thèse, le corps de recherche présenté visait à fournir de nouvelles perspectives sur l'évolution de l'hémodynamique avec le vieillissement (Partie I) et la physiologie de l'interaction ventriculaire-artérielle (Partie II) en exploitant le potentiel d'un modèle unidimensionnel (1D) de la circulation systémique. Un objectif majeur de cette thèse était également le développement, la mise en œuvre et la validation de nouveaux outils non invasifs pour surveiller les biomarqueurs d'importance (Partie III), ainsi que l'évaluation de techniques existantes ou nouvelles pour obtenir des propriétés biomécaniques aortiques (Partie IV).

Dans la Partie I, nous avons présenté un modèle 1D validé de la circulation systémique qui a été ajusté pour tenir compte des effets du vieillissement, comme indiqué dans la littérature précédente. Le modèle de vieillissement s'est révélé très cohérent avec les données publiées d'études à grande échelle en termes d'évolution de la pression, de forme d'onde aortique et d'indices de réflexion de l'onde. L'examen du profil de réflexion des ondes a révélé une augmentation de l'amplitude des ondes au fil du temps, qui constitue le principal déterminant de l'augmentation de la pression systolique induite par l'âge. De plus, nous avons souligné l'importance de considérer les effets hétérogènes du vieillissement sur la distensibilité artérielle lors de l'adaptation des propriétés du modèle d'arbre artériel, afin de prédire correctement l'hémodynamique centrale. Une méthode de personnalisation des paramètres de l'arbre artériel en fonction de la mesure du débit aortique et de la pression périphérique a ensuite été proposée et validée.

Dans la Partie II, nous avons démontré l'importance de la fonction systolique cardiaque sur l'hémodynamique centrale et périphérique dans des conditions physiologiques et pathologiques. Au moyen de notre modèle informatique 1D, nous avons montré qu'une augmentation physiologique de la contractilité cardiaque conduit à une onde de pression plus forte pompée par le cœur, qui, par la suite, modifie considérablement les ondes de pression et de débit, centrales et périphériques, et augmente l'amplification de la pression à partir de l'aorte à la périphérie. Une découverte majeure a été que les phénotypes de pression caractéristiques (type A et type C), qui sont couramment associés à la rigidité de la paroi artérielle, dépendent également fortement de la contractilité du VG. Ces résultats de calcul étaient en bon accord avec notre étude in vivo ultérieure, menée dans un groupe de patients soumis à un remplacement de valve aortique transcathéter (TAVR). L'ablation de la sténose valvulaire aortique a conduit à une amélioration immédiate de l'onde directe, qui était liée à un changement de forme des ondes aortiques et au développement d'une hypertension systolique post-TAVR.

La Partie III de cette thèse a été consacrée à la conception, au développement, aux tests et à la validation d'une méthode pour réaliser une surveillance cardiaque et hémodynamique basée sur des mesures simples, facilement disponibles et non invasives. Le concept est basé sur la personnalisation des paramètres du modèle mathématique du système cardiovasculaire en fonction des données des patients provenant de la sphygmomanométrie et de l'échocardiographie de routine, et la dérivation ultérieure des propriétés cardiovasculaires dans une approche de rétro-ingénierie. Une attention particulière a été accordée à la dérivation de l'élastance terminale systolique (E_{es}), couramment utilisée comme indice de la fonction systolique VG ou de la contractilité ventriculaire. La méthode proposée pour dériver E_{es} a été testée in vivo et a été validée par rapport à des mesures invasives, démontrant une grande précision et robustesse.

Enfin, dans la Partie IV, nous avons évalué les méthodes existantes et nouvelles pour l'évaluation des propriétés biomécaniques de l'aorte. Nous avons d'abord cherché à savoir si la compliance de la zone aortique locale, mesurée lorsque la surface de la lumière change au cours de la pression du pouls, est un indice approprié de compliance ou de distensibilité du volume lorsqu'elle est appliquée à l'aorte proximale. Nous avons trouvé à la fois *in silico* et *in vivo* que le fait de négliger la déformation longitudinale de l'aorte proximale pendant la contraction pourrait conduire à une sous-estimation sévère de la distensibilité. Surtout, cette sous-estimation pourrait être incohérente entre les différentes populations et les groupes de patients. Dans une deuxième analyse, nous avons concentré notre attention sur les mesures de la conformité aortique régionale. Plus précisément, nous avons examiné le potentiel de l'IRM à détection compressée (CS) 4D pour estimer de manière fiable la vitesse des ondes de pouls aortiques (PWV). Après avoir utilisé divers algorithmes pour calculer le délai entre les signaux de flux, nous avons démontré qu'une corrélation élevée et un bon accord entre le CS-4D et les estimations PWV du contrat de phase 2D (PC) à haute résolution peuvent être atteints pour l'aorte proximale et distale. L'IRM CS-4D a également été en mesure de saisir l'augmentation prévue de la PWV aortique proximale avec l'âge.

Mots-clés : Vieillesse • Modélisation cardiovasculaire • Surveillance non invasive • Méthodes inverses • Interaction ventriculaire-artérielle • IRM en flux 4D

Contents

| | |
|---|-------------|
| Acknowledgements | i |
| Abstract | iii |
| Résumé | v |
| List of Figures | xi |
| List of Tables | xiii |
| List of Equations | xv |
| Chapter 1 Introduction | 1 |
| 1.1 Motivation | 1 |
| 1.2 Scope and Summary of Chapters | 2 |
| 1.3 Current state of knowledge | 2 |
| 1.3.1 The Cardiovascular Physiology | 2 |
| 1.3.2 The Ventricular-Arterial Coupling..... | 3 |
| 1.3.3 Cardiovascular Ageing..... | 4 |
| 1.3.4 Cardiac and Hemodynamic Monitoring | 7 |
| 1.3.5 <i>In vivo</i> Assessment of Aortic Compliance..... | 8 |
| 1.3.6 Mathematical Models of the Cardiovascular System..... | 10 |
| 1.4 Bibliography | 11 |
| Chapter 2 Hemodynamics of Ageing..... | 17 |
| 2.1 Evolution of aortic pressure during normal ageing: a model-based study | 17 |
| 2.1.1 Introduction | 18 |
| 2.1.2 Methods..... | 18 |
| 2.1.3 Results | 21 |
| 2.1.4 Discussion | 24 |
| 2.1.5 Bibliography..... | 26 |
| 2.2 On the importance of the non-uniform aortic stiffening in the hemodynamics of physiological ageing . | 29 |
| 2.2.1 Introduction | 30 |
| 2.2.2 Methods..... | 30 |
| 2.2.3 Results | 33 |
| 2.2.4 Discussion | 36 |
| 2.2.5 Bibliography..... | 39 |

| | | |
|------------------|--|-----------|
| Chapter 3 | Influence of Heart on Arterial Hemodynamics | 43 |
| 3.1 | The effect of left ventricular contractility on arterial hemodynamics: a model-based investigation | 43 |
| 3.1.1 | Introduction | 44 |
| 3.1.2 | Methods..... | 44 |
| 3.1.3 | Results..... | 46 |
| 3.1.4 | Discussion | 50 |
| 3.1.5 | Bibliography..... | 52 |
| 3.2 | Acute effects of Transcatheter Aortic Valve Replacement on the ventricular-aortic interaction..... | 55 |
| 3.2.1 | Introduction | 56 |
| 3.2.2 | Methods..... | 56 |
| 3.2.3 | Results..... | 59 |
| 3.2.4 | Discussion | 64 |
| 3.2.5 | Bibliography..... | 66 |
| Chapter 4 | Inverse Methods for Noninvasive Monitoring of Hemodynamics..... | 69 |
| 4.1 | Estimating left ventricular elastance from aortic flow waveform, ventricular ejection fraction, and brachial pressure: an <i>in silico</i> study..... | 69 |
| 4.1.1 | Introduction | 70 |
| 4.1.2 | Methods..... | 70 |
| 4.1.3 | Results..... | 73 |
| 4.1.4 | Discussion | 78 |
| 4.1.5 | Bibliography..... | 82 |
| 4.2 | <i>In vivo</i> application and validation of a novel noninvasive method to estimate the end-systolic elastance | 85 |
| 4.2.1 | Introduction | 86 |
| 4.2.2 | Methods..... | 86 |
| 4.2.3 | Results..... | 89 |
| 4.2.4 | Discussion | 94 |
| 4.2.5 | Bibliography..... | 96 |
| Chapter 5 | Methods for Assessing Bio-mechanical Properties of the Aorta | 99 |
| 5.1 | The effect of the elongation of the proximal aorta on the estimation of the aortic wall distensibility | 99 |
| 5.1.1 | Introduction | 100 |
| 5.1.2 | Methods..... | 100 |
| 5.1.3 | Results..... | 106 |
| 5.1.4 | Discussion | 108 |
| 5.1.5 | Bibliography..... | 111 |
| 5.2 | Assessing regional aortic Pulse Wave Velocity with compressed-sensing accelerated 4D flow MRI: an <i>in vivo</i> comparison with 2D phase contrast MRI | 113 |
| 5.2.1 | Introduction | 114 |
| 5.2.2 | Methods..... | 114 |
| 5.2.3 | Results..... | 118 |
| 5.2.4 | Discussion | 122 |
| 5.2.5 | Bibliography..... | 125 |

| | | |
|-------------------------|------------------------------------|------------|
| Chapter 6 | Conclusions..... | 127 |
| 6.1 | Summary of results | 127 |
| 6.2 | Perspectives and future work | 128 |
| 6.3 | Biobibliography | 129 |
| Publications | | 131 |
| Curriculum Vitae | | 133 |

List of Figures

| | | |
|---------------|--|----|
| Figure 1.1:1 | Ageing and cardiovascular disease worldwide..... | 1 |
| Figure 1.3:1 | Pressure evolution in the arterial and venous system..... | 3 |
| Figure 1.3:2 | The law of Laplace and ventricular adaptation to pressure overload..... | 4 |
| Figure 1.3:3 | Changes in vascular structure with age..... | 5 |
| Figure 1.3:4 | Evolution of brachial systolic and diastolic pressure with age and gender..... | 5 |
| Figure 1.3:5 | Wave reflections as the major determinant of age-induced hypertension according to O'Rourke et al..... | 6 |
| Figure 1.3:6 | Cardiac ageing..... | 7 |
| Figure 1.3:7 | The end-systolic pressure-volume relation as an index of cardiac systolic function..... | 8 |
| Figure 1.3:8 | Carotid-to-femoral tonometry for the estimation of PWV..... | 9 |
| Figure 1.3:9 | Example of aortic flow data acquired with 4D Flow MRI for PWV measurement..... | 9 |
| Figure 1.3:10 | Schematic representation of the arterial tree developed by Reymond et al. [11] consisting of 55 main arteries of the systemic circulation, the circulation in the coronaries, the principal abdominal aortic branches, and the circle of Willis..... | 10 |
| Figure 2.1:1 | Model pressure predictions against clinical data for the time frame of 30 to 80 years of age..... | 22 |
| Figure 2.1:2 | Aortic and brachial pressure waveforms for different age decades..... | 23 |
| Figure 2.1:3 | Model predictions against clinical data from Mitchell et al. [13] and Torjesen et al. [15]. (A) Augmentation Pressure, (B) Augmentation index, (C) Inflection Point..... | 23 |
| Figure 2.1:4 | Contribution of forward pressure wave to pressure augmentation during ageing, as assessed by the PPforward/PPcentral ratio. 1D model results compared to the 0-D model results [18]..... | 24 |
| Figure 2.2:1 | Pressure waveforms at the proximal ascending aorta for the control case, after local proximal stiffening and global arterial stiffening for the same pulse pressure increase (+45%)..... | 32 |
| Figure 2.2:2 | Method-estimated c-f PWV values against the reference SphygmoCor values..... | 34 |
| Figure 2.2:3 | Comparison of the method-predicted aortic SBP and central augmentation index against the values predicted by the Mobil-O-Graph device..... | 35 |
| Figure 2.2:4 | Aortic pressure waveforms derived from the model simulations for two subjects: (left) the characteristic Type A pressure phenotype of a 52-year-old male and (right) the Type C phenotype of a 30-year-old female..... | 36 |
| Figure 3.1:1 | Intraventricular pressure-volume loops for two scenarios of high ($E_{es} = 3$ mmHg/mL, $V_d = -2$ mL) and low ($E_{es} = 1$ mmHg/mL, $V_d = -60$ mL) LV contractility with a maintained stroke volume..... | 46 |
| Figure 3.1:2 | Effect of LV contractility on central hemodynamics..... | 49 |
| Figure 3.1:3 | Central and peripheral arterial pressure for the two cases of LV contractility..... | 50 |
| Figure 3.2:1 | Flow diagram of study patients according to the inclusion/exclusion criteria..... | 57 |
| Figure 3.2:2 | Aortic pressure and flow pulse wave analysis in the time domain and frequency-based wave separation of the pressure wave into its forward and backward components..... | 58 |
| Figure 3.2:3 | Representative case of a patient with severe AS before and after TAVR..... | 63 |
| Figure 3.2:4 | Scatterplot (left) and Bland-Altman plot (right) comparing the cardiac output estimated prior to the TAVR procedure via echocardiography and thermodilution..... | 64 |
| Figure 4.1:1 | Schematic description of the two-step inverse problem-solving algorithm..... | 72 |

| | | |
|--------------|--|-----|
| Figure 4.1:2 | Optimization of cardiac preload..... | 74 |
| Figure 4.1:3 | Comparison of the E_{es} and E_{ed} values as estimated by the proposed method to the real ones..... | 76 |
| Figure 4.1:4 | Comparison of the E_{es} values as estimated by the method of Chen et al. [8] to the real ones..... | 76 |
| Figure 4.1:5 | (left) Aortic flow waveform used as the input signal for this particular case. (right) Model-derived brachial pressure waveforms for the 'real' arterial compliance and after inducing a +20% and a -20% change in arterial compliance..... | 77 |
| Figure 4.2:1 | Two-step optimization algorithm to compute the ESPVR..... | 88 |
| Figure 4.2:2 | Example of the optimization process of the ESPVR for a specific HFpEF patient..... | 91 |
| Figure 4.2:3 | Scatterplots (left) and Bland-Altman plots (right) for E_{es} , Vd and $V100$ as predicted by the method against invasive measurements..... | 92 |
| Figure 4.2:4 | Scatterplot (left) and Bland-Altman plot (right) for the EDP approximated using its experimental correlation with E/e' [10] against invasive measurements..... | 93 |
| Figure 4.2:5 | Method sensitivity to the estimated diastolic LV properties..... | 94 |
| Figure 5.1:1 | (A) Raw MR data of the aorta and its main branches acquired with ToF MR Angiography on a healthy young male [12]. (B) Reconstruction of the 3D geometry. (C) Cropping of the aorta at the main supra-aortic branches and above the celiac trunk..... | 101 |
| Figure 5.1:2 | Boundary conditions. (left) Schematic representation of the viscoelastic boundary conditions applied along the vessel wall to mimic the support provided by the external tissues and organs. (right) Different regions of the wall domain considered for assigning viscoelastic boundary properties..... | 103 |
| Figure 5.1:3 | Motion of the aortic root in 2 planes..... | 104 |
| Figure 5.1:4 | Imaging of the proximal aorta of the 38-year-old male during diastole (left) and systole (right) in the sagittal plane along with the segmented 3D geometries..... | 106 |
| Figure 5.1:5 | (left) Unloaded configuration after 6 cycles of the fixed-point optimization algorithm [23]. (right) The corresponding error map between the measured geometry and the configuration inflated to diastolic pressure..... | 106 |
| Figure 5.1:6 | Generic model results for the lumen volumetric changes with increasing pressure..... | 107 |
| Figure 5.2:1 | (A) 2D PC MRI data acquisition strategy. (B) Processing of the CS-4D MRI data using 4D Flow Demonstrator (Free-type Project, Siemens Healthineers, Erlangen, Germany)..... | 115 |
| Figure 5.2:2 | Examples of flow signals acquired with 2D MRI (left) and the corresponding CS-4D flows (right) for one young volunteer..... | 116 |
| Figure 5.2:3 | Schematic representation of four previously proposed PTT algorithms..... | 118 |
| Figure 5.2:4 | Box plots of the 2D and CS-4D PWV calculated at the aortic arch (left) and descending aorta (right), using four previously proposed algorithms..... | 119 |
| Figure 5.2:5 | Scatterplots and Bland-Altman plots of the PWV estimated from the 2D and the CS-4D data using the FFT algorithm..... | 121 |
| Figure 5.2:6 | Association between age and the CS-4D aortic arch PWV estimated using three PTT algorithms..... | 122 |

List of Tables

| | | |
|-------------|--|-----|
| Table 2.1:1 | Inverse relation coefficients a and b and goodness of fit R^2 for each age decade. | 20 |
| Table 2.1:2 | Overview of the ageing cardiac parameters. | 21 |
| Table 2.1:3 | Simulation derived hemodynamic parameters according to age category. | 21 |
| Table 2.2:1 | Hemodynamic values of the study population categorized into the two age groups. | 33 |
| Table 2.2:2 | Indices of correlation, accuracy and agreement between the measured and method-derived c-f PWV values. | 34 |
| Table 3.1:1 | Model parameters used to set up the two scenarios of high and low LV contractility. | 45 |
| Table 3.1:2 | Comparison of hemodynamic characteristics between the two contractility simulations. | 47 |
| Table 3.2:1 | Demographic characteristics, comorbidities and presenting symptoms of the study participants. | 60 |
| Table 3.2:2 | Invasive hemodynamic and echocardiographic characteristics of the study population before and after TAVR. | 61 |
| Table 3.2:3 | Effect of TAVR on vascular parameters assessed via the PPM and on the aortic pressure wave components assessed via frequency-based wave separation analysis. | 62 |
| Table 4.1:1 | The effect of cardiac preload on method estimates for a specific case. | 74 |
| Table 4.1:2 | Cardiac parameters and hemodynamic characteristics of the 50 simulated cases. | 75 |
| Table 4.1:3 | Correlation, agreement and accuracy between ‘real’ and estimated E_{es} and E_{ed} values. | 77 |
| Table 4.1:4 | Estimation of E_{es} and E_{ed} after inducing a +20% increase and a -20% decrease in arterial compliance. | 77 |
| Table 4.1:5 | Estimation of E_{es} and E_{ed} after simulating measurement errors: a +10% increase in aortic flow amplitude and a +10% increase in brachial systolic blood pressure. | 78 |
| Table 4.2:1 | Descriptive and clinical characteristics of study population (n=19). | 90 |
| Table 4.2:2 | Method sensitivity to the approximation of the end-diastolic pressure (EDP). The results pertain to a specific HFpEF case. | 93 |
| Table 5.1:1 | Simulation results after varying key model parameters. The table includes the reference distensibility value along with the estimate without considering elongation. The respective errors are shown. | 107 |
| Table 5.1:2 | Participant demographic characteristics, measured aortic root displacement and distensibility estimation. | 108 |
| Table 5.2:1 | Demographic and clinical characteristics of study volunteers. | 119 |
| Table 5.2:2 | Indices of correlation, accuracy and agreement between the 2D and CS-4D measurements of PWV as evaluated via four PTT algorithms. The results for both the aortic arch and the descending aorta are provided. | 120 |
| Table 5.2:3 | Intra- and inter-observer variability of 2D PWV estimation. | 122 |

List of Equations

| | |
|--|-----|
| Equation 1.3:1 – The Bramwell-Hill equation relating pulse wave velocity and local arterial compliance. | 3 |
| Equation 2.1:1 – Aortic valve model with inertia and turbulence terms | 19 |
| Equation 2.1:2 – Pulse wave velocity as a function of mean lumen diameter..... | 19 |
| Equation 2.2:1 – Arterial compliance as a function of the pulse wave velocity..... | 31 |
| Equation 3.1:1 – LV pressure-volume relation..... | 44 |
| Equation 4.1:1 – Time-varying elastance relating left ventricular pressure and volume..... | 71 |
| Equation 4.1:2 – Single-beat method of Chen et al. for the noninvasive estimation of the end-systolic elastance | 73 |
| Equation 4.2:1 – Updated LV pressure-volume relation accounting for the non-linear LV diastolic properties | 86 |
| Equation 5.1:1 – Volumetric changes expressed as changes in area and centerline length..... | 100 |
| Equation 5.1:2 – The strain-energy function according to the HGO model | 102 |
| Equation 5.1:3 – Stain-like quantities $E1$ and $E2$ that characterize the deformation of the two families of fibres | 102 |
| Equation 5.1:4 – Boundary condition applied along the outer aortic wall comprising an elastic and a viscoelastic response | 103 |
| Equation 5.1:5 – Formula for calculation of the volume of a conical cylinder | 105 |

Chapter 1 Introduction

1.1 Motivation

The average lifespan of the human population steadily increases and, in consequence, larger parts of the world's population belong to aged groups [1]. By 2050, it is expected that one in six people will be over 65 years old [1]. Within this age group, cardiovascular diseases (CVD) are currently the leading cause of morbidity and mortality globally [2]. Put in numbers, the prevalence of CVDs, such as hypertension, atherosclerosis, ischemic injury, myocardial infarction and stroke, is almost 70-75% for people aged 60-79 years and steadily increases after 80 [3] (Figure 1.1:1). With the population of elderly constantly growing, it is expected that in the near future almost 1 in 2 deaths will be due to CVDs, with major socio-economic implications [4].

Therefore, it is of outmost importance to understand how ageing affects hemodynamics and cardiovascular function, and elucidate the pathways that connect it with cardiovascular disease. Additionally, the medical community is in dire need of tools to assess and monitor cardiovascular health. Such tools should be easy-to-operate, noninvasive, and personalized, in order to assist clinicians with early disease detection and targeted therapy.

Ageing and Cardiovascular Disease Worldwide

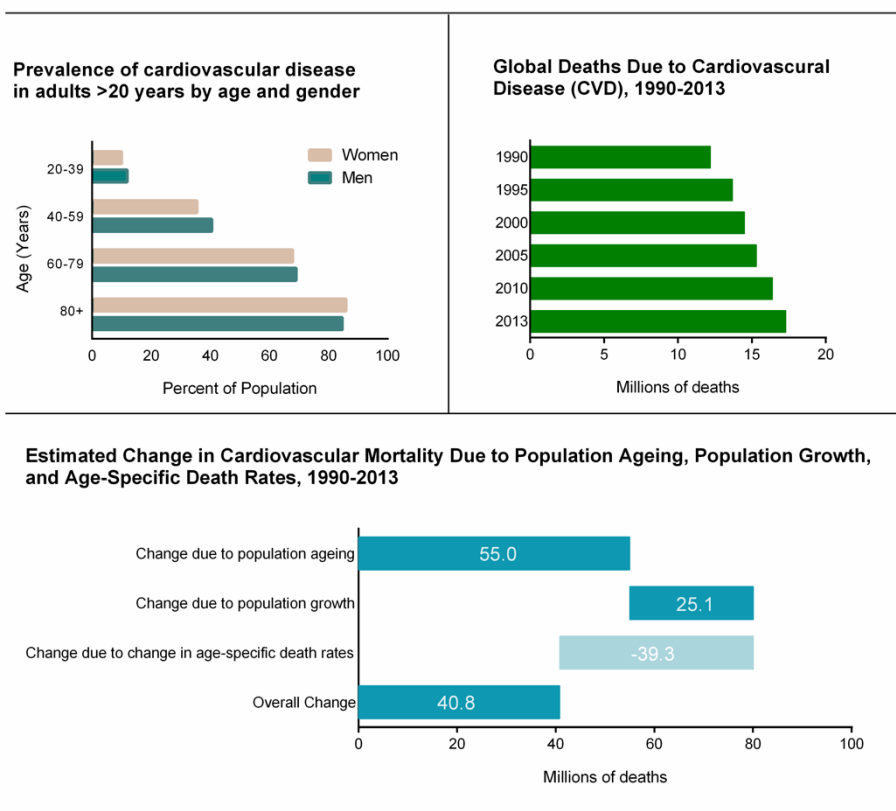


Figure 1.1:1 Ageing and cardiovascular disease worldwide. Data based on the National Health and Nutrition examination Survey 2009-2012 [3] as well as the Global Burden of Disease 2013 study [5].

1.2 Scope and Summary of Chapters

The primary goal of this dissertation was to investigate the age-related changes in hemodynamics and achieve a better understanding of the physiology of the ventricular-arterial interaction by leveraging the potential of a state-of-the-art one-dimensional (1D) model of the systemic circulation. The second major goal was to evaluate existing or novel techniques for the assessment of biomechanical properties as well as design, develop and implement novel noninvasive tools for monitoring biomarkers of importance.

In more detail, this thesis is organized in four parts, which focus on the following subjects:

- 1) **Hemodynamics of ageing (Chapter 2).** In the first part of this dissertation, we sought to provide *in silico* insights into the effects of ageing on central hemodynamics as well as expose ageing mechanisms that contribute to the physiological increase in systolic pressure. Particular attention was given to understanding how the parameters of mathematical models of the cardiovascular system should be adjusted in order to incorporate effects of age.
- 2) **Influence of heart on arterial hemodynamics (Chapter 3).** Given that the interaction between the heart and the arterial system is recognized as a key component of cardiovascular function, this chapter was devoted to the investigation of the effect of cardiac contractility on central and peripheral hemodynamics under physiological and pathological conditions. This subject was approached initially from a computational standpoint and, subsequently, was assessed *in vivo* during acute change of cardiac afterload.
- 3) **Inverse methods for noninvasive monitoring of hemodynamics (Chapter 4).** In the third major part of this thesis, we used the insights gained from simulating mechanisms of ageing (Chapter 2) and from studying the ventricular-arterial interaction (Chapter 3) in order to design, implement and validate novel tools for the derivation of biomarkers of importance, with an emphasis on the assessment of cardiac contractility. The concept is based on the personalization of a mathematical model of the cardiovascular system according to a few, readily available noninvasive measurements, and the subsequent derivation of parameters of interest via a reverse-engineering approach. These techniques will be hereafter called “inverse methods”.
- 4) **Methods for assessing biomechanical properties of the aorta (Chapter 5).** The final part of this dissertation focused on the evaluation of the accuracy of existing and novel Magnetic Resonance Imaging (MRI) techniques for the estimation of aortic biomechanical properties. First, we examined the importance of the axial stretch of the proximal aorta during cardiac contraction on the estimation of local area compliance. Additionally, we aimed to evaluate the potential of using a novel time-resolved three-dimensional (3D) MRI sequence to derive measures of aortic wall elasticity.

1.3 Current state of knowledge

1.3.1 The Cardiovascular Physiology

With each contraction, the left ventricle (LV) of the heart pumps blood through the systemic circulation in order to provide tissues with oxygen and nutrients and remove waste products. The aorta plays an important role in physiology: it acts both as a conduit vessel and a buffering chamber [6]. The aortic wall is compliant, which entails that, during systole, it distends to accommodate the blood ejected by the LV. In diastole, it releases the stored energy and forwards the remaining blood volume to the peripheral circulation, thus achieving a nearly continuous perfusion of peripheral beds [7]. This buffering capacity is known as the Windkessel function.

In the healthy young man, elastic properties decrease progressively as the vessels approach the periphery [8]. Contrarily, the resistance of the aorta and conduit arteries is low, so that the mean pressure is roughly maintained from heart to the more muscular peripheral vessels until it drops significantly at the level of arterioles [9] (Figure 1.3:1). This implies that conduit arteries can be seen as a supply reservoir and peripheral resistances adjust themselves to regulate the blood flow to the tissues. Accordingly, arterial load can be expressed as the combination of a pulsatile component influenced mostly by the elasticity (or compliance) of the major arteries and a steady component (total peripheral resistance) regulated mostly by microvascular properties [10].

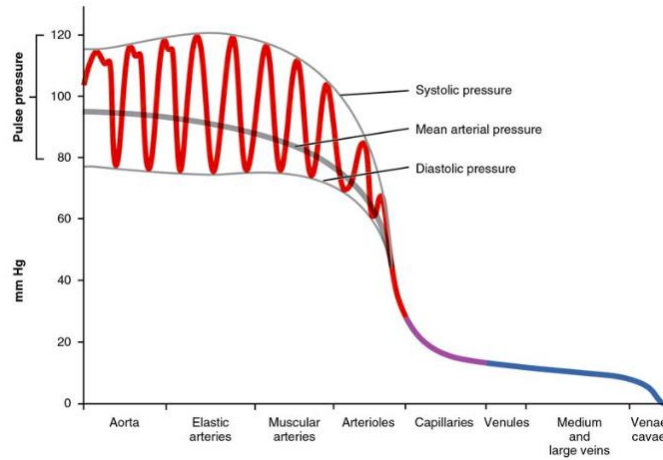


Figure 1.3:1 Pressure evolution in the arterial and venous system. Reproduced from [9] with permission.

During systole, the heart generates blood pressure and flow pulse waves. Due to the elasticity of the arterial walls, the pulse waves are not instantaneously transmitted to the periphery, but propagate along the arterial tree with a certain speed, which is called the pulse wave velocity (PWV) [11]. The PWV can be calculated as the distance travelled by the wave over the time delay and is directly linked with the local arterial wall compliance (C_A) via the Bramwell-Hill equation:

$$PWV = \sqrt{\frac{A}{\rho C_A}}$$

Equation 1.3:1 – The Bramwell-Hill equation relating pulse wave velocity and local arterial compliance.

An important aspect of wave propagation is reflections: the pulse waves generated by the heart get reflected when they encounter sites of impedance mismatch, e.g. bifurcations. This means that at any given point in the arterial tree, the pressure and flow waves can be expressed as the sum of a total forward wave travelling from the proximal aorta to the periphery and a total backward wave travelling back to the heart [12].

1.3.2 The Ventricular-Arterial Coupling

The arterial blood pressure is the result of the instantaneous interaction between the heart and the arterial system. The left ventricle and the arterial circulation form a coupled biological system and are interdependent, as evidenced by the common physiological mechanisms that coordinate their function [13], [14]. The importance of the ventricular-arterial coupling (VAC) is recognized in both the physiology of cardiac and aortic mechanics, as well as in the pathophysiology of cardiovascular diseases [14].

Acute changes in either ventricular or vascular function activate neurohumoral mechanisms that restore the matching between the two systems, e.g. via changes in heart rate, vascular tone or cardiac contractility [15]. Under chronic hemodynamic overload, the optimization of the cardiovascular function is achieved by structural changes, i.e., remodeling [13], [16]–[18]. Concretely, in the case of pressure overload, cardiovascular remodeling aims at maintaining the tensile stress acting on the vascular or ventricular wall within the normal range [19]. To better appreciate this concept, we may consider the law of Laplace, according to which tensile stress is directly proportional to pressure and radius and inversely proportional to wall thickness. In response to increases in pressure, the ventricular or arterial wall needs to thicken in order for the tensile stress to be maintained constant. Accordingly, the compensatory mechanism to pressure overload is hypertrophy and decrease in the ratio of lumen radius to wall thickness, as has been demonstrated by studies on chronic hypertension [13], [16]–[20] (Figure 1.3:2).

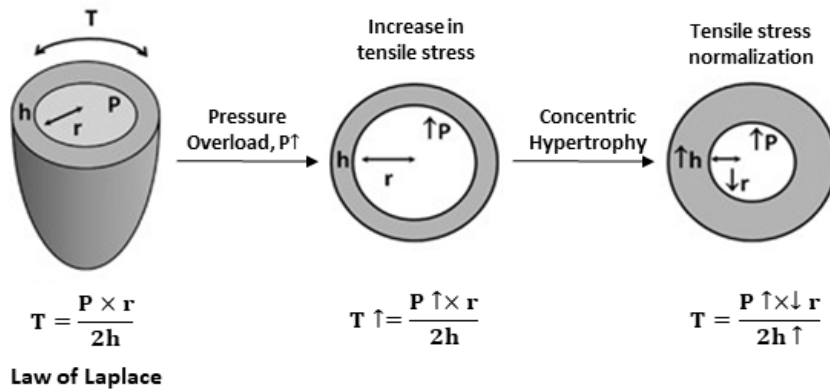


Figure 1.3:2 The law of Laplace and ventricular adaptation to pressure overload. Adapted from [20] and reproduced with permission.

1.3.3 Cardiovascular Ageing

Although the exact mechanisms that pave the way for the development of cardiovascular disease with age are not fully elucidated, it is understood that ageing leads to gradual changes in the structure and function of both the cardiac and arterial systems [21], [22], resulting in arterial stiffening and increase in systolic blood pressure. The following paragraphs summarize the major points of cardiovascular ageing as reported in the literature.

Vascular Ageing and Hemodynamics

Extensive research on the impact of older age on the structure of arteries has reported an increase in degradation of the extracellular matrix (ECM) of the vascular wall, increased collagen and calcium deposition, and elastin fragmentation in the media layer [23], [24]. These changes occur predominantly in large arteries and contribute to the reduction of the arterial compliance [8], [25]. In peripheral arteries, endothelial function demonstrates a progressive decline with age as shown for the brachial [26], [27] and femoral [28] arteries. The endothelium is a single layer of cells that plays a key role in modulating arterial structure and vasodilatory, thrombolytic and vasoprotective functions, hence endothelial dysfunction may contribute to the development of atherosclerosis and other vascular disorders [29]. From a pathophysiological standpoint, the increase in collagen and decrease in elastin content precedes endothelial damage [30].

A common observation in human ageing studies is the increase in the arterial intima-media thickness that is fairly linear with age [31], [32]. The arterial wall thickening can be understood as a compensatory mechanism in response to the elevation of blood pressure exerted on the wall, as explained by the law of Laplace. A second frequently reported observation is vascular dilation [33]. Although the mechanism behind the age-related enlargement of lumen diameters is still not clear, it could constitute a compensatory adaptation to the stiffening of the vasculature as well as to the increase in wall thickness, in order to maintain luminal area.

Morphologically, the above-described alterations are predominantly present in the aorta. The aorta thickens, dilates, elongates and becomes more tortuous with age [33]. Interestingly, previous studies have shown that aortic regional lengths and diameters increase at different rates with age, with the proximal aorta being more affected than its distal counterparts [34]. The aortic arch region has also been reported to undergo remodeling, usually increasing in length [35]. The effect of these aortic morphological changes on the local hemodynamics might offer important insight into the link between age and disease and, therefore, is currently the subject of intense research.

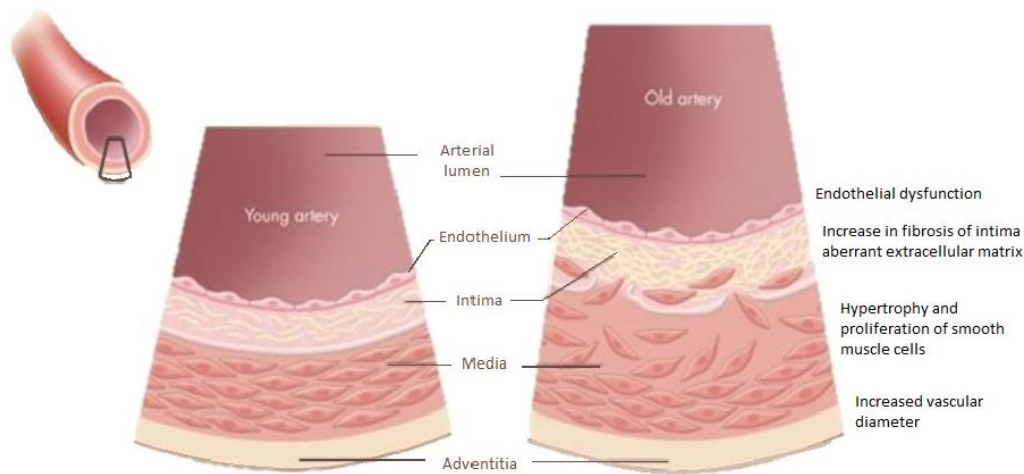


Figure 1.3:3 Changes in vascular structure with age.

Vascular stiffening, as a consequence of the changes in the structure of the arteries, is a crucial component of ageing (and pathology), with important implications for wave propagation and pressure evolution. In young adults, the proximal aorta is highly compliant, accounting for approximately 50% of the total compliance of the arterial tree [36]. Pressure and flow waves travel, therefore, slowly within the arteries, aortic PWV is typically around 4 ± 1 m/s for healthy subjects under 30 years old [37], [38]. As a result, reflected waves return to the heart during diastole, augmenting the diastolic pressure [39] and improving coronary perfusion. With increasing age, the arterial tree stiffens in a non-uniform way [40], [41], the proximal aorta loses its elasticity more markedly than its distal counterpart and the periphery [37], [42]. This entails an increase in the aortic PWV, which might rise to 6 ± 2 m/s for 40-60 year-old adults [37]. As the aorta becomes stiffer and more tortuous, the wave reflection topology is modified; the pulse wave is reflected downstream more rapidly and returns back to the heart before diastole, leading to augmentation of the late systolic blood pressure [23]. Several investigations support the importance of late systolic load from wave reflections as a determinant of diastolic and systolic dysfunction, and heart failure [43]–[46].

Large-scale longitudinal studies have shown that systolic blood pressure (SBP) increases continuously with age [47], [48] (Figure 1.3:4). Diastolic blood pressure (DBP), on the other hand, has a varying pattern with ageing; increasing until the fifth decade of life and slowly decreasing thereafter (Figure 1.3:4). The underlying mechanisms that cause the decrease of DBP after 60 years are still being investigated, nevertheless, it is clear that lower DBP compromises coronary perfusion that occurs primarily during diastole, favoring the development of myocardial ischemia [49]. Overall, there is a steep rise in pulse pressure after the age of 60 years old, which exposes the microcirculation to greater pulsatility, causing damage to end organs such as the kidneys and the brain [50], [51]. The increase in pulse pressure is the most powerful predictor of risk in the elderly [52].

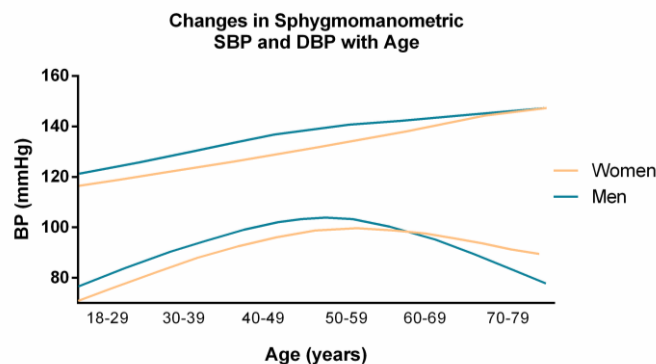


Figure 1.3:4 Evolution of brachial systolic and diastolic pressure with age and gender according to [46].

The relative contribution of the forward and backward wave components to the increase in blood pressure with age remains a subject of scientific debate. Until recently, the line of thinking was that the major determinant of the systolic pressure increase with age is wave reflections, since the earlier return of the augmented reflected waves to the heart affects end-systolic pressure O'Rourke et al. [53], [54] (Figure 1.3:5). However, this point of view has been challenged by subsequent studies [55], which suggest that the non-uniform aortic stiffening leads to an increase in the characteristic impedance predominantly in the proximal aorta, causing a significant augmentation in the forward pressure wave amplitude, which drives the increase in systolic blood pressure.

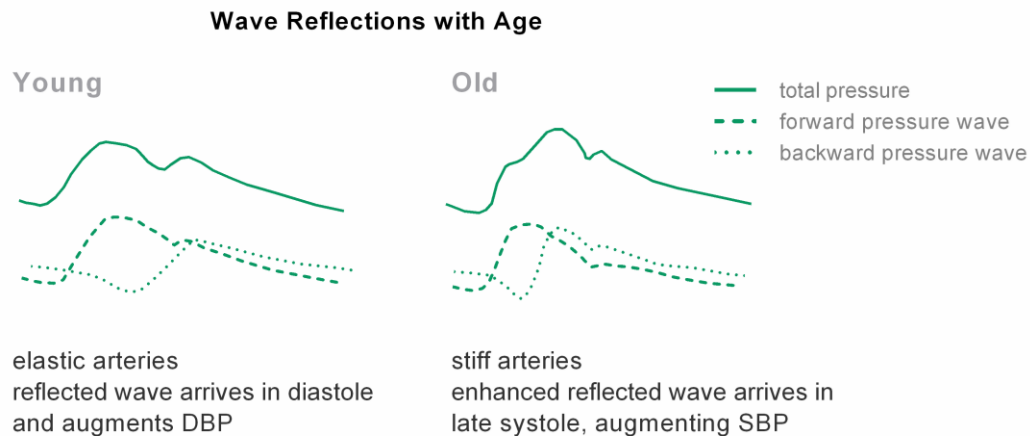


Figure 1.3:5 Wave reflections as the major determinant of age-induced hypertension according to O'Rourke et al. [52], [53].

Cardiac Ageing

Age-induced changes in vascular structure and function are accompanied by cardiac remodeling [4]. The heart responds to the pressure overload by increasing the thickness of the ventricular wall, usually in the form of concentric hypertrophy [21], and promoting fibroblast proliferation, which results in additional fibrotic tissue [21], [56]. LV hypertrophy is a powerful mechanism to reduce wall stress during systole (Figure 1.3:2) and thus to preserve ejection in case of afterload excess. On a structural level, previous autopsy studies have shown an increase in collagen type I (higher tensile strength) and a decrease in collagen type III (higher distensibility) in the elderly [57]. The higher ratio of collagen type I may contribute to left ventricle stiffness [57]–[59], which has important implications for cardiac function. For the stiffer heart to achieve the same perfusion and maintain cardiac output, more effort is required which poses restrictions to heart rate variability [60].

There have been conflicting data concerning the evolution of LV mass with age, but recent analyses report a modest sex-specific decrease in men only [21] or no effect whatsoever [61]. The fairly preserved LV mass with age despite the increase in wall thickness could be explained by the concurrent change in the shape of the LV from conical to spherical, i.e., preservation of short axis length but decrease of long axis length [62]. These morphological changes entail a decrease in the LV end-diastolic volume (EDV) [63]. Importantly, the combination of LV concentric hypertrophy with a decreased LV cavity volume are associated with diastolic dysfunction, the hallmark of heart failure with preserved ejection fraction (HFpEF) [64].

Finally, at the electrophysiological level, the calcification of the cardiac skeleton results in electrical conduction delay, which causes increased incidence of atrial and ventricular arrhythmias with age at rest and during exercise [65].

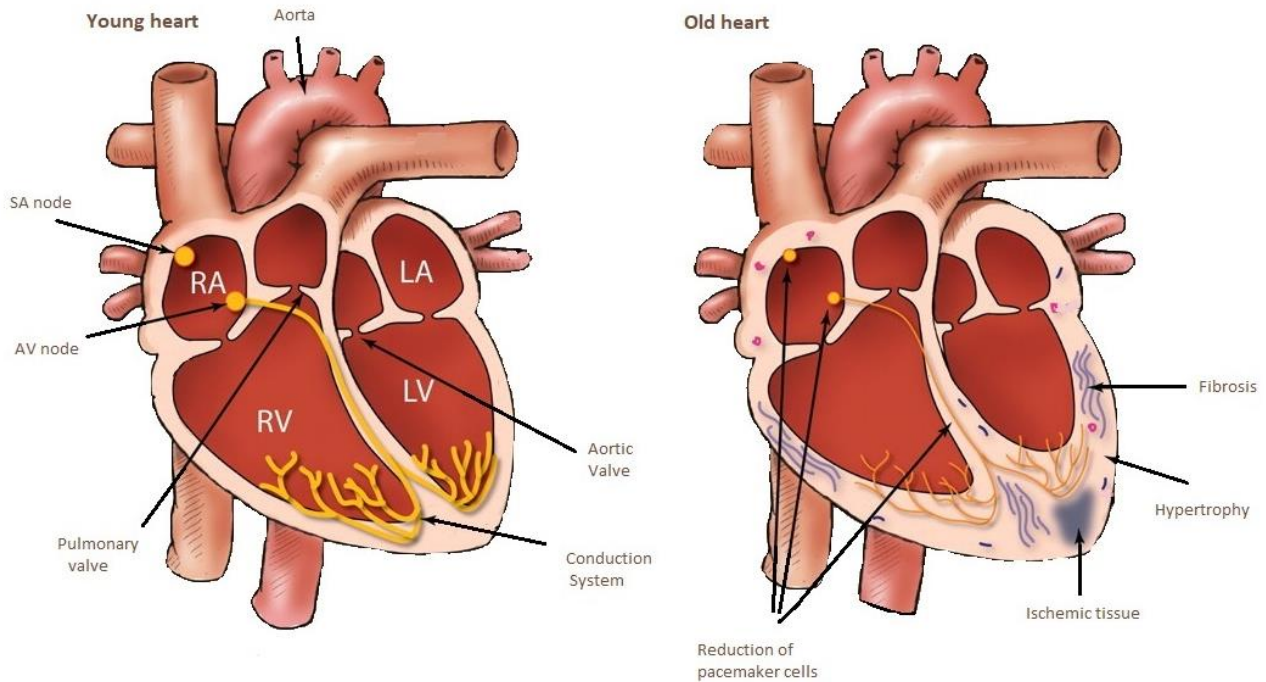


Figure 1.3:6 Cardiac ageing. Adapted from [4] and reproduced with permission.

1.3.4 Cardiac and Hemodynamic Monitoring

Arguably, accurate assessment and monitoring of the relevant hemodynamic indices are crucial to the investigation of cardiovascular ageing. Hemodynamic parameters and cardiac biomarkers are valuable in clinical practice as they offer insight on cardiovascular health and act as prognostic tools of cardiovascular risk. Established monitoring methods are, however, frequently invasive and not always sensitive enough to detect differences between different age groups [66]. Accordingly, there is increasing interest in providing clinicians with noninvasive, precise and fast tools to assess and preserve cardiovascular health [67].

Central hemodynamics. Several noninvasive monitoring methods are proposed for the derivation of proximal hemodynamics, typically revolving around aortic pressure estimation. Central pressure derivation usually entails measurement of the radial artery pulse with applanation tonometry, calibration against brachial sphygmomanometric pressure [68]–[71] and use of either a generalized transfer function [72]–[74], a waveform feature [75], or a mathematical moving average model [76]. Most of these methods have succeeded in providing a statistical relation between the waveforms at these two arterial sites, lacking, however, a physiological basis [72], [77].

Cardiac contractility. Global LV systolic function is indirectly assessed in clinical routine by echocardiography, focusing on indications such as cardiac output (CO), LV volumes and particularly the ejection fraction (EF), defined as the ratio of stroke volume (SV) over the end-diastolic volume [78]. Despite its popularity, EF is in fact limited in offering a complete characterization of the cardiac inotropic state [79] as it is preload- and afterload-dependent. The gold standard method for assessing LV systolic function to date is the invasive measurement of LV pressure-volume (P-V) loops under varying load conditions, from which the end-systolic pressure-volume relation (ESPVR) can be calculated [80], [81] (Figure 1.3 :7). Suga et al. [81] found this relation to be fairly linear within physiologic ranges. The ESPVR is described by its slope, i.e., the end-systolic elastance E_{es} , and its volume axis intercept, i.e., the dead volume V_d , and has been proven less load sensitive than other indices of ventricular contractility [82]. For an increased E_{es} , the ventricle is able to eject more blood volume against the same afterload, which is indicative of increased contractility [81].

Despite the importance of E_{es} for the characterization of cardiac systolic performance, its bedside use is not established due to the invasive and expensive nature of the P-V loop measurement. To overcome this limitation, investigators have focused their attention on developing novel noninvasive methods to derive E_{es} [83]–[85]. Such methods are based on simple single-beat measurements, i.e.,

without loading interventions, and include among others peripheral arm-cuff pressure, echo-derived ventricular volume and cardiac output. The methodology of Chen et al. [83] is particularly acknowledged in this field of research.

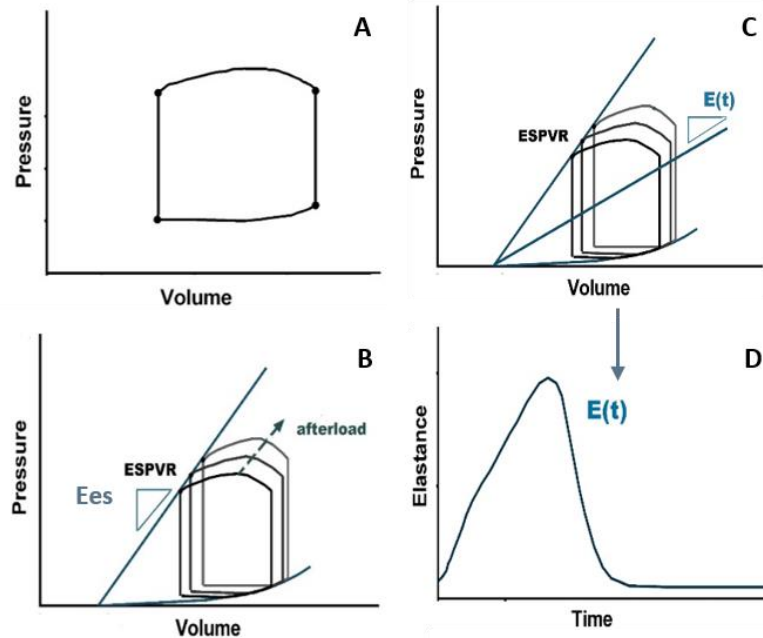


Figure 1.3:7 The end-systolic pressure-volume relation as an index of cardiac systolic function. (A) The LV P-V loop. (B) The LV P-V loop under afterload manipulation and the derivation of the ESPVR. (C) The instantaneous elastance as pressure over volume ratio. (D) The time-varying elastance function.

1.3.5 *In vivo* Assessment of Aortic Compliance

An important aspect of cardiovascular health monitoring is the ability to estimate aortic stiffness. Aortic stiffening plays an important role in the development of CVD and its use is recommended in guidelines in order to improve cardiovascular risk stratification [25], [86]. For that purpose, several invasive and noninvasive methods have been described [87]. Some depend on the assessment of the ratio between lumen volumetric changes and pulse pressure, $\Delta V/PP$. This index can be assessed noninvasively by combination of MR Angiography and sphygmomanometry. Under the assumption of only radial deformation, compliance measurement can also be simplified to local area changes over pulse pressure, called the cross-sectional area compliance, $\Delta A/PP$. Local area compliance is extensively used in the literature for purpose of investigating effects of ageing [88], [89], training [88] and different pathologies [88], [90]–[92] on the ascending aortic distensibility. A major limitation of this technique is that it does not take into account the longitudinal deformation of the vessel, which might be important in the case of the ascending aorta. Additionally, these indices of aortic stiffness rely on precise aortic blood pressure measurement.

The most widely used and validated techniques for assessing aortic stiffness involve PWV assessment [87]. The gold standard method for measuring pulse wave velocity is catheterization; however, its application is limited to specific populations and clinical settings. Global indices of PWV are often derived using tonometry, whereby the pressure waveforms at two distinct locations (commonly the carotid-femoral or carotid-radial arteries) are measured. The pressure signals are processed to acquire the time delay, called the pulse transit time (PTT), and PWV is calculated as ratio of the distance between the measuring sites over the PTT (Figure 1.3:8).

Carotid-to-Femoral Tonometry

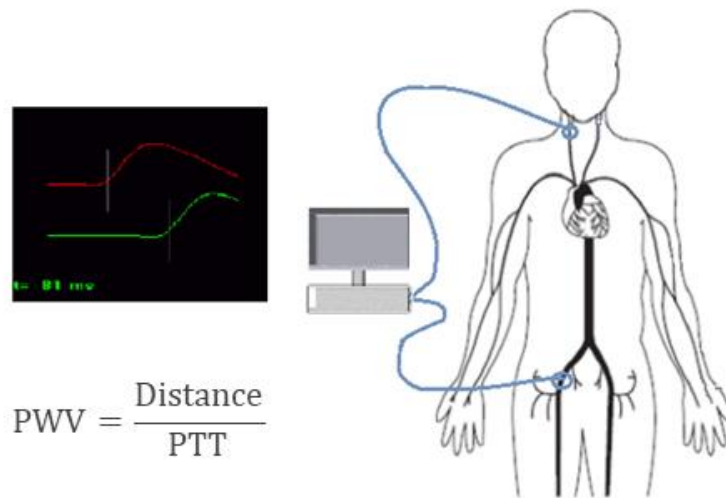


Figure 1.3:8 Carotid-to-femoral tonometry for derivation of PWV.

As ageing affects predominantly the elasticity of the proximal aorta, there is increasing interest towards techniques that offer more detailed insight into the regional aortic PWV. Typically, this is achieved by acquiring aortic blood flow curves using two-dimensional (2D) phase contrast (PC) MRI acquisitions with through-plane velocity encoding [93], [94]. 2D PC MRI can achieve high temporal and spatial resolution, which is vital for the correct identification of the PTT [95], and, therefore, is widely used in the literature. Of note, PWV measurement with this technique requires combination of blood flow data with MR Angiography in order to obtain the distance between the flow signals.

The latest advances in MR technology have made possible the time-resolved imaging of blood flow in the 3 spatial dimensions, a technique called 4D Flow MRI [96]. 4D Flow MRI allows for the volumetric, functional coverage of the entire aorta and the calculation of any arbitrary direction of flow and distance. Accordingly, the potential of using 4D Flow MRI to acquire regional aortic PWV has garnered increasing scientific attention and is currently the subject of intense investigation [97].

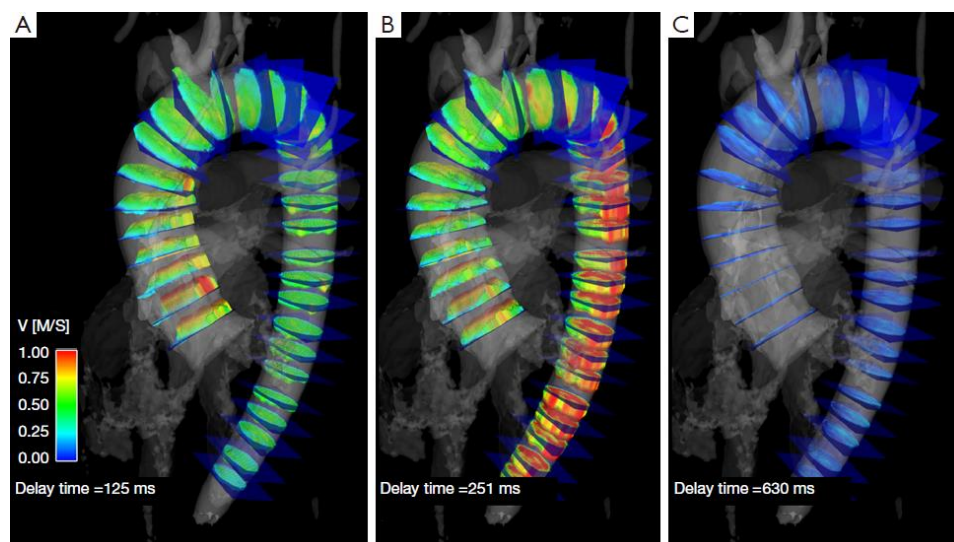


Figure 1.3:9 Example of aortic flow data acquired with 4D Flow MRI for PWV measurement. Reproduced from [98] with permission.

1.3.6 Mathematical Models of the Cardiovascular System

Mathematical modeling of the cardiovascular system is a valuable tool that can be used to investigate patient-specific aspects of aortic hemodynamics, which are difficult to assess *in vivo*. Numerical modeling can contribute in this aspect thanks to advances in imaging technology, which allow for the extraction of high-definition, person-specific data. Particularly, 1D models of the vasculature are regarded as a reliable and convenient tool for investigating wave transmission phenomena in the cardiovascular system, whereas 0D models of the contractility of the heart (time-varying elastance) have already been used to simulate physiological as well as pathological conditions. 3D analysis of fluid dynamics, structural mechanics or even the combination of both in fluid-structure interaction frameworks can be used to investigate more complex hemodynamic phenomena that cannot be captured in one dimension. Although these techniques are still limited by their considerable computational burden, advances in automated meshing and computation parallelization might promote their popularity in the future.

In this dissertation, we extensively used a mathematical model of systemic circulation, which was previously developed and validated in our laboratory [99]–[101] and has since received great recognition by the scientific community.

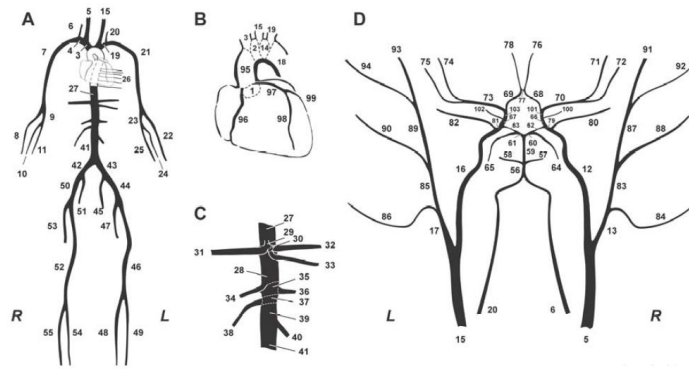


Figure 1.3:10 Schematic representation of the arterial tree developed by Reymond et al. [99] consisting of (A) 55 main arteries of the systemic circulation, (B) the circulation in the coronaries, (C) the principal abdominal aortic branches, and (D) the circle of Willis. Reproduced from Reymond et al. [99] with permission.

This computational framework comprises a detailed 1D wave propagation model of the systemic arterial tree (103 vessels), including 55 systemic arteries, the circle of Willis and the coronary circulation. Blood pressure and flow waveforms are obtained throughout the vasculature through numerical integration of the 1D form of the Navier-Stokes equations. The mass and momentum conservation equations are coupled with a constitutive relation that describes arterial wall elasticity. The arterial wall model includes a viscoelastic response as in Holenstein et al. [102] and a nonlinear elastic response that relates local lumen area to location and distending pressure. Dependency of wall elasticity on distending pressure is described by Langewouters et al. [103] and assumed to have the same functional form in all arterial locations. Pulsatility effects are included using the Witzig Womersley theory [104]. In order to include the effect of distal vessels of the arterial tree, 3-element Windkessel models are coupled to the terminal arterial segments. The 1D model of the arterial tree is coupled with a 0D time-varying elastance model for the LV contractility, which assumes a linear LV P-V relation at each time point and is mathematically expressed as a double hill function of time.

The generic 1D model was thoroughly validated by Reymond et al. [99]. A patient-specific model variant was further validated with *in vivo* measurements and was found capable of faithfully reproducing the flow and pressure waveform characteristics [100].

The importance and utility of this model in the context of the present thesis was multifold. The model was used in order to investigate pathophysiological mechanisms, as well as to simulate the effect of interventions. Additionally, it constituted the foundation for the design, development, testing and validation of novel techniques for noninvasive cardiac and hemodynamic monitoring techniques. This entails both the generation of a virtual patient database that can be used to evaluate the performance of monitoring methods, as well as the personalization of the model itself in order to obtain cardiovascular parameters of interest.

1.4 Bibliography

- [1] United Nations, Department of Economic and Social Affairs, and Population Division, *World population ageing, 2019 highlights*. 2020.
- [2] World Health Organization, "Cardiovascular diseases." <https://www.who.int/westernpacific/health-topics/cardiovascular-diseases> (accessed Jun. 30, 2020).
- [3] Mozaffarian Dariush *et al.*, "Executive Summary: Heart Disease and Stroke Statistics—2016 Update," *Circulation*, vol. 133, no. 4, pp. 447–454, Jan. 2016, doi: 10.1161/CIR.0000000000000366.
- [4] B. J. North and D. A. Sinclair, "The Intersection Between Aging and Cardiovascular Disease," *Circ. Res.*, vol. 110, no. 8, pp. 1097–1108, Apr. 2012, doi: 10.1161/CIRCRESAHA.111.246876.
- [5] V. L. Feigin *et al.*, "Global burden of stroke and risk factors in 188 countries, during 1990–2013: a systematic analysis for the Global Burden of Disease Study 2013," *Lancet Neurol.*, vol. 15, no. 9, pp. 913–924, Aug. 2016, doi: 10.1016/S1474-4422(16)30073-4.
- [6] M. F. O'Rourke and J. Hashimoto, "Mechanical factors in arterial aging: a clinical perspective," *J. Am. Coll. Cardiol.*, vol. 50, no. 1, pp. 1–13, Jul. 2007, doi: 10.1016/j.jacc.2006.12.050.
- [7] J. E. WAGENSEIL and R. P. MECHAM, "Vascular Extracellular Matrix and Arterial Mechanics," *Physiol. Rev.*, vol. 89, no. 3, pp. 957–989, Jul. 2009, doi: 10.1152/physrev.00041.2008.
- [8] C. M. McEniery *et al.*, "Normal vascular aging: differential effects on wave reflection and aortic pulse wave velocity: the Anglo-Cardiff Collaborative Trial (ACCT)," *J. Am. Coll. Cardiol.*, vol. 46, no. 9, pp. 1753–1760, Nov. 2005, doi: 10.1016/j.jacc.2005.07.037.
- [9] J. Gordon Betts *et al.*, "Blood Flow, Blood Pressure and Resistance," in *Anatomy and Physiology*, OpenStax, 2013.
- [10] J. Mayet and A. Hughes, "Cardiac and vascular pathophysiology in hypertension," *Heart*, vol. 89, no. 9, pp. 1104–1109, Sep. 2003.
- [11] N. Westerhof, N. Stergiopulos, M. I. M. Noble, and B. E. Westerhof, *Snapshots of Hemodynamics: An Aid for Clinical Research and Graduate Education*. Springer, 2018.
- [12] N. Westerhof, P. Sipkema, G. C. van den Bos, and G. Elzinga, "Forward and backward waves in the arterial system," *Cardiovasc. Res.*, vol. 6, no. 6, pp. 648–656, Nov. 1972.
- [13] G. M. London, "The concept of ventricular/vascular coupling: functional and structural alterations of the heart and arterial vessels go in parallel," *Nephrol. Dial. Transplant.*, vol. 13, no. 2, pp. 250–253, Feb. 1998, doi: 10.1093/oxfordjournals.ndt.a027813.
- [14] I. Ikonomidis *et al.*, "The role of ventricular–arterial coupling in cardiac disease and heart failure: assessment, clinical implications and therapeutic interventions. A consensus document of the European Society of Cardiology Working Group on Aorta & Peripheral Vascular Diseases, European Association of Cardiovascular Imaging, and Heart Failure Association," *Eur. J. Heart Fail.*, vol. 21, no. 4, pp. 402–424, 2019, doi: 10.1002/ehf.1436.
- [15] G. Jackson, C. R. Gibbs, M. K. Davies, and G. Y. H. Lip, "Pathophysiology," *BMJ*, vol. 320, no. 7228, pp. 167–170, Jan. 2000.
- [16] R. B. Devereux, T. G. Pickering, M. H. Alderman, S. Chien, J. S. Borer, and J. H. Laragh, "Left ventricular hypertrophy in hypertension. Prevalence and relationship to pathophysiologic variables," *Hypertens. Dallas Tex* 1979, vol. 9, no. 2 Pt 2, pp. II53–60, Feb. 1987, doi: 10.1161/01.hyp.9.2_pt_2.ii53.
- [17] C. V. Ioannou *et al.*, "Left Ventricular Hypertrophy Induced by Reduced Aortic Compliance," *J. Vasc. Res.*, vol. 46, no. 5, pp. 417–425, 2009, doi: 10.1159/000194272.
- [18] W. S. Aronow, "Hypertension and left ventricular hypertrophy," *Ann. Transl. Med.*, vol. 5, no. 15, Aug. 2017, doi: 10.21037/atm.2017.06.14.
- [19] G. G. Schiattarella and J. A. Hill, "Inhibition of Hypertrophy Is a Good Therapeutic Strategy in Ventricular Pressure Overload," *Circulation*, vol. 131, no. 16, pp. 1435–1447, Apr. 2015, doi: 10.1161/CIRCULATIONAHA.115.013894.
- [20] W. Nadruz, "Myocardial remodeling in hypertension," *J. Hum. Hypertens.*, vol. 29, no. 1, pp. 1–6, Jan. 2015, doi: 10.1038/jhh.2014.36.
- [21] J. B. Strait and E. G. Lakatta, "Aging-associated cardiovascular changes and their relationship to heart failure," *Heart Fail. Clin.*, vol. 8, no. 1, pp. 143–164, Jan. 2012, doi: 10.1016/j.hfc.2011.08.011.
- [22] U. Quinn, L. A. Tomlinson, and J. R. Cockcroft, "Arterial stiffness," *JRSM Cardiovasc. Dis.*, vol. 1, no. 6, Sep. 2012, doi: 10.1258/cvd.2012.012024.
- [23] M. F. O'Rourke, "Arterial aging: pathophysiological principles," *Vasc. Med.*, vol. 12, no. 4, pp. 329–341, Nov. 2007, doi: 10.1177/1358863X07083392.

- [24] O. Fritze *et al.*, "Age-related changes in the elastic tissue of the human aorta," *J. Vasc. Res.*, vol. 49, no. 1, pp. 77–86, 2012, doi: 10.1159/000331278.
- [25] L. de R. Mikael *et al.*, "Vascular Aging and Arterial Stiffness," *Arq. Bras. Cardiol.*, vol. 109, no. 3, pp. 253–258, Sep. 2017, doi: 10.5935/abc.20170091.
- [26] D. S. Celermajer, K. E. Sorensen, D. J. Spiegelhalter, D. Georgakopoulos, J. Robinson, and J. E. Deanfield, "Aging is associated with endothelial dysfunction in healthy men years before the age-related decline in women," *J. Am. Coll. Cardiol.*, vol. 24, no. 2, pp. 471–476, Aug. 1994, doi: 10.1016/0735-1097(94)90305-0.
- [27] M. A. Black, N. T. Cable, D. H. J. Thijssen, and D. J. Green, "Impact of age, sex, and exercise on brachial artery flow-mediated dilatation," *Am. J. Physiol. - Heart Circ. Physiol.*, vol. 297, no. 3, pp. H1109–H1116, Sep. 2009, doi: 10.1152/ajpheart.00226.2009.
- [28] D. H. J. Thijssen *et al.*, "Assessment of flow-mediated dilation in humans: a methodological and physiological guideline," *Am. J. Physiol. - Heart Circ. Physiol.*, vol. 300, no. 1, pp. H2–H12, Jan. 2011, doi: 10.1152/ajpheart.00471.2010.
- [29] K.-H. Park and W. J. Park, "Endothelial Dysfunction: Clinical Implications in Cardiovascular Disease and Therapeutic Approaches," *J. Korean Med. Sci.*, vol. 30, no. 9, pp. 1213–1225, Sep. 2015, doi: 10.3346/jkms.2015.30.9.1213.
- [30] Z. Sun, "Aging, Arterial Stiffness and Hypertension," *Hypertension*, vol. 65, no. 2, pp. 252–256, Feb. 2015, doi: 10.1161/HYPERTENSIONAHA.114.03617.
- [31] S. Homma, N. Hirose, H. Ishida, T. Ishii, and G. Araki, "Carotid plaque and intima-media thickness assessed by b-mode ultrasonography in subjects ranging from young adults to centenarians," *Stroke*, vol. 32, no. 4, pp. 830–835, Apr. 2001, doi: 10.1161/01.str.32.4.830.
- [32] I. C. L. van den Munckhof *et al.*, "Relation between age and carotid artery intima-medial thickness: a systematic review," *Clin. Cardiol.*, vol. 41, no. 5, pp. 698–704, May 2018, doi: 10.1002/clc.22934.
- [33] Y. Ohyama, A. Redheui, N. Kachenoura, B. A. Venkatesh, and J. A. C. Lima, "Imaging Insights on the Aorta in Aging," *Circ. Cardiovasc. Imaging*, vol. 11, no. 4, p. e005617, Apr. 2018, doi: 10.1161/CIRCIMAGING.117.005617.
- [34] J. Sugawara, K. Hayashi, T. Yokoi, and H. Tanaka, "Age-associated elongation of the ascending aorta in adults," *JACC Cardiovasc. Imaging*, vol. 1, no. 6, pp. 739–748, Nov. 2008, doi: 10.1016/j.jcmg.2008.06.010.
- [35] A. Redheuil *et al.*, "Reduced ascending aortic strain and distensibility: earliest manifestations of vascular aging in humans," *Hypertens. Dallas Tex 1979*, vol. 55, no. 2, pp. 319–326, Feb. 2010, doi: 10.1161/HYPERTENSIONAHA.109.141275.
- [36] C. V. Ioannou *et al.*, "Hemodynamics induced after acute reduction of proximal thoracic aorta compliance," *Eur. J. Vasc. Endovasc. Surg. Off. J. Eur. Soc. Vasc. Surg.*, vol. 26, no. 2, pp. 195–204, Aug. 2003.
- [37] V. Taviani *et al.*, "Age-related changes of regional pulse wave velocity in the descending aorta using Fourier velocity encoded M-mode," *Magn. Reson. Med.*, vol. 65, no. 1, pp. 261–268, 2011, doi: 10.1002/mrm.22590.
- [38] S. S. Hickson *et al.*, "The relationship of age with regional aortic stiffness and diameter," *JACC Cardiovasc. Imaging*, vol. 3, no. 12, pp. 1247–1255, Dec. 2010, doi: 10.1016/j.jcmg.2010.09.016.
- [39] N. A. Shirwany and M. Zou, "Arterial stiffness: a brief review," *Acta Pharmacol. Sin.*, vol. 31, no. 10, pp. 1267–1276, Oct. 2010, doi: 10.1038/aps.2010.123.
- [40] E. Kimoto *et al.*, "Preferential stiffening of central over peripheral arteries in type 2 diabetes," *Diabetes*, vol. 52, no. 2, pp. 448–452, Feb. 2003.
- [41] P. Boutouyrie, S. Laurent, A. Benetos, X. J. Girerd, A. P. Hoeks, and M. E. Safar, "Opposing effects of ageing on distal and proximal large arteries in hypertensives," *J. Hypertens. Suppl. Off. J. Int. Soc. Hypertens.*, vol. 10, no. 6, pp. S87–91, Aug. 1992.
- [42] E. Kimoto *et al.*, "Preferential stiffening of central over peripheral arteries in type 2 diabetes," *Diabetes*, vol. 52, no. 2, pp. 448–452, Feb. 2003.
- [43] J. A. Chirinos, "Ventricular–arterial coupling: Invasive and non-invasive assessment," *Artery Res.*, vol. 7, no. 1, Mar. 2013, doi: 10.1016/j.artres.2012.12.002.
- [44] T. Weber and J. A. Chirinos, "Pulsatile arterial haemodynamics in heart failure," *Eur. Heart J.*, vol. 39, no. 43, pp. 3847–3854, Nov. 2018, doi: 10.1093/eurheartj/ehy346.
- [45] J. A. Chirinos *et al.*, "Late Systolic Myocardial Loading Is Associated With Left Atrial Dysfunction in Hypertension," *Circ. Cardiovasc. Imaging*, vol. 10, no. 6, p. e006023, Jun. 2017, doi: 10.1161/CIRCIMAGING.116.006023.
- [46] G. W. Yip, J. W. H. Fung, Y.-T. Tan, and J. E. Sanderson, "Hypertension and heart failure: a dysfunction of systole, diastole or both?," *J. Hum. Hypertens.*, vol. 23, no. 5, Art. no. 5, May 2009, doi: 10.1038/jhh.2008.141.
- [47] S. S. Franklin *et al.*, "Hemodynamic patterns of age-related changes in blood pressure. The Framingham Heart Study," *Circulation*, vol. 96, no. 1, pp. 308–315, Jul. 1997.
- [48] C. M. McEniery *et al.*, "Central pressure: variability and impact of cardiovascular risk factors: the Anglo-Cardiff Collaborative Trial II," *Hypertens. Dallas Tex 1979*, vol. 51, no. 6, pp. 1476–1482, Jun. 2008, doi: 10.1161/HYPERTENSIONAHA.107.105445.

- [49] J. W. McEvoy *et al.*, "Diastolic blood pressure, subclinical myocardial damage, and cardiac events: Implications for blood pressure control," *J. Am. Coll. Cardiol.*, vol. 68, no. 16, pp. 1713–1722, Oct. 2016, doi: 10.1016/j.jacc.2016.07.754.
- [50] C.-P. Chung, H.-Y. Lee, P.-C. Lin, and P.-N. Wang, "Cerebral Artery Pulsatility is Associated with Cognitive Impairment and Predicts Dementia in Individuals with Subjective Memory Decline or Mild Cognitive Impairment," *J. Alzheimers Dis. JAD*, vol. 60, no. 2, pp. 625–632, 2017, doi: 10.3233/JAD-170349.
- [51] G. F. Mitchell *et al.*, "Arterial stiffness, pressure and flow pulsatility and brain structure and function: the Age, Gene/Environment Susceptibility--Reykjavik study," *Brain J. Neurol.*, vol. 134, no. Pt 11, pp. 3398–3407, Nov. 2011, doi: 10.1093/brain/awr253.
- [52] A. Benetos, "Pulse pressure and cardiovascular risk," *J. Hypertens. Suppl. Off. J. Int. Soc. Hypertens.*, vol. 17, no. 5, pp. S21–24, Dec. 1999.
- [53] M. F. O'Rourke and W. W. Nichols, "Changes in Wave Reflection With Advancing Age in Normal Subjects," *Hypertension*, vol. 44, no. 6, pp. E10–E11, Dec. 2004, doi: 10.1161/01.HYP.0000146403.99648.c6.
- [54] M. F. O'Rourke and W. W. Nichols, "Aortic Diameter, Aortic Stiffness, and Wave Reflection Increase With Age and Isolated Systolic Hypertension," *Hypertension*, vol. 45, no. 4, pp. 652–658, Apr. 2005, doi: 10.1161/01.HYP.0000153793.84859.b8.
- [55] G. F. Mitchell *et al.*, "Changes in arterial stiffness and wave reflection with advancing age in healthy men and women: the Framingham Heart Study," *Hypertens. Dallas Tex 1979*, vol. 43, no. 6, pp. 1239–1245, Jun. 2004, doi: 10.1161/01.HYP.0000128420.01881.aa.
- [56] A. U. Ferrari, A. Radaelli, and M. Centola, "Invited Review: Aging and the cardiovascular system," *J. Appl. Physiol.*, vol. 95, no. 6, pp. 2591–2597, Dec. 2003, doi: 10.1152/jappphysiol.00601.2003.
- [57] C. A. Meschiari, O. K. Ero, H. Pan, T. Finkel, and M. L. Lindsey, "The impact of aging on cardiac extracellular matrix," *GeroScience*, vol. 39, no. 1, pp. 7–18, Feb. 2017, doi: 10.1007/s11357-017-9959-9.
- [58] M. A. Horn and A. W. Trafford, "Aging and the cardiac collagen matrix: Novel mediators of fibrotic remodelling," *J. Mol. Cell. Cardiol.*, vol. 93, pp. 175–185, Apr. 2016, doi: 10.1016/j.yjmcc.2015.11.005.
- [59] Querejeta Ramón *et al.*, "Increased Collagen Type I Synthesis in Patients With Heart Failure of Hypertensive Origin," *Circulation*, vol. 110, no. 10, pp. 1263–1268, Sep. 2004, doi: 10.1161/01.CIR.0000140973.60992.9A.
- [60] M. Reardon and M. Malik, "Changes in heart rate variability with age," *Pacing Clin. Electrophysiol. PACE*, vol. 19, no. 11 Pt 2, pp. 1863–1866, Nov. 1996.
- [61] D. U. Akasheva *et al.*, "Age-Related Left Ventricular Changes and Their Association with Leukocyte Telomere Length in Healthy People," *PLoS ONE*, vol. 10, no. 8, Aug. 2015, doi: 10.1371/journal.pone.0135883.
- [62] B. Grüner Sveälv, G. Fritzon, and B. Andersson, "Gender and age related differences in left ventricular function and geometry with focus on the long axis," *Eur. J. Echocardiogr.*, vol. 7, no. 4, pp. 298–307, Aug. 2006, doi: 10.1016/j.euje.2005.06.008.
- [63] Cheng Susan, Fernandes Verônica R.S., Bluemke David A., McClelland Robyn L., Kronmal Richard A., and Lima João A.C., "Age-Related Left Ventricular Remodeling and Associated Risk for Cardiovascular Outcomes," *Circ. Cardiovasc. Imaging*, vol. 2, no. 3, pp. 191–198, May 2009, doi: 10.1161/CIRCIMAGING.108.819938.
- [64] A. M. Katz and E. L. Rolett, "Heart failure: when form fails to follow function," *Eur. Heart J.*, vol. 37, no. 5, pp. 449–454, Feb. 2016, doi: 10.1093/eurheartj/ehv548.
- [65] N. S. V. Singam, C. Fine, and J. L. Fleg, "Cardiac changes associated with vascular aging," *Clin. Cardiol.*, vol. 43, no. 2, pp. 92–98, 2020, doi: 10.1002/clc.23313.
- [66] K. E. Covinsky *et al.*, "Loss of independence in activities of daily living in older adults hospitalized with medical illnesses: increased vulnerability with age," *J. Am. Geriatr. Soc.*, vol. 51, no. 4, pp. 451–458, Apr. 2003.
- [67] J.-L. Vincent *et al.*, "Clinical review: Update on hemodynamic monitoring - a consensus of 16," *Crit. Care*, vol. 15, no. 4, p. 229, 2011, doi: 10.1186/cc10291.
- [68] M. J. Roman *et al.*, "Central pressure more strongly relates to vascular disease and outcome than does brachial pressure: the Strong Heart Study," *Hypertens. Dallas Tex 1979*, vol. 50, no. 1, pp. 197–203, Jul. 2007, doi: 10.1161/HYPERTENSIONAHA.107.089078.
- [69] M. E. Safar *et al.*, "Central pulse pressure and mortality in end-stage renal disease," *Hypertens. Dallas Tex 1979*, vol. 39, no. 3, pp. 735–738, Mar. 2002.
- [70] R. Pini *et al.*, "Central but not brachial blood pressure predicts cardiovascular events in an unselected geriatric population: the ICARE Dicomano Study," *J. Am. Coll. Cardiol.*, vol. 51, no. 25, pp. 2432–2439, Jun. 2008, doi: 10.1016/j.jacc.2008.03.031.
- [71] P. Jankowski *et al.*, "Pulsatile but not steady component of blood pressure predicts cardiovascular events in coronary patients," *Hypertens. Dallas Tex 1979*, vol. 51, no. 4, pp. 848–855, Apr. 2008, doi: 10.1161/HYPERTENSIONAHA.107.101725.
- [72] C. H. Chen *et al.*, "Estimation of central aortic pressure waveform by mathematical transformation of radial tonometry pressure. Validation of generalized transfer function," *Circulation*, vol. 95, no. 7, pp. 1827–1836, Apr. 1997.

- [73] M. Karamanoglu, M. F. O'Rourke, A. P. Avolio, and R. P. Kelly, "An analysis of the relationship between central aortic and peripheral upper limb pressure waves in man," *Eur. Heart J.*, vol. 14, no. 2, pp. 160–167, Feb. 1993.
- [74] D. B. McCombie, A. T. Reisner, and H. H. Asada, "Laguerre-model blind system identification: cardiovascular dynamics estimated from multiple peripheral circulatory signals," *IEEE Trans. Biomed. Eng.*, vol. 52, no. 11, pp. 1889–1901, Nov. 2005, doi: 10.1109/TBME.2005.856260.
- [75] K. Takazawa, N. Tanaka, K. Takeda, F. Kurosu, and C. Ibukiyama, "Underestimation of vasodilator effects of nitroglycerin by upper limb blood pressure," *Hypertens. Dallas Tex* 1979, vol. 26, no. 3, pp. 520–523, Sep. 1995.
- [76] B. Williams, P. S. Lacy, P. Yan, C.-N. Hwee, C. Liang, and C.-M. Ting, "Development and validation of a novel method to derive central aortic systolic pressure from the radial pressure waveform using an n-point moving average method," *J. Am. Coll. Cardiol.*, vol. 57, no. 8, pp. 951–961, Feb. 2011, doi: 10.1016/j.jacc.2010.09.054.
- [77] G. Swamy and R. Mukkamala, "Estimation of the aortic pressure waveform and beat-to-beat relative cardiac output changes from multiple peripheral artery pressure waveforms," *IEEE Trans. Biomed. Eng.*, vol. 55, no. 5, pp. 1521–1529, May 2008, doi: 10.1109/TBME.2007.913408.
- [78] S. Chengode, "Left ventricular global systolic function assessment by echocardiography," *Ann. Card. Anaesth.*, vol. 19, no. Suppl 1, pp. S26–S34, Oct. 2016, doi: 10.4103/0971-9784.192617.
- [79] M. A. Konstam and F. M. Abboud, "Ejection Fraction: Misunderstood and Over-rated (Changing the Paradigm in Categorizing Heart Failure)," *Circulation*, vol. 135, no. 8, pp. 717–719, Feb. 2017, doi: 10.1161/CIRCULATIONAHA.116.025795.
- [80] K. Sagawa, H. Suga, A. A. Shoukas, and K. M. Bakalar, "End-systolic pressure/volume ratio: a new index of ventricular contractility," *Am. J. Cardiol.*, vol. 40, no. 5, pp. 748–753, Nov. 1977.
- [81] H. Suga and K. Sagawa, "Instantaneous pressure-volume relationships and their ratio in the excised, supported canine left ventricle," *Circ. Res.*, vol. 35, no. 1, pp. 117–126, Jul. 1974.
- [82] H. W. Paley, I. G. McDonald, J. Blumenthal, and J. Mailhot, "The effects of posture and isoproterenol on the velocity of left ventricular contraction in man. The reciprocal relationship between left ventricular volume and myocardial wall force during ejection on mean rate of circumferential shortening," *J. Clin. Invest.*, vol. 50, no. 11, pp. 2283–2294, Nov. 1971, doi: 10.1172/JCI106726.
- [83] C.-H. Chen *et al.*, "Noninvasive single-beat determination of left ventricular end-systolic elastance in humans," *J. Am. Coll. Cardiol.*, vol. 38, no. 7, pp. 2028–2034, Dec. 2001, doi: 10.1016/S0735-1097(01)01651-5.
- [84] B. Bonnet, F. Jourdan, G. du Cailar, and P. Fesler, "Noninvasive evaluation of left ventricular elastance according to pressure-volume curves modeling in arterial hypertension," *Am. J. Physiol. Heart Circ. Physiol.*, vol. 313, no. 2, pp. H237–H243, Aug. 2017, doi: 10.1152/ajpheart.00086.2017.
- [85] T. Shishido, K. Hayashi, K. Shigemitsu, T. Sato, M. Sugimachi, and K. Sunagawa, "Single-Beat Estimation of End-Systolic Elastance Using Bilinearly Approximated Time-Varying Elastance Curve," *Circulation*, vol. 102, no. 16, pp. 1983–1989, Oct. 2000, doi: 10.1161/01.CIR.102.16.1983.
- [86] S. Laurent *et al.*, "Expert consensus document on arterial stiffness: methodological issues and clinical applications," *Eur. Heart J.*, vol. 27, no. 21, pp. 2588–2605, Nov. 2006, doi: 10.1093/eurheartj/ehl254.
- [87] R. R. Townsend, "Arterial Stiffness: Recommendations and Standardization," *Pulse*, vol. 4, no. Suppl 1, pp. 3–7, Jan. 2017, doi: 10.1159/000448454.
- [88] R. H. Mohiaddin *et al.*, "Regional aortic compliance studied by magnetic resonance imaging: the effects of age, training, and coronary artery disease," *Heart*, vol. 62, no. 2, pp. 90–96, Aug. 1989, doi: 10.1136/hrt.62.2.90.
- [89] D. A. Duprez, C. Swingen, R. Sih, T. Lefebvre, D. R. Kaiser, and M. Jerosch-Herold, "Heterogeneous remodelling of the ascending and descending aorta with age," *J. Hum. Hypertens.*, vol. 21, no. 8, pp. 689–691, Aug. 2007, doi: 10.1038/sj.jhh.1002216.
- [90] Resnick Lawrence M., Militianu Daniela, Cunnings Amy J., Pipe James G., Evelhoch Jeffrey L., and Soulen Renate L., "Direct Magnetic Resonance Determination of Aortic Distensibility in Essential Hypertension," *Hypertension*, vol. 30, no. 3, pp. 654–659, Sep. 1997, doi: 10.1161/01.HYP.30.3.654.
- [91] A. Lalande *et al.*, "Compliance and pulse wave velocity assessed by MRI detect early aortic impairment in young patients with mutation of the smooth muscle myosin heavy chain," *J. Magn. Reson. Imaging JMRI*, vol. 28, no. 5, pp. 1180–1187, Nov. 2008, doi: 10.1002/jmri.21565.
- [92] S. Soljanlahti, T. Autti, L. Hyttinen, A. F. Vuorio, P. Keto, and K. Lauerma, "Compliance of the aorta in two diseases affecting vascular elasticity, familial hypercholesterolemia and diabetes: a MRI study," *Vasc. Health Risk Manag.*, vol. 4, no. 5, pp. 1103–1109, Oct. 2008.
- [93] R. H. Mohiaddin *et al.*, "Regional aortic compliance studied by magnetic resonance imaging: the effects of age, training, and coronary artery disease," *Heart*, vol. 62, no. 2, pp. 90–96, Aug. 1989, doi: 10.1136/hrt.62.2.90.

-
- [94] J. M. Boese, M. Bock, S. O. Schoenberg, and L. R. Schad, "Estimation of aortic compliance using magnetic resonance pulse wave velocity measurement," *Phys. Med. Biol.*, vol. 45, no. 6, pp. 1703–1713, Jun. 2000, doi: 10.1088/0031-9155/45/6/320.
 - [95] B. D. Bolster, E. Atalar, C. J. Hardy, and E. R. McVeigh, "Accuracy of Arterial Pulse-Wave Velocity Measurement Using MR," *J. Magn. Reson. Imaging JMRI*, vol. 8, no. 4, pp. 878–888, 1998.
 - [96] P. Dyverfeldt *et al.*, "4D flow cardiovascular magnetic resonance consensus statement," *J. Cardiovasc. Magn. Reson. Off. J. Soc. Cardiovasc. Magn. Reson.*, vol. 17, p. 72, Aug. 2015, doi: 10.1186/s12968-015-0174-5.
 - [97] P. Dyverfeldt, T. Ebbers, and T. L  nne, "Pulse wave velocity with 4D flow MRI: systematic differences and age-related regional vascular stiffness," *Magn. Reson. Imaging*, vol. 32, no. 10, pp. 1266–1271, Dec. 2014, doi: 10.1016/j.mri.2014.08.021.
 - [98] A. L. Wentland, T. M. Grist, and O. Wieben, "Review of MRI-based measurements of pulse wave velocity: a biomarker of arterial stiffness," *Cardiovasc. Diagn. Ther.*, vol. 4, no. 2, pp. 193–206, Apr. 2014, doi: 10.3978/j.issn.2223-3652.2014.03.04.
 - [99] P. Reymond, F. Merenda, F. Perren, D. R  fenacht, and N. Stergiopulos, "Validation of a one-dimensional model of the systemic arterial tree," *Am. J. Physiol. - Heart Circ. Physiol.*, vol. 297, no. 1, pp. H208–H222, Jul. 2009, doi: 10.1152/ajpheart.00037.2009.
 - [100] P. Reymond, Y. Bohraus, F. Perren, F. Lazeyras, and N. Stergiopulos, "Validation of a patient-specific one-dimensional model of the systemic arterial tree," *Am. J. Physiol. Heart Circ. Physiol.*, vol. 301, no. 3, pp. H1173–1182, Sep. 2011, doi: 10.1152/ajpheart.00821.2010.
 - [101] N. Stergiopulos, M. Spiridon, F. Pythoud, and J. J. Meister, "On the wave transmission and reflection properties of stenoses," *J. Biomech.*, vol. 29, no. 1, pp. 31–38, Jan. 1996.
 - [102] R. Holenstein, P. Niederer, and M. Anliker, "A viscoelastic model for use in predicting arterial pulse waves," *J. Biomech. Eng.*, vol. 102, no. 4, pp. 318–325, Nov. 1980.
 - [103] Langewouters G. J., "Visco-elasticity of the human aorta in vitro in relation to pressure and age.," PhD Thesis, Free University of Amsterdam, The Netherlands, 1982.
 - [104] J. Womersley, "An Elastic Tube Theory of Pulse Transmission and Oscillatory Flow in Mammalian Arteries," *WADC Tech. Rep. - TR56-614*, 1957.

Chapter 2 Hemodynamics of Ageing

2.1 Evolution of aortic pressure during normal ageing: a model-based study

Stamatia Pagoulatou and Nikolaos Stergiopoulos

Laboratory of Hemodynamics and Cardiovascular Technology (LHTC), Institute of Bioengineering, Ecole Polytechnique Fédérale de Lausanne (EPFL), Lausanne, Switzerland

Abstract

The age-related increase in pulse pressure (PP) and systolic blood pressure (SBP) is often attributed to alterations in the wave reflection profile and augmented contributions of the reflected waves. However, clinical evidence shows that the stiffening of the proximal aorta with age and the consequent augmentation of the forward pressure wave plays an equally important role. The relative importance of the forward and reflected wave components in essential hypertension has not yet been fully elucidated. The aim of the current investigation was to simulate the major ageing mechanisms in the arterial system and the heart using a mathematical one-dimensional model of the arterial tree and to assess the evolution of systolic and pulse pressure during normal (nonpathological) ageing. Our state-of-the-art 1D model was extended to include turbulence and inertial effects of the flow exiting the left ventricle. Literature data on the age-associated changes in arterial stiffness, peripheral resistance and cardiac contractility were gathered and used as an input for the simulations. The predicted evolution of pressure and augmentation index with age followed accurately the curves obtained in a number of large-scale clinical studies. Analysis of the relative contribution of the forward and backward wave components showed that the forward wave becomes the major determinant of the increase in central and peripheral SBP and PP with advancing age. The 1D model of the ageing tree and heart captures faithfully and with great accuracy the central pressure evolution with ageing. The stiffening of the proximal aorta and the resulting augmentation of the forward pressure wave is the major contributor of the systolic pressure augmentation with age.

Key words: Ageing • 1D Model • Wave Reflection • Augmentation Index

Published in PLoS ONE (2017)

2.1.1 Introduction

Hypertension has been recognized as a major contributor to cardiovascular morbidity and mortality [1], [2]. The continuous rise of systolic blood pressure (SBP) and pulse pressure (PP) over time is mainly attributed to age-associated changes in the big elastic vessels, i.e. the aorta and its major branches, which undergo gradual stiffening and dilation [3], [4]. These alterations in the arterial properties and the resulting augmentation in cardiac afterload affect the cardiac structure and function, which in turn further contribute to the development of hypertension [5], [6].

Even in the absence of clinical hypertension [7], age-induced arterial stiffening can be detected by an increase in the aortic Pulse Wave Velocity (PWV), a measure which serves as an independent predictor of cardiovascular and total mortality [8]–[10]. Central Augmentation Index (Alx), which is a composite index illustrating the augmenting effect caused by the reflected wave, has also been proposed and used extensively as a surrogate measure of arterial stiffness, although its reliability has been questioned lately [11], [12]. In fact, several studies initially suggested a linear increase in both PWV and Alx with age across different populations. However, findings from Mitchell et al. [13], which were later corroborated by a number of studies [14], [15], revealed a steep increase in Alx in younger individuals, followed by a slight decrease in the elderly. In this context, Alx was proposed as a rather sensitive marker of vascular ageing in younger adults [14]. The nature of Alx as well as its clinical significance are still not fully understood and require further investigation.

Another topic that has engendered controversy among researchers is the contribution of the forward and backward travelling waves on the increase of SBP with age. One possible theory proposed by O’Rourke et al. [16] is that global arterial stiffening causes the augmentation and earlier arrival of the reflected waves. This point of view was challenged by Mitchell et al. [17], who suggested that the non-uniform aortic stiffening leads to an increase in the characteristic impedance predominantly in the proximal aorta, causing an augmentation in the forward pressure wave amplitude.

The use of mathematical models of the cardiovascular system to simulate ageing could shed light to these debates and broaden our general understanding on the ageing process. Previous work from Maksuti et al. [18] has tried to do so by employing a lumped parameter (4-element Windkessel) model of the arterial tree. This simple ageing model did manage to predict systolic (SBP) and diastolic (DBP) pressure evolution quite accurately. However, the arterial tree being represented by a 4-element Windkessel model, it lacked spatial dimension and thus it was unable to capture wave transmission effects.

The objective of this study was to predict the evolution of pressure during physiological ageing using a simple heart model and a one-dimensional model of the arterial tree. We aimed in predicting faithfully not only the evolution of systolic and diastolic pressure, but also the wave characteristics, so that the forward and reflected wave components can be analyzed and other indices characterizing wave reflections (i.e., Alx) can be derived as well. Particular attention is paid on the contribution of the earlier-arriving and amplified reflection wave and the augmented forward wave with goal to assess their relative contribution in the development of isolated systolic hypertension.

2.1.2 Methods

Description of the 1D model of the arterial tree

The ageing cardiovascular system was simulated using a detailed one-dimensional wave propagation model of the systemic arterial tree, which was first developed by Stergiopoulos et al. [19] and later improved by Reymond et al. [20]. A brief overview of the *in silico* model, emphasizing on the most important modeling assumptions, is presented below. For a more thorough description, the reader is referred to the original publications [19]–[21].

In the 1D model, blood pressure and flow waveforms are obtained throughout the vasculature through numerical integration of the 1D form of the Navier-Stokes equations. Following Holenstein et al. [22], the viscoelastic properties of the arterial wall are included by a constitutive relation relating pressure and cross-sectional area. Dependency of local area compliance on pressure is described by Langewouters et al. [23] and assumed to have the same functional form in all arterial locations. Pulsatile effects on the velocity profile are modeled according to the Witzig-Womersley theory. In order to include the distal vessels of the arterial tree, 3-element Windkessel models are coupled to the terminal arterial segments. Cardiac contractility is represented by a time-varying elastance model of the left ventricle, as proposed by Sagawa [24].

The generic 1D model was thoroughly validated by Reymond et al. [20]. A patient-specific model variant was further validated with *in vivo* measurements and was found capable of faithfully reproducing the flow and pressure waveform characteristics [21].

For the needs of our study, an improved version of this mathematical model was developed. Ventricular-vascular coupling was modified in order to include the opening of the aortic valve and the phenomena of inertia and turbulence in the flow exiting the ventricle, according to Mynard et al. [25]. Therefore, ventricular pressure, P_{lv} , and proximal aortic pressure, P_a , were no longer assumed to be equal during ejection. Instead:

$$\Delta p = P_{lv} - P_a = BQ|Q| + L \frac{dQ}{dt}$$

Equation 2.1:1 – Aortic valve model with inertia and turbulence terms

where B and L are the time-varying blood resistance and inertance, respectively.

Physiological ageing

Previous work by Maksuti et al. [18] stressed the importance of taking into consideration changes in both the arterial network and the heart when simulating ageing. Indeed, concurrently with the gradual stiffening of the elastic vessels and the increase in peripheral resistance with age, the heart undergoes remodeling, usually under the form of ventricular wall thickening and stiffening. Cardiac changes affect cardiovascular performance and further contribute to the development of hypertension [18].

Arterial stiffening

Arterial stiffness is usually assessed by measurement of PWV, which is known to increase with distance from the heart. In Reymond's model [20], PWV was approximated as a function of mean arterial lumen diameter by fitting the following inverse relation to the data reported for different arteries [26]–[31]:

$$PWV(\bar{d}) \cong a/\bar{d}^b$$

Equation 2.1:2 – Pulse wave velocity as a function of mean lumen diameter

where $a=13.3$ and $b=0.3$, with goodness of fit $R^2=0.6$.

This $PWV(\bar{d})$ relation represents a normal arterial system, where arterial stiffness increases steeply as one moves from central to peripheral arteries. In a young adult, PWV is approximately 5 m/s in the elastic proximal aorta [32] and increases to approximately 10 m/s in the stiffer femoral artery [33]. It has been shown, however, that during normal ageing the elastic properties of different aortic regions do not undergo uniform alterations. In fact, with advancing age, proximal vessels lose their elasticity more markedly than the periphery does, to an extent that proximal aorta might even become stiffer than distal sites in the elderly [13], [34].

Following Reymond's concept [20], we created different empirical inverse relations between artery size and PWV for all age decades, using the local PWV increase reported by Rogers et al. [32]. Geometry –and, thus, mean arterial lumen diameter– was assumed to remain unchanged with age. Relation coefficients a and b as well as goodness of fit R^2 are shown in Table 2.1:1 for each decade. Despite some dispersion, the relations yielded a good functional fit to literature data for all ages ($R^2>0.75$), which was a significant improvement compared to the original relation.

Table 2.1:1 Inverse relation coefficients a and b and goodness of fit R^2 for each age decade.

| Parameters | Age (years) | | | | | |
|------------|-------------|-------|-------|-------|-------|-------|
| | 30 | 40 | 50 | 60 | 70 | 80 |
| a | 15.48 | 15.59 | 16.33 | 16.68 | 15.91 | 15.29 |
| b | 0.502 | 0.458 | 0.447 | 0.428 | 0.372 | 0.345 |
| R^2 | 0.95 | 0.90 | 0.93 | 0.93 | 0.81 | 0.75 |

Peripheral resistance

For a given cardiac output (CO), the mean arterial pressure (MAP), i.e. the steady state component of blood pressure, is regulated solely by the peripheral arterial system. A number of studies have reported a rather insignificant decrease of CO with age [35], [36], indicating that the age-induced increase in MAP is driven mainly by the increase in the resistance of the smaller vessels of the periphery. In our model, the total peripheral resistance (TPR) was calculated for each decade as the ratio of the expected MAP (see Clinical pressure data) to CO. The latter was assumed unchanged with age and equal to the average value reported by Katori [35], CO=6.6 L/min. Based on the increase in the total peripheral resistance, all terminal resistances were then adapted accordingly in a uniform way.

Cardiac function

Age-induced changes in cardiac function and shape are still subject to intense investigation. One widely acknowledged cardiac change with age is the left ventricular wall thickening, which is present even in adults apparently free of any cardiovascular disease [37]. The reported augmentation in myocardial wall thickness occurs usually under the form of concentric hypertrophy [38]. With this compensation mechanism, the heart usually succeeds to bear the extra afterload without a significant increase in ventricular wall stress. Only under extreme conditions hypertrophy might develop to a point where wall stress becomes subnormal [39].

Surprisingly, these age-related changes in cardiac shape have been proven not to influence the overall shape of the normalized elastance curve, $E_N(t_N)$ (normalized both by time and amplitude), which seems independent of loading conditions, heart rate, and contractility in both canine and human hearts [40]–[42]. The thickening -and thus stiffening- of left ventricular wall is reflected by an increase in the end-systolic elastance (E_{es}). For the needs of our study, we assumed that ventricular wall stress is preserved with advancing age and thus E_{es} was increased in proportion to SBP, following the concept first developed by Maksuti et al. [18].

Stiffening of the ventricular wall renders ventricular filling slower, shifting the bulk of the atrial outflow later in diastole and thus gravely affecting diastolic function [6]. In our model, we assumed that end-diastolic elastance (E_{ed}) was augmented proportionally to E_{es} increase.

Following the argumentation of Maksuti et al. [18], we made the assumption of an unchanged end-diastolic volume (EDV) during cardiac remodeling. In order to achieve a constant EDV, end-diastolic pressure (P_{ven}) (which is almost equal to venous pressure) was increased appropriately with advancing age. Regarding heart rate (HR), studies have shown a decrease with age, hence we chose to vary HR values according to the physiological data reported by McEniery et al. [14] (average values between males and females per decade).

An overview of the ageing cardiac parameters is presented in Table 2.1:2.

Table 2.1:2 Overview of the ageing cardiac parameters.

| Parameter | Age (years) | | | | | |
|-----------------------|-------------|------|------|------|------|------|
| | 30 | 40 | 50 | 60 | 70 | 80 |
| E_{es} (x108 Pa/m3) | 1.37 | 1.45 | 1.55 | 1.65 | 1.80 | 2.01 |
| E_{ed} (x106 Pa/m3) | 3.43 | 3.63 | 3.67 | 4.13 | 4.50 | 5.03 |
| P_{ven} (Pa) | 861 | 895 | 937 | 987 | 1046 | 1131 |
| HR (bpm) | 73.3 | 72.1 | 70.9 | 69.7 | 68.5 | 67.3 |

E_{es} : end-systolic elastance, E_{ed} : end-diastolic elastance, P_{ven} : end-diastolic pressure, HR : heart rate

Clinical pressure data

Reference peripheral SBP and DBP values were obtained from the Framingham Heart Study reported by Franklin et al. [43], using the average values between normotensive groups 1 and 2. Expected central SBP was later computed using the mean pressure amplification from the proximal aorta to the brachial artery for each age decade, as documented by the Anglo-Cardiff Collaborate Trail II [44].

Data analysis: 1D model vs Clinical data

The difference between the model pressure predictions and the clinical data was quantified by calculation of the normalized root-mean squared error (n-RMSE). From the model-derived pressure waveforms, the contribution of the reflected wave amplitude to the total PP was assessed by changes in augmentation pressure (AP). Subsequently, aortic pressure wave shape was assessed by calculation of the central augmentation index (Aix), i.e. the ratio of AP to central pulse pressure (PP_{central}), following the methodology previously described in Murgo et al. [31].

Data analysis: 1D model vs 0-D model

Aortic pressure waves were separated into their forward and backward wave components, following the standard analysis in frequency domain [45]. Characteristic impedance at the root of the ascending aorta was estimated by averaging the input impedance modulus (Z_c) in the frequency range of 3-15 Hz. Forward wave pulse pressure (PP_{forward}) was defined as the difference between the systolic and diastolic pressure of the forward wave component. Wave separation analysis was applied to the 0-D model of Maksuti et al. [18], as well as to the 1D model and the ratios of forward wave PP to central PP at the ascending aorta were plotted as a function of age.

2.1.3 Results

The values of the simulation-derived hemodynamic parameters are presented in Table 2.1:3, grouped by decade of age.

Table 2.1:3 Simulation derived hemodynamic parameters according to age category.

| Parameter | Age (years) | | | | | |
|---------------------------------|-------------|-------|-------|-------|-------|-------|
| | 30 | 40 | 50 | 60 | 70 | 80 |
| Brachial SBP (mmHg) | 109.7 | 114.0 | 121.9 | 129.0 | 136.8 | 141.3 |
| Aortic SBP (mmHg) | 97.7 | 105.1 | 112.1 | 117.8 | 126.2 | 129.8 |
| MAP (mmHg) | 84.8 | 88.8 | 91.6 | 94.8 | 95.8 | 95.4 |
| DBP (mmHg) | 73.9 | 77.0 | 77.0 | 77.9 | 74.1 | 73.3 |
| PP _{peripheral} (mmHg) | 37.4 | 37.7 | 45.5 | 51.3 | 61.4 | 68.8 |
| PP _{central} (mmHg) | 23.9 | 28.1 | 35.2 | 39.9 | 52.1 | 56.5 |

| | | | | | | |
|-----------------------|------|------|------|------|------|------|
| PP ampl (ratio) | 1.57 | 1.34 | 1.29 | 1.28 | 1.18 | 1.21 |
| AP (mmHg) | 0.6 | 2.4 | 6.1 | 7.2 | 6.3 | 7.1 |
| Alx (%) | 2.7 | 8.6 | 17.0 | 18.1 | 12.5 | 12.5 |
| Inflection Point (ms) | 154 | 136 | 123 | 114 | 124 | 120 |

SBP : systolic blood pressure, MAP : mean arterial pressure, DBP : diastolic blood pressure, PP : pulse pressure, PP ampl : pulse pressure amplification, AP : augmentation pressure, Alx : augmentation index.

The evolution of brachial SBP and aortic SBP and DBP with age is depicted also in Figure 2.1:1 A in comparison to the clinical pressure data described above. As expected, the model predicted that both central and peripheral SBP increased progressively over time. Aortic SBP increased from 98 mmHg at 30 years to 130 mmHg at 80 years of age, while brachial SBP increased from 110 mmHg to 141 mmHg during the same time period. In contrast, DBP initially increased until 50 years and then followed the well anticipated decline. This resulted in the expected widening of both central and peripheral PP with age. Goodness of fit parameter n-RMSE was calculated and found equal to 2.2%.

Central SBP increased more with age than peripheral SBP did, resulting in a loss of PP amplification (defined as the ratio of brachial PP to aortic PP). As depicted in Figure 2.1:1 B, the ratio varied from 1.57 at 30 years to less than 1.22 at 80 years of age and was in close agreement with the data from the Anglo-Cardiff Collaborate Trial II (ACCT) [44]. Note that the decrease in PP augmentation was steeper for young adults, conforming to the ACCT findings.

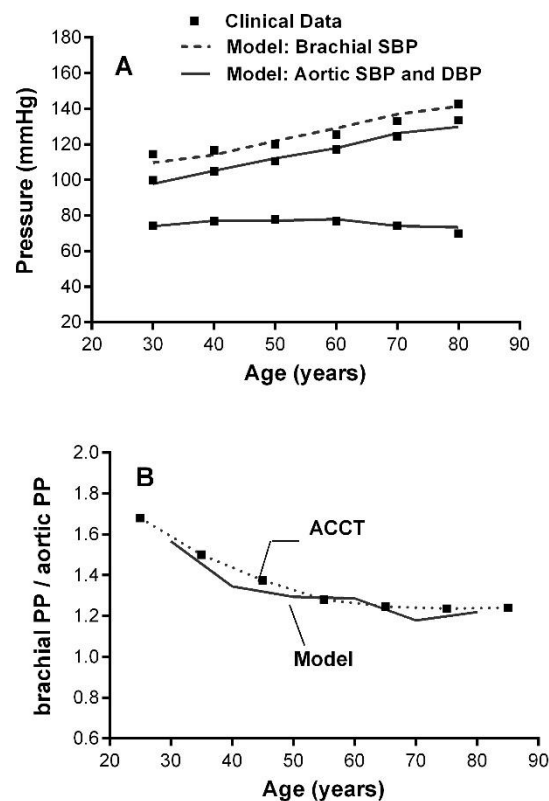


Figure 2.1:1 Model pressure predictions against clinical data for the time frame of 30 to 80 years of age. (A) Model-derived brachial SBP (dashed line) and aortic SBP and DBP (solid line) against the reference data [43], [44] (squares). (B) Model-derived ratio of peripheral (brachial) PP to central (aortic) PP (solid line) against the measurements from ACCT trial [44] (squares-dotted line).

Figure 2.1:2 shows predicted pressure waveforms at the ascending aorta and the brachial artery and their evolution from 30 to 80 years of age. As expected, the pressure pulse wave is shown to arrive earlier in the brachial artery with advancing age due to the higher PWV.

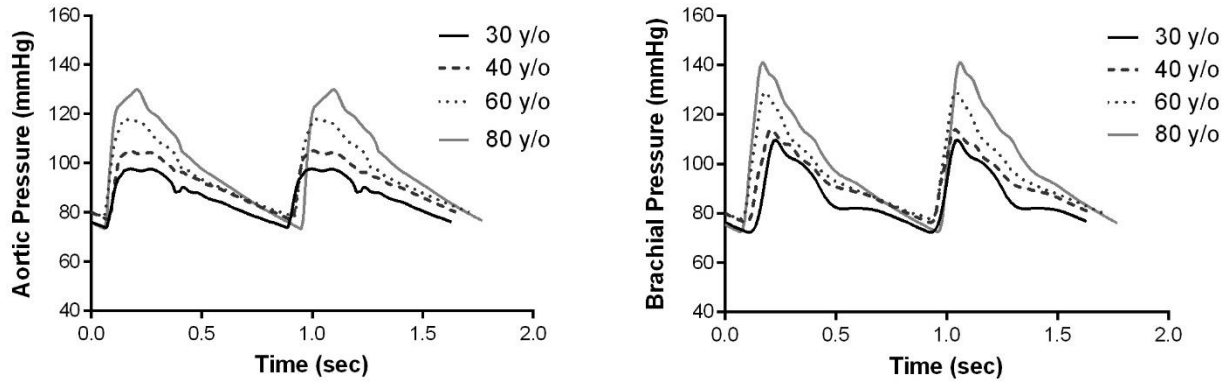


Figure 2.1:2 Aortic (*left*) and brachial (*right*) pressure waveforms for different age decades.

Augmentation pressure (AP) is plotted in Figure 2.1:3 A against the reference AP values [13]. As previously suggested by Mitchell et al. [13], we found that AP changed minimally with advancing age. Aortic augmentation index as well as inflection point were also computed for each age decade. In our model AIx was found to increase steeply in young adults and actually decline after 60 years of age. Our results were highly consistent with the findings of Torjesen et al. [15] (average values between males and females), as shown in Figure 2.1:3 B and Figure 2.1:3 C.

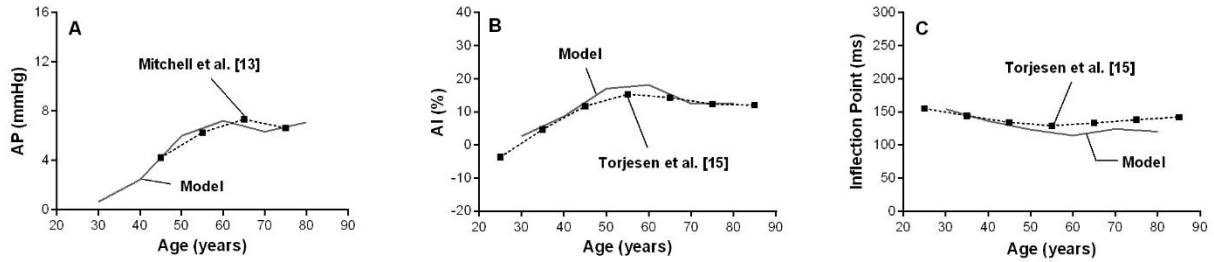


Figure 2.1:3 Model predictions (solid line) against clinical data from Mitchell et al. [13] and Torjesen et al. [15] (black squares). (A) Augmentation Pressure, (B) Augmentation index, (C) Inflection Point.

Forward wave pulse pressure (PPforward), computed after the wave separation analysis, was used in order to assess the contribution of the forward wave to systolic pressure augmentation during ageing. The ratio of the forward wave pulse pressure to the central pulse pressure (PPforward/PPcentral) is presented in Figure 2.1:4, compared to the results obtained by the 0-D model of Maksuti et al. [18]. In our model, the ratio increased from 0.78 to 0.83 between the ages of 30 to 80 years old, while the 0-D model predicted a decline.

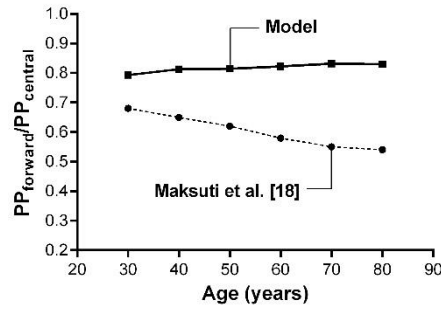


Figure 2.1:4 Contribution of forward pressure wave to pressure augmentation during ageing, as assessed by the $PP_{\text{forward}}/PP_{\text{central}}$ ratio. 1D model results (squares - solid line) compared to the 0-D model results [18] (dots - dashed line).

2.1.4 Discussion

The present study aimed to achieve three goals. First, to simulate the evolution of arterial pressures during the physiological ageing process using a realistic 1D model of the systemic arterial tree. The original 1D model, upon which our work was based, was developed in our laboratory [19], [20] and is considered to be one of the most complete and thoroughly validated models available in literature. This powerful computational tool has successfully provided a solid foundation for a number of subsequent studies [46]–[49].

In order to gain in-depth insight into the ageing cardiovascular system, we decided to modify the original version of the 1D model, which previously assumed left ventricular and aortic pressure to be equal during ejection. This assumption is limiting since there are flow phenomena created in the aortic valve that lead to differences between the ventricular and aortic pressure waveforms both in magnitude and phase [25]. An elevated pressure difference might even be indicative of aortic stenosis. Although in our work no pathological cases were simulated, omitting inertial effects and turbulence losses at the aortic valve, a key component of the ventricular-arterial coupling, would reduce the accuracy of the aortic wave shape even in physiological conditions. Indeed, after including in our simulations the inertia and turbulence model proposed by Mynard et al. [25], Aix predictions were significantly improved, with the n-RMSE decreasing almost threefold.

Based on data from a wide range of literature, we expanded the generic 1D model - representative of a young healthy male - into a model of the arterial tree adaptable to all adult ages. A key point in simulating arterial ageing was to describe in a mathematical way the progressive and heterogeneous stiffening of the arterial network, which has been widely recognized as a determinant for the rise in SBP. To achieve this, we first examined closely the inverse relation between artery size and PWV that was originally proposed by Raymond et al. [20]. This relation was created combining reference data on local aortic and peripheral PWV measurements from different populations and exhibited a relatively poor correlation coefficient of $R^2=0.6$. What was not taken into consideration by Raymond et al. [20], however, was the fact that the aforementioned populations were of different age groups, some even exceeding 55 years old. Given the high dependency of PWV on age, this contributed to the significant dispersion observed between the average “fitted” curve and the literature data. Indeed, after the age factor was accounted for, the age-dependent $PWV(\bar{d})$ relations fitted well to the literature data and the dispersion decreased for all age decades ($R^2>0.75$ in all cases).

The second goal was to validate the predictions of the ageing model via a comparison to published data from large-scale clinical studies. Despite the simplicity of the rules we applied, and despite the fact that we did not take into consideration how the arterial geometry evolves with time, our simulations were surprisingly accurate; our prediction of SBP and DBP reproduced the pattern reported by the Framingham heart study [43] and the Anglo-Cardiff Collaborate Trial II [44]. We achieved an n-RMSE of 2.2%, whereas the 0-D model from Maksuti et al. [18] achieved a n-RMSE of 5.1% when compared to the same clinical data. In addition, our *in silico* ageing model provided pressure waveforms that, from a qualitative point of view, captured faithfully the actual wave characteristics at the ascending aorta and the brachial artery.

Furthermore, we evaluated the change with age of the brachial to aortic PP ratio and found that our model was able to follow the anticipated evolution: a marked decrease in young ages followed by a less marked change in senescence. This decrease in PP augmentation is a key feature of ageing and has become the subject of intense investigation, since it serves as a sign of adverse

clinical outcomes [50]. Mitchell et al. [13] interpreted this decrease as the combination of changes in both the wave reflection and arterial stiffness. He suggested that in young adults, as arterial stiffness increases steeply from the proximal aorta towards the distal branches, local reflections occur relatively earlier in time, leading to a greater PP augmentation. With advancing age, the significant increase in proximal PWV reduces or might even reverse the arterial stiffness gradient, shifting the reflection sites distally and apparently reducing amplification.

According to Avolio et al. [51], the factor most closely associated with PP amplification is Alx. In prior studies, Alx has been extensively used as a surrogate measure of arterial stiffness, although it seems to be a rather composite measure that synthesizes the impact of different parameters, i.e. arterial stiffness, heart rate, and reflection wave properties. In contrast to findings from Hayward et al. [52], our model results revealed a clearly non-linear relationship between age and Alx. In young individuals, Alx was found to rise steeply with age in contrast to older individuals, whose Alx decreased minimally. This pattern has been previously reported by a plethora of studies [13]–[15]. In this context, we agree that Alx might serve as a rather sensitive measure of vascular ageing in younger adults, as suggested by McEniery et al. [14].

These outcomes, which are clearly associated with non-uniform alterations in the wave reflection profile, inspired us to further investigate the relative changes in the aortic forward and backward pressure waveforms during ageing. Therefore, we set as third goal of our study to quantify and assess the contribution of each wave component to the development of essential hypertension. Absolute values of forward wave amplitude were found to increase with age, whereas AP (which serves as an index of the reflected wave amplitude) changed only minimally. The relative contribution of the wave components was assessed by the ratio of the forward wave PP to central PP, which increased with advancing age. Hence, our findings supported the theory proposed by Mitchell et al. [13], [17], according to which it is the forward wave that becomes the major determinant of the increase in central and peripheral SBP and PP with advancing age. This finding is contradicting the predictions of the 0-D model [18], which failed to capture the wave transmission effects.

Limitations and Future Work

Limitations of the 1D model with respect to the formulation of the governing equations are acknowledged and discussed in detail in the original publication by Reymond et al. [20].

Cardiac function was adapted for each decade according to the physiological rules employed by Maksuti et al. [18]. The shape of the normalized elastance function $EN(tN)$ (in time and magnitude), is suggested to be invariable among hearts, particularly during early contraction [40]–[42]. In fact, the isovolumic relaxation phase of the cardiac cycle is prolonged in older individuals, due to the slower ventricular filling [6]. The magnitude of the alteration in the timing of the relaxation and contraction phase is, however, rather negligible in healthy adults.

Central arterial geometry is known to change significantly during normal ageing [53]–[55]. To adapt to the changes in hemodynamic stresses acting on the arterial wall, the proximal aorta thickens, lengthens, enlarges in diameter and becomes tortuous in older individuals, as described in [55]. The same study has demonstrated a close relationship between these geometrical alterations in proximal aorta and the increase in central and brachial SBP. This seems reasonable given that an alteration in regional aortic diameter and length would clearly affect PWV and pulse transit time. Whether arterial diameter changes themselves are an important pathophysiological factor remains unknown. In an attempt to address this question, we assessed the effects of aortic geometric changes in model predictions, using the *in vivo* data provided by Redheuil et al. [55] on the evolution of the ascending, proximal and distal aortic diameters with age. Surprisingly, central systolic and diastolic pressure values were minimally affected (n-RMSE changed by less than 3%), suggesting that geometric changes in the aorta alone are not the determining factor in the alteration of central aortic hemodynamics with age. Nevertheless, more literature data on the aforementioned geometric changes will enable us to include in our simulations more precise models of the arterial remodeling and study in depth its significance.

Furthermore, gender-related differences in cardiovascular ageing are important, as supported by a substantial volume of literature. The increase in central SBP and PP with age is less prominent in men than women [14]. This variation is often correlated with the fact that large artery stiffness and pulsatility is on average more pronounced in older females [3]. Prior studies have documented significant wave reflection differences between the two sexes, with women systematically demonstrating higher Alx values and larger reflection waves than men [13]. This characteristic is often attributed to their shorter height and the closer physical proximity between the heart and the reflection sites, although this explication might not be sufficient [56]. Moreover, given that women have a significantly longer life span and a lower risk of cardiovascular disease, it is likely that cardiac structure is better preserved in the feminine heart [57]. All these observations possibly reflect intrinsic differences in the cardiac and arterial properties between the

two genders. However, gender-related variations in cardiovascular anatomy and physiology were not accounted for in the present study due to paucity of clinical data and thus the present work is most pertinent for the evolution of pressure in males.

Future work will focus on generating more data in order to allow for a quantitative validation of the ageing model on a patient-specific and gender-specific approach, where the generic 1D model will be tuned according to the measured cardiovascular geometry and properties of each patient. This way, the model-derived pressure and flow waveforms will be quantitatively and qualitatively compared with the measured ones.

Conclusions

We developed a 1D model of the ageing cardiovascular system, which can serve as a tool for investigating how cardiac and arterial changes influence hemodynamic characteristics. The model output has been found highly consistent with published data from large-scale studies, particularly in terms of systolic and diastolic pressures, wave shape and reflection indices. Examination of the model-derived wave reflection profile revealed a pronounced correlation between the augmentation in the forward wave amplitude and the increase in SBP and PP over time.

This study lays the ground for further investigation of the ageing mechanisms which contribute to the development of essential hypertension and lead to cardiovascular disease. New detailed information about age-related changes in aortic geometry and properties would help further improve the accuracy of the mathematical models of the ageing cardiovascular tree.

2.1.5 Bibliography

- [1] M. Ezzati, A. D. Lopez, A. Rodgers, S. Vander Hoorn, and C. J. Murray, "Selected major risk factors and global and regional burden of disease," *The Lancet*, vol. 360, no. 9343, pp. 1347–1360, Nov. 2002, doi: 10.1016/S0140-6736(02)11403-6.
- [2] C. M. M. Lawes, S. Vander Hoorn, A. Rodgers, and International Society of Hypertension, "Global burden of blood-pressure-related disease, 2001," *Lancet Lond. Engl.*, vol. 371, no. 9623, pp. 1513–1518, May 2008, doi: 10.1016/S0140-6736(08)60655-8.
- [3] B. Jani and C. Rajkumar, "Ageing and vascular ageing," *Postgrad. Med. J.*, vol. 82, no. 968, pp. 357–362, Jun. 2006, doi: 10.1136/pgmj.2005.036053.
- [4] H.-Y. Lee and B.-H. Oh, "Aging and arterial stiffness," *Circ. J. Off. J. Jpn. Circ. Soc.*, vol. 74, no. 11, pp. 2257–2262, Nov. 2010.
- [5] A. U. Ferrari, A. Radaelli, and M. Centola, "Invited Review: Aging and the cardiovascular system," *J. Appl. Physiol.*, vol. 95, no. 6, pp. 2591–2597, Dec. 2003, doi: 10.1152/japplphysiol.00601.2003.
- [6] J. B. Strait and E. G. Lakatta, "Aging-associated cardiovascular changes and their relationship to heart failure," *Heart Fail. Clin.*, vol. 8, no. 1, pp. 143–164, Jan. 2012, doi: 10.1016/j.hfc.2011.08.011.
- [7] P. V. Vaitkevicius *et al.*, "Effects of age and aerobic capacity on arterial stiffness in healthy adults," *Circulation*, vol. 88, no. 4, pp. 1456–1462, Oct. 1993, doi: 10.1161/01.CIR.88.4.1456.
- [8] G. F. Mitchell *et al.*, "Arterial Stiffness and Cardiovascular Events," *Circulation*, vol. 121, no. 4, pp. 505–511, Feb. 2010, doi: 10.1161/CIRCULATIONAHA.109.886655.
- [9] S. S. Najjar *et al.*, "Pulse Wave Velocity Is an Independent Predictor of the Longitudinal Increase in Systolic Blood Pressure and of Incident Hypertension in the Baltimore Longitudinal Study of Aging," *J. Am. Coll. Cardiol.*, vol. 51, no. 14, pp. 1377–1383, avril 2008, doi: 10.1016/j.jacc.2007.10.065.
- [10] C. Vlachopoulos, K. Aznaouridis, and C. Stefanadis, "Prediction of Cardiovascular Events and All-Cause Mortality With Arterial Stiffness: A Systematic Review and Meta-Analysis," *J. Am. Coll. Cardiol.*, vol. 55, no. 13, pp. 1318–1327, Mar. 2010, doi: 10.1016/j.jacc.2009.10.061.
- [11] L.-T. Cheng, L.-J. Tang, L. Cheng, H.-Y. Huang, and T. Wang, "Limitation of the Augmentation Index for Evaluating Arterial Stiffness," *Hypertens. Res.*, vol. 30, no. 8, pp. 713–722, août 2007, doi: 10.1291/hypres.30.713.
- [12] M. Sakurai *et al.*, "The relationship between aortic augmentation index and pulse wave velocity: an invasive study," *J. Hypertens.*, vol. 25, no. 2, pp. 391–397, Feb. 2007, doi: 10.1097/HJH.0b013e3280115b7c.
- [13] G. F. Mitchell *et al.*, "Changes in arterial stiffness and wave reflection with advancing age in healthy men and women: the Framingham Heart Study," *Hypertens. Dallas Tex 1979*, vol. 43, no. 6, pp. 1239–1245, Jun. 2004, doi: 10.1161/01.HYP.0000128420.01881.aa.

- [14] C. M. McEniery *et al.*, "Normal vascular aging: differential effects on wave reflection and aortic pulse wave velocity: the Anglo-Cardiff Collaborative Trial (ACCT)," *J. Am. Coll. Cardiol.*, vol. 46, no. 9, pp. 1753–1760, Nov. 2005, doi: 10.1016/j.jacc.2005.07.037.
- [15] A. A. Torjesen *et al.*, "Forward and Backward Wave Morphology and Central Pressure Augmentation in Men and Women in the Framingham Heart Study," *Hypertension*, vol. 64, no. 2, pp. 259–265, Aug. 2014, doi: 10.1161/HYPERTENSIONAHA.114.03371.
- [16] M. F. O'Rourke and W. W. Nichols, "Aortic Diameter, Aortic Stiffness, and Wave Reflection Increase With Age and Isolated Systolic Hypertension," *Hypertension*, vol. 45, no. 4, pp. 652–658, Apr. 2005, doi: 10.1161/01.HYP.0000153793.84859.b8.
- [17] G. F. Mitchell *et al.*, "Aortic diameter, wall stiffness, and wave reflection in systolic hypertension," *Hypertens. Dallas Tex 1979*, vol. 51, no. 1, pp. 105–111, Jan. 2008, doi: 10.1161/HYPERTENSIONAHA.107.099721.
- [18] E. Maksuti, N. Westerhof, B. E. Westerhof, M. Broomé, and N. Stergiopulos, "Contribution of the Arterial System and the Heart to Blood Pressure during Normal Aging - A Simulation Study," *PloS One*, vol. 11, no. 6, p. e0157493, 2016, doi: 10.1371/journal.pone.0157493.
- [19] N. Stergiopulos, D. F. Young, and T. R. Rogge, "Computer simulation of arterial flow with applications to arterial and aortic stenoses," *J. Biomech.*, vol. 25, no. 12, pp. 1477–1488, Dec. 1992.
- [20] P. Reymond, F. Merenda, F. Perren, D. Rüfenacht, and N. Stergiopulos, "Validation of a one-dimensional model of the systemic arterial tree," *Am. J. Physiol. - Heart Circ. Physiol.*, vol. 297, no. 1, pp. H208–H222, Jul. 2009, doi: 10.1152/ajpheart.00037.2009.
- [21] P. Reymond, Y. Bohraus, F. Perren, F. Lazeyras, and N. Stergiopulos, "Validation of a patient-specific one-dimensional model of the systemic arterial tree," *Am. J. Physiol. Heart Circ. Physiol.*, vol. 301, no. 3, pp. H1173–1182, Sep. 2011, doi: 10.1152/ajpheart.00821.2010.
- [22] R. Holenstein, P. Niederer, and M. Anliker, "A viscoelastic model for use in predicting arterial pulse waves," *J. Biomech. Eng.*, vol. 102, no. 4, pp. 318–325, Nov. 1980.
- [23] Langewouters G. J., "Visco-elasticity of the human aorta in vitro in relation to pressure and age," PhD Thesis, Free University of Amsterdam, The Netherlands, 1982.
- [24] K. Sagawa, "The end-systolic pressure-volume relation of the ventricle: definition, modifications and clinical use," *Circulation*, vol. 63, no. 6, pp. 1223–1227, Jun. 1981.
- [25] J. P. Mynard, M. R. Davidson, D. J. Penny, and J. J. Smolich, "A simple, versatile valve model for use in lumped parameter and one-dimensional cardiovascular models," *Int. J. Numer. Methods Biomed. Eng.*, vol. 28, no. 6–7, pp. 626–641, juin 2012, doi: 10.1002/cnm.1466.
- [26] J.-P. Baguet, B. A. Kingwell, A. L. Dart, J. Shaw, K. E. Ferrier, and G. L. Jennings, "Analysis of the regional pulse wave velocity by Doppler: methodology and reproducibility," *J. Hum. Hypertens.*, vol. 17, no. 6, pp. 407–412, Jun. 2003, doi: 10.1038/sj.jhh.1001566.
- [27] C. A. Giller and R. Aaslid, "Estimates of pulse wave velocity and measurement of pulse transit time in the human cerebral circulation," *Ultrasound Med. Biol.*, vol. 20, no. 2, pp. 101–105, 1994.
- [28] K. Hayashi, S. Nagasawa, Y. Naruo, A. Okumura, K. Moritake, and H. Handa, "Mechanical properties of human cerebral arteries," *Biorheology*, vol. 17, no. 3, pp. 211–218, 1980.
- [29] R. D. Latham, N. Westerhof, P. Sipkema, B. J. Rubal, P. Reuderink, and J. P. Murgo, "Regional wave travel and reflections along the human aorta: a study with six simultaneous micromanometric pressures," *Circulation*, vol. 72, no. 6, pp. 1257–1269, Dec. 1985.
- [30] P. C. Luchsinger and R. E. Snell, "Instantaneous Pressure Distribution Along the Human Aorta," *Circ. Res.*, no. 15, pp. 503–510, 1964.
- [31] J. P. Murgo, N. Westerhof, J. P. Giolma, and S. A. Altobelli, "Aortic input impedance in normal man: relationship to pressure wave forms," *Circulation*, vol. 62, no. 1, pp. 105–116, Jul. 1980, doi: 10.1161/01.CIR.62.1.105.
- [32] W. J. Rogers *et al.*, "Age-associated changes in regional aortic pulse wave velocity," *J. Am. Coll. Cardiol.*, vol. 38, no. 4, pp. 1123–1129, Oct. 2001.
- [33] E. Kimoto *et al.*, "Preferential stiffening of central over peripheral arteries in type 2 diabetes," *Diabetes*, vol. 52, no. 2, pp. 448–452, Feb. 2003.
- [34] P. Boutouyrie, S. Laurent, A. Benetos, X. J. Girerd, A. P. Hoeks, and M. E. Safar, "Opposing effects of ageing on distal and proximal large arteries in hypertensives," *J. Hypertens. Suppl. Off. J. Int. Soc. Hypertens.*, vol. 10, no. 6, pp. S87–91, Aug. 1992.
- [35] R. Katori, "Normal cardiac output in relation to age and body size," *Tohoku J. Exp. Med.*, vol. 128, no. 4, pp. 377–387, Aug. 1979.

- [36] E. G. Lakatta, J. H. Mitchell, A. Pomerance, and G. G. Rowe, "Human aging: Changes in structure and function," *J. Am. Coll. Cardiol.*, vol. 10, no. 2, pp. 42A-47A, août 1987, doi: 10.1016/S0735-1097(87)80447-3.
- [37] G. Gerstenblith, J. Frederiksen, F. C. Yin, N. J. Fortuin, E. G. Lakatta, and M. L. Weisfeldt, "Echocardiographic assessment of a normal adult aging population," *Circulation*, vol. 56, no. 2, pp. 273-278, Aug. 1977, doi: 10.1161/01.CIR.56.2.273.
- [38] B. H. Lorell and B. A. Carabello, "Left ventricular hypertrophy: pathogenesis, detection, and prognosis," *Circulation*, vol. 102, no. 4, pp. 470-479, Jul. 2000.
- [39] G. P. Aurigemma and W. H. Gaasch, "Gender differences in older patients with pressure-overload hypertrophy of the left ventricle," *Cardiology*, vol. 86, no. 4, pp. 310-317, 1995.
- [40] H. Senzaki, C.-H. Chen, and D. A. Kass, "Single-Beat Estimation of End-Systolic Pressure-Volume Relation in Humans," *Circulation*, vol. 94, no. 10, pp. 2497-2506, Nov. 1996, doi: 10.1161/01.CIR.94.10.2497.
- [41] H. Suga and K. Sagawa, "Instantaneous Pressure-Volume Relationships and Their Ratio in the Excised, Supported Canine Left Ventricle," *Circ. Res.*, vol. 35, no. 1, pp. 117-126, Jul. 1974, doi: 10.1161/01.RES.35.1.117.
- [42] H. Suga, K. Sagawa, and A. A. Shoukas, "Load Independence of the Instantaneous Pressure-Volume Ratio of the Canine Left Ventricle and Effects of Epinephrine and Heart Rate on the Ratio," *Circ. Res.*, vol. 32, no. 3, pp. 314-322, Mar. 1973, doi: 10.1161/01.RES.32.3.314.
- [43] S. S. Franklin *et al.*, "Hemodynamic patterns of age-related changes in blood pressure. The Framingham Heart Study," *Circulation*, vol. 96, no. 1, pp. 308-315, Jul. 1997.
- [44] C. M. McEniery *et al.*, "Central pressure: variability and impact of cardiovascular risk factors: the Anglo-Cardiff Collaborative Trial II," *Hypertens. Dallas Tex 1979*, vol. 51, no. 6, pp. 1476-1482, Jun. 2008, doi: 10.1161/HYPERTENSIONAHA.107.105445.
- [45] N. Westerhof, P. Sipkema, G. C. van den Bos, and G. Elzinga, "Forward and backward waves in the arterial system," *Cardiovasc. Res.*, vol. 6, no. 6, pp. 648-656, Nov. 1972.
- [46] L. Aslanidou, B. Trachet, P. Reymond, R. A. Fraga-Silva, P. Segers, and N. Stergiopulos, "A 1D model of the arterial circulation in mice," *ALTEX*, vol. 33, no. 1, pp. 13-28, 2016, doi: 10.14573/altex.1507071.
- [47] P. Reymond, N. Westerhof, and N. Stergiopulos, "Systolic hypertension mechanisms: effect of global and local proximal aorta stiffening on pulse pressure," *Ann. Biomed. Eng.*, vol. 40, no. 3, pp. 742-749, Mar. 2012, doi: 10.1007/s10439-011-0443-x.
- [48] O. Vardoulis, T. G. Papaioannou, and N. Stergiopulos, "On the estimation of total arterial compliance from aortic pulse wave velocity," *Ann. Biomed. Eng.*, vol. 40, no. 12, pp. 2619-2626, Dec. 2012, doi: 10.1007/s10439-012-0600-x.
- [49] O. Vardoulis, T. G. Papaioannou, and N. Stergiopulos, "Validation of a novel and existing algorithms for the estimation of pulse transit time: advancing the accuracy in pulse wave velocity measurement," *Am. J. Physiol. Heart Circ. Physiol.*, vol. 304, no. 11, pp. H1558-1567, Jun. 2013, doi: 10.1152/ajpheart.00963.2012.
- [50] M. E. Safar *et al.*, "Central pulse pressure and mortality in end-stage renal disease," *Hypertens. Dallas Tex 1979*, vol. 39, no. 3, pp. 735-738, Mar. 2002.
- [51] A. P. Avolio *et al.*, "Role of Pulse Pressure Amplification in Arterial Hypertension," *Hypertension*, vol. 54, no. 2, pp. 375-383, Aug. 2009, doi: 10.1161/HYPERTENSIONAHA.109.134379.
- [52] C. S. Hayward and R. P. Kelly, "Gender-Related Differences in the Central Arterial Pressure Waveform," *J. Am. Coll. Cardiol.*, vol. 30, no. 7, pp. 1863-1871, décembre 1997, doi: 10.1016/S0735-1097(97)00378-1.
- [53] D. Craiem, M. E. Casciaro, S. Graf, G. Chironi, A. Simon, and R. L. Armentano, "Effects of aging on thoracic aorta size and shape: a non-contrast CT study," *Conf. Proc. Annu. Int. Conf. IEEE Eng. Med. Biol. Soc. IEEE Eng. Med. Biol. Soc. Annu. Conf.*, vol. 2012, pp. 4986-4989, 2012, doi: 10.1109/EMBC.2012.6347112.
- [54] A. V. Kamenskiy, I. I. Pipinos, J. S. Carson, J. N. MacTaggart, and B. T. Baxter, "Age and disease-related geometric and structural remodeling of the carotid artery," *J. Vasc. Surg.*, vol. 62, no. 6, pp. 1521-1528, Dec. 2015, doi: 10.1016/j.jvs.2014.10.041.
- [55] A. Redheuil *et al.*, "Age-related changes in aortic arch geometry: relationship with proximal aortic function and left ventricular mass and remodeling," *J. Am. Coll. Cardiol.*, vol. 58, no. 12, pp. 1262-1270, Sep. 2011, doi: 10.1016/j.jacc.2011.06.012.
- [56] C. D. Gatzka *et al.*, "Gender differences in the timing of arterial wave reflection beyond differences in body height," *J. Hypertens.*, vol. 19, no. 12, pp. 2197-2203, Dec. 2001.
- [57] G. Olivetti *et al.*, "Gender differences and aging: effects on the human heart," *J. Am. Coll. Cardiol.*, vol. 26, no. 4, pp. 1068-1079, Oct. 1995, doi: 10.1016/0735-1097(95)00282-8.

2.2 On the importance of the non-uniform aortic stiffening in the hemodynamics of physiological ageing

Stamatia Pagoulatou ¹, Vasiliki Bikia ¹, Bram Trachet ^{1,2}, Theodore G. Papaioannou ³, Athanase D. Protogerou ⁴ and Nikolaos Stergiopoulos ¹

¹ Laboratory of Hemodynamics and Cardiovascular Technology (LHTC), Institute of Bioengineering, Ecole Polytechnique Fédérale de Lausanne (EPFL), Lausanne, Switzerland

² Institute of Biomedical Technology, IBiTech-bioMMeda, Ghent University, Ghent, Belgium

³ Biomedical Engineering Unit, First Department of Cardiology, Medical School, National and Kapodistrian University of Athens, Athens, Greece

⁴ Cardiovascular Prevention and Research Unit, Department of Pathophysiology, National and Kapodistrian University Athens School of Medicine, Athens, Greece

Abstract

Mathematical models of the arterial tree constitute a valuable tool to investigate the hemodynamics of ageing and pathology. Rendering such models patient-specific could allow for the assessment of central hemodynamic variables of clinical interest. However, this task is challenging, particularly with respect to the tuning of the local area compliance that varies significantly along the arterial tree. Accordingly, in this study, we demonstrate the importance of taking into account the differential effects of ageing on the stiffness of central and peripheral arteries when simulating a person's hemodynamic profile. More specifically, we propose a simple method for effectively adapting the properties of a generic 1D model of the arterial tree based on the subject's age and noninvasive measurements of aortic flow and brachial pressure. Key element for the success of the method is the implementation of different mechanisms of arterial stiffening for young and old individuals. The designed methodology was tested and validated against in vivo data from a population of n=20 adults. Carotid-to-femoral pulse wave velocity (c-f PWV) was accurately predicted by the model (mean error=0.14 m/s, SD=0.77 m/s), with the greatest deviations being observed for older subjects. In regard to aortic pressure, model-derived systolic blood pressure and augmentation index were both in good agreement (mean difference of 2.3 mmHg and 4.25%, respectively) with the predictions of a widely used commercial device (Mobil-O-Graph). These preliminary results encourage us to further validate the method in larger samples and consider its potential as a noninvasive tool for hemodynamic monitoring.

Key words: Noninvasive • Hemodynamic monitoring • 1D simulations

Published in the American Journal of Physiology – Heart and Circulatory Physiology (2019)

2.2.1 Introduction

Central hemodynamic parameters, such as aortic blood pressure and cardiac output, may have a greater prognostic value for assessing cardiovascular risk than peripheral hemodynamic indices [1]. Although central hemodynamics are crucial for accurate diagnosis and optimal treatment management, there is an inherent difficulty in their noninvasive estimation in clinical practice. Most relevant central hemodynamic monitoring techniques proposed in the literature often involve statistical correlations [2], generalized transfer functions [3], [4] or formulas based on pulse wave analysis [5], [6].

The personalization of mathematical models of the cardiovascular system constitutes a physiologically relevant way for the derivation of central hemodynamic variables, a desirable alternative to most of the aforementioned techniques or commercial devices that lack a physiological/mathematical background. Particularly, patient-specific, one-dimensional (1D) simulations could serve as a valuable tool for the assessment of pressure and flow in the entire arterial network, which is crucial to disease initiation and progression [7]. This is, of course, a challenging task, primarily due to the large amount of input data needed for the effective personalization of a distributed arterial tree model.

In a previous publication, we proposed a methodology for tuning the parameters of a validated, generalized 1D model of the arterial tree and the subsequent derivation of the cardiac contractility based on noninvasive measurements of brachial pressure and aortic flow [8]. Using the measured aortic flow as the model input, we achieved the parameter tuning by essentially altering the compliance of all arterial vessels in a uniform way until the model predicted brachial pressure accurately. The assumption of a uniform scaling of the arterial compliance between different individuals and different physio-pathological situations (i.e., ageing, disease, etc.) is oversimplifying. Indeed, stiffening can take place locally or affect heterogeneously the local elastic properties of the arterial tree and, hence, the assumption of uniform global stiffening may compromise the accuracy of the model predictions.

On this note, a number of studies have published findings supporting the preferential stiffening of the central arteries with increasing age [9]. In young adults, the distensibility gradient from proximal aorta to peripheral arteries is steep, with proximal aorta being very compliant (local pulse wave velocity, PWV, typically less than 4 m/s) and the peripheral muscular arteries significantly stiffer. Arterial stiffening with age takes place in a non-uniform way, with stiffening being much more pronounced in the proximal aorta than in the peripheral arteries [9]. In a previous work, we studied the implications of this age-related non-uniform stiffening on the wave transmission characteristics and reported a significant increase in the forward wave amplitude with age as well as a decrease in pulse pressure amplification from central to peripheral arteries [10].

In consideration of the aforementioned facts, the present work aimed at highlighting the importance of considering the age-related non-uniform stiffening of the arteries when adapting the parameters of the arterial tree. Concretely, we developed a methodology that uses as model inputs the subject's age, aortic flow and peripheral blood pressure and accordingly adjusts the arterial parameters. More particularly, the compliance of the central and peripheral arterial segments are adjusted differently for younger and older individuals according to literature trends on the evolution of the aortic stiffness with ageing. The proposed methodology was tested and validated against *in vivo* data from a population of both healthy and diseased adults. We find that the tuned arterial tree models are capable of accurately capturing the elastic properties of the aorta and the hemodynamic profile of each subject, reproducing the expected pressure phenotypes. Finally, these tools could possibly be further exploited to derive central hemodynamic indices of importance, such as central pressures.

2.2.2 Methods

Brief description of the 1D model of the arterial tree

The generic 1D model of the systemic circulation, previously developed by Reymond et al. [11] and validated by [12], consists of 103 arterial segments (Figure 1.3:10) which are considered as flexible tapered tubes. The governing equations are based on the integration of the continuity and momentum conservation equations over the arterial cross-section complemented with a constitutive relation relating distending pressure and cross-sectional area. The wall shear stress is approximated using the Witzig-Womersley theory [13]. The arterial wall behavior is viscoelastic and nonlinearly elastic [14], whereby the local arterial compliance has a pressure-dependent component (C_p) and a location-dependent component (C_d) [15]. The latter function can be calculated for a reference pressure of $P_{ref}=100$ mmHg and for an average cross-sectional area (A) according to the local pulse wave velocity:

$$C_d(d) = \frac{A}{\rho PWV^2(d)}$$

Equation 2.2:1 – Arterial compliance as a function of the pulse wave velocity

In the initial 1D model of Reymond et al. [11], a global empirical relationship relating PWV and vessel diameter was developed based on previously published data for a healthy young male adult. At the terminal sites, the vascular beds are modeled using 3-element Windkessel models, where the distribution of terminal resistance in proximal and distal resistances was chosen so that it yields minimal reflections. At the proximal end, the arterial tree either receives a prescribed aortic flow waveform or is coupled with a time-varying elastance model of the left ventricle [16], [17].

Considerations on non-uniform arterial stiffening along the aorta

The arterial compliance and especially its location-dependent component $C_d(d)$ vary significantly between individuals. Compliance is affected by many factors, with age being the predominant one. A study by Cho et al. [18] compared young and old patients with untreated hypertension and showed that the young hypertensive group had significantly lower central PWVs than the older age group despite showing higher levels of peripheral blood pressure. This suggests that PWV is mainly affected by age rather than blood pressure levels.

In terms of model personalization, the local PWV should ideally be known for all arterial locations in order to precisely calculate the compliance of a patient's arterial tree. Of particular interest is the compliance gradient along the aorta, which is substantially altered during ageing. Ageing leads to gradual and non-uniform loss of the elasticity of the arteries, whereby the central aorta is more affected than the periphery [9]. As a result of this heterogeneous alteration, the pressure waveforms in older subjects -often referred to as Type A waveforms- are characterized by a dominant late systolic peak and a shoulder with inflection on the upstroke [19]. The dominant late systolic peak is primarily attributed to augmented forward wave component amplitude due to the stiffened proximal aorta and to a lesser extent to augmented and earlier arriving reflections [10], [19]. In previous work, we incorporated this non-uniform stiffening of the arterial tree with age into the model by developing averaged distensibility curves for each age decade from 30 to 80 years old based on literature data and were able to reproduce the expected aortic pressure wave shapes [10].

To show the importance of non-uniform aortic stiffening in the development of aortic systolic hypertension while preserving the "correct" aortic phenotype, Reymond et al. [20] simulated aortic stiffening with age in two ways: first, by equally reducing compliance uniformly in all arteries ("global stiffening") and, second, by applying a non-uniform stiffening whereby, in accordance to observations, proximal aorta is stiffened more than peripheral vessels ("local stiffening"). The results are shown in Figure 2.2:1. The reduction in total arterial compliance was the same (-29%) in both global and local stiffening. Both global and local stiffening yielded the same pulse pressure increase of 45% and the same systolic pressure in the root of the proximal aorta, however, local non-uniform stiffening was the one that produced a physiologically relevant aortic pressure phenotype, resembling more the *Type A* waveforms. Reymond et al. [20] noted also that a decrease in compliance under local proximal aortic stiffening leads to higher carotid-to-femoral pulse wave velocities (c-f PWV) when compared to global stiffening, the difference being attributed to the more pronounced stiffening of the aorto-femoral path.

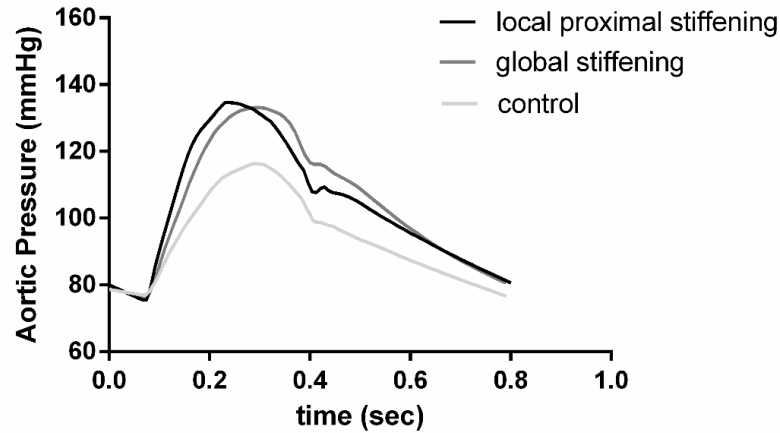


Figure 2.2:1 Pressure waveforms at the proximal ascending aorta for the control case (light gray line), after local proximal stiffening (black line) and global arterial stiffening (gray line) for the same pulse pressure increase (+45%).

Method for adaptation of the distensibility-diameter curve

Based on the aforementioned observations we put forward the following methodology for incorporating the effects of ageing during the adaptation of the 1D arterial model. For young subjects, we simply apply global stiffening of the arterial tree, meaning that the area compliances of all arteries are scaled with one global scaling factor. For older individuals we apply the local stiffening approach, whereby compliance of only the aortic segments (segments 1-95-2-14-18-27 of the arterial tree as shown in Figure 1.3:10) is adjusted. In detail, the subject is initially categorized according to his/her age in the younger or older age group. The age of 50 years was used as the cut-off value for grouping in the present study, as vascular ageing is reported to accelerate after this threshold [18]. As an initial approximation of the subject's arterial tree we use the "average" arterial compliance values expected for his/her age, as presented in our previous ageing model [10]. The simulation runs using as model input the recorded aortic flow. Subsequently, we compare the model-predicted brachial systolic (SBP) and diastolic blood pressure (DBP) to the measured values and if the error is significant, we adjust the arterial compliance applying either global or local stiffening. Peripheral resistance is also calculated and adjusted as the ratio of the mean arterial pressure over the measured cardiac output. Finally, the arterial geometry is adjusted according to the measured aortic diameter via multiplication of all internal diameters with a uniform factor.

Validation against *in vivo* data

The method described above was tested with *in vivo* data collected previously by Papaioannou et al. [21]. Method accuracy and bias were assessed by comparing a) the model-estimated carotid-to-femoral PWV with the corresponding values measured by a reference technique (SphygmoCor, AtCor, Sydney Australia) and b) the model-estimated aortic pressure (in terms of both magnitude and shape) with the predictions from the Mobil-O-Graph device (IEM GmbH, Stolberg, Germany).

The database included the hemodynamic and cardiovascular recordings from 24 patients who underwent noninvasive cardiovascular risk assessment. Out of the 24 patients, four were excluded from the study as their cardiac ultrasound or applanation tonometry data were lacking or unreliable for use. The study population included both genders and covered a variety of health conditions, including hypertension, cardiovascular disease and stroke [21].

Data recording and analysis

During the *in vivo* investigation two repeated measurements of the proximal aortic peak velocity profile were acquired via transthoracic 2D Doppler echocardiography. Both measurements were conducted by an experienced cardiologist at supine position and according to the recommendations of [22]. Blood flow was calculated from the peak velocity profiles following the Witzig-Womersley theory [13] and assuming a constant cross-sectional area. The model input aortic flow was set equal to the average of the two measured flow curves.

Peripheral systolic and diastolic pressure values were recorded at the brachial artery using the Mobil-O-Graph device, which has been thoroughly validated in the past [23]. This device also allows for the reconstruction of the aortic pressure and the extraction of key waveform features, such as the central Augmentation Index (Alx). The central Alx is a measure of wave reflections and reflects the percentage of the total pulse pressure that can be attributed to the reflected pulse wave [19]. A number of studies have previously validated the use of the Mobil-O-Graph for noninvasive estimating central pressure [24]–[27]. Accordingly, good agreement has been shown between the Mobil-O-Graph-derived Alx and other common tonometric devices [28]. In our study, both estimates of aortic SBP and Alx were extracted and were thereafter used as reference values.

Carotid-to-femoral PWV was measured via applanation tonometry using the SphygmoCor system, which has the advantage of recording signals of carotid and femoral pressure in parallel – thus avoiding the need of synchronization. This device is also often used for the reconstruction of the aortic pressure wave [3] from the recorded radial pressure waves [29] and has shown quite reliable results in previous validation studies [30], [31]. However, in the present study we used as reference for the aortic pressure the Mobil-O-Graph data so as to ensure that the recordings of peripheral pressure and the estimates of central pressure were simultaneous, as discussed below. More details on the measurement protocol can be found in the original publication [21].

For each patient, we used the recorded data and the methodology described above to tune the arterial tree parameters proximally and distally. The tuned models allowed for the derivation of the c-f PWV, which was calculated analytically by the compliance of each arterial segment in the aortic-femoral path based on the Bramwell-Hill equation (Equation 1.3:1). Furthermore, the model-produced proximal aortic pressure curves were processed to derive the SBP and the central Alx, as explained in [19]. The computed values were then compared with the corresponding estimates of the Mobil-O-Graph device.

Statistical analysis

Correlation, accuracy and agreement between the model-based estimates and the *in vivo* recordings of c-f PWV were assessed using the Pearson's (r) and Spearman's (ρ) correlation coefficients, the intraclass correlation coefficient (ICC), the normalized root mean square error (nRMSE) and the Bland-Altman analysis [32]. High values of r and ρ reflect good correlation in terms of linearity and direction. Bias was estimated by the mean difference (\bar{d}) and the standard deviation of the differences (SD). The limits of agreement were set at $\bar{d} + 2SD$ and $\bar{d} - 2SD$, as 95% of the prediction errors for a normal distribution are expected to lie in this range. The Bland-Altman analysis was further used to assess the agreement between the model-derived aortic pressure and Alx with the respective estimates of the Mobil-O-Graph. The Mann-Whitney non-parametric test was used for the evaluation of differences of continuous variables between the two age groups. Statistical significance was accepted for p-values lower than 0.05. Data analysis was performed using the GraphPad Prism software and Matlab.

2.2.3 Results

Table 2.2:1 summarizes the hemodynamic parameters of the 20 patients, separated in two age groups (below and above 50 years old). Cardiac output, central and peripheral blood pressure and c-f PWV are reported. As expected, the younger age group ($n=16$) exhibited significantly lower carotid-to-femoral pulse wave velocities than the older group ($n=4$).

Table 2.2:1 Hemodynamic values of the study population categorized into the two age groups.

| | Total sample ($n=20$) | Age group I (age < 50 years old) ($n=16$) | Age group II (age \geq 50 years old) ($n=4$) | p-value |
|-----------------------|----------------------------|---|--|---------|
| Males/Females, n | 11/9 | 8/8 | 3/1 | 0.59 |
| Age (years) | 38.4 ± 13.6 | 32.3 ± 5.1 | 62.5 ± 7.9 | <0.05 |
| Central SBP (mmHg) | 110.0 ± 11.2 | 108.9 ± 11.6 | 114.4 ± 9.2 | 0.33 |
| Central DBP (mmHg) | 78.6 ± 8.8 | 77.3 ± 8.4 | 83.6 ± 10.0 | 0.26 |
| Peripheral SBP (mmHg) | 116.3 ± 10.7 | 115.0 ± 11.1 | 121.5 ± 8.2 | 0.24 |
| Peripheral DBP (mmHg) | 77.6 ± 8.7 | 76.4 ± 8.2 | 82.4 ± 10.1 | 0.35 |

| | | | | |
|---------------|-----------------|-----------------|-----------------|-------|
| c-f PWV (m/s) | 6.9 ± 1.9 | 6.0 ± 0.6 | 10.3 ± 0.9 | <0.05 |
| HR (bpm) | 70.4 ± 10.3 | 69.7 ± 10.6 | 73.0 ± 10.1 | 0.70 |
| CO (L/min) | 4.2 ± 1.0 | 4.0 ± 0.9 | 5.1 ± 1.1 | 0.07 |

SBP: systolic blood pressure, DBP: diastolic blood pressure, c-f PWV: carotid-to-femoral pulse wave velocity, HR: heart rate, CO: cardiac output

Figure 2.2:2 (left) shows a box plot of the model estimates against the measured c-f PWV values along with their confidence intervals. The Bland-Altman plot in Figure 2.2:2 (right) depicts the difference between the model-derived c-f PWV values and the respective SphygmoCor c-f PWV values against their mean. The limits of agreement are also illustrated by the two horizontal, continuous lines. The mean error in the estimation of c-f PWV was 0.14 m/s, with limits of agreement equal to 1.7 and -1.4 m/s. The greatest deviations are observed at high c-f PWVs; it should be noted, however, that for these c-f PWV values the confidence intervals of the reference device were wide, in the order of magnitude of 1 m/s. An overview of statistical parameters of agreement, accuracy and correlation is also given in Table 2.2:2.

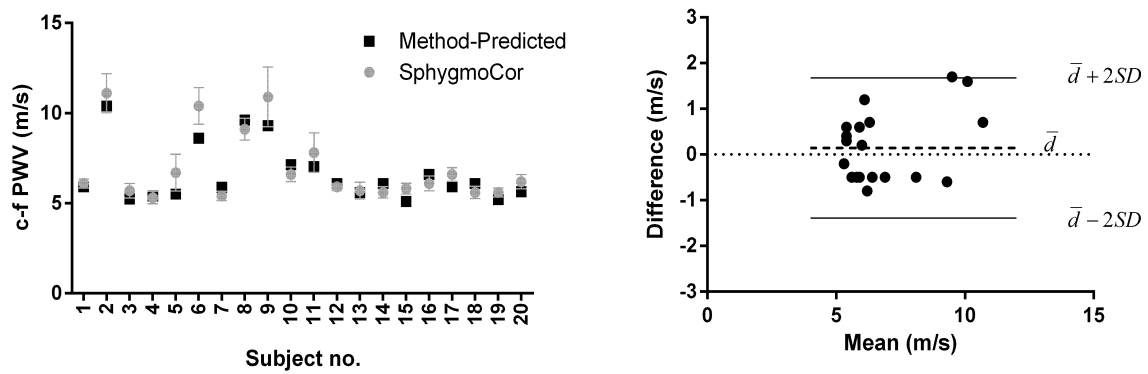


Figure 2.2:2 (left) Method-estimated c-f PWV values plotted against the reference SphygmoCor values along with their respective confidence intervals. (right) The Bland-Altman plot of the difference between the estimated and reference c-f PWV values against their means. Mean difference (\bar{d}) as well as 95% confidence intervals ($\pm 2SD$ around the mean difference) are depicted with a continuous and dashed lines respectively.

Table 2.2:2 Indices of correlation, accuracy and agreement between the measured and method-derived c-f PWV values.

| | | |
|--------------------|--|-------------|
| Correlation | Pearson's correlation coefficient, r | 0.92 |
| | Spearman's correlation coefficient, ρ | 0.99 |
| | Intraclass correlation coefficient, ICC | 0.90 |
| Accuracy | Normalized root mean square error, nRMSE | 11.1% |
| Agreement | Mean difference, \bar{d} (m/s) | 0.14 |
| | Standard deviation of difference, SD (m/s) | 0.77 |
| | Limits of agreement (m/s) | 1.68, -1.39 |

The scatterplots and Bland-Altman plots for the aortic systolic pressure and augmentation index as derived by the Mobil-O-Graph device and as predicted by the model are also shown in Figure 2.2:3. The mean difference of aortic systolic pressure was equal to 2.3 mmHg, with SD of difference 3.0 mmHg. The nRMSE was 3.3%. It is noted that there is no particular trend of the differences to vary with the mean SBP. Accordingly, the model predictions for the Alx were in good agreement with the Mobil-O-Graph estimates; the mean difference was 4.25% with an SD of 3.7%.

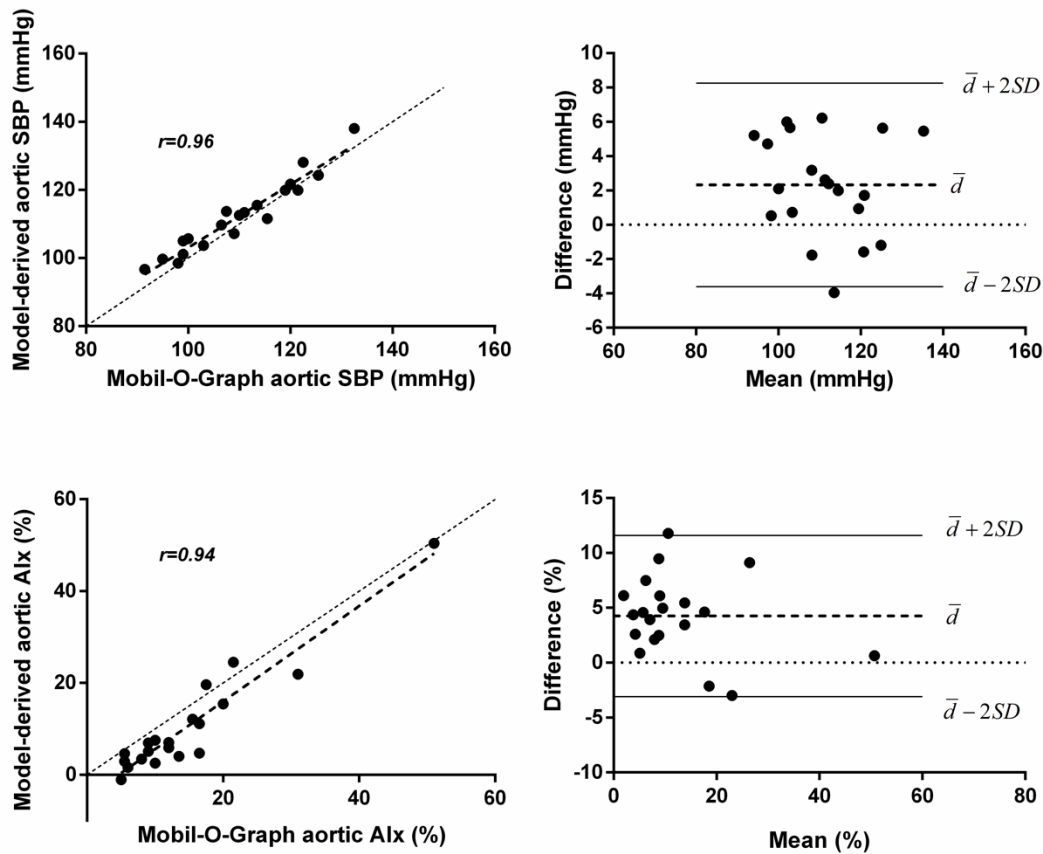


Figure 2.2:3 Comparison of the method-predicted aortic SBP and central augmentation index against the values predicted by the Mobil-O-Graph device. (top left) Scatterplot of the aortic SBP as computed by the method and as predicted by the Mobil-O-Graph device. (top right) The Bland-Altman plot of the difference between the model-estimated and Mobil-O-Graph aortic SBP values against their means. (bottom left and right) The respective scatterplot and Bland-Altman plot for the central augmentation index as computed by the method and as predicted by the Mobil-O-Graph device. Mean difference (\bar{d}) as well as 95% confidence intervals ($\pm 2SD$ around the mean difference) are depicted with a continuous and dashed lines respectively.

Moreover, Figure 2.2:4 depicts the aortic pressure waveforms as predicted by the tuned model for two different subjects. The left plot corresponds to the simulation results of a 52-year-old male and the right plot to a 30-year-old female. We clearly observe that the pressure waveform for the older subject resembles the characteristic Type A phenotype, producing the anticipated shoulder with inflection at the upstroke. Conversely, for the younger subject the model predicts a smooth upstroke, which resembles the Type C phenotype.

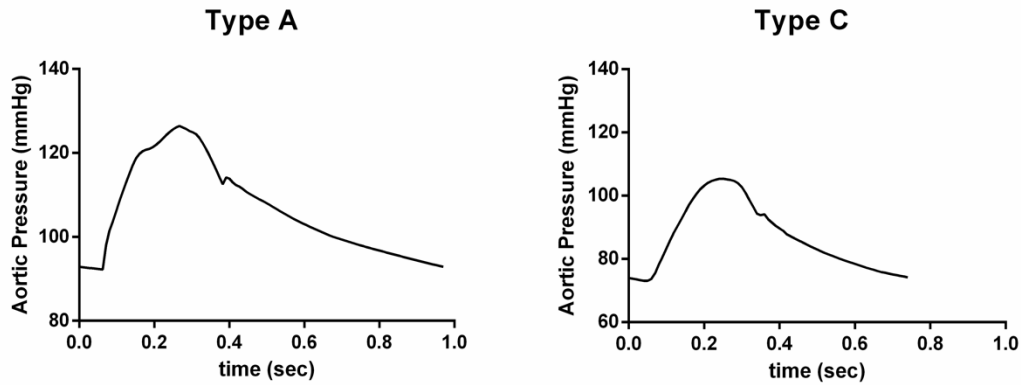


Figure 2.2:4 Aortic pressure waveforms derived from the model simulations for two subjects: (left) the characteristic Type A pressure phenotype of a 52-year-old male and (right) the Type C phenotype of a 30-year-old female.

2.2.4 Discussion

In this study, we presented a simple technique to tune the parameters of a previously validated 1D model of the systemic circulation based on noninvasive measurements of proximal aortic flow and brachial sphygmomanometric pressure alone. This was motivated by: a) our observations and experience from modelling the heterogeneous effects of ageing on arterial distensibility, b) previous work from our group on the differential effects of different mechanisms of arterial stiffening on central hemodynamics [20]. We hypothesized that it is possible to effectively tune the distensibility-diameter curve of the arterial tree by applying either a local proximal or a global stiffness adjustment factor according to the patient's age.

The validation of the proposed arterial tree tuning methodology against *in vivo* data of both healthy and diseased adults yielded encouraging results. It was shown that the estimated carotid-to-femoral PWV, which is the most commonly used quantity as surrogate to aortic compliance, was in good agreement with the respective measurement of c-f PWV made by applanation tonometry (SphygmoCor apparatus). We reported a small bias, $d=0.14$ m/s, and SD of differences, $SD=0.77$ m/s. This small bias is quite lower than the observed intra-observed reproducibility of c-f PWV measurement [33]. In general, the estimation errors were greater for the older subjects, whose c-f PWVs were higher. Although the older sample was small ($n=4$) – a limitation that is discussed more thoroughly below –, we noted that the proposed technique was able to capture the expected pattern of increased c-f PWV for older ages. On the contrary, if we had employed only the global stiffening mechanism for the older adults, this would have led to a severe underestimation of the computed c-f PWVs, namely it would have increased the average estimation error for the older group from -0.9 m/s to -3.7 m/s.

Interestingly, we found that, irrespective of the stiffening mechanism employed, the resulting increase in pulse pressure is dictated primarily by the loss in the total arterial compliance of the tree. In other words, the increase in pulse pressure seems not to be affected by the exact topology where the stiffening occurs (non-uniform local or global) but rather by the overall compliance of the arterial tree. This finding is in good agreement with previous studies and supports the methodology by Stergiopoulos et al. [34], who proposed the Pulse Pressure Method (PPM), a simple 2-element Windkessel-based method for the estimation of total arterial compliance.

It is important to note that the proposed technique might not achieve the exact personalization of the distributed model of the arterial tree, as it is based on an average model adjusted following population-averaged trends. However, as discussed before, the exact personalization of the arterial tree model presents major challenges, primarily due to the need of a large amount of input data. Conversely, our aim here was to highlight the importance of considering the non-uniform stiffening of the arterial tree when adjusting the model parameters for aged individuals. Accordingly, we developed 'approximate' distributed models, which were capable of faithfully capturing key features of the hemodynamics of ageing. In our simulations, we showed that we are able to replicate the characteristic aortic pressure phenotypes only by employing different stiffening mechanisms according to the subject's age (Figure 2.2:4).

In that context, it is important to consider the possible application of these simulations to derive central indices noninvasively. For example, this technique could be combined with our previously proposed methodology [8] for the noninvasive estimation of the end-systolic elastance, an index which serves as the gold-standard measure of cardiac contractility and is, therefore, of particular interest to clinicians.

Another potential application of the presented method is the derivation of the central aortic pressure, which carries more valuable prognostic value for cardiovascular damage than peripheral pressure [35]. Due to the importance of the central aortic pressure, a number of previous studies have proposed noninvasive methods for its derivation.

A recent study by Tosello et al. [36] developed and validated a technique for the estimation of central blood pressure via adjustment of a multiscale mathematical model according to brachial pressure, height, weight, age, left-ventricular end-systolic and end-diastolic volumes and central pulse wave velocity. The validation of their method showed significant overestimation of systolic blood pressure and underestimation of diastolic pressure when compared to the SphygmoCor device, with mean differences equal to 7.8 mmHg and -3.2 mmHg, respectively.

Another study [37] proposed a methodology for the adjustment of the distributed model parameters from measures of the proximal and distal radial pulse waves and the subsequent calculation of the aortic-to-radial transfer function. Their experimental results for central pressure estimation showed better performance than the broadly clinically used generalized transfer function and n-point moving average techniques.

A promising technique for deriving central blood pressure via standard automatic arm cuff was proposed by [38]. Their method leverages physiologic modeling to first accurately derive brachial blood pressure from the oscillogram and then calculates the central pressure via variable transfer functions, in which the pulse transit time is adjusted accordingly. Their technique was validated and was found more reliable than other noninvasive devices. This paper presents a novel multiple measurement information fusion approach to the estimation of cardiovascular risk predictors from noninvasive pulse volume waveforms measured at the body's diametric (arm and ankle) locations. Leveraging the fact that diametric pulse volume waveforms originate from the common central pulse waveform, the approach estimates cardiovascular risk predictors in three steps by: (1) deriving lumped-parameter models of the central-diametric arterial lines from diametric pulse volume waveforms, (2) estimating central blood pressure waveform by analyzing the diametric pulse volume waveforms using the derived arterial line models, and (3) estimating cardiovascular risk predictors (including central systolic and pulse pressures, pulse pressure amplification, and pulse transit time) from the arterial line models and central blood pressure waveform in conjunction with the diametric pulse volume waveforms. Experimental results obtained from 164 human subjects with a wide blood pressure range (systolic 144 mmHg and diastolic 103 mmHg) showed that the approach could estimate cardiovascular risk predictors accurately ($r \geq 0.78$). Further analysis showed that the approach outperformed a generalized transfer function regardless of the degree of pulse pressure amplification. The approach may be integrated with already available medical devices to enable convenient out-of-clinic cardiovascular risk prediction.

Ghasemi et al. [39] recently published a paper on the estimation of cardiovascular risk from noninvasive pulse volume waveforms. Their method leverages the fact that pulse wave measured at peripheral sites, i.e. arm and ankle, both originate from the ascending aorta. Consequently, in a first step, they fit the parameters of a transmission line model according to multiple peripheral measurements. In a second step, they derive the central blood pressure waveform and then estimate cardiovascular risks. Their model was trained and validated with *in vivo* data from 164 subjects and showed better performance than the generalized transfer function. Ebrahimi et al. [40] also published a similar concept that relies on a model-parameter identification approach to assess cardiovascular risk. Their methodology employs a tube-load model of wave propagation and reflection, where the proximal and distal blood pressure waveforms are inputted. The lumped parameter model is, subsequently, individualized and the algorithm recognizes unphysiological patterns in the model parameters. Although this is a preliminary work and consists of a simplified model, it demonstrates the great potential of using vascular models for disease diagnosis.

The current method presents a significant advantage, as it employs a complete, distributed 1D model of the arterial tree, in which the heterogeneous effects of ageing on the arterial stiffness can be incorporated. In our study, we found that the estimated aortic systolic pressure was in good agreement with the estimates given by the Mobil-O-Graph device, the mean difference being 2.3 mmHg. We did not notice a particular trend for errors in the aortic SBP estimation as function of age or hypertension. Accordingly, the method yielded accurate estimation of the aortic Alx. The central Alx is a hemodynamic parameter of importance, as it depends on the arterial stiffness and the reflective properties of the arteries [41]. It is related to risk factors for cardiovascular disease and serves as predictor of morbidity and mortality [42]–[44]. Therefore, there is potential in applying the proposed technique in the clinic as a

noninvasive tool for central pressure monitoring and risk stratification. Our future work will investigate this potential by validating the method against invasive pressure data.

An interesting potential of the proposed modelling approach is that there can be an interchange between the model inputs and the output qualities. We showed that when age, aortic flow and brachial pressure are known, it is possible to estimate accurately the compliance of the central arteries and thus effectively describe the arterial tree of a patient. This scheme could potentially be reformulated and adjusted in order to receive as inputs the age, central compliance and brachial pressure of the patient and yield his/her cardiac output, the monitoring of which constitutes a major hurdle in the actual clinical practice [45].

General considerations and limitations

An important point to be made pertains to the use of the carotid-to-femoral PWV as an accurate index of the aortic wall elasticity. Previous studies have questioned the utility of c-f PWV as a clinical measure of central stiffness and hence as a diagnostic marker for early vascular stiffening. More specifically, Cuomo et al. [46] undertook a fluid-structure interaction (FSI) study to simulate the effects of ageing on the regional wall properties of the human aorta and showed that c-f PWV correlated poorly with the circumferential stiffness (imposed on the model). Conversely, other metrics which are directly linked to arterial geometry, such as the local distensibility, demonstrated better correlation with structural stiffness. These results were also corroborated by their subsequent study [47], which combined *in vivo* and *in vitro* data to build state-of-the-art, patient-specific FSI mouse models; they reported that changes in PWV did not capture well the regional differences in the corresponding material stiffness properties, particularly when comparing between males and females. They suggested that this discrepancy can be attributed mainly to two factors, namely the dependency of PWV on the non-uniform arterial geometry (which is not accounted for in the simplified equation by Moens-Korteweg), and the use of an approximate path length between the two signal recordings (commonly assumed 80% of the direct tape-measured distance [48]).

Although these computational studies show poor correlation between c-f PWV and material properties, c-f PWV agrees well with regional measures of compliance. Previous studies, such as [49]–[51], have shown that the c-f PWV is strongly related to measures of aortic arch compliance, but with a trend to overestimate it; conversely, it correlates better with descending and abdominal distensibility. This might be attributed to the fact that the carotid-to-femoral path excludes the ascending aorta and the aortic arch, which are highly compliant in the young.

In that context, we recognize that the c-f PWV is an average index of the aortic elasticity and might reflect more the properties of the descending thoracic and abdominal part. Therefore, in the present study, we can only maintain that the methodology captures well the average elastic properties of the aorta. Our future work will be oriented towards investigating the accuracy of the proposed method against detailed *in vivo* data on the regional PWV measured at multiple aortic sites.

As discussed above, despite having access to both the SphygmoCor and Mobil-O-Graph aortic pressure estimates, we chose to use only the latter values as a reference for our comparisons. This was done primarily to ensure that the reference aortic pressure was simultaneously recorded with the brachial pressure that drove the optimization process. Using the SphygmoCor reconstructed aortic pressure waves as reference values would significantly affect the accuracy of the estimation of aortic SBP reported, namely the nRMSE would increase from 3.3% to 13.4%.

Furthermore, a few limitations of the present study need to be acknowledged. This method is based on a generalized model of the ageing systemic circulation that was previously developed according to published data [10]. As briefly discussed above, this entails that the tuned model does not necessarily represent the patient-specific conditions. It is rather an ‘approximately personalized’ model, which however captures key hemodynamical indices. The tuning technique could be better refined to incorporate factors such as gender, body mass index, etc. Moreover, as the tuning algorithm was designed based on physiological data, the effects of certain pathologies (e.g. atherosclerosis, coronary artery disease, etc.) are not taken into account and hence the quality of the tuning process and the resulting predictions may be compromised. Nevertheless, it should be noted that the *in vivo* validation of the method was conducted on a population of both physiological and pathological cases.

Methodological considerations regarding the measurement protocol have been presented in detail in the previous publication by Papaioannou et al. [21]. As discussed above, the Mobil-O-graph device does not provide a direct measurement of the aortic pressure, but makes use of transfer functions to noninvasively estimate it. However, the use of this device is well justified, given its good performance in previous validation studies. Although ageing is related to an increase in SBP with a concomitant decrease in DBP [52], in our sample the difference in SBP and DBP values between the two age groups was not found statistically significant. This can be

attributed to the small sample size used as well as to the fact that the study population included both healthy and diseased adults. The older age group includes only 4 subjects, limiting our ability to generalize our conclusions. Our database was extracted from a previous study that aimed at the validation of a novel method for cardiac output monitoring and thus did not focus on an equal distribution between young and old patients. Nevertheless, it is important to point out that this was essentially a proof-of-concept study. Despite the small sample size, our method was able to predict a significant difference in the estimated c-f PWV between the two age groups and to produce the characteristic Type A pressure waveforms for the older subjects. This encourages us to continue the validation process in a greater sample of both genders with different age groups and on a wider range of pathologic conditions.

Conclusions

In this study, we showed the importance of considering the heterogeneous effects of ageing on the arterial distensibility when adapting the properties of a distributed model. We showed that if we differentiate between young and old subjects and accordingly employ different mechanisms of arterial stiffening we are able to capture : i) the expected increase in the carotid-to-femoral PWV with age and ii) physiologically relevant aortic pressure waveforms, both in terms of magnitude (SBP) and wave reflections (Aix). Accordingly, we proposed a technique for effectively tuning a 1D model of the arterial tree using noninvasive measurements and a previously developed model of the ageing cardiovascular system. The proposed methodology was tested using *in vivo* data from a population of healthy and diseased subjects and showed encouraging results. The tuned models predicted accurately the carotid-to-femoral PWV and the central systolic blood pressure, which encourages us to further investigate the method validity in larger samples. This *in silico* approach could find wide application in the derivation of central hemodynamic variables that are indispensable in the clinical reality, improving our understanding of central hemodynamics and paving the way for novel personalized diagnostic tools.

2.2.5 Bibliography

- [1] G. F. Mitchell *et al.*, "Arterial stiffness and cardiovascular events: The Framingham Heart Study," *Circulation*, vol. 121, no. 4, pp. 505–511, Feb. 2010, doi: 10.1161/CIRCULATIONAHA.109.886655.
- [2] L. S. Nguyen and P. Squara, "Non-Invasive Monitoring of Cardiac Output in Critical Care Medicine," *Front. Med.*, vol. 4, Nov. 2017, doi: 10.3389/fmed.2017.00200.
- [3] M. Karamanoglu, M. F. O'Rourke, A. P. Avolio, and R. P. Kelly, "An analysis of the relationship between central aortic and peripheral upper limb pressure waves in man," *Eur. Heart J.*, vol. 14, no. 2, pp. 160–167, Feb. 1993.
- [4] C. H. Chen *et al.*, "Estimation of central aortic pressure waveform by mathematical transformation of radial tonometry pressure. Validation of generalized transfer function," *Circulation*, vol. 95, no. 7, pp. 1827–1836, Apr. 1997.
- [5] A. A. Udy, M. Altukroni, P. Jarett, J. A. Roberts, and J. Lipman, "A comparison of pulse contour wave analysis and ultrasonic cardiac output monitoring in the critically ill," *Anaesth. Intensive Care*, vol. 40, no. 4, pp. 631–637, Jul. 2012.
- [6] M. T. Ganter *et al.*, "Continuous cardiac output measurement by un-calibrated pulse wave analysis and pulmonary artery catheter in patients with septic shock," *J. Clin. Monit. Comput.*, vol. 30, no. 1, pp. 13–22, Feb. 2016, doi: 10.1007/s10877-015-9672-0.
- [7] G. F. Mitchell *et al.*, "Arterial stiffness, pressure and flow pulsatility and brain structure and function: the Age, Gene/Environment Susceptibility--Reykjavik study," *Brain J. Neurol.*, vol. 134, no. Pt 11, pp. 3398–3407, Nov. 2011, doi: 10.1093/brain/awr253.
- [8] S. Z. Pagouladou and N. Stergiopoulos, "Estimating Left Ventricular Elastance from Aortic Flow Waveform, Ventricular Ejection Fraction, and Brachial Pressure: An In Silico Study," *Ann. Biomed. Eng.*, vol. 46, no. 11, pp. 1722–1735, Nov. 2018, doi: 10.1007/s10439-018-2072-0.
- [9] E. Kimoto *et al.*, "Preferential stiffening of central over peripheral arteries in type 2 diabetes," *Diabetes*, vol. 52, no. 2, pp. 448–452, Feb. 2003.
- [10] S. Pagouladou and N. Stergiopoulos, "Evolution of aortic pressure during normal ageing: A model-based study," *PLoS ONE*, vol. 12, no. 7, Jul. 2017, doi: 10.1371/journal.pone.0182173.
- [11] P. Reymond, F. Merenda, F. Perren, D. Rüfenacht, and N. Stergiopoulos, "Validation of a one-dimensional model of the systemic arterial tree," *Am. J. Physiol. - Heart Circ. Physiol.*, vol. 297, no. 1, pp. H208–H222, Jul. 2009, doi: 10.1152/ajpheart.00037.2009.

- [12] P. Reymond, Y. Bohraus, F. Perren, F. Lazeyras, and N. Stergiopulos, "Validation of a patient-specific one-dimensional model of the systemic arterial tree," *Am. J. Physiol. Heart Circ. Physiol.*, vol. 301, no. 3, pp. H1173–1182, Sep. 2011, doi: 10.1152/ajpheart.00821.2010.
- [13] J. Womersley, "An Elastic Tube Theory of Pulse Transmission and Oscillatory Flow in Mammalian Arteries," *WADC Tech. Rep. - TR56-614*, 1957.
- [14] R. Holenstein, P. Niederer, and M. Anliker, "A viscoelastic model for use in predicting arterial pulse waves," *J. Biomech. Eng.*, vol. 102, no. 4, pp. 318–325, Nov. 1980.
- [15] Langewouters G. J., "Visco-elasticity of the human aorta in vitro in relation to pressure and age," PhD Thesis, Free University of Amsterdam, The Netherlands, 1982.
- [16] K. Sagawa, "The end-systolic pressure-volume relation of the ventricle: definition, modifications and clinical use," *Circulation*, vol. 63, no. 6, pp. 1223–1227, Jun. 1981.
- [17] H. Suga and K. Sagawa, "Instantaneous pressure-volume relationships and their ratio in the excised, supported canine left ventricle," *Circ. Res.*, vol. 35, no. 1, pp. 117–126, Jul. 1974.
- [18] S. K. Cho *et al.*, "Effects of age on arterial stiffness and blood pressure variables in patients with newly diagnosed untreated hypertension," *Korean Circ. J.*, vol. 45, no. 1, pp. 44–50, Jan. 2015, doi: 10.4070/kcj.2015.45.1.44.
- [19] J. P. Murgo, N. Westerhof, J. P. Giolma, and S. A. Altobelli, "Aortic input impedance in normal man: relationship to pressure wave forms," *Circulation*, vol. 62, no. 1, pp. 105–116, Jul. 1980.
- [20] P. Reymond, N. Westerhof, and N. Stergiopulos, "Systolic hypertension mechanisms: effect of global and local proximal aorta stiffening on pulse pressure," *Ann. Biomed. Eng.*, vol. 40, no. 3, pp. 742–749, Mar. 2012, doi: 10.1007/s10439-011-0443-x.
- [21] T. G. Papaioannou *et al.*, "First in vivo application and evaluation of a novel method for non-invasive estimation of cardiac output," *Med. Eng. Phys.*, vol. 36, no. 10, pp. 1352–1357, Oct. 2014, doi: 10.1016/j.medengphy.2014.06.019.
- [22] M. A. Quiñones, C. M. Otto, M. Stoddard, A. Waggoner, and W. A. Zoghbi, "Recommendations for quantification of Doppler echocardiography: A report from the Doppler quantification task force of the nomenclature and standards committee of the American Society of Echocardiography," *J. Am. Soc. Echocardiogr.*, vol. 15, no. 2, pp. 167–184, Feb. 2002, doi: 10.1067/mje.2002.120202.
- [23] W. Wei, M. Tölle, W. Zidek, and M. van der Giet, "Validation of the mobil-O-Graph: 24 h-blood pressure measurement device," *Blood Press. Monit.*, vol. 15, no. 4, pp. 225–228, Aug. 2010, doi: 10.1097/MBP.0b013e328338892f.
- [24] L. Luzardo *et al.*, "24-h ambulatory recording of aortic pulse wave velocity and central systolic augmentation: a feasibility study," *Hypertens. Res. Off. J. Jpn. Soc. Hypertens.*, vol. 35, no. 10, pp. 980–987, Oct. 2012, doi: 10.1038/hr.2012.78.
- [25] A. D. Protogerou *et al.*, "Feasibility and reproducibility of noninvasive 24-h ambulatory aortic blood pressure monitoring with a brachial cuff-based oscillometric device," *Am. J. Hypertens.*, vol. 25, no. 8, pp. 876–882, Aug. 2012, doi: 10.1038/ajh.2012.63.
- [26] T. Weber *et al.*, "Validation of a brachial cuff-based method for estimating central systolic blood pressure," *Hypertens. Dallas Tex 1979*, vol. 58, no. 5, pp. 825–832, Nov. 2011, doi: 10.1161/HYPERTENSIONAHA.111.176313.
- [27] W. Weiss, C. Gohlisch, C. Harsch-Gladisch, M. Tolle, W. Zidek, and M. van der Giet, "Oscillometric estimation of central blood pressure: validation of the Mobil-O-Graph in comparison with the SphygmoCor device," *Blood Press. Monit.*, vol. 17, no. 3, pp. 128–31, Jun. 2012.
- [28] S. Wassertheurer *et al.*, "A new oscillometric method for pulse wave analysis: comparison with a common tonometric method," *J. Hum. Hypertens.*, vol. 24, no. 8, pp. 498–504, Aug. 2010, doi: 10.1038/jhh.2010.27.
- [29] T. G. Papaioannou, A. D. Protogerou, K. S. Stamatelopoulos, M. Vavuranakis, and C. Stefanadis, "Non-invasive methods and techniques for central blood pressure estimation: procedures, validation, reproducibility and limitations," *Curr. Pharm. Des.*, vol. 15, no. 3, pp. 245–253, 2009.
- [30] T. G. Papaioannou *et al.*, "Accuracy of commercial devices and methods for noninvasive estimation of aortic systolic blood pressure a systematic review and meta-analysis of invasive validation studies," *J. Hypertens.*, vol. 34, no. 7, pp. 1237–1248, 2016, doi: 10.1097/HJH.0000000000000921.
- [31] A. L. Pauca, M. F. O'Rourke, and N. D. Kon, "Prospective evaluation of a method for estimating ascending aortic pressure from the radial artery pressure waveform," *Hypertens. Dallas Tex 1979*, vol. 38, no. 4, pp. 932–937, Oct. 2001.
- [32] J. M. Bland and D. G. Altman, "Statistical methods for assessing agreement between two methods of clinical measurement," *Lancet Lond. Engl.*, vol. 1, no. 8476, pp. 307–310, Feb. 1986.
- [33] T. G. Papaioannou *et al.*, "Assessment of differences between repeated pulse wave velocity measurements in terms of 'bias' in the extrapolated cardiovascular risk and the classification of aortic stiffness: is a single PWV measurement enough?," *J. Hum. Hypertens.*, vol. 26, no. 10, pp. 594–602, Oct. 2012, doi: 10.1038/jhh.2011.76.

- [34] N. Stergiopoulos, J. J. Meister, and N. Westerhof, "Evaluation of methods for estimation of total arterial compliance," *Am. J. Physiol.*, vol. 268, no. 4 Pt 2, pp. H1540-1548, Apr. 1995, doi: 10.1152/ajpheart.1995.268.4.H1540.
- [35] C. Vlachopoulos, K. Aznaouridis, M. F. O'Rourke, M. E. Safar, K. Baou, and C. Stefanadis, "Prediction of cardiovascular events and all-cause mortality with central haemodynamics: a systematic review and meta-analysis," *Eur. Heart J.*, vol. 31, no. 15, pp. 1865–1871, Aug. 2010, doi: 10.1093/eurheartj/ehq024.
- [36] F. Tosello *et al.*, "Central Pressure Appraisal: Clinical Validation of a Subject-Specific Mathematical Model," *PLOS ONE*, vol. 11, no. 3, p. e0151523, Mar. 2016, doi: 10.1371/journal.pone.0151523.
- [37] S. Jiang, Z.-Q. Zhang, F. Wang, and J.-K. Wu, "A personalized-model-based central aortic pressure estimation method," *J. Biomech.*, vol. 49, no. 16, pp. 4098–4106, Dec. 2016, doi: 10.1016/j.jbiomech.2016.11.007.
- [38] K. Natarajan *et al.*, "Central Blood Pressure Monitoring via a Standard Automatic Arm Cuff," *Sci. Rep.*, vol. 7, no. 1, p. 14441, Oct. 2017, doi: 10.1038/s41598-017-14844-5.
- [39] Z. Ghasemi *et al.*, "Estimation of Cardiovascular Risk Predictors from Non-Invasively Measured Diametric Pulse Volume Waveforms via Multiple Measurement Information Fusion," *Sci. Rep.*, vol. 8, no. 1, p. 10433, Jul. 2018, doi: 10.1038/s41598-018-28604-6.
- [40] S. Ebrahimi Nejad, J. P. Carey, M. S. McMurtry, and J.-O. Hahn, "Model-based cardiovascular disease diagnosis: a preliminary in-silico study," *Biomech. Model. Mechanobiol.*, vol. 16, no. 2, pp. 549–560, 2017, doi: 10.1007/s10237-016-0836-8.
- [41] M. F. O'Rourke, A. Pauca, and X.-J. Jiang, "Pulse wave analysis," *Br. J. Clin. Pharmacol.*, vol. 51, no. 6, pp. 507–522, Jun. 2001, doi: 10.1046/j.0306-5251.2001.01400.x.
- [42] London Gérard M., Blacher Jacques, Pannier Bruno, Guérin Alain P., Marchais Sylvain J., and Safar Michel E., "Arterial Wave Reflections and Survival in End-Stage Renal Failure," *Hypertension*, vol. 38, no. 3, pp. 434–438, Sep. 2001, doi: 10.1161/01.HYP.38.3.434.
- [43] M. J. C. A. Van Trijp, C. S. P. M. Uiterwaal, W. J. W. Bos, A. Oren, D. E. Grobbee, and M. L. Bots, "Noninvasive arterial measurements of vascular damage in healthy young adults: relation to coronary heart disease risk," *Ann. Epidemiol.*, vol. 16, no. 2, pp. 71–77, Feb. 2006, doi: 10.1016/j.annepidem.2005.09.005.
- [44] T. Weber *et al.*, "Increased arterial wave reflections predict severe cardiovascular events in patients undergoing percutaneous coronary interventions," *Eur. Heart J.*, vol. 26, no. 24, pp. 2657–2663, Dec. 2005, doi: 10.1093/eurheartj/ehi504.
- [45] A. J. Lee, J. H. Cohn, and J. S. Ranasinghe, "Cardiac Output Assessed by Invasive and Minimally Invasive Techniques," *Anesthesiol. Res. Pract.*, vol. 2011, 2011, doi: 10.1155/2011/475151.
- [46] F. Cuomo, S. Roccabianca, D. Dillon-Murphy, N. Xiao, J. D. Humphrey, and C. A. Figueroa, "Effects of age-associated regional changes in aortic stiffness on human hemodynamics revealed by computational modeling," *PLOS ONE*, vol. 12, no. 3, p. e0173177, Mar. 2017, doi: 10.1371/journal.pone.0173177.
- [47] Cuomo Federica *et al.*, "Sex-dependent differences in central artery haemodynamics in normal and fibulin-5 deficient mice: implications for ageing," *Proc. R. Soc. Math. Phys. Eng. Sci.*, vol. 475, no. 2221, p. 20180076, Jan. 2019, doi: 10.1098/rspa.2018.0076.
- [48] Reference Values for Arterial Stiffness' Collaboration, "Determinants of pulse wave velocity in healthy people and in the presence of cardiovascular risk factors: 'establishing normal and reference values,'" *Eur. Heart J.*, vol. 31, no. 19, pp. 2338–2350, Oct. 2010, doi: 10.1093/eurheartj/ehq165.
- [49] H. Boardman *et al.*, "Aortic stiffness and blood pressure variability in young people: a multimodality investigation of central and peripheral vasculature," *J. Hypertens.*, vol. 35, no. 3, pp. 513–522, Mar. 2017, doi: 10.1097/HJH.0000000000001192.
- [50] A. Dogui *et al.*, "Consistency of aortic distensibility and pulse wave velocity estimates with respect to the Bramwell-Hill theoretical model: a cardiovascular magnetic resonance study," *J. Cardiovasc. Magn. Reson. Off. J. Soc. Cardiovasc. Magn. Reson.*, vol. 13, p. 11, Jan. 2011, doi: 10.1186/1532-429X-13-11.
- [51] Redheuil Alban *et al.*, "Reduced Ascending Aortic Strain and Distensibility," *Hypertension*, vol. 55, no. 2, pp. 319–326, Feb. 2010, doi: 10.1161/HYPERTENSIONAHA.109.141275.
- [52] C. M. McEniery *et al.*, "Normal vascular aging: differential effects on wave reflection and aortic pulse wave velocity: the Anglo-Cardiff Collaborative Trial (ACCT)," *J. Am. Coll. Cardiol.*, vol. 46, no. 9, pp. 1753–1760, Nov. 2005, doi: 10.1016/j.jacc.2005.07.037.

Chapter 3 Influence of Heart on Arterial Hemodynamics

3.1 The effect of left ventricular contractility on arterial hemodynamics: a model-based investigation

Stamatia Pagoulidou¹, Dionysios Adamopoulos², Georgios Rovas¹, Vasiliki Bikia¹, and Nikolaos Stergiopoulos¹

¹ Laboratory of Hemodynamics and Cardiovascular Technology (LHTC), Institute of Bioengineering, Ecole Polytechnique Fédérale de Lausanne (EPFL), Lausanne, Switzerland

² Cardiology Department, Geneva University Hospitals (HUG), Geneva, Switzerland

Abstract

Ventricular-arterial coupling is a major determinant of cardiovascular performance, however, there are still inherent difficulties in distinguishing ventricular from vascular effects on arterial pulse phenotypes. In the present study, we employed an extensive mathematical model of the cardiovascular system to investigate how sole changes in cardiac contractility might affect central and peripheral hemodynamics. First, we simulated two physiologically relevant cases of high and low left ventricular contractility by altering the end-systolic elastance, E_{es} , (3 versus 1 mmHg/mL) under constant cardiac output and afterload. The simulation results were used for pulse wave analysis and wave separation. Increased contractility resulted in a steeper aortic flow waveform with a higher peak value. The aortic pressure waveform changed from the characteristic Type A phenotype to Type C when E_{es} increased, which was accompanied with a decrease in augmentation index, AIx (-2.4% $E_{es} \uparrow$ versus +18.1% $E_{es} \downarrow$). The aortic forward pressure wave component was steeper for high E_{es} , while its amplitude remained unchanged. In the periphery, the radial SBP was higher when E_{es} increased, which caused the pulse pressure amplification to rise drastically (1.86 versus 1.39) and the peripheral AIx to decrease (47.1% versus 76.5%). Our results show that an increase in cardiac contractility alone, with no concomitant change in arterial properties, alters the shape of the forward pressure wave, which, consequently, changes central and peripheral pulse phenotypes. Indices based on the pressure waveform, like AIx , are affected by changes in ventricular function and thus cannot be assumed to reflect only changes in the arterial system.

Key words: Ventricular-arterial coupling • Forward pressure wave • Pulse pressure amplification • Augmentation index

Manuscript submitted for publication

3.1.1 Introduction

The arterial blood pressure is the result of the instantaneous interaction between the left ventricle (LV) of the heart and the arterial system. The ventricular-arterial coupling is a major determinant of left ventricular function and global cardiovascular health [1]–[3]. Accordingly, several physiological and pathological processes are linked with deleterious alterations in one component of the interaction, which gradually compromise the function and structure of its counterpart. Ageing, for example, is linked with the stiffening of the arterial tree [4], [5]; the increase in vascular load triggers remodeling of the LV, which leads to further increases in systemic pressure and so on [6].

Distinguishing myocardial from vascular effects is critical to deciphering the interaction between the two systems and assessing cardiovascular performance. Previous clinical-epidemiological studies have undertaken this task by investigating arterial hemodynamics in normal and diseased human hearts under varying loading conditions and inotropic states [1], [7]–[9]. Particularly, different states of cardiac contractility are often assessed via the use of medication that increases heart rate and cardiac output [7], [8].

However, there are inherent difficulties in studying *in vivo* the hemodynamic effect of purely inotropic changes. First, such studies require invasive techniques to measure intraventricular pressures and volumes, which pose significant risks and are applicable to only special settings. Second, it is practically impossible to isolate myocardial effects, as the agents used influence also the vascular system, often altering mean arterial pressure [7], [8]. To overcome this limitation, physiology-based models of the cardiovascular system can be of use, as they allow for changes of cardiac parameters while keeping the arterial system unchanged.

In the present study, we employed an extensive, previously validated mathematical model of the cardiovascular system to investigate how sole changes in cardiac contractility might affect central and peripheral hemodynamics. To that aim, we simulated two physiologically relevant cases of high and low LV contractility under constant cardiac output and afterload. Particularly, we analyzed the effect of changes in cardiac contractility on key features of the aortic and radial pressure and flow waves, wave propagation characteristics, as well as the pulse pressure amplification from the ascending aorta to the radial artery.

3.1.2 Methods

Brief description of the model of the cardiovascular system

The mathematical model [10] solves the one-dimensional (1D) Navier-Stokes equations combined with a constitutive law for the wall elasticity along the centerline of each artery. The arterial tree consists of a network of 103 arteries, including 55 main systemic arteries, the coronary circulation and a representation of the circle of Willis. Proximally, the ascending aorta is coupled with a 0D model of the left ventricle based on the varying elastance model [11], [12]. Importantly, the contractility of the LV is described by the linear end-systolic pressure-volume relationship (*ESPVR*) and particularly its slope, the end-systolic elastance (E_{es}), which is sensitive enough to detect pathologies such as hypertrophic and dilated cardiomyopathies [13].

The complete mathematical model was proposed by Reymond et al. in 2009 [10] and was thoroughly validated against *in vivo* data [14]. Over the past years, the original model has been improved to include a better description of the valve dynamics [15]. Additionally, the intraventricular pressure-volume relation has been updated to consider the non-linearity of the end-diastolic pressure-volume relation (*EDPVR*) [16]. In the present work, the LV pressure (P_{LV}) is the addition of a linear *ESPVR* and an exponential *EDPVR*. The contraction is modulated by a time-varying activation function, $\epsilon(t)$, which varies from 0 to 1 and controls the weights of the two terms as follows:

$$P_{LV}(V_{LV}) = \epsilon(t) * ESPVR + (1 - \epsilon(t)) * EDPVR$$

Equation 3.1:1 – Updated LV pressure-volume relation accounting for the non-linear LV diastolic properties

Where *ESPVR* is equal to $E_{es} * (V_{LV} - V_d)$, with E_{es} being the end-systolic elastance and V_d the dead volume [12], and *EDPVR* is equal to $P_0 * \exp(\beta * V_{LV})$, with P_0 being the dead pressure and β a diastolic stiffness parameter.

Setup of Modelling Parameters

In this work, we used the cardiovascular model described above to run two discrete simulations. The first simulation pertained to a virtual healthy subject who had high LV contractility and an arterial tree of physiological parameters, representative of a middle-aged male. The second simulation corresponded to a different virtual healthy subject who shared the exact same arterial tree with the first one, but had lower LV contractility.

The cardiovascular parameters of these two subjects were chosen according to the physiological ranges and mechanisms reported in the literature (Table 3.1:1). More specifically, for the first subject we imposed a steep $ESPVR$, with maximal end-systolic elastance $E_{es} = 3$ mmHg/mL. This value is in the upper limit of the physiological range reported in the publication by Senzaki et al. [13] for normal hearts. The dead volume, V_d , was set at -2 mL, which is in the normal range of [-100, 100] mL [17], [18]. For this high contractility scenario, the LV preload (i.e., the end-diastolic pressure, EDP) was set at 8.2 mmHg [19] and the end-diastolic volume (EDV) at 97 mL [20]. The simulation yielded a physiologic stroke volume (SV) of 65mL, with a high-normal EF of 68% [20].

For the second subject, we introduced a decrease in LV contractility. Concretely, we set $E_{es} = 1$ mmHg/mL, which is in the lower limit of the range proposed for normal hearts [13], and $V_d = -60$ mL. In absence of compensatory mechanisms, this decrease of E_{es} would lead to a drop in the stroke volume. The physiological mechanism to restore the SV is through increase of the preload as explained by the Frank-Starling law. Therefore, in our simulation, in order to maintain the stroke volume constant for both subjects, $SV=65$ mL, the preload had to increase by 2.8 mmHg, i.e. from 8.2 to 11mmHg. The increase of preload was accompanied by a mild dilation of the LV, i.e. EDV increased to 120 mL and EF dropped to 54%. Both changes in the EDV and EF are still in the physiological range [20]. Figure 3.1:1 demonstrates the resulting intraventricular P-V loops for the high and low contractility scenarios. These two scenarios will be hereafter denoted as $E_{es} \uparrow$ for high and $E_{es} \downarrow$ for low contractility.

Table 3.1:1 Model parameters used to set up the two scenarios of high and low LV contractility.

| Parameters | High Contractility Simulation | Low Contractility Simulation |
|--|-------------------------------|------------------------------|
| LV parameters | | |
| <i>ESPVR</i> | | |
| End-systolic elastance, E_{es} (mmHg/mL) | 3.0 | 1.0 |
| Dead volume, V_d (mL) | -2 | -60 |
| Ejection Fraction, EF | 68% | 54% |
| <i>EDPVR</i> | | |
| Preload, EDP (mmHg) | 8.2 | 11.0 |
| End-diastolic volume, EDV (mL) | 97 | 120 |
| Dead pressure, P_0 (mmHg) | | 2.3 |
| Diastolic stiffness, β (mL-1) | | 0.013 |
| Heart rate, HR (bpm) | | 70 |
| Arterial Parameters | | |
| Arterial compliance, C_A (mL/mmHg) | | 0.62 |
| Terminal compliance, C_T (mL/mmHg) | | 0.26 |
| Total vascular compliance, TVC (mL/mmHg) | | 0.88 |
| Total vascular resistance, TVR (mmHg·sec/mL) | | 1.22 |
| Aortic characteristic impedance, Z_c (mmHg·sec/mL) | | 0.04 |

The diastolic properties of the LV were set at normal values [21] and were equal for both simulations (Table 3.1:1). To isolate the cardiac effects, we employed for both cases the same arterial tree model, which had physiologically relevant parameters representative of a healthy middle-aged adult [22] (Table 3.1:1). Normal valve properties were chosen according to [15]. Cardiac and arterial parameters for the two simulations can be found in Table 3.1:1.

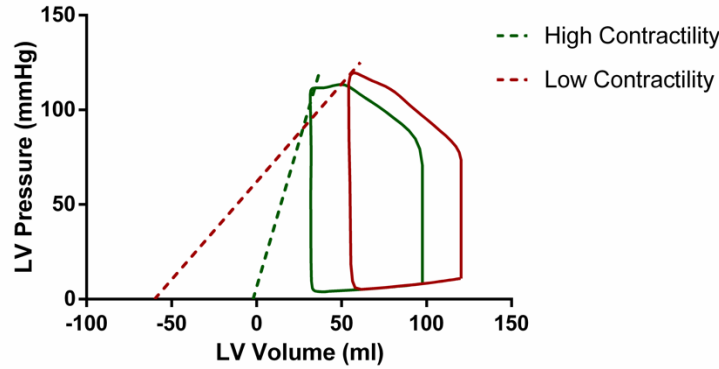


Figure 3.1:1: Intraventricular pressure-volume loops for two scenarios of high ($E_{es} = 3$ mmHg/mL, $V_d = -2$ mL - green curve) and low ($E_{es} = 1$ mmHg/mL, $V_d = -60$ mL - red curve) LV contractility with a maintained stroke volume. Note that for the low E_{es} scenario an increase in preload was needed in order to restore stroke volume. The dashed lines represent the respective linear ESPVRs.

Data Analysis and Wave Separation

From the results of the two simulations, key features of the flow and pressure waveforms were extracted including: the magnitude and timing of the peak of the aortic flow, the aortic and radial systolic (SBP), diastolic (DBP) and pulse (PP) pressure, the maximal slope of the aortic pressure upstroke (dP/dt_{max}). The pulse pressure amplification (PP_{amp}) between the proximal aorta and the radial artery was calculated as the ratio PP_{radial}/PP_{aortic} [23]. Central (aortic) Augmentation Pressure (cAP) was defined according to the characteristic inflection point or “shoulder” on the aortic pressure waveform. Accordingly, central Augmentation Index ($cAIx$) was expressed as the ratio of central augmented pressure to the central pulse pressure cAP/cPP [24]. The two aortic pressure waveforms were also classified into 2 types according to the timing of the inflection point as previously described by Murgo et al. [24]: the Type A pressure waveform, whereby the peak systolic pressure occurs after the shoulder and $cAIx > 12\%$, and the Type C pressure waveform, whereby the peak systolic pressure precedes the inflection point and $cAIx < 0$. Peripheral (radial) Augmentation Index ($pAIx$) was the ratio of the amplitude of the late systolic peak to the amplitude of the early systolic peak [25].

Subsequently, aortic pressure waveforms were separated into their forward and backward traveling components as in Westerhof et al. [26]. Aortic characteristic impedance was calculated by averaging the modulus of the input impedance in the frequency range between 3-9 harmonics [26]. The amplitude, peak and upstroke steepness for the forward and backward pressure waves were quantified. Reflection coefficient was defined as the ratio of backward wave amplitude over forward wave amplitude.

3.1.3 Results

The main pressure and flow characteristics for the increased and decreased contractility simulated cases are presented in Table 3.1:2 as well as in Figures 3.1:2 and 3.1:3. We find that changes in the $ESPVR$ have a major impact on both central and peripheral hemodynamics. For $E_{es} \uparrow$ the LV pressure curve has a steep upstroke ($14.9 \cdot 10^2$ mmHg/sec), reaches its peak early in systole (0.14 sec after beginning of ejection) and then slowly decreases until the end of systole (Figure 3.1:2A left and Table 3.1:2). Contrarily, for $E_{es} \downarrow$ the slope of the LV pressure is almost halved ($8.7 \cdot 10^2$ mmHg/sec), the aortic pressure meets the LV curve towards the end of systole, when the LV pressure peak occurs (0.23 sec after beginning of ejection) (Figure 3.1:2A right and Table 3.1:2). It is of interest to observe that the maximal LV pressure is lower in the case of high contractility (113.6 mmHg for $E_{es} \uparrow$ versus 119.7 mmHg for $E_{es} \downarrow$). These features can also be observed on the P-V loops depicted in Figure 3.1:1.

Table 3.1:2 Comparison of hemodynamic characteristics between the two contractility simulations.

| Parameters | High Contractility Simulation | Low Contractility Simulation |
|--|-------------------------------|------------------------------|
| <u>Aortic flow</u> | | |
| Cardiac Output (L/min) (maintained) | 4.6 | 4.6 |
| Maximal Aortic Flow (mL/sec) | 453 | 359 |
| Timing of Maximal Aortic Flow (sec) (since beginning of ejection) | 0.06 | 0.07 |
| Maximal slope, dF/dt max (mL/sec ²) | 1.53e4 | 1.09e4 |
| <u>LV P-V</u> | | |
| Maximal P_{LV} (mmHg) | 113.6 | 119.7 |
| Timing of maximal P_{LV} (sec) (since beginning of ejection) | 0.14 | 0.23 |
| LV dP/dt max (mmHg/sec) | 14.9e2 | 8.7e2 |
| <u>Arterial pressure</u> | | |
| Aortic SBP (mmHg) | 113.2 | 119.6 |
| Aortic DBP (mmHg) | 66.9 | 67.9 |
| Aortic MAP (mmHg) | 91.1 | 92.0 |
| Aortic PP (mmHg) | 46.3 | 51.8 |
| Aortic AP (mmHg) | -1.0 | 9.4 |
| Aortic Alx (%) | -2.4 | 18.1 |
| Aortic dP/dt max (mmHg/sec) | 6.6e2 | 4.6e2 |
| Radial SBP (mmHg) | 148.3 | 135.1 |
| Radial DBP (mmHg) | 62.4 | 63.3 |
| Radial MAP (mmHg) | 87.4 | 88.3 |
| Radial PP (mmHg) | 85.9 | 71.9 |
| Radial Alx (%) | 47.1 | 76.5 |
| PP Amplification | 1.86 | 1.39 |
| <u>Wave Separation Analysis</u> | | |
| Forward pressure wave component amplitude (mmHg) | 28.1 | 29.5 |
| Forward pressure wave peak (mmHg) | 61.5 | 63.3 |
| Forward pressure wave peak timing (sec) (since beginning of ejection) | 0.12 | 0.23 |
| Maximal slope forward dP/dt (mmHg/sec) | 6.6e2 | 4.4e2 |
| Backward pressure wave component amplitude (mmHg) | 20.7 | 22.7 |
| Backward pressure wave peak (mmHg) | 54.3 | 56.9 |
| Backward pressure wave peak timing (sec) (since beginning of ejection) | 0.25 | 0.25 |
| Reflection coefficient (%) | 73.7 | 76.9 |

SBP: Systolic Blood Pressure, DBP: Diastolic Blood Pressure, MAP: Mean Arterial Pressure, PP: Pulse Pressure, AP: Augmentation Pressure, Alx: Augmentation Index.

Accordingly, for increased E_{es} both aortic flow and pressure curves have steeper upstrokes at the beginning of ejection and reach their respective peaks earlier (Figure 3.1:2B-C and Table 3.1:2). Importantly, we note that the aortic flow wave shape is distinctively different between the two cases. Even though cardiac output is preserved, the maximal flow value is significantly higher for $E_{es} \uparrow$ (453 mL/sec for $E_{es} \uparrow$ versus 359 mL/sec for $E_{es} \downarrow$) (Figure 3.1:2C and Table 3.1:2). Additionally, we observe differences in the shape of the aortic pressure waves: although both simulations refer to the same total compliance and the same characteristic impedance of the proximal aorta (Table 3.1:1), the aortic pressure waveform resembles the characteristic Type C phenotype for $E_{es} \uparrow$, while for $E_{es} \downarrow$ the curve resembles the Type A phenotype (Figure 3.1:2B). Naturally, this is also reflected on the central AIX, which rises from -2.4% for $E_{es} \uparrow$ to +18.1% for $E_{es} \downarrow$.

Figure 3.1:2D contains an overview of the results of the wave separation analysis. For both cases, the amplitudes of the aortic forward and backward pressure wave components are approximately the same, which leads to the preservation of their ratio, i.e. the same reflection coefficient (Table 3.1:2). Overall, the backward wave seems relatively unaffected by the change in contractility. However, this does not hold true for the shape of the forward wave. Concretely, the peak of the forward pressure wave is pushed earlier in systole when LV contractility is increased (0.12 sec for $E_{es} \uparrow$ versus 0.23 sec for $E_{es} \downarrow$), which entails the increase of the steepness of its upstroke ($6.6 \cdot 10^2$ mmHg/sec for $E_{es} \uparrow$ versus $4.4 \cdot 10^2$ mmHg/sec for $E_{es} \downarrow$). This finding is in line with previous observations [27], [28].

The effect of $ESPVR$ is not limited to only central hemodynamics. In Figure 3.1:3, we demonstrate the pressure waveforms at the distal radial artery as predicted by the model for the high and low E_{es} values. The radial mean pressure is rather conserved (Table 3.1:2). However, we note that an increase in E_{es} leads to a pronounced increase in radial SBP (148.3 mmHg for $E_{es} \uparrow$ versus 135.1 mmHg for $E_{es} \downarrow$) and radial PP (85.9 mmHg for $E_{es} \uparrow$ versus 71.9 mmHg for $E_{es} \downarrow$) (Table 3.1:2). Evidently, this causes the pulse pressure amplification from the ascending aorta to the radial artery to rise drastically, i.e. PP_{amp} is 1.86 for $E_{es} \uparrow$ versus 1.39 for $E_{es} \downarrow$. With respect to the shape of the radial pressure curve, the late systolic peak has similar timing for both cases, however, its value is lower for $E_{es} \uparrow$. This is translated in a drop in the peripheral augmentation index, i.e. $pAIX$ is 47.1% for $E_{es} \uparrow$ vs 76.5% for $E_{es} \downarrow$.

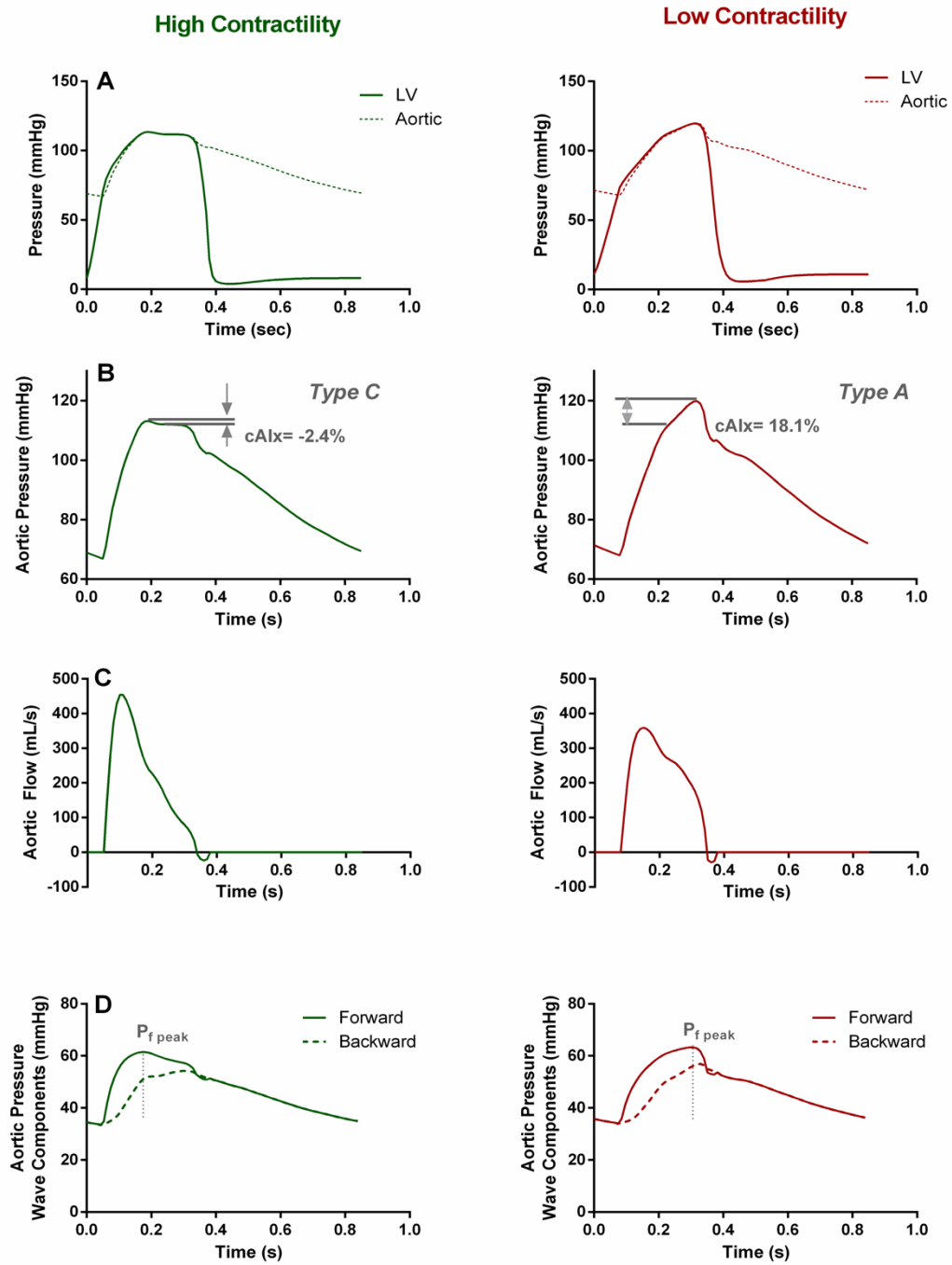


Figure 3.1:2 Effect of LV contractility on central hemodynamics. (A) LV and aortic pressure as a function of time. (B) Characteristic Type C and Type A aortic pressure phenotypes reproduced by high and low contractility, respectively. (C) Aortic flow. (D) Forward and backward travelling pressure waves. Note that the forward peak occurs significantly earlier in the high contractility simulation, while the amplitudes of the forward and backward pressure waves are left unchanged.

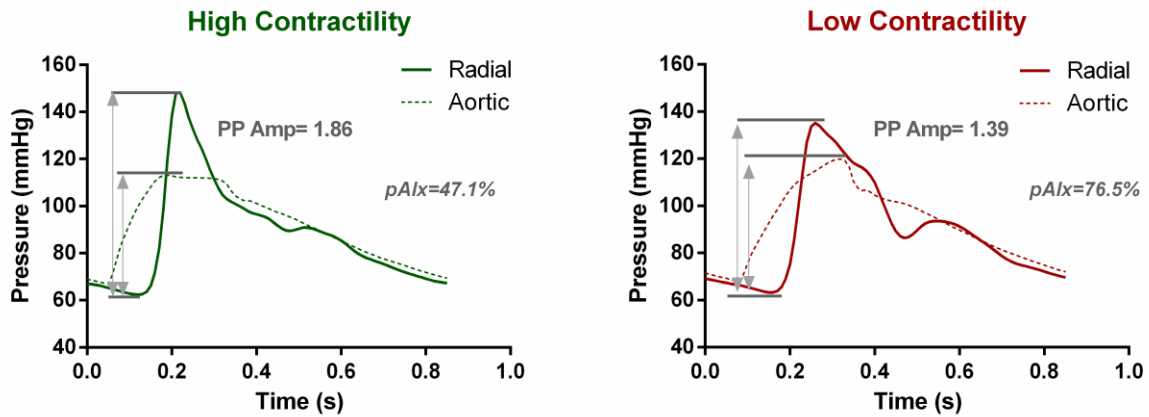


Figure 3.1:3 Central and peripheral arterial pressure for the two cases of LV contractility. Note the rise in the radial systolic pressure as well as in the pulse pressure amplification when E_{es} is higher; in this case, $pAlx$ is significantly lower.

3.1.4 Discussion

In the present study, we demonstrated that an increase in LV contractility alone could directly result in alterations in both central and peripheral hemodynamics even for an unchanged arterial load and cardiac output. This was achieved by employing an extensive, physiologically relevant mathematical model of the cardiovascular system, and manipulating the end-systolic pressure-volume relation in order to simulate higher and lower systolic function. This work addresses the hemodynamic footprint of contractility on multiple levels, touching upon its effect on the central pressure and flow waveforms as well as the distal radial pressure phenotypes.

Importantly, we found that an increase in LV contractility as expressed by a steeper $ESPVR$ has an effect on the shape of the initial forward travelling wave pumped by the left ventricle; the forward wave shows a pronounced upstroke and an early peak, without, however, changing its amplitude (Figure 3.1:2D). On the other hand, the wave reflections are not particularly affected, as they depend primarily on vascular properties (Figure 3.1:2D).

The increased steepness of the forward wave due to increased contractility orchestrates a number of changes in both central and peripheral arterial hemodynamics. The respective proximal aortic pressure and flow waveforms change drastically in shape, i.e. they become steeper, reach their peak values earlier in systole, and particularly for the aortic waveform the peak value is significantly increased. Of interest is the fact that when E_{es} is decreased the aortic pressure curve resembles the characteristic Type A phenotype, while for increased E_{es} it resembles the Type C phenotype. Accordingly, we note alterations in the aortic inflection point and Alx ; for increased LV contractility the Alx drops and might even become negative (Figure 3.1:2B and Table 3.1:2).

In addition to central hemodynamics, changes in cardiac contractility affect also peripheral hemodynamic phenotypes. Radial systolic and pulse pressure increases for higher E_{es} , although the mean pressure is preserved (Figure 3.1:3 and Table 3.1:2). This finding might seem rather counter-intuitive at first. Since we employ the same arterial tree for both simulations, the transmission line theory dictates that there should be no change in the transmission/reflection coefficients from the central aorta to the radial artery. Indeed, the reflection coefficient calculated as the ratio of the backward to forward wave amplitude remains constant. Therefore, one would expect that the pulse pressure amplification should also be maintained despite the changes in LV contractility. This disparity can be explained by the effect of E_{es} on the slope/timing of forward wave. In other words, even though the transmission network is not altered, the initial forward wave pumped by the heart is. The fact that the forward wave is characteristically steeper and reaches its peak early suggests that at a specific time point in early systole, the forward pressure wave has a higher value, which will result in an also amplified radial pressure (Figure 3.1:2).

In light of this evidence, we can better appreciate observations made in previous clinical works [29], [30]. Particularly, we recently investigated the hemodynamic profile of patients with severe aortic valve stenosis (AS) before and acutely after they underwent Transcatheter Aortic Valve Replacement (TAVR) (25). Interestingly, we found significant differences between the shape of central

pressure and flow waves before and after TAVR. We showed that resolution of aortic stenosis led to an enhanced forward traveling wave, which was associated with changes in the central pressure and flow waveforms as well as a decrease in the aortic Alx. We hypothesized that post-TAVR hemodynamics might be related to the hyperdynamic state of the LV, which cannot acutely adapt to the improved loading conditions. The present work supports this hypothesis and offers a mathematical explanation of this clinical observation.

Clinical implications

Our findings have several implications. First, central as well as peripheral pressure and flow waveforms might contain crucial information on cardiac systolic function. This point has also been evoked in previous studies that proposed [9], [31] and used [29], [32], [33] aortic dP/dt_{max} as a measure of LV contractility. A recent clinical study by [9] suggested that this does not apply only to central waveforms but also extends to peripheral measures, i.e. radial and femoral dP/dt_{max} were also able to track reasonably well LV inotropic changes. Here, we provide a mathematical justification of why this holds true: LV contractility affects primarily the forward wave and it is in fact the slope of the forward wave that is captured in both central and peripheral dP/dt_{max} measures.

Further advancing this line of thinking, we suggest that the forward wave might be an important element of the ventricular-arterial coupling, given that its slope and the timing of its peak seem to be informative of the LV systolic function. Contrarily, the total backward travelling wave is rather a vascular index and provides information on the cumulative effect of reflections occurring throughout the arterial tree. Even though wave separation analysis is not currently being performed as part of the clinical routine, it can potentially offer a complete image of the cardiovascular coupling and assist clinicians with better assessing LV performance.

A second finding of major clinical importance is that high peripheral SBP might not necessarily be indicative of central systolic hypertension. Aortic pressure, which is directly “seen” by the heart, strongly relates to vascular disease and clinical outcomes [34]. However, since access to aortic pressure requires invasive measurements, peripheral pressure measurements are used instead. Here, we demonstrate that PP amplification from the aorta to the radial artery changes with changes in E_{es} , which partly explains previous doubts expressed on the reliability of peripheral pressure as a surrogate of central pressure [34]–[36]. Arguably, peripheral pressure is a well-studied marker with prognostic value for cardiovascular morbidity and mortality [37]. Nevertheless, we suggest that it might be meaningful to focus more attention on deriving central pressure as it offers a better description of the afterload.

On that note, one should also exert caution when interpreting the shape of the central pressure waveform to assess vascular stiffness. In the present study, we were able to reproduce both Type A and Type C aortic pressure phenotypes [24] by changing only the cardiac systolic properties, while maintaining the arterial tree parameters of an average middle-aged male. Traditionally, Type A pressure curves are associated with increased aortic stiffness and advanced age, whereby large reflections arrive earlier back to the aortic root. Contrarily, Type C pressure curves are understood to represent younger individuals, with lower amplitude reflections and lower pulse pressures [24]. Here, we demonstrate that these particular phenotypes are not solely dictated by vascular stiffness and reflections, but are actually strongly related to cardiac contractility. This comment also extends to the central Alx, which was until recently regarded as a purely vascular parameter [38]. We show that cardiac contractility is also an important determinant of central Alx, a finding that corroborates previous statements that Alx might not be a measure of wave reflections solely [27], [39].

Considerations on the analysis and study limitations

When interpreting our results the reader should consider that the data presented pertain to mathematical simulations and not *in vivo* human measurements. Nevertheless, this limitation is mitigated by the facts that: i) the mathematical model used in the present study has been thoroughly validated against *in vivo* data before and has been found capable of accurately representing physiologic and pathologic hemodynamics [14], [22], ii) the model parameters were chosen in a way to reflect plausible physiological states, according to normal ranges proposed in the literature (the choice of each model parameter was respectively justified).

On that note, we should acknowledge that we do not have complete understanding on how changes in LV contractility will exactly affect the volume intercept, V_d , of the $ESPVR$. Arguably, we anticipate that when contractility decreases, the preload should increase due to the Frank-Starling law, thus reducing the EF; however, this change in preload and EF largely depends on the chosen V_d values. Here, we chose the V_d values, so that a drastic change in LV contractility would lead to an equally drastic change in EF, i.e. when E_{es} dropped from 3 mmHg/mL to 1 mmHg/mL, EF also decreased from 68% to 54%. In an exaggerated version, this mechanism describes systolic heart failure: when LV contractility is compromised, the increase in preload does no longer suffice to restore the stroke volume and EF gradually drops to pathologic values.

Nevertheless, it should be noted that repeating the analysis for different, physiologically relevant V_d values would not affect the study results. In other words, our observations regarding the alteration of central and peripheral wave characteristics would still hold true even if EF were less decreased. Additionally, our findings match well previously reported data from clinical and modeling studies [27], [28], [39]. Our next step should be the corroboration of our model-based results with *in vivo* or *in vitro* data.

The cardiac model of time-varying elastance implemented here is based on the assumption that the normalized elastance, $E_N(t)$, shares a uniform shape among different individuals [12]. This view has been challenged as previous studies showed a significant variation of $E_N(t)$ according to afterload and introduced correction models [40]. This feature is not yet included in our simulations, but will be incorporated in our future studies. However, since vascular load was kept constant in the present study we do not expect that it would significantly affect our results.

Additionally to the concept of elastance, other mathematical models have been proposed to describe the contractility of the LV. Particularly, more detailed finite-element models exist [41], [42] that couple cavity mechanics with sarcomere mechanics. The use of such a model (like the one proposed by [41]) might be more relevant for the investigation of hemodynamic changes under varying inotropic states. Future work will be oriented towards this direction. Further model-related limitations can be found in the original publication [10].

Conclusions

In the present study, we demonstrated by means of a mathematical model of the cardiovascular system that a physiological increase in cardiac contractility leads to a steeper forward pressure wave pumped by the LV, which, subsequently, drastically alters central and peripheral pressure and flow waves. This might have important implications for the assessment of cardiac contractility through measurement of noninvasive pressure waveforms. Additionally, the characteristic Type A and Type C aortic pressure phenotypes, and accordingly the central AIx, are not solely dictated by vascular stiffness but also majorly depend on LV contractility. Last, we found that the amplification of the pulse pressure from the central aorta to the periphery is also affected by the cardiac contractile state and, hence, suggest that caution should be exerted when using peripheral measurements as surrogate for central pressure.

3.1.5 Bibliography

- [1] M. R. Starling, "Left ventricular-arterial coupling relations in the normal human heart," *Am. Heart J.*, vol. 125, no. 6, pp. 1659–1666, Jun. 1993, doi: 10.1016/0002-8703(93)90756-y.
- [2] W. C. Little and M. Pu, "Left Ventricular-Arterial Coupling," *J. Am. Soc. Echocardiogr.*, vol. 22, no. 11, pp. 1246–1248, Nov. 2009, doi: 10.1016/j.echo.2009.09.023.
- [3] F. Antonini-Canterin, S. Poli, O. Vriz, D. Pavan, V. D. Bello, and G. L. Nicolosi, "The Ventricular-Arterial Coupling: From Basic Pathophysiology to Clinical Application in the Echocardiography Laboratory," *J. Cardiovasc. Echography*, vol. 23, no. 4, pp. 91–95, 2013, doi: 10.4103/2211-4122.127408.
- [4] Z. Sun, "Aging, Arterial Stiffness and Hypertension," *Hypertension*, vol. 65, no. 2, pp. 252–256, Feb. 2015, doi: 10.1161/HYPERTENSIONAHA.114.03617.
- [5] H.-Y. Lee and B.-H. Oh, "Aging and arterial stiffness," *Circ. J. Off. J. Jpn. Circ. Soc.*, vol. 74, no. 11, pp. 2257–2262, Nov. 2010, doi: 10.1253/circj.cj-10-0910.
- [6] J. B. Strait and E. G. Lakatta, "Aging-associated cardiovascular changes and their relationship to heart failure," *Heart Fail. Clin.*, vol. 8, no. 1, pp. 143–164, Jan. 2012, doi: 10.1016/j.hfc.2011.08.011.
- [7] E. Mikulic, J. N. Cohn, and J. A. Franciosa, "Comparative hemodynamic effects of inotropic and vasodilator drugs in severe heart failure," *Circulation*, vol. 56, no. 4 Pt 1, pp. 528–533, Oct. 1977, doi: 10.1161/01.cir.56.4.528.
- [8] L. C. Argenta *et al.*, "A comparison of the hemodynamic effects of inotropic agents," *Ann. Thorac. Surg.*, vol. 22, no. 1, pp. 50–57, Jul. 1976, doi: 10.1016/s0003-4975(10)63953-7.
- [9] M. I. Monge Garcia *et al.*, "Performance comparison of ventricular and arterial dP/dtmax for assessing left ventricular systolic function during different experimental loading and contractile conditions," *Crit. Care*, vol. 22, no. 1, p. 325, Nov. 2018, doi: 10.1186/s13054-018-2260-1.
- [10] P. Reymond, F. Merenda, F. Perren, D. Rüfenacht, and N. Stergiopoulos, "Validation of a one-dimensional model of the systemic arterial tree," *Am. J. Physiol. Heart Circ. Physiol.*, vol. 297, no. 1, pp. H208–222, Jul. 2009, doi: 10.1152/ajpheart.00037.2009.

- [11] H. Suga and K. Sagawa, "Instantaneous pressure-volume relationships and their ratio in the excised, supported canine left ventricle," *Circ. Res.*, vol. 35, no. 1, pp. 117–126, Jul. 1974.
- [12] K. Sagawa, H. Suga, A. A. Shoukas, and K. M. Bakalar, "End-systolic pressure/volume ratio: a new index of ventricular contractility," *Am. J. Cardiol.*, vol. 40, no. 5, pp. 748–753, Nov. 1977.
- [13] H. Senzaki, C. H. Chen, and D. A. Kass, "Single-beat estimation of end-systolic pressure-volume relation in humans. A new method with the potential for noninvasive application," *Circulation*, vol. 94, no. 10, pp. 2497–2506, Nov. 1996.
- [14] P. Reymond, Y. Bohraus, F. Perren, F. Lazeyras, and N. Stergiopoulos, "Validation of a patient-specific one-dimensional model of the systemic arterial tree," *Am. J. Physiol. Heart Circ. Physiol.*, vol. 301, no. 3, pp. H1173–H1182, Sep. 2011, doi: 10.1152/ajpheart.00821.2010.
- [15] J. P. Mynard, M. R. Davidson, D. J. Penny, and J. J. Smolich, "A simple, versatile valve model for use in lumped parameter and one-dimensional cardiovascular models," *Int. J. Numer. Methods Biomed. Eng.*, vol. 28, no. 6–7, pp. 626–641, Jul. 2012, doi: 10.1002/cnm.1466.
- [16] D. Burkhoff, I. Mirsky, and H. Suga, "Assessment of systolic and diastolic ventricular properties via pressure-volume analysis: a guide for clinical, translational, and basic researchers," *Am. J. Physiol.-Heart Circ. Physiol.*, vol. 289, no. 2, pp. H501–H512, Aug. 2005, doi: 10.1152/ajpheart.00138.2005.
- [17] C.-H. Chen *et al.*, "Noninvasive single-beat determination of left ventricular end-systolic elastance in humans," *J. Am. Coll. Cardiol.*, vol. 38, no. 7, pp. 2028–2034, Dec. 2001, doi: 10.1016/S0735-1097(01)01651-5.
- [18] H. Senzaki, C. H. Chen, and D. A. Kass, "Single-beat estimation of end-systolic pressure-volume relation in humans. A new method with the potential for noninvasive application," *Circulation*, vol. 94, no. 10, pp. 2497–2506, Nov. 1996, doi: 10.1161/01.cir.94.10.2497.
- [19] E. A. ten Brinke *et al.*, "Noninvasive estimation of left ventricular filling pressures in patients with heart failure after surgical ventricular restoration and restrictive mitral annuloplasty," *J. Thorac. Cardiovasc. Surg.*, vol. 140, no. 4, pp. 807–815, Oct. 2010, doi: 10.1016/j.jtcvs.2009.11.039.
- [20] R. M. Lang *et al.*, "Recommendations for cardiac chamber quantification by echocardiography in adults: an update from the American Society of Echocardiography and the European Association of Cardiovascular Imaging," *J. Am. Soc. Echocardiogr. Off. Publ. Am. Soc. Echocardiogr.*, vol. 28, no. 1, pp. 1–39.e14, Jan. 2015, doi: 10.1016/j.echo.2014.10.003.
- [21] K. Kadry *et al.*, "Biomechanics of diastolic dysfunction: a model-based approach," *Submitt. Publ.*
- [22] S. Pagoulatou and N. Stergiopoulos, "Evolution of aortic pressure during normal ageing: A model-based study," *PLoS ONE*, vol. 12, no. 7, Jul. 2017, doi: 10.1371/journal.pone.0182173.
- [23] Avolio Alberto P. *et al.*, "Role of Pulse Pressure Amplification in Arterial Hypertension," *Hypertension*, vol. 54, no. 2, pp. 375–383, Aug. 2009, doi: 10.1161/HYPERTENSIONAHA.109.134379.
- [24] Murgo J P, Westerhof N, Giolma J P, and Altobelli S A, "Aortic input impedance in normal man: relationship to pressure wave forms," *Circulation*, vol. 62, no. 1, pp. 105–116, Jul. 1980, doi: 10.1161/01.CIR.62.1.105.
- [25] Munir Shahzad *et al.*, "Peripheral Augmentation Index Defines the Relationship Between Central and Peripheral Pulse Pressure," *Hypertension*, vol. 51, no. 1, pp. 112–118, Jan. 2008, doi: 10.1161/HYPERTENSIONAHA.107.096016.
- [26] N. Westerhof, P. Sipkema, G. C. van den Bos, and G. Elzinga, "Forward and backward waves in the arterial system," *Cardiovasc. Res.*, vol. 6, no. 6, pp. 648–656, Nov. 1972, doi: 10.1093/cvr/6.6.648.
- [27] M. H. G. Heusinkveld *et al.*, "Augmentation index is not a proxy for wave reflection magnitude: mechanistic analysis using a computational model," *J. Appl. Physiol.*, vol. 127, no. 2, pp. 491–500, Aug. 2019, doi: 10.1152/jappphysiol.00769.2018.
- [28] Fok Henry *et al.*, "Dominance of the Forward Compression Wave in Determining Pulsatile Components of Blood Pressure," *Hypertension*, vol. 64, no. 5, pp. 1116–1123, Nov. 2014, doi: 10.1161/HYPERTENSIONAHA.114.04050.
- [29] C. Müller *et al.*, "Transcatheter aortic valve replacement (TAVR) leads to an increase in the subendocardial viability ratio assessed by pulse wave analysis," *PLOS ONE*, vol. 13, no. 11, p. e0207537, Nov. 2018, doi: 10.1371/journal.pone.0207537.
- [30] S. Pagoulatou *et al.*, "Hemodynamics before and acutely after Transcatheter Aortic Valve Implantation (TAVI)," *Submitt. Publ.*
- [31] A. G. Wallace, N. S. Skinner, and J. H. Mitchell, "Hemodynamic determinants of the maximal rate of rise of left ventricular pressure," *Am. J. Physiol.*, vol. 205, pp. 30–36, Jul. 1963, doi: 10.1152/ajplegacy.1963.205.1.30.
- [32] P. Ostadal, D. Vondrakova, A. Krüger, M. Janotka, and J. Naar, "Continual measurement of arterial dP/dtmax enables minimally invasive monitoring of left ventricular contractility in patients with acute heart failure," *Crit. Care*, vol. 23, no. 1, p. 364, Nov. 2019, doi: 10.1186/s13054-019-2654-8.
- [33] P. Morimont, B. Lambermont, T. Desai, N. Janssen, G. Chase, and V. D'Orio, "Arterial dP/dtmax accurately reflects left ventricular contractility during shock when adequate vascular filling is achieved," *BMC Cardiovasc. Disord.*, vol. 12, no. 1, p. 13, Mar. 2012, doi: 10.1186/1471-2261-12-13.

- [34] C. M. McEniery, J. R. Cockcroft, M. J. Roman, S. S. Franklin, and I. B. Wilkinson, "Central blood pressure: current evidence and clinical importance," *Eur. Heart J.*, vol. 35, no. 26, pp. 1719–1725, Jul. 2014, doi: 10.1093/eurheartj/ehu565.
- [35] R. Pini *et al.*, "Central but not brachial blood pressure predicts cardiovascular events in an unselected geriatric population: the ICARE Dicomano Study," *J. Am. Coll. Cardiol.*, vol. 51, no. 25, pp. 2432–2439, Jun. 2008, doi: 10.1016/j.jacc.2008.03.031.
- [36] M. Roman *et al.*, "Central Pressure More Strongly Relates to Vascular Disease and Outcome Than Does Brachial Pressure: The Strong Heart Study," *Hypertension*, vol. 50, pp. 197–203, Jul. 2007, doi: 10.1161/HYPERTENSIONAHA.107.089078.
- [37] F. Turnbull and Blood Pressure Lowering Treatment Trialists' Collaboration, "Effects of different blood-pressure-lowering regimens on major cardiovascular events: results of prospectively-designed overviews of randomised trials," *Lancet Lond. Engl.*, vol. 362, no. 9395, pp. 1527–1535, Nov. 2003, doi: 10.1016/s0140-6736(03)14739-3.
- [38] C. Vlachopoulos, M. O'Rourke, W. W. Nichols, M. O'Rourke, and W. W. Nichols, *McDonald's Blood Flow in Arteries : Theoretical, Experimental and Clinical Principles*. CRC Press, 2011.
- [39] Sharman James E., Davies Justin E., Jenkins Carly, and Marwick Thomas H., "Augmentation Index, Left Ventricular Contractility, and Wave Reflection," *Hypertension*, vol. 54, no. 5, pp. 1099–1105, Nov. 2009, doi: 10.1161/HYPERTENSIONAHA.109.133066.
- [40] T. Shishido, K. Hayashi, K. Shigemitsu, T. Sato, M. Sugimachi, and K. Sunagawa, "Single-Beat Estimation of End-Systolic Elastance Using Bilinearly Approximated Time-Varying Elastance Curve," *Circulation*, vol. 102, no. 16, pp. 1983–1989, Oct. 2000, doi: 10.1161/01.CIR.102.16.1983.
- [41] J. Lumens, T. Delhaas, B. Kirn, and T. Arts, "Three-wall segment (TriSeg) model describing mechanics and hemodynamics of ventricular interaction," *Ann. Biomed. Eng.*, vol. 37, no. 11, pp. 2234–2255, Nov. 2009, doi: 10.1007/s10439-009-9774-2.
- [42] R. C. P. Kerckhoffs, M. L. Neal, Q. Gu, J. B. Bassingthwaighe, J. H. Omens, and A. D. McCulloch, "Coupling of a 3D Finite Element Model of Cardiac Ventricular Mechanics to Lumped Systems Models of the Systemic and Pulmonic Circulation," *Ann. Biomed. Eng.*, vol. 35, no. 1, pp. 1–18, Jan. 2007, doi: 10.1007/s10439-006-9212-7.

3.2 Acute effects of Transcatheter Aortic Valve Replacement on the ventricular-aortic interaction

Stamatia Pagoulatou ¹, Nikolaos Stergiopoulos ¹, Vasiliki Bikia ¹, Georgios Rovas ¹, Marc-Joseph Licker ³, Hajo Müller ², Stéphane Noble ², and Dionysios Adamopoulos ²

¹ Laboratory of Hemodynamics and Cardiovascular Technology (LHTC), Institute of Bioengineering, Ecole Polytechnique Fédérale de Lausanne (EPFL), Lausanne, Switzerland

² Cardiology Division, Department of Medicine, Geneva University Hospitals (HUG), Geneva, Switzerland

³ Division of Anesthesiology, Geneva University Hospitals (HUG), Geneva, Switzerland

Abstract

TAVR is increasingly used to treat severe aortic stenosis (AS) patients. However, little is known regarding the direct effect of TAVR on the ventricular-arterial coupling (VAC). In the present study, we aimed to investigate changes in central hemodynamics after successful transcatheter aortic valve replacement (TAVR). We retrospectively examined the medical files of 33 severe AS patients (84±6 years) who underwent TAVR. Invasive measurements of left ventricular and aortic pressures as well as echocardiographic aortic flow were acquired before and after TAVR (maximum within 5 days post-TAVR). We examined alterations in key features of central pressure and flow waveforms, including the aortic augmentation index (AIx), and assessed changes in the VAC via wave separation analysis. Arterial parameters were determined via parameter-fitting on a 2-element Windkessel model. Resolution of AS resulted in direct increase in the aortic systolic pressure and maximal aortic flow (131±22 versus 157±25 mmHg and 237±49 versus 302±69 mL/sec, $p<0.001$ for all), while the ejection duration decreased ($p<0.001$). We noted a significant decrease in the AIx (from 42±12% to 19±11%, $p<0.001$). Noteworthy, the arterial properties remained unchanged. There was a comparable increase in both forward (61±20 versus 77±20 mmHg, $p<0.001$) and backward (35±14 versus 42±10 mmHg, $p=0.013$) pressure wave amplitudes, while their ratio, i.e., the reflection coefficient, was preserved ($p=NS$). Our results highlight the importance of the VAC on the amplitude, shape and related attributes of the aortic pressure and flow pulse and challenge the interpretation of AIx as a solely vascular measure in AS patients.

Key words: Aortic valve stenosis • Aortic valve replacement • Contraction • Coupling

Manuscript submitted for publication

3.2.1 Introduction

Severe aortic valve stenosis (AS) currently affects 2% to 9% of adults older than 65 years old, and its prevalence is likely to increase in the future as the population steadily ages [1]. In the presence of AS, cardiovascular hemodynamics are significantly affected [2]. Importantly, the valvular stenosis poses an obstruction to the left ventricular (LV) outflow, hence causing a rise in the LV afterload. Chronic pressure overload triggers LV remodeling, usually in the form of hypertrophy [3], and gradually leads to inadequate cardiac output (CO) and ultimately heart failure [4].

Accordingly, symptomatic severe AS is correlated with high mortality rates [5] and requires aortic valve replacement. Transcatheter aortic valve replacement (TAVR) has emerged in the past years as a desirable alternative to open-heart surgery and has transformed the outlook for high and intermediate surgical-risk patients. Several studies have confirmed the improvement of clinical outcomes after TAVR, even showing significantly higher rate of survival at 1 year as compared to classical surgical valve replacement even in low surgical-risk patients [6]–[8].

In the following years, TAVR has the potential to become the gold standard technique for all patients with severe AS, depending on the still unknown long-term valve durability [9]. However, we have only limited understanding of the effect of TAVR on cardiovascular hemodynamics. On that note, the work of Muller et al. [10] recently analyzed the periprocedural changes in pulse wave features by examining noninvasive measures of carotid and radial pressure as well as echocardiographic indices. They demonstrated that TAVR leads to an improvement of endomyocardial perfusion and LV contractility. They also reported changes in the reconstructed aortic pressure features -commonly regarded as vascular parameters [11]-, i.e. the augmentation pressure (AP) and augmentation index (Alx).

In the present study, we aimed to extend previous literature on the direct effect of TAVR on cardiovascular hemodynamics by acquiring invasive measurements of LV and aortic pressure as well as echocardiographic flow data. The analysis examined alterations in key features of both central pressure and flow waveforms. We further investigated changes in the ventricular-arterial coupling by means of wave separation analysis. Particular attention was given to the interpretation of Alx as a vascular measure in the setting of AS.

3.2.2 Methods

Study Population

In this retrospective study, we examined the medical files of all patients who underwent TAVR at the Geneva University Hospitals between September 2018 and January 2020 (n=110). These patients were referred for TAVR according to standard indications after evaluation by the local Heart Team. 4 TAVR interventions were performed on a previously implanted prosthetic valve (“valve in valve” procedure) for either severe stenosis (n=2) or aortic regurgitation (n=2) and thus were excluded from the final cohort. 23 patients were excluded because of missing or low-quality hemodynamic recordings during the intervention and 8 because of significant arrhythmia compromising pulse wave analysis. 1 patient was excluded because of a periprocedural myocardial infarction and 3 patients because the TAVR was performed in an emergency setting due to a baseline cardiogenic shock state. In order to avoid the potential confounding effect of low myocardial contractility, patients with moderate or severe left ventricular dysfunction (LVEF <40%, n=8) were also excluded. Only patients with available data on baseline CO measured by thermodilution were included in the final cohort. Finally, we only considered successful TAVR interventions as defined by 1) the absence of periprocedural mortality, 2) the correct positioning of a single prosthetic heart valve in the right anatomical location and 3) intended performance of the prosthetic heart valve (mean transprosthetic gradient < 20 mmHg and no moderate or severe prosthetic valve regurgitation) according to the VARC-2 criteria [12]. A detailed description of the study population inclusion/exclusion criteria is presented in Figure 3.2:1.

The final cohort consisted of 33 patients. Baseline demographics, clinical and echocardiographic data was available for all subjects. 17 patients received an Evolut Pro (Medtronic®), 6 an Evolut R (Medtronic®), 5 an Edwards Sapien (Edwards Lifesciences®) and 5 an Accurate Neo (Boston Scientific®) prosthetic valve. Transfemoral access was preferred for all interventions. The 30 days composite safety endpoint was reached for all patients [12]. Patient data was anonymized prior to analysis. Informed written consent had been previously obtained from each patient for inclusion in the local TAVR database as part of the Swiss prospective registry (NCT1368250) that was approved by the local Ethics Committee.

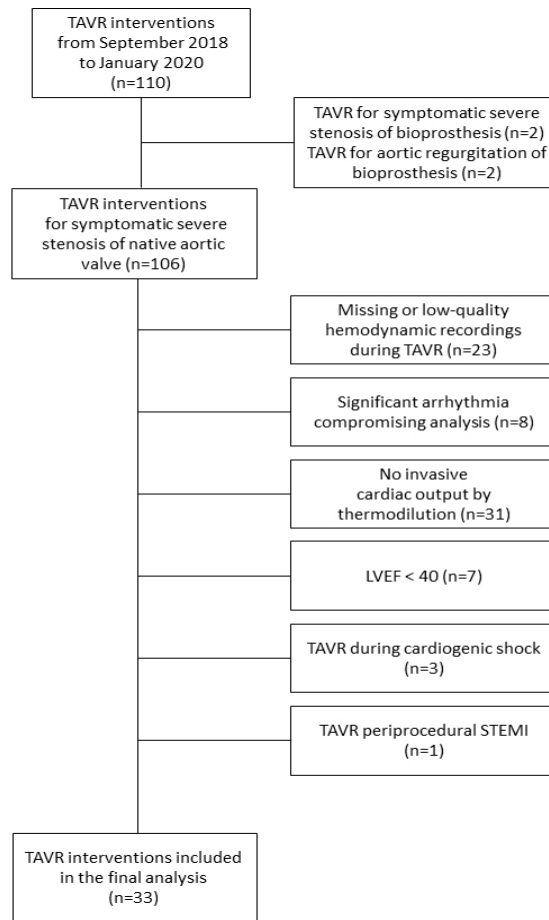


Figure 3.2:1 Flow diagram of study patients according to the inclusion/exclusion criteria.

Pressure measurements during the TAVR procedure

The routine TAVR procedure included a baseline left heart catheterization with simultaneous recording of the pressure in both the left ventricle and the aortic root. A first 6F “pigtail” catheter (Cordis®) was advanced through the stenotic valve into the left ventricle from the vascular access for the transcatheter heart valve and a second 6F pigtail catheter was advanced to the aortic root using the second vascular access, both were then connected to a pressure line and transducer. The pressure curves in the left ventricle and in the ascending aorta were simultaneously recorded over several heartbeats after careful calibration of the pressure transducer. The TAVR procedure was then performed and a second set of pressure measurements was taken immediately after the TAVR procedure.

On a separate day prior to the TAVR, all patients underwent a baseline diagnostic left and right heart catheterization. For all patients, invasive measurements of CO by the gold standard thermodilution method were collected.

Analysis of invasive data

Multiple LV and ascending aortic pressure curves captured before and after the TAVR procedure were digitized for each patient. A custom, in-house Matlab® code was developed to automatically identify the beginning and end of each heartbeat and the average pressure curves were computed. Subsequently, key features of the pressure waveforms were determined, including: i) the peak LV pressure, ii) the invasive mean ventricular-aortic pressure gradient, which is the gradient between the LV and aortic pressures integrated throughout the ejection period and is considered as the optimal indicator of AS severity in the presence of normal LV systolic function and stroke volume [13], [14], iii) the aortic systolic (SBP), diastolic (DBP), mean (MAP) and pulse (PP) pressure, iv) the timing of the aortic SBP, v) the maximal slope of the aortic pressure upstroke $\left[\left(\frac{dp}{dt}_{max}\right)\right]$, vi) the characteristic inflection point of

the aortic pressure curve [pressure (P_{inf}) and timing (t_{inf})], provided that such a point could be explicitly identified, vii) the aortic AP, calculated as the difference between the aortic SBP and P_{inf} , and viii) the aortic AIx, defined as the ratio AP/PP according to previous literature [15], [16] (Figure 3.2:2).

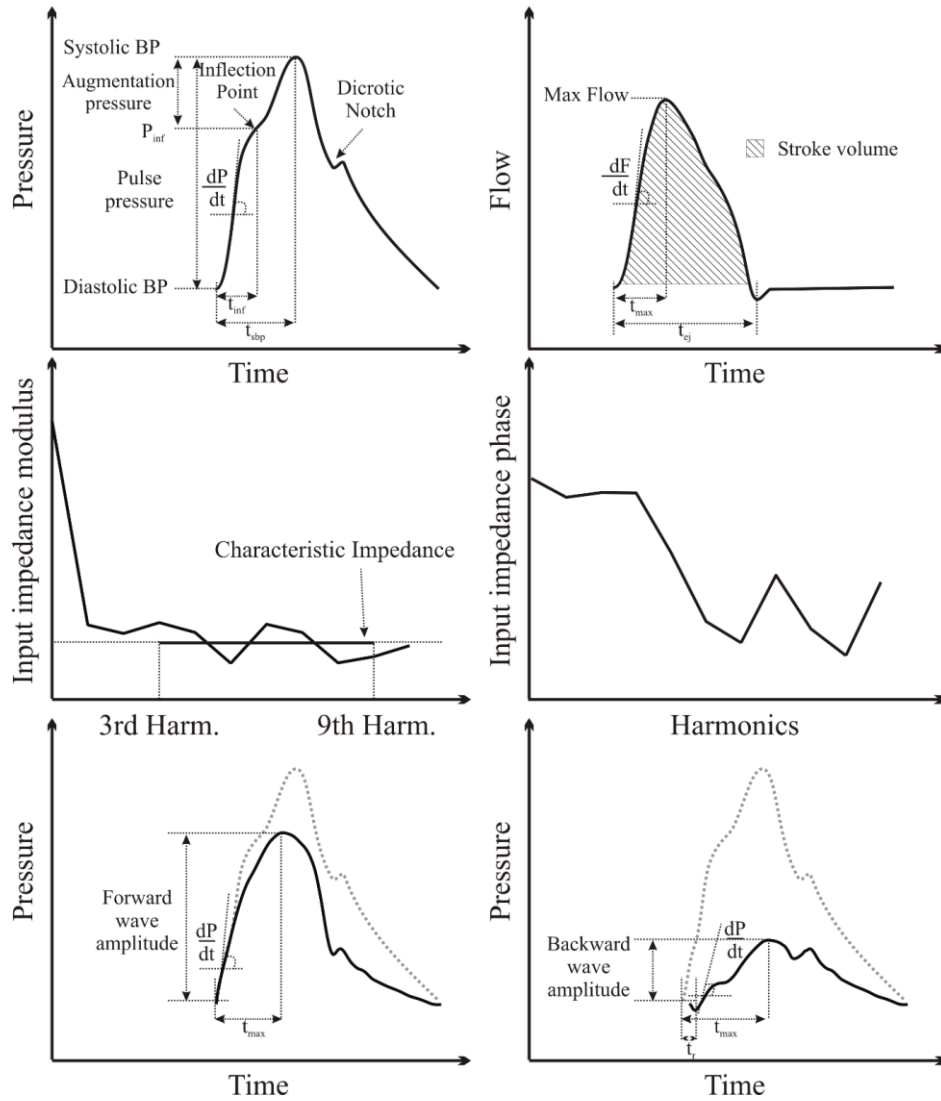


Figure 3.2:2 Aortic pressure and flow pulse wave analysis in the time domain and frequency-based wave separation of the pressure wave into its forward and backward components. BP: Blood pressure; P_{inf} : Pressure at the inflection point; t_{inf} : Time to the inflection point; dP/dt : Maximal slope of the pressure waveform during the ejection period; dF/dt : maximal slope of the flow waveform during the ejection period; t_{ej} : Ejection duration; t_{max} : time to the maximal point of the waveform; t_r : transit time.

Echocardiography

A complete transthoracic echocardiographic examination was performed prior to the TAVR and after the procedure (for 32 patients within 48 hours and for 1 patient 5 days after TAVR). The diameter of the left ventricular outflow track (LVOT) was measured in the parasternal long axis view during mid-systole. The proximal peak velocity profile was acquired at the level of the LVOT via transthoracic Pulsed Wave Doppler echocardiography in the apical 5-chamber view. The aortic flow waveform was subsequently calculated using the measured instantaneous peak velocity. This was done by assuming an appropriate velocity profile based on the Witzig-Womersley theory [17] and integrating the velocity over the corresponding circular cross-sectional area. End-diastolic (EDV) and end-systolic (ESV) left ventricular volumes were also measured retrospectively according to Simpson's method in monoplane (4 chamber view). The measurements were conducted by an experienced cardiologist with the patient in supine position and according to standard recommendations for echocardiography [18]. Transvalvular and transprosthetic pressure gradients as well as qualitative evaluation of valve abnormalities were collected retrospectively from the echocardiography reports.

Data analysis and wave separation

The proximal aortic pressure curve acquired invasively, and the flow curves obtained from echocardiography were interpolated and combined for subsequent analysis. Note that any difference in heart rate between the pressure and flow measurements was accounted for by truncating or extending the diastolic portion of the aortic flow wave. As pressure and flow were not measured simultaneously, synchronization of the signals was required. To this aim, we adopted the second derivative approach, whereby the time lag between the two signals was corrected by calculating the maxima of the second time derivatives [19]. After synchronization, the signals were used for the calculation of the equivalent total vascular resistance (TVR) and total arterial compliance (C). This was achieved via parameter-fitting on a 2-element Windkessel model, as described in the Pulse Pressure Method (PPM) by Stergiopoulos et al. [20].

Wave separation analysis was performed by applying the standard methodology in the frequency domain (Figure 3.2:2). The characteristic impedance was calculated by averaging the input impedance modulus of the 3rd to 9th harmonics. The waves were then separated into their corresponding forward and backward components as described by Westerhof et al. [21]. Key features of the forward and backward pressure waves were identified, including the magnitude and timing of the peak pressure as well as the wave amplitude. Finally, the reflection coefficient was evaluated as the ratio of the backward wave to the forward wave amplitudes (Figure 3.2:2).

Statistical Analysis

Data is reported as a mean \pm SD for continuous variables, and as percentages for categorical variables. For comparing continuous variables before and after TAVR paired t-test was used. The inflection point could not be explicitly identified on the aortic pressure upstroke of seven patients; hence these seven cases were excluded from the AIx analysis (n=26). Pearson's correlation coefficient (r), normalized root mean squared error (nRMSE) and Bland-Altman analysis were used to assess the correlation, accuracy and agreement between the echocardiographic and thermodilution-derived CO values obtained prior to the TAVR procedure. Statistical significance was considered for p-values lower than 0.05. Statistical analysis was performed in SPSS (version 13.0, Chicago, Illinois).

3.2.3 Results

The demographic characteristics, comorbidities and presenting symptoms of the study participants are summarized in Table 3.2:1. Average age was 84 ± 6 years, 17 (52%) were females and 24 (72.7%) presented with baseline arterial hypertension, which was the most common risk factor. Most patients (n=22, 66.6%) presented with moderate to severe dyspnea (NYHA III or IV) before the TAVR.

Table 3.2:1 Demographic characteristics, comorbidities and presenting symptoms of the study participants.

| | <i>n=33</i> |
|---------------------------------|--------------------|
| Age (years) | 84±6 |
| Gender (males, %) | 16 (48.5) |
| Height (cm) | 166±8 |
| Weight (kg) | 76±15 |
| BMI (kg/m ²) | 27.5±5.5 |
| BSA (m ²) | 1.8±0.2 |
| Smokers (%) | 1 (3) |
| Ex-Smokers (%) | 16 (48.5) |
| Arterial Hypertension (%) | 24 (72.7) |
| Dyslipidaemia (%) | 22 (66.7) |
| Diabetes (%) | 11 (33.4) |
| Previous stroke or TIA (%) | 6 (18.2) |
| Coronary artery disease (%) | 17 (51.5) |
| Peripheral artery disease (%) | 4 (12.1) |
| COPD (%) | 4 (12.1) |
| Renal failure (%) | 17 (51.5) |
| Atrial fibrillation/Flutter (%) | 11 (33.3) |
| Oncological disease (%) | 8 (24.2) |
| EuroSCORE 1 | 13.4±7.2 |
| EuroSCORE 2 | 4.5±3.0 |
| STS Score | 3.4±1.8 |
| NYHA III or IV (%) | 22 (66.6) |
| Angina (%) | 4 (12.1) |
| Syncope (%) | 7 (21.2) |

TIA: Transient ischemic attack; COPD: Chronic obstructive pulmonary disease; STS: Society of Thoracic Surgeons

As expected TAVR acutely decreased LV peak pressure, ventricular-aortic pressure gradients, echocardiographic maximal aortic velocity and valvular-arterial impedance in all patients, as shown in Table 3.2:2. Aortic surface increased from 0.8 ± 0.2 cm² for the native valve to 1.9 ± 0.4 cm² for the prosthetic valve ($p < 0.001$). Table 3.2:2 also contains information on the LV ejection fraction, end-systolic and end-diastolic volumes as assessed by Simpson's monoplane in 4 chamber view in standard echocardiography. We noted that the LV ejection fraction increased after TAVR ($63 \pm 15\%$ versus $68 \pm 14\%$, $p = 0.001$). This was mainly driven by a significant decrease in the end-systolic volume (from 27 ± 15 ml to 23 ± 14 ml, $p = 0.007$).

Table 3.2:2 Invasive hemodynamic and echocardiographic characteristics of the study population before and after TAVR.

| Parameter | Pre TAVR | Post TAVR | P-value |
|--|-----------|-----------|---------|
| Heart rate (bpm) | 64±11 | 70±12 | 0.002 |
| Invasive LV peak pressure (mmHg) | 179±25 | 161±24 | <0.001 |
| Invasive mean ventricular-aortic pressure gradient (mmHg·sec) | 16.1±6.2 | 1.8±1.2 | <0.001 |
| Ejection fraction (Simpson 4C, %) | 63±15 | 68±14 | 0.001 |
| End-diastolic volume (Simpson 4C, ml) | 69±26 | 68±28 | 0.60 |
| End-systolic volume (Simpson 4C, ml) | 27±15 | 23±14 | 0.007 |
| Echocardiographic mean ventricular-aortic pressure gradient (mmHg) | 44±14 | 8±3 | <0.001 |
| Echocardiographic max ventricular-aortic pressure gradient (mmHg) | 75±21 | 15±6 | <0.001 |
| Max aortic velocity (cm/sec) | 427±62 | 193±40 | <0.001 |
| Aortic/prosthetic valve surface (cm ²) | 0.8±0.2 | 1.9±0.4 | <0.001 |
| Valvular-arterial impedance (mmHg/mL/m ²) | 6.1±1.7 | 4.3±1.0 | <0.001 |
| Aortic regurgitation (%) | | | |
| NS or minimal | 15 (43.4) | 14 (42.5) | |
| Discrete or discrete to moderate | 18 (56.6) | 19 (57.5) | |
| Mitral regurgitation (%) | | | |
| NS or discrete | 30 (91) | 30 (91) | |
| Discrete to moderate | 1 (3) | 2 (6) | |
| Moderate | 1 (3) | 1 (3) | |
| Moderate to severe | 1 (3) | 0 (0) | |

LV: left ventricle; NS: Not significant.

Table 3.2:3 summarizes the major hemodynamic changes related to TAVR. After valve replacement, aortic flow had a higher maximal value (237±49 versus 302±69 mL/sec, $p<0.001$) and reached its maximal value earlier in the systole (0.14±0.03 versus 0.10±0.02 sec, $p<0.001$). Concurrently, the duration of ejection decreased (0.35±0.04 versus 0.31±0.04 sec, $p<0.001$). The heart rate as well as the stroke volume showed an increase after TAVR (64±11 to 70±12 bpm, $p=0.002$, and 58±13 versus 63±17 mL, $p=0.05$, respectively). This led to a rise in cardiac output (4.1 ±0.7 versus 4.7±1.2 L/min, $p=0.003$).

TAVR acutely affected the aortic pressure waveform (Table 3.2:3, Figure 3.2:3). Within minutes after the resolution of AS, we observed an increase in the aortic SBP (from 131±22 to 157±25 mmHg, $p<0.001$) and DBP (from 53±11 to 57±12 mmHg, $p=0.04$). This entailed a rise in PP (78±17 versus 100±21 mmHg, $p<0.001$) and MAP (79±13 versus 91±14 mmHg, $p<0.001$). The invasive aortic pressure curve became steeper at early ejection (512±149 versus 1001±408 mmHg/sec, $p<0.001$) and the peak pressure occurred earlier in the systole (0.26±0.04 versus 0.23±0.03 sec, $p=0.001$). Subsequently, we applied pulse wave analysis to study the periprocedural changes in the aortic AP and AIx. We found that the inflection point occurred at significantly higher pressures (101±16

versus 135 ± 25 mmHg, $p < 0.001$). Consequently, AP decreased after the procedure (34 ± 14 mmHg versus 19 ± 12 mmHg, $p < 0.001$) and aortic AIx presented a decrease from $42 \pm 12\%$ to $19 \pm 11\%$ ($p < 0.001$, Table 3.2:3).

Immediately after TAVR, the properties of the arterial system remained unchanged as assessed via the PPM (Table 3.2:3). Concretely, because of the moderate increase in MAP combined with the improved CO, the total arterial resistance did not change (1.40 ± 0.32 versus 1.39 ± 0.38 mmHg·sec/mL, $p = \text{NS}$). The total arterial compliance had a minor decreasing trend (0.45 ± 0.12 versus 0.42 ± 0.15 mL/mmHg) as a result of increases in aortic MAP (by $\sim +15\%$) and PP (by $\sim +27\%$), which, however, did not reach statistical significance ($p = 0.11$).

Table 3.2:3 Effect of TAVR on vascular parameters assessed via the PPM and on the aortic pressure wave components assessed via frequency-based wave separation analysis.

| | Pre TAVR | Post TAVR | P-value |
|--|-----------------|-----------------|-----------|
| Aortic flow | | | |
| Ejection duration (sec) | 0.35 ± 0.04 | 0.31 ± 0.04 | < 0.001 |
| Maximal aortic flow (mL/sec) | 237 ± 49 | 302 ± 69 | < 0.001 |
| Time to max aortic flow (sec) | 0.14 ± 0.03 | 0.10 ± 0.02 | < 0.001 |
| Stroke volume (mL) | 58 ± 13 | 63 ± 17 | 0.05 |
| Cardiac output (L/min) | 4.1 ± 0.7 | 4.7 ± 1.2 | 0.003 |
| Aortic pressure waveform | | | |
| Aortic SBP (mmHg) | 131 ± 22 | 157 ± 25 | < 0.001 |
| Aortic DBP (mmHg) | 53 ± 11 | 57 ± 12 | 0.04 |
| Aortic PP (mmHg) | 78 ± 17 | 100 ± 21 | < 0.001 |
| Aortic MAP (mmHg) | 79 ± 13 | 91 ± 14 | < 0.001 |
| Time to aortic SBP (sec) | 0.26 ± 0.04 | 0.23 ± 0.03 | 0.001 |
| Maximal aortic pressure slope (mmHg/sec) | 512 ± 149 | 1001 ± 408 | < 0.001 |
| Aortic inflection point (mmHg) | 101 ± 16 | 135 ± 25 | < 0.001 |
| Time to aortic inflection point (sec) | 0.13 ± 0.04 | 0.13 ± 0.03 | 0.98 |
| Aortic augmentation pressure (mmHg) | 34 ± 14 | 19 ± 12 | < 0.001 |
| Aortic augmentation index (%) | 42 ± 12 | 19 ± 11 | < 0.001 |
| Wave separation analysis | | | |
| Characteristic impedance (mmHg·sec/mL) | 0.22 ± 0.12 | 0.22 ± 0.10 | 0.87 |
| Forward wave amplitude (mmHg) | 61 ± 20 | 77 ± 20 | < 0.001 |
| Time to forward wave peak (sec) | 0.21 ± 0.03 | 0.16 ± 0.03 | < 0.001 |
| Maximal forward wave slope (mmHg/sec) | 730 ± 395 | 1290 ± 551 | < 0.001 |
| Backward wave amplitude (mmHg) | 35 ± 14 | 42 ± 10 | 0.013 |
| Time to backward wave peak (sec) | 0.31 ± 0.06 | 0.27 ± 0.05 | < 0.001 |
| Maximal backward wave slope (mmHg/sec) | 278 ± 113 | 415 ± 151 | < 0.001 |
| Backward wave transit time (sec) | 0.11 ± 0.06 | 0.09 ± 0.06 | 0.16 |
| Reflection coefficient | 0.57 ± 0.13 | 0.56 ± 0.14 | 0.57 |
| 2-element Windkessel parameters | | | |
| Total vascular resistance (mmHg·sec/mL) | 1.40 ± 0.32 | 1.39 ± 0.38 | 0.84 |
| Total arterial compliance (mL/mmHg) | 0.45 ± 0.12 | 0.42 ± 0.15 | 0.11 |

SBP: systolic blood pressure; DBP: diastolic blood pressure; PP: pulse pressure; MAP: mean arterial pressure.

After analyzing the input impedance in the frequency domain, we estimated that the characteristic impedance was unaffected by the valve replacement (Table 3.2:3). By further applying wave separation analysis, we found that both forward (61 ± 20 versus 77 ± 20 mmHg, $p<0.001$) and backward pressure wave (35 ± 14 mmHg versus 42 ± 10 mmHg, $p=0.013$) components were amplified, had steeper upstrokes and reached their respective peaks at earlier time points (Table 3.2:3, Figure 3.2:3). The increase in the wave amplitudes was not associated with any change in their ratio, which served as a measure of the reflection coefficient (0.57 ± 0.13 versus 0.56 ± 0.14 , $p=0.57$). Figure 3.2:3 demonstrates the periprocedural changes in the central hemodynamics for a severe AS patient, representative of the study population.

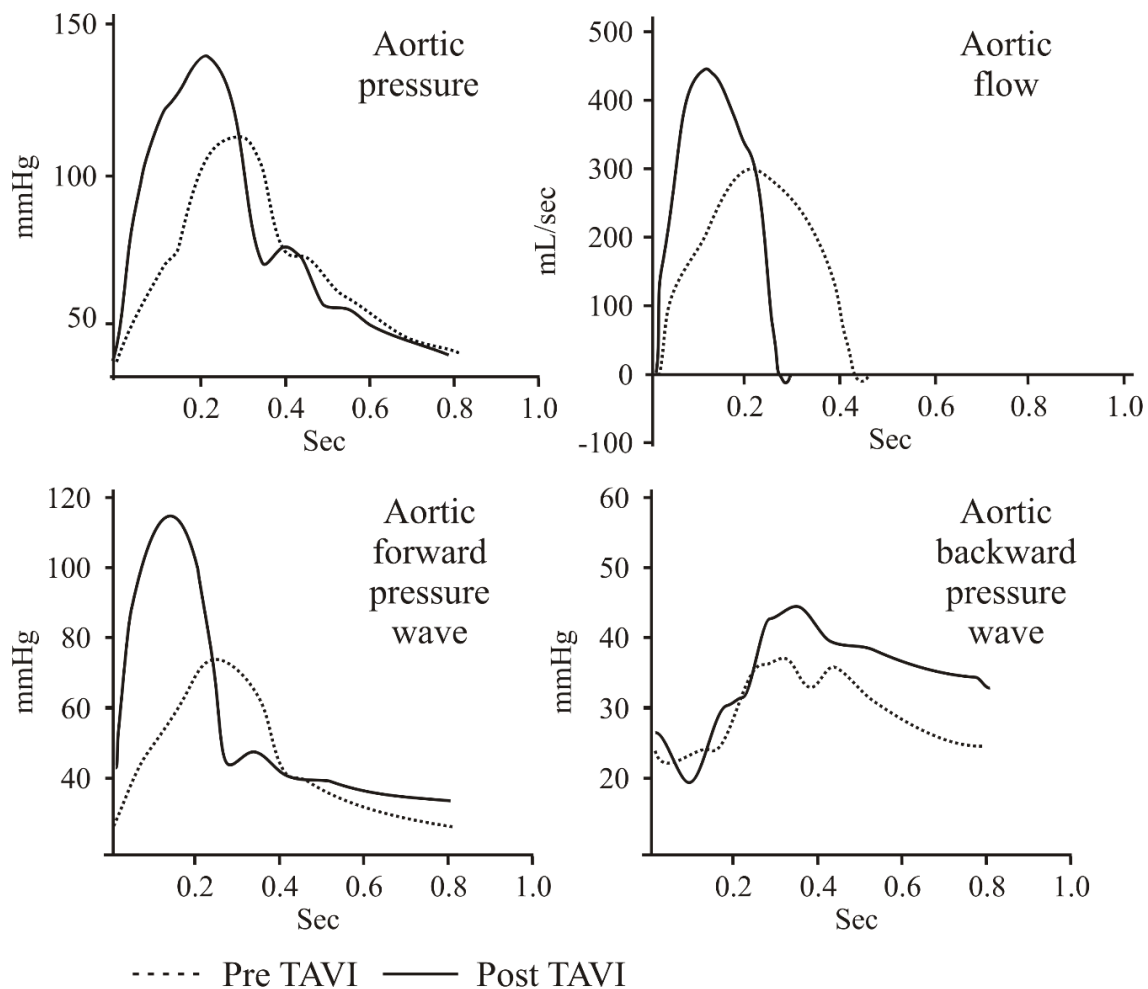


Figure 3.2:3 Representative case of a patient with severe AS before and after TAVR. Hemodynamic changes with respect to central pressure and flow waves are depicted. Changes in aortic pressure wave features include an increase in the systolic blood pressure, pressure at the inflection point and pulse pressure, while augmentation pressure and augmentation index decrease. Changes in aortic flow waveform characteristics include increase in maximal flow and slope. Forward and backward pressure components present a rise in both wave amplitudes and slope. Their ratio is maintained after TAVR.

Reliability of echocardiographic flow measurements

Figure 3.2:4 depicts the correlation and agreement between the CO measured by echocardiography and thermodilution performed prior to the TAVR procedure. The correlation coefficient was $r=0.57$, with $nRMSE=21\%$. The bias of the echocardiographic measurement was low ($\bar{d}=-0.2$ L/min) with acceptable limits of agreements ($LA=[-1.8, 1.3]$ L/min). Importantly, there was no statistically significant difference between the CO assessed by the two methods ($p=0.08$). The median difference in time between the two exams was 1 day (range: 25th quartile :1 day – 75th quartile 14 days).

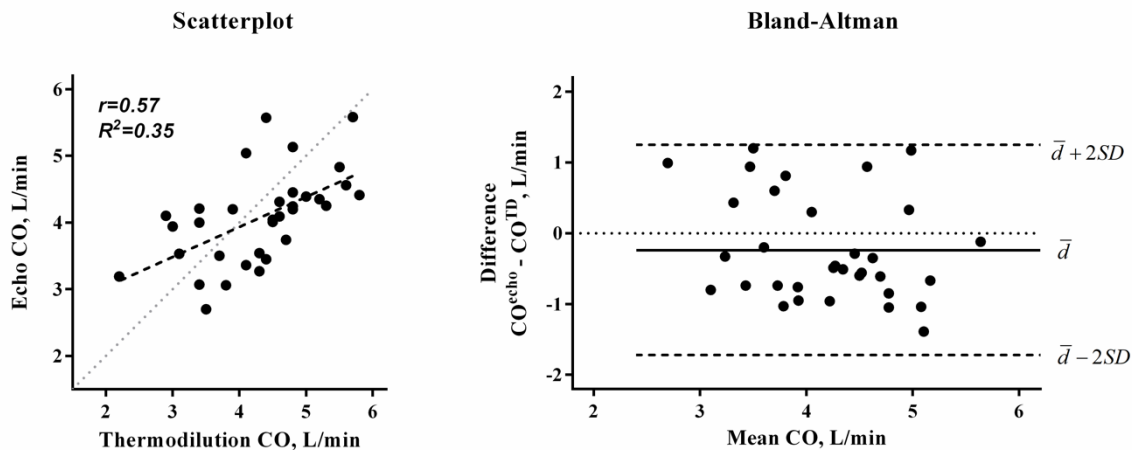


Figure 3.2:4 Scatterplot (left) and Bland-Altman plot (right) comparing the cardiac output estimated prior to the TAVR procedure via echocardiography and thermodilution. In the scatterplot, the line of equality (dotted line) and the linear fit of the data (dashed line) are shown. In the Bland-Altman plot, bias, \bar{d} , and limits of agreement, $\bar{d} \pm 2SD$, are also depicted. CO: cardiac output, TD: thermodilution

3.2.4 Discussion

In the present study, we investigated the acute effects of TAVR on central hemodynamics based on invasive measures of LV, aortic pressure and echocardiographic flow data by means of standard pulse wave and wave separation analysis. Our main findings are: 1) TAVR resulted in an immediate increase in aortic pressures with no significant changes in the total vascular resistance of the arterial tree, 2) wave separation analysis showed a comparable amplification of both the forward and backward pressure waves, while timing and reflection coefficient remained unchanged and 3) a notable decrease in the aortic A_{1x} after the TAVR procedure was noted despite an unaffected arterial compliance and reflection coefficient.

In all 33 AS cases, TAVR successfully resulted in the relief of the blood flow obstruction as confirmed by the immediate and substantial decrease in the transvalvular resistance. The decreased mean ventricular-aortic pressure gradient was accompanied by a significant drop in the systolic LV pressure demonstrating the expected beneficial influence of TAVR on cardiac afterload.

In the present cohort, valve replacement was also associated with an increase in aortic pressures, mainly systolic. This observation is in line with previous literature; some investigators suggest the development of hypertension within the first hours and days after the procedure [22], [23], while others also show long-term effects [24]. The prognostic significance and optimal management of the post TAVR hypertension remains unknown since neither compliance nor vascular resistance is the responsible mechanism.

Considering CO, most previous works showed a significant improvement after TAVR [22], [23]. Namely, Chrissoheris et al. [22], reported in their invasive examination of 52 cases a rise in CO from 3.8 ± 1.3 L/min to 5.4 ± 1.7 L/min as measured with thermodilution. In our study, we also reported a significant improvement of the LV output after the valve replacement by approximately 0.6 L/min.

TAVR and the ventricular-arterial coupling

With regard to the cardiovascular coupling, all hemodynamic cases examined in this study support the following paradigm. In the presence of chronic AS, the cardiovascular system gradually develops compensatory mechanisms to adapt to the high afterload [3]. In other words, the system reaches a ventricular-arterial coupling that is optimal in order to overcome the great valvular resistance and achieve adequate perfusion of the arterial system. As TAVR successfully resolves the aortic stenosis in a matter of minutes, the LV cannot adapt acutely to the new conditions. Downstream of the aortic valve, there is no radical alteration in the arterial properties immediately after TAVR (i.e. characteristic impedance, vascular resistance and compliance).

Therefore, for an unchanged arterial system, the left ventricle is expected to pump a more pronounced forward wave. Indeed, we found that, after the procedure, the forward pressure wave is enhanced in amplitude, has a steeper upstroke and reaches its peak earlier. The steeper upstroke, as can be observed in the early systolic part of the total aortic pressure curve, has also been reported by other groups. Muller et al. [10] showed an increase in the maximal rate of rise of aortic pressure and interpreted it as indicative of better LV contractility after valve replacement.

Subsequently, the enhanced forward wave propagates into the arterial system until it is reflected at peripheral sites of impedance mismatch. We found that the reflected pressure wave arriving back to the aorta is also enhanced in amplitude, while overall the reflection coefficient is maintained. This seems reasonable, given that there is no major change in the properties of the arterial tree.

Alx in patients with severe aortic stenosis

Following this paradigm, it is relevant to consider its implications for the interpretation of the Alx. The Alx is defined according to the inflection point observed on the upstroke of the pressure waveform. Traditionally, this inflection point is understood as the marker of the arrival of the backward traveling wave and of its superposition with the forward wave. Accordingly, Alx is often regarded as a vascular measure of aortic stiffness and wave reflection [11]. However, there is concrete evidence suggesting that the Alx might not be a suitable marker for aortic stiffening. Previous investigations showed a non-linear relationship between Alx and age [25], [26] as well as associations between lower Alx and higher cardiovascular risk factor burden [27].

In the present work, we demonstrated a significant drop in the aortic Alx due to TAVR. This finding was also previously reported by Muller et al. [10], who examined reconstructed aortic pressure waveforms in a similar setting. If the paradigm of Alx as a sole measure of stiffness and reflections were valid, then one would expect a concomitant decrease also in wave reflections after the valve replacement. However, as shown by means of wave separation analysis, TAVR had no effect on the reflection coefficient. This observation seriously challenges the view of Alx as a marker of stiffness in AS patients. Our data suggest that the decrease in Alx reflects changes in the ventricular-arterial coupling due to the resolution of AS. A plausible explanation for the decrease in Alx is that it is associated with the timing/slope of the enhanced forward wave. An earlier and steeper increase in early systolic (forward mainly) wave will result in much higher pressures before the arrival of the reflected wave, leading to a smaller relative contribution of wave reflections to the total pulse pressure and thus a lower Alx. This explanation is clearly supported by the typical features of the aortic waves before and after TAVR shown in Figure 3.2:3. The concept of Alx reflecting both cardiac and vascular properties was also previously evoked in a recent study [28].

Study considerations and limitations

Arguably, echocardiography has limitations in the evaluation of aortic flow when compared to the gold standard techniques, i.e., catheterization and thermodilution. In the present study, we examined the reliability of the echocardiographic flow measurements performed prior to the TAVR procedure by direct comparison with thermodilution measurements. We found that echocardiography tended to slightly underestimate cardiac output; this result is in line with previous literature [29]. Nevertheless, the bias was low and importantly there was no statistically significant difference between the two methods. These findings are corroborated by the observations of Antonini-Canterin et al. [29]. Additionally, we acknowledge that the aortic pressure and flow measurements were not performed simultaneously. Regarding the wave separation analysis, we accounted for the fact that the two measurements were not simultaneous by employing synchronization techniques to improve the quality of the results.

The cohort included mostly elderly with severe AS, given that this is the typical population selected for TAVR. Therefore, caution should be exerted in generalizing these results for other patient groups. Particularly younger subjects undergoing TAVR might not develop these compensatory mechanisms to the same extent. On that note, the study group was selected to exclude comorbidities that might influence the validity of our interpretations (e.g. hemodynamic shock, moderate or severe aortic valve regurgitation, left ventricular dysfunction).

Conclusions

The present study offers novel insights into the alterations in the ventricular-arterial coupling due to successful TAVR. Our findings support the development of systolic hypertension shortly after TAVR, as previously demonstrated. Additionally, we found that TAVR was linked with the enhancement of the forward wave pumped by the heart. We demonstrated that Alx was markedly decreased after TAVR; a decrease which was not associated with any significant change in the stiffness of the vascular system or the wave reflection coefficient. Therefore, these results challenge the interpretation of Alx as a solely vascular measure in the setting of AS.

3.2.5 Bibliography

- [1] C. Rostagno, "Heart valve disease in elderly," *World J. Cardiol.*, vol. 11, no. 2, p. 71, Feb. 2019, doi: 10.4330/wjc.v11.i2.71.
- [2] A. Călin *et al.*, "The left ventricle in aortic stenosis – imaging assessment and clinical implications," *Cardiovasc. Ultrasound*, vol. 13, no. 1, p. 22, Apr. 2015, doi: 10.1186/s12947-015-0017-4.
- [3] S. Sasayama, J. Ross, D. Franklin, C. M. Bloor, S. Bishop, and R. B. Dille, "Adaptations of the left ventricle to chronic pressure overload," *Circ. Res.*, vol. 38, no. 3, pp. 172–178, Mar. 1976, doi: 10.1161/01.res.38.3.172.
- [4] Z. Hachicha, J. G. Dumesnil, P. Bogaty, and P. Pibarot, "Paradoxical low-flow, low-gradient severe aortic stenosis despite preserved ejection fraction is associated with higher afterload and reduced survival," *Circulation*, vol. 115, no. 22, pp. 2856–2864, Jun. 2007, doi: 10.1161/CIRCULATIONAHA.106.668681.
- [5] G. H. Bevan, D. A. Zidar, R. A. Josephson, and S. G. Al-Kindi, "Mortality Due to Aortic Stenosis in the United States, 2008-2017," *JAMA*, vol. 321, no. 22, pp. 2236–2238, Jun. 2019, doi: 10.1001/jama.2019.6292.
- [6] C. R. Smith *et al.*, "Transcatheter versus surgical aortic-valve replacement in high-risk patients," *N. Engl. J. Med.*, vol. 364, no. 23, pp. 2187–2198, Jun. 2011, doi: 10.1056/NEJMoa1103510.
- [7] D. H. Adams *et al.*, "Transcatheter aortic-valve replacement with a self-expanding prosthesis," *N. Engl. J. Med.*, vol. 370, no. 19, pp. 1790–1798, May 2014, doi: 10.1056/NEJMoa1400590.
- [8] M. J. Mack *et al.*, "Transcatheter Aortic-Valve Replacement with a Balloon-Expandable Valve in Low-Risk Patients," *N. Engl. J. Med.*, vol. 380, no. 18, pp. 1695–1705, 02 2019, doi: 10.1056/NEJMoa1814052.
- [9] Thyregod Hans Gustav Hørsted *et al.*, "Five-Year Clinical and Echocardiographic Outcomes From the NOTION Randomized Clinical Trial in Patients at Lower Surgical Risk," *Circulation*, vol. 139, no. 24, pp. 2714–2723, Jun. 2019, doi: 10.1161/CIRCULATIONAHA.118.036606.
- [10] C. Müller *et al.*, "Transcatheter aortic valve replacement (TAVR) leads to an increase in the subendocardial viability ratio assessed by pulse wave analysis," *PLOS ONE*, vol. 13, no. 11, p. e0207537, Nov. 2018, doi: 10.1371/journal.pone.0207537.
- [11] C. Vlachopoulos, M. O'Rourke, W. W. Nichols, M. O'Rourke, and W. W. Nichols, *McDonald's Blood Flow in Arteries: Theoretical, Experimental and Clinical Principles*. CRC Press, 2011.
- [12] A. P. Kappetein *et al.*, "Updated standardized endpoint definitions for transcatheter aortic valve implantation: The Valve Academic Research Consortium-2 consensus document*," *J. Thorac. Cardiovasc. Surg.*, vol. 145, no. 1, pp. 6–23, Jan. 2013, doi: 10.1016/j.jtcvs.2012.09.002.
- [13] Nishimura Rick A. and Carabello Blase A., "Hemodynamics in the Cardiac Catheterization Laboratory of the 21st Century," *Circulation*, vol. 125, no. 17, pp. 2138–2150, May 2012, doi: 10.1161/CIRCULATIONAHA.111.060319.
- [14] B. A. Carabello, "What is new in the 2006 ACC/AHA guidelines on valvular heart disease?," *Curr. Cardiol. Rep.*, vol. 10, no. 2, pp. 85–90, Mar. 2008, doi: 10.1007/s11886-008-0016-2.
- [15] R. Kelly, C. Hayward, A. Avolio, and M. O'Rourke, "Noninvasive determination of age-related changes in the human arterial pulse," *Circulation*, vol. 80, no. 6, pp. 1652–1659, Dec. 1989, doi: 10.1161/01.cir.80.6.1652.
- [16] Murgo J P, Westerhof N, Giolma J P, and Altobelli S A, "Aortic input impedance in normal man: relationship to pressure wave forms," *Circulation*, vol. 62, no. 1, pp. 105–116, Jul. 1980, doi: 10.1161/01.CIR.62.1.105.
- [17] J. Womersley, "An Elastic Tube Theory of Pulse Transmission and Oscillatory Flow in Mammalian Arteries," *WADC Tech. Rep.* - TR56-614, 1957.
- [18] H. Baumgartner *et al.*, "Echocardiographic assessment of valve stenosis: EAE/ASE recommendations for clinical practice," *J. Am. Soc. Echocardiogr. Off. Publ. Am. Soc. Echocardiogr.*, vol. 22, no. 1, pp. 1–23; quiz 101–102, Jan. 2009, doi: 10.1016/j.echo.2008.11.029.
- [19] D. J. Penny, J. P. Mynard, and J. J. Smolich, "Aortic wave intensity analysis of ventricular-vascular interaction during incremental dobutamine infusion in adult sheep," *Am. J. Physiol. Heart Circ. Physiol.*, vol. 294, no. 1, pp. H481–489, Jan. 2008, doi: 10.1152/ajpheart.00962.2006.

- [20] N. Stergiopoulos, J.-J. Meister, and N. Westerhof, "Simple and accurate way for estimating total and segmental arterial compliance: The pulse pressure method," *Ann. Biomed. Eng.*, vol. 22, no. 4, pp. 392–397, Jul. 1994, doi: 10.1007/BF02368245.
- [21] N. Westerhof, P. Sipkema, G. C. van den Bos, and G. Elzinga, "Forward and backward waves in the arterial system," *Cardiovasc. Res.*, vol. 6, no. 6, pp. 648–656, Nov. 1972, doi: 10.1093/cvr/6.6.648.
- [22] M. Chrissoheris *et al.*, "Acute Invasive Hemodynamic Effects of Transcatheter Aortic Valve Replacement," *J. Heart Valve Dis.*, vol. 25, no. 2, pp. 162–172, 2016.
- [23] V. Di Bello *et al.*, "Acute improvement in arterial-ventricular coupling after transcatheter aortic valve implantation (CoreValve) in patients with symptomatic aortic stenosis," *Int. J. Cardiovasc. Imaging*, vol. 28, no. 1, pp. 79–87, Jan. 2012, doi: 10.1007/s10554-010-9772-3.
- [24] G. Y. Perlman *et al.*, "Post-Procedural Hypertension Following Transcatheter Aortic Valve Implantation: Incidence and Clinical Significance," *JACC Cardiovasc. Interv.*, vol. 6, no. 5, pp. 472–478, May 2013, doi: 10.1016/j.jcin.2012.12.124.
- [25] F. Fantin, A. Mattocks, C. J. Bulpitt, W. Banya, and C. Rajkumar, "Is augmentation index a good measure of vascular stiffness in the elderly?," *Age Ageing*, vol. 36, no. 1, pp. 43–48, Jan. 2007, doi: 10.1093/ageing/afl115.
- [26] C. M. McEniery, Yasmin, I. R. Hall, A. Qasem, I. B. Wilkinson, and J. R. Cockcroft, "Normal Vascular Aging: Differential Effects on Wave Reflection and Aortic Pulse Wave Velocity: The Anglo-Cardiff Collaborative Trial (ACCT)," *J. Am. Coll. Cardiol.*, vol. 46, no. 9, pp. 1753–1760, Nov. 2005, doi: 10.1016/j.jacc.2005.07.037.
- [27] G. F. Mitchell *et al.*, "Arterial stiffness and cardiovascular events: The Framingham Heart Study," *Circulation*, vol. 121, no. 4, p. 505, Feb. 2010, doi: 10.1161/CIRCULATIONAHA.109.886655.
- [28] M. H. G. Heusinkveld *et al.*, "Augmentation index is not a proxy for wave reflection magnitude: mechanistic analysis using a computational model," *J. Appl. Physiol. Bethesda Md 1985*, vol. 127, no. 2, pp. 491–500, Aug. 2019, doi: 10.1152/japplphysiol.00769.2018.
- [29] F. Antonini-Canterin, S. Poli, O. Vriz, D. Pavan, V. D. Bello, and G. L. Nicolosi, "The Ventricular-Arterial Coupling: From Basic Pathophysiology to Clinical Application in the Echocardiography Laboratory," *J. Cardiovasc. Echography*, vol. 23, no. 4, pp. 91–95, 2013, doi: 10.4103/2211-4122.127408.

Chapter 4 Inverse Methods for Noninvasive Monitoring of Hemodynamics

4.1 Estimating left ventricular elastance from aortic flow waveform, ventricular ejection fraction, and brachial pressure: an *in silico* study

Stamatia Pagoulatou and Nikolaos Stergiopoulos

Laboratory of Hemodynamics and Cardiovascular Technology (LHTC), Institute of Bioengineering, Ecole Polytechnique Fédérale de Lausanne (EPFL), Lausanne, Switzerland

Abstract

Although left ventricular end-systolic elastance (E_{es}) serves as a major index of cardiac contractility, a widely-accepted noninvasive estimation of E_{es} does not exist. To overcome this limitation, we developed a two-step inverse method that allows for its noninvasive estimation from measurements of aortic flow and brachial pressure using a previously validated one-dimensional model of the cardiovascular system. In a first step, aortic flow is set as the model input and the output brachial pressure is compared with the 'real' values. Subsequently, the basic properties of the arterial tree are tuned according to an optimization algorithm. In a second step, the same optimization method is used to estimate the elastance parameters that produce an aortic flow waveform that matches the 'real' one. Additional knowledge of the ejection fraction can allow for the accurate estimation of the entire P-V loop, including end-diastolic elastance. The method was tested on a database of 50 different *in silico* hemodynamic cases generated after varying cardiac and arterial model parameters. Implementation of the method yielded good agreement ($r=0.99$) and accuracy ($n\text{-RMSE}=4\%$) between 'real' and estimated values of E_{es} . Furthermore, a sensitivity analysis revealed that errors due to poor arterial adjustment and measurements are small ($\leq 8\%$ for E_{es}).

Key words: Cardiac contractility • Noninvasive • 1D model • Hemodynamics

Published in Annals of Biomedical Engineering (2018)

4.1.1 Introduction

The clinical need of effectively monitoring cardiac performance and thus detecting possible myocardial disorders is well established. However, accurate assessment of the myocardial inotropic state, independently from preload and afterload, remains still a challenge. As a result, research has been oriented over the past decades towards deriving a reliable and easily obtainable cardiac index, which would carry significant diagnostic value by being a determinant of myocardial contractility and which would enable comparison between different patho-physiological states or different individuals by being insensitive to loading conditions [1].

In this respect, past efforts to assess contractile state by measurement of myocardial shortening velocity were quickly abandoned after the emergence of the widely accepted concept of elastance, first proposed by Suga et al. [2], [3]. In a series of invasive studies of the left ventricular pressure-volume (P-V) loops in canine hearts, Suga et al. demonstrated that end-systolic elastance (E_{es}), i.e. the slope of the end-systolic pressure-volume relation (ESPVR), is a major determinant of left ventricular (LV) systolic performance and heart interaction with the systemic vasculature [2]–[4]. The concept of the time-varying elastance, ($E(t)$), was introduced shortly after the observation that there is a fairly linear pressure-volume relationship at any given moment of the cardiac cycle.

Although this approach has been proven to be a fertile area of research and is often used in animal research, its clinical applicability is severely hampered by two factors: the need for inducing *in vivo* acute load alterations and the method's invasive nature. The former aspect was addressed in a number of studies [5], [6], which proposed and validated invasive methods for estimating E_{es} from a single cardiac cycle (single-beat methods). Building upon this framework, investigators have subsequently focused their efforts on establishing a reliable noninvasive method to derive end-systolic elastance from simple single-beat measurements [7], [8].

The use of mathematical models of the cardiovascular system could serve as a valuable tool to assess cardiac contractility and estimate end-systolic and end-diastolic elastance, E_{es} and E_{ed} , respectively. In this study, we introduce a novel, noninvasive, *in silico* method for deriving left ventricular elastance in humans from measured proximal aortic flow waveforms and brachial pressure values. This methodology was developed according to an inverse problem-solving concept. Method feasibility and validity were tested under different hemodynamic conditions via the use of an accurate and validated, one-dimensional (1D) model of the arterial tree [9], [10] coupled with a typical time-varying elastance model for the left ventricle [5], [11]. Estimated values of E_{es} were compared to those obtained by prior methods in terms of accuracy and agreement.

4.1.2 Methods

Brief description of the 1D model of the arterial tree

The aforementioned 1D wave propagation model was developed in our laboratory by Reymond et al. [10] and was validated with *in vivo* measurements [9]. A brief overview of its basic features is presented below, focusing mainly on the ventricular-arterial coupling. A more thorough description of the model assumptions can be found in the original publications [9], [10].

The arterial tree, as depicted in Figure 1.3:10, consists of 103 arterial segments, including the main arteries of the systemic circulation, a detailed network representing the circle of Willis and the coronary circulation. Pressure and flow waveforms are obtained throughout the vasculature via numerical integration of the 1D form of the continuity and momentum equations over the arterial cross-section. Arterial wall behavior is nonlinear and viscoelastic and defined according to Holenstein et al. [12]. Local arterial compliance is related to pressure based on the function proposed by Langewouters et al. [13]. Vessel distensibility is calculated after approximating pulse wave velocity (PWV) as an inverse power function of arterial lumen diameter, following the physiological values reported in the literature. Resistance of the peripheral vasculature is accounted for by coupling the terminal branches of the arterial tree with 3-element Windkessel models.

This open-loop model can receive two possible input signals at the proximal end of the arterial tree, i.e. the root of the ascending aorta. One option is to solve the governing equations by prescribing as model input a recorded aortic flow waveform and, thus, completely excluding the cardiac function. Alternatively, the arterial system can be coupled with a model for the LV contractility [11]. This heart model consists of a constant pressure source (filling pressure, P_{fill}), which drives the filling of the left ventricle, and a time-varying elastance model, which relates left ventricular pressure, P_{lv} , and volume, V_{lv} , as follows:

$$E(t) = \frac{P_{lv}(t)}{V_{lv}(t) - V_o}$$

Equation 4.1:1 – Time-varying elastance relating left ventricular pressure and volume

where V_o is the dead volume of the left ventricle. Arterial-ventricular coupling is regulated by an updated aortic valve model [14], which can capture both normal and dysfunctional valve conditions. The normalized (both in time and magnitude) elastance curve used was proposed by Senzaki et al. [5] as the combined averaged curve of different patient groups (normal hearts to chronic heart diseases) and test conditions.

According to Senzaki et al. [5], this normalized time-varying elastance curve demonstrates little variance among humans, a finding which has also been corroborated by previous canine heart studies [2], [3]. Consequently, it can be inferred that the contractile state of any individual can be fully determined by only three cardiac parameters: (1) the end-systolic elastance, E_{es} , (2) the end-diastolic elastance, E_{ed} , and (3) time to reach E_{es} , t_{max} .

Basic principle of the two-step inverse method for E_{es} and E_{ed} estimation

The dual character of the model input inspired us with the following two-step inverse problem-solving algorithm for estimating left ventricular elastance (Figure 4.1:1). For a given preload and afterload, there is only one particular set of elastance parameters (E_{es} , E_{ed}) for which a given proximal aortic flow waveform is produced. Therefore, if, in a first step, we adjust the properties of the arterial tree (i.e. the compliance of each segment which determines pulse pressure and the resistance of the peripheral vessels which sets mean pressure), then it is possible to derive, in a second step, the elastance parameters from recorded aortic flow curves either on a trial-and-error basis or by developing an iterative (optimization) algorithm.

Accurate adjustment of the default arterial parameters (vessel compliance and peripheral resistance) into patient-specific settings is of course a challenging task. The arterial trees of different individuals may vary regarding their geometries, the compliance of each segment and resistance of the periphery. A simple approach followed in this crucial first step was to modify globally the compliance of the arterial segments and the peripheral resistance until brachial systolic (SBP) and diastolic (DBP) blood pressures are accurately predicted for the recorded aortic flow input.

Effect of Preload

The concept described above requires a few arterial measurements for the derivation of E_{es} and E_{ed} . End-diastolic elastance is, however, majorly affected by preload. Indeed, to implement this method under the assumption of a constant filling pressure would be limiting, as it would fix cardiac preload. In order to encompass this sensitivity, our method was extended to allow for the additional estimation of filling pressure and thus the derivation of E_{ed} . More specifically, for a “false” value of P_{fill} , the aforementioned technique calculates a pressure-volume loop that does not correspond to the “real” LV end-diastolic and end-systolic volumes, as argued in the following paragraphs (Figure 4.1:2), and, therefore, leads to an erroneous estimation of E_{es} and E_{ed} . If the method is supplemented by an additional independent measurement of EDV and ESV, then we possess all the information to estimate the correct filling pressure and thus define totally the pressure-volume loop.

In silico estimation of E_{es} and E_{ed}

To assess the feasibility of this technique, a database of 50 different hemodynamic cases was generated by varying key cardiac and arterial parameters in a physiologically and pathologically relevant range. More specifically, end-systolic and end-diastolic elastance varied in the range of [1.0, 3.5] mmHg/mL and [0.05, 0.20] mmHg/mL, respectively [15]–[17], whereas the value of dead volume, $V_o=15$ mL, was left unaltered. The filling pressure was altered in the range of [7, 23] mmHg in order to yield physiologically relevant end-diastolic pressures [5]. The time when maximal elastance occurs in the cardiac cycle (t_{max}) was kept constant for all cases and equal to the average value of $t_{max}=340$ ms reported by previous studies [10], [18]. Heart rate was also altered between 60 to 100 bpm throughout the simulations. Different arterial tree configurations were set by altering uniformly the reference vessel compliance of each segment (total compliance, C_{ref}) and the reference resistance of each terminal branch of the arterial tree (total peripheral resistance, R_{ref}) based on scaling factors ranging from 0.5 to 1.5 and 0.90 to 1.15, respectively. These values were chosen so that the generated aortic and brachial pressures were representative of a wide range of populations in terms of pulse pressure and mean arterial pressure. Arterial geometry was left unchanged for all cases. A variety of different hemodynamic cases were thus simulated, reflecting diverse cardiac and vascular mechanical properties representative of both healthy (low normotensive and normotensive) and unhealthy or aged (hypertensive) humans (Table 4.1:2).

After creating this pool of different cases, we tested the theoretical concept in practice by following the inverse problem-solving algorithm described above. For each hemodynamic case, the aortic flow was initially isolated and, henceforth, treated as the ‘real’ signal, such as a signal which could have been obtained from an Ultrasound measurement, for example. Using as a model input this aortic flow wave, the governing equations were solved throughout the vasculature keeping the default arterial configuration of the generic model. As expected, this led to computation of peripheral SBP and DBP values that deviated significantly from the ‘real’ ones. Subsequently, arterial compliance and peripheral resistance were altered globally by scaling factors determined via a gradient-based optimization algorithm (steepest descent) until brachial SBP and DBP predictions matched as close as possible the “real” ones.

Having tuned the arterial properties to the case-specific settings, we coupled the tuned 1D model of the arterial tree with the normalized elastance model of the heart. For an initial approximation of the filling pressure, we employed a similar optimization algorithm and estimated the E_{es} and E_{ed} values for which the model-derived aortic flow waveforms matched as close as possible the ‘real’ aortic flow wave. The resulting set of $\{E_{es}, E_{ed}, P_{fill}\}$ was evaluated by comparing the model-derived EDV to the ‘real’ value. The filling pressure was, subsequently, changed via an external optimization cycle until the process converged to a triplet of $\{E_{es}, E_{ed}, P_{fill}\}$ that led to the correct estimation of the end-diastolic volume.

A schematic description of the algorithm presented above is shown in Figure 4.1:1.

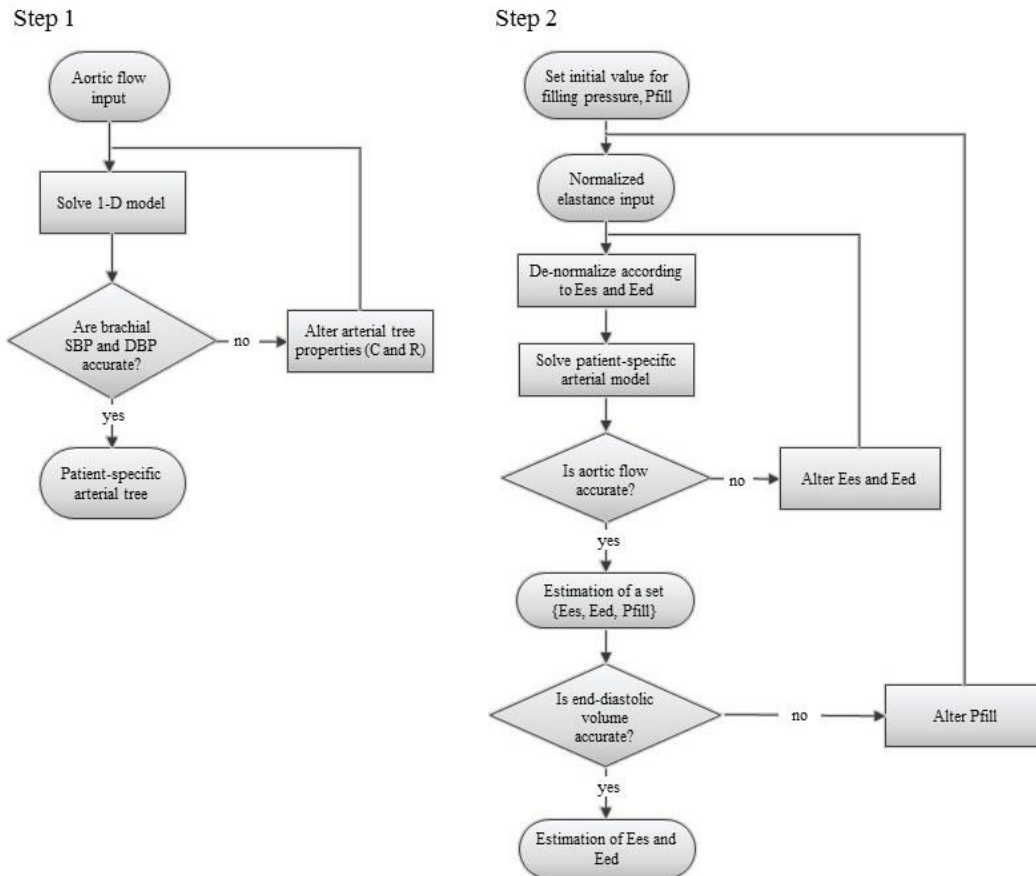


Figure 4.1:1 Schematic description of the two-step inverse problem-solving algorithm.

Comparison with previous noninvasive method for E_{es} estimation

LV end-systolic elastance was also estimated for each case following the method proposed by Chen et al. [8], which refers to the noninvasive single-beat estimation of maximal elastance from simple hemodynamic indices, i.e. systolic (SBP) and diastolic (DBP) arm-cuff pressures (brachial), echo-derived stroke volume (SV) and ejection fraction (EF):

$$E_{es} = \frac{DBP - E_{Nd(est)} \cdot 0.9 \cdot SBP}{SV \cdot E_{Nd(est)}}$$

Equation 4.1:2 – Single-beat method of Chen et al. for the noninvasive estimation of the end-systolic elastance

where the term $0.9 \cdot SBP$ is an approximation [19] of the end-systolic LV pressure (ESP) and DBP an approximation of the LV pressure at the end of the isovolumic contraction (Pad). $E_{Nd(est)}$ was suggested as a noninvasive estimate of the normalized ventricular elastance at the onset of ejection, which is based on the group-averaged normalized curve value $E_{Nd(avg)}$ proposed by Senzaki et al. [5]. In their original work, $E_{Nd(est)}$ was further altered according to hemodynamic indices (EF, brachial pressures) in order to account for the individual contractile effects, which cause deviation from the anticipated value $E_{Nd(avg)}$. In our study, however, since we made the assumption of a load-independent normalized elastance, we employed the method of Chen et al. [8] considering $E_{Nd(est)}$ and $E_{Nd(avg)}$ to be equal.

Statistical methods

Correlation, agreement and accuracy indices between the ‘real’ elastance values and the ones derived from the novel and the existing method were evaluated. Pearson’s correlation coefficient (r) was calculated to assess the strength of their relation, both in terms of linearity and direction, with $r=1$ reflecting perfect correlation. Furthermore, since a high r value does not necessarily mean that the data points lie along the line of equality, agreement was tested following the Bland-Altman method [20]. Bias was estimated by the mean difference (\bar{d}) and the standard deviation of the differences (SD). Limits of agreement were set at $\bar{d} + 2SD$ and $\bar{d} - 2SD$, given that if prediction errors are normally distributed then 95% of them are expected to lie in this range. Accuracy between model-predicted values and the real ones was measured by calculation of the root-mean-square error (RMSE) normalized to the average.

Sensitivity to arterial configuration tuning

To assess the robustness of the novel inverse method, we examined how errors deriving from the estimation of the arterial load influence the computed elastance parameters in a particular case of physiological cardiac and arterial properties ($E_{es}=2.25$ mmHg/mL, $E_{ed}=0.11$ mmHg/mL, $V_0=15$ mL, $P_{fill}=10.9$ mmHg and $C=1.1C_{ref}$, $R=R_{ref}$). Supposing that arterial compliance was erroneously estimated globally by +20%, we run the optimization algorithm and assessed the error in the new E_{es} and E_{ed} estimates. We repeated the same process by inducing a 20% global decrease in vessel compliance.

Sensitivity to measurement errors

In addition to examining the errors deriving from the implementation of the algorithm, we quantified the contribution of “measurement errors” on the elastance estimates. Using the same physiological case as before ($E_{es}=2.25$ mmHg/mL, $E_{ed}=0.11$ mmHg/mL, $V_0=15$ mL, $P_{fill}=10.9$ mmHg and $C=1.1C_{ref}$, $R=R_{ref}$) we introduced an increase of 10% in the amplitude of the input aortic flow and evaluated the variation in the E_{es} and E_{ed} estimates after the execution of the two-step algorithm. Finally, we investigated one more scenario where systolic blood pressure at the periphery was erroneously recorded at +10% of its real value.

4.1.3 Results

How preload affects E_{es} and E_{ed} estimates

Figure 4.1:2A shows the ‘real’ pressure-volume loop which was generated for a specific case with the following characteristics: $E_{es}=2.25$ mmHg/mL, $E_{ed}=0.11$ mmHg/mL, $P_{fill}=10.9$ mmHg, $V_0=15$ mL and $C=1.1C_{ref}$, $R=R_{ref}$, as shown in Table 4.1:1. Following Step 1 and after the adjustment of the arterial tree parameters, total arterial compliance and peripheral resistance were estimated with small errors (-1% and -5%, respectively). In Step 2, the preload was set to a default value of $P_{fill}=13.5$ mmHg and the derived pressure-volume loop is shown in Figure 4.1:2B. We observe a shift of the pressure-volume loop to the right, however, both the shape of the ejection part of the loop as well as the stroke volume are preserved. This shift towards higher volumes led to an underestimation of the ejection fraction, from 0.53 to 0.50 (Table 4.1:1). The fact that stroke volume is preserved with an increase in end-diastolic volume

(EDV) led to an increase in E_{ed} by 15% and decrease in E_{es} by 12%. Consequently, their ratio decreased by overall 24%, a finding which is in line with previous studies [21].

This analysis shows that if the filling pressure is not a priori known, the inverse method will fail to estimate the correct end-diastolic and end-systolic volume (ESV), although the stroke volume will be correctly captured, simply because aortic flow is prescribed and drives the optimization process. Therefore, additionally to aortic flow and brachial pressure, optimization for an independent measurement of EDV and ESV can allow us to define totally the pressure-volume loop, as depicted in Figure 4.1:2C.

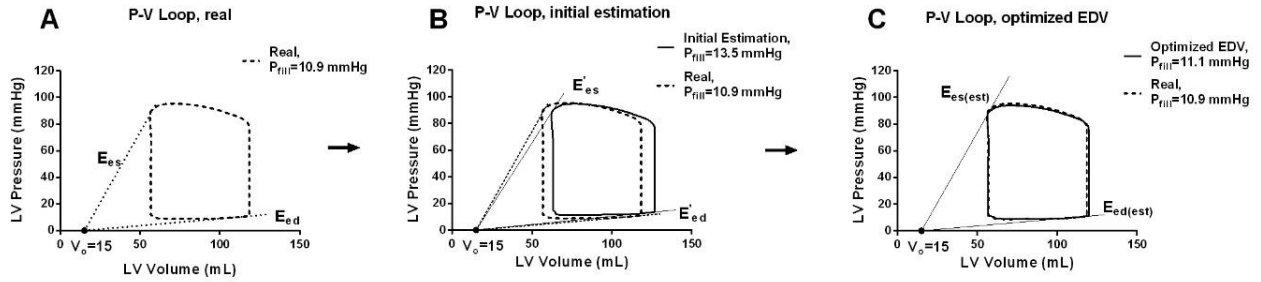


Figure 4.1:2 Optimization of cardiac preload. (A) The real P-V loop that corresponds to $P_{fill}=10.9$ mmHg. (B) First estimation with the default filling pressure set at $P_{fill}=13.5$ mmHg. (C) Final results after a second external optimization loop is added in order to reach the ‘measured’ EDV.

Table 4.1:1 The effect of cardiac preload on method estimates for a specific case.

| Parameter | Real | Initial Estimates, (error) | Second optimization with regards to EDV, (error) |
|--------------------|-------|----------------------------|--|
| E_{es} (mmHg/mL) | 2.25 | 1.97, (-12%) | 2.19, (-3%) |
| E_{ed} (mmHg/mL) | 0.105 | 0.121, (15%) | 0.106, (1%) |
| E_{es} / E_{ed} | 21.4 | 16.3, (-24%) | 20.7, (-3%) |
| EF | 0.527 | 0.501, (-5%) | 0.530, (1%) |
| EDV (mL) | 118.5 | 126.6, (7%) | 119.5, (1%) |
| P_{fill} (mmHg) | 10.9 | 13.5, (24%) | 11.1, (2%) |

***In silico* validation of the proposed method and comparison with other techniques**

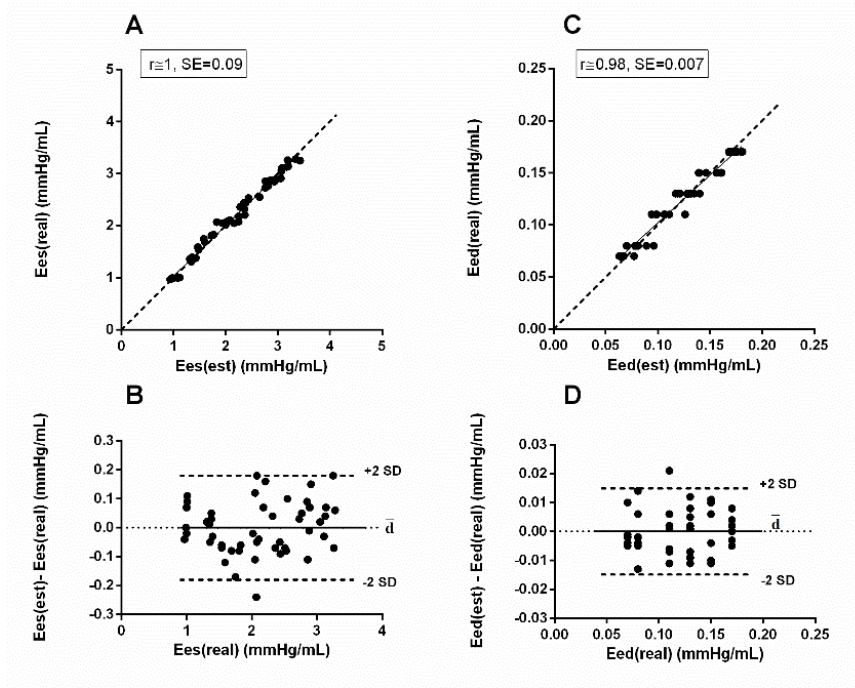
A summary of the cardiovascular properties as well as the simulation-derived hemodynamic characteristics of the 50 cases is presented in Table 4.1:2.

Table 4.1:2 Cardiac parameters and hemodynamic characteristics of the 50 simulated cases.

| Parameter | Max | Min | Mean | SD |
|---------------------|-------|------|-------|------|
| E_{es} (mmHg/mL) | 3.28 | 1.00 | 2.11 | 0.71 |
| E_{ed} (mmHg/mL) | 0.18 | 0.07 | 0.12 | 0.04 |
| P_{fill} (mmHg) | 23 | 7 | 15 | 5.4 |
| EF (%) | 68.9 | 32.5 | 50.5 | 8.6 |
| EDV (mL) | 245 | 88 | 145 | 33 |
| TPR (mmHg·s/mL) | 1.20 | 0.85 | 1.02 | 0.09 |
| brachial SBP (mmHg) | 193.7 | 75.1 | 123.1 | 33.8 |
| brachial DBP (mmHg) | 133.4 | 52.9 | 82.4 | 19.4 |
| brachial PP (mmHg) | 110.0 | 11.9 | 40.6 | 21.0 |
| MAP (mmHg) | 152.1 | 61.4 | 94.6 | 23.1 |
| aortic SBP (mmHg) | 186.0 | 71.2 | 116.8 | 32.7 |
| aortic DBP (mmHg) | 135.2 | 53.9 | 83.6 | 19.8 |
| aortic PP (mmHg) | 98.9 | 8.0 | 33.3 | 19.1 |

TPR: total peripheral resistance, SBP: systolic blood pressure, DBP: diastolic blood pressure, PP: pulse pressure, MAP: mean arterial pressure

For the 50 hemodynamic cases, the first step of the estimation of the scaling factors for compliance and peripheral resistance was achieved with small errors, namely $n\text{-RMSE}=0.07$ for C_{ref} and $n\text{-RMSE}=0.04$ for R_{ref} . The second step of optimization led to a good approximation of filling pressure, which was captured with an overall $n\text{-RMSE}$ of 6.0%. Correlation and agreement between the ‘real’ and estimated from the proposed method E_{es} and E_{ed} values are shown by scatter plots and the Bland-Altman plots in Figure 4.1:3. The respective plots for the E_{es} values derived from the Chen et al. [8] method are presented in Figure 4.1:4.



$E_{es}(\text{real})$: real end-systolic elastance, $E_{es}(\text{est})$: estimated end-systolic elastance, $E_{ed}(\text{real})$: real end-diastolic elastance, $E_{ed}(\text{est})$: estimated end-diastolic elastance.

Figure 4.1:3 Comparison of the E_{es} and E_{ed} values as estimated by the proposed method to the real ones. A. Scatter plot comparing 'real' end-systolic elastance ($E_{es}(\text{real})$) to estimated end-systolic elastance ($E_{es}(\text{est})$) for the 50 simulated cases. Line of equality (dashed line) and linear regression (solid line) are shown. B. Bland-Altman plot of $E_{es}(\text{est}) - E_{es}(\text{real})$ difference against $E_{es}(\text{real})$. Mean difference (\bar{d}) as well as 95% confidence intervals ($\pm 2SD$ around the mean difference) are included. (C and D) Same analysis followed as in A and B for the comparison of 'real' and estimated end-diastolic elastance.

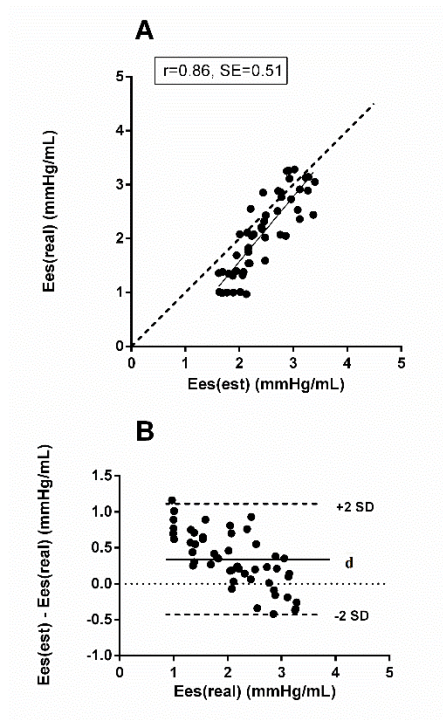


Figure 4.1:4 Comparison of the E_{es} values as estimated by the method of Chen et al. [8] to the real ones. A. Scatter plot comparing 'real' end-systolic elastance ($E_{es}(\text{real})$) to estimated end-systolic elastance ($E_{es}(\text{est})$) from Chen et al. [8]. Line of equality (dashed line) and linear regression (solid line) are shown. B. Bland-Altman plot of $E_{es}(\text{est}) - E_{es}(\text{real})$ difference against $E_{es}(\text{real})$. Mean difference (\bar{d}) as well as 95% confidence intervals ($\pm 2SD$ around the mean difference) are included.

Overall, the proposed method gave accurate estimates of E_{es} and E_{ed} , with E_{es} prediction achieving an n-RMSE of 4.2%. The errors deriving from the estimation of the filling pressures affected more the end-diastolic elastance estimates, which were captured with an n-RMSE of 6.1%. Bland-Altman plots revealed a good agreement between the ‘real’ and the estimated E_{es} and E_{ed} values with low bias. Likewise, the method proposed by Chen et al. [8] captured the expected E_{es} values with an n-RMSE equal to 24.4%, a standard error of estimate of 0.51 mmHg/mL and a relatively small bias. A similar level of accuracy was reported in their original *in vivo* validation [8].

Indices of correlation, accuracy and agreement between the ‘real’ and estimated E_{es} and E_{ed} values, determined for each method, are summarized in Table 4.1:3.

Table 4.1:3 Correlation, agreement and accuracy between ‘real’ and estimated E_{es} and E_{ed} values.

| Method | Parameter | Correlation | Accuracy | Agreement - Bias | | |
|-------------|-----------|-------------|-----------|------------------|-------|---------------|
| | | r | n-RMSE, % | \bar{d} | SDd | LoA |
| Proposed | E_{es} | 0.99 | 4.2 | 0.00 | 0.09 | 0.18, -0.18 |
| | E_{ed} | 0.98 | 6.1 | 0.000 | 0.007 | 0.015, -0.015 |
| Chen et al. | E_{es} | 0.85 | 24.4 | 0.34 | 0.39 | 1.11, -0.43 |

r : Pearson’s correlation coefficient, n-RMSE: normalized squared mean standard error, \bar{d} : mean of differences, SDd: standard deviation of differences, LoA: limits of agreement ($\bar{d} + 2SD_d$, $\bar{d} - 2SD_d$)

Sensitivity of E_{es} estimation to arterial tuning

Changes in elastance estimates after inducing globally an unaccounted +20% increase and a -20% decrease in arterial compliance are shown in Table 4.1:4. E_{es} was minimally influenced by the mistuning, namely it was altered by -4% to +1%, respectively, whereas E_{ed} was more affected, namely altered by +15% to -4%, respectively. Figure 4.1:5 shows the respective alterations in brachial pressure predictions as well as the aortic flow waveform of this particular case.

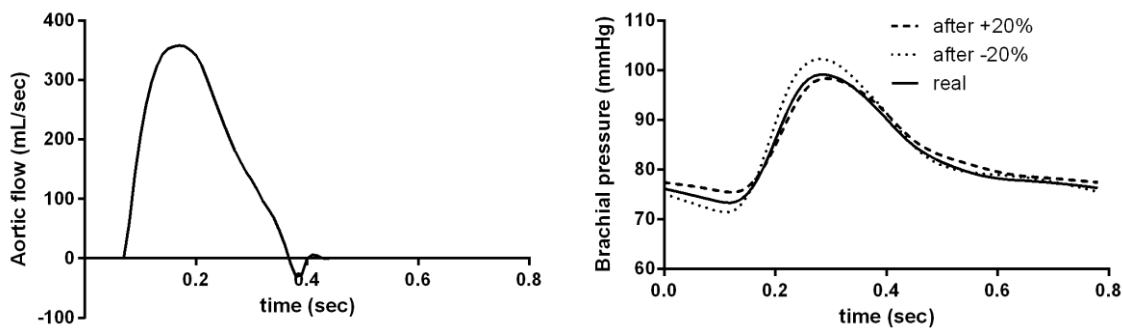


Figure 4.1:5 Left. Aortic flow waveform used as the input signal for this particular case. Right. Model-derived brachial pressure waveforms for the ‘real’ arterial compliance (solid line) and after inducing a +20% (dashed line) and a -20% (dotted line) change in arterial compliance.

Table 4.1:4 Estimation of E_{es} and E_{ed} after inducing a +20% increase and a -20% decrease in arterial compliance.

| Parameter | Real | Method estimates | after +20% in C | after -20% in C |
|--------------------|-------|------------------|-----------------|-----------------|
| E_{es} (mmHg/mL) | 2.25 | 2.19 | 2.17 | 2.27 |
| E_{ed} (mmHg/mL) | 0.105 | 0.106 | 0.121 | 0.101 |

Sensitivity of E_{es} estimation to measurement errors

An increase in the aortic flow amplitude by 10% resulted in a modified arterial tree configuration as shown in Table 4.1:5. The overestimation of the arterial compliance (from $1.1C_{ref}$ to $1.17C_{ref}$) was a rather expected outcome, in the sense that, for the peripheral pressure to remain unchanged, the arterial tree has to adapt to the augmented aortic flow by decreasing wall stiffness. Overall, cardiac elastance values were minimally affected (Table 4.1:5).

Similarly, an augmented systolic pressure had a significant impact on the adjustment of the arterial tree and was correlated with a pronounced decrease of arterial wall compliance (from $1.1C_{ref}$ to $0.82C_{ref}$) and an increase in peripheral resistance (from $R=R_{ref}$ to $R=1.04R_{ref}$) as seen in Table 4.1:5. Overall, this miscalculation of both arterial tree parameters led to small errors in the E_{es} (+8%) and E_{ed} (-15%) estimation.

Table 4.1:5 Estimation of E_{es} and E_{ed} after simulating measurement errors: a +10% increase in aortic flow amplitude and a +10% increase in brachial systolic blood pressure.

| Parameter | Real | Method estimates | +10% aortic flow | +10% SBP |
|--------------------|-------|------------------|------------------|----------|
| C/C_{ref} | 1.10 | 1.09 | 1.17 | 0.82 |
| R/R_{ref} | 1.00 | 0.95 | 0.87 | 1.04 |
| E_{es} (mmHg/mL) | 2.25 | 2.19 | 2.32 | 2.42 |
| E_{ed} (mmHg/mL) | 0.105 | 0.106 | 0.094 | 0.090 |

4.1.4 Discussion

In the present study, we developed and tested a novel noninvasive method for estimating end-systolic and end-diastolic elastance from aortic flow waveform, ejection fraction and brachial systolic and diastolic pressures.

The method was designed using a state-of-the-art 1D model of the arterial tree, which is considered one of the most complete and accurate ones in the literature [9], [10], and was validated after simulating a variety of hemodynamic cases reflecting both healthy and pathological conditions. These cases pertained to normal hearts [15] (physiological E_{es} values near 2.0 mmHg/mL) and hearts which have undergone remodeling under the form of concentric hypertrophy [17] (increased E_{es} near 3.5 mmHg/mL accompanied by hypertension) and eccentric hypertrophy [16] (decreased E_{es} less than 1.2 mmHg/mL with decreased EF). Accordingly, arterial properties were chosen to alter in order to simulate a wide range of pulse pressures and mean pressures, which could be representative of both normotensive and hypertensive adults.

Preload

Our original methodology focused on the optimization of the arterial and cardiac parameters assuming a constant preload (filling pressure). During the ejection phase of the cardiac cycle, left ventricular pressure is approximately equal to aortic pressure with a slight difference in phase and magnitude that is mainly dictated by the flow phenomena occurring at the aortic valve (inertia and turbulence losses). During the diastolic phase, however, the aortic valve is closed and thus there is little interaction between the left ventricle and the arterial tree. Consequently, diastolic function is mostly defined by cardiac preload and, therefore, it was anticipated that the method accuracy would be sensitive to the chosen value for filling pressure.

To elucidate this sensitivity, we initially tested how an erroneous reservoir pressure would affect the algorithm's estimates and reported a few interesting findings. For a different P_{fill} , the P-V loop was shifted to a different volume range, preserving, however, the ejection P-V curve. This led to significant errors in the estimation of both elastance parameters. We showed, however, that for a certain V_0 and for a measured ejection fraction, it is possible to calculate the P_{fill} for which the P-V loop corresponds to the true values of end-systolic and end-diastolic volumes, and, therefore, estimate correctly elastance values.

After the extension of the algorithm to include this sensitivity, the *in silico* validation of the method yielded satisfying results, with 'real' and estimated elastance values being in agreement over the full range. The correlation between the two measures was good,

with the data points falling along the line of equality. Bland-Altman plots demonstrated that the proposed method has low bias and narrow limits of agreement for both E_{es} and E_{ed} estimation.

Arterial load adjustment

One challenge we faced when developing the proposed method was to find an effective way to translate the default arterial tree configuration into patient-specific standards. In general, resistance of the peripheral vessels can be adjusted with accuracy after having measured peripheral pressure –i.e. mean arterial pressure (MAP) - and cardiac output (CO). On the contrary, determining arterial wall distensibility is a more demanding task. Arterial stiffness is known to increase as one moves away from the heart, creating a stiffness gradient, which is highly inconsistent among individuals in regards to age, gender and disease [22].

This suggests that the original PWV(d) curve proposed by Raymond et al. [10], –which is representative of a healthy young male– varies among different individuals not only in amplitude but also in shape, and thus requires adjustment. In order to get detailed insight into the local vessel compliance and arterial geometry of each patient, one could turn to cumbersome and time-consuming MRI and Ultrasound measurements. However, this approach would render the method rather useless in clinical practice. To overcome this dilemma, we decided to follow a simple reasoning and adjust the original PWV(d) inverse relation by scaling factors according to easily obtained brachial pressure measurements. The reliability of this approach remains to be validated with *in vivo* measurements. Naturally, errors in the estimation of vessel compliance are expected, hence we proceeded to quantify their possible effect on the estimation of elastance. After varying arterial distensibility by +20% to -20%, we found that both E_{es} and E_{ed} changed little (absolute errors less than 4% and 15%, respectively), with changes in E_{ed} being more marked, suggesting that small errors around arterial compliance are not a major source of error in the estimation process. This finding is in good agreement with a previous study by Stergiopoulos et al. [21].

Nevertheless, it should be noted that changing uniformly arterial compliances and thus inducing global stiffening is in general a good approach for younger adults, whereas in older individuals local stiffening has to be accounted for [23]. In our future steps, we plan to integrate the age factor into the analysis and develop a more refined algorithm that tunes the arterial tree parameters through local changes.

Sensitivity to measurement errors

A second question that may arise regarding the robustness of the method is how measurement errors, namely during the aortic flow and brachial pressure recordings, may affect the E_{es} and E_{ed} estimates. Although previous studies on the variability of measurements of aortic flow by Doppler Ultrasound have indicated in general good accuracy and reliability of this technique [24], we decided to examine the effect of an overestimation of aortic flow amplitude by +10%. The introduction of this error resulted, in the first step, in a subsequent erroneous adjustment of the arterial tree, which became more compliant. However, it appears that these errors in both the flow input and the arterial tree parameters yielded, in the second step, a fairly accurate estimation of both E_{es} and E_{ed} , with the errors being smaller than 3% and -11%, respectively.

Similarly, the augmentation of the systolic pressure input led to a much stiffer and resistant arterial tree and, in the end, to a greater E_{es} estimate. This result was anticipated, given that these vascular changes have been previously correlated with an augmented cardiac contractility (similarly to the cardiovascular interaction during ageing). Overall, the effect of both measurement errors was quite small (generally less than 15%).

Prior single-beat algorithms

E_{es} being a powerful tool in defining ventricular properties and performance, there have been also previous attempts to associate this measure with noninvasive single-beat parameters. Chen et al. [8] were the first ones to develop a fully noninvasive method, which was validated with invasive multiple-beat analysis and was found to be highly accurate. In their work, they proposed a simple and concise equation to estimate E_{es} from easily measured parameters, obtained from pressure arm-cuffs, echo-Doppler cardiography and electrocardiograms. In deriving this equation, they substituted intraventricular pressures with distal pressures, which were adjusted accordingly: diastolic pressure was assumed unchanged throughout the vasculature, whereas end-systolic LV pressure was approximated as the product of brachial systolic pressure and a factor of pressure amplification (0.9SBP). The latter approximation was proposed in previous studies [19].

Therefore, the accuracy of their E_{es} estimates depends mainly on the value chosen for the normalized elastance at the onset of ejection, $E_{Nd(est)}$. $E_{Nd(est)}$ would theoretically be equal to the group-averaged value reported by Senzaki et al. [5], had there been no

evidence of load-dependence of the normalized elastance. This point of view, however, has been challenged by studies that demonstrated significant variance of the normalized elastance according to load [25], [26]. Subsequently, investigators have improved the original approach of Senzaki et al. [5] by developing models for adjusting the normalized elastance curve based on the individual contractility and load conditions. Shishido et al. [6] proposed one such technique for adjusting the upstroke of the normalized elastance curve according to a load-sensitive shape index. Concurrently, Chen et al. [8] developed their own method for assessing E_{Nd} from ejection fraction and arterial diastolic and systolic pressures, a model which was found to be accurate when validated against *in vivo* measurements. In our simulations, however, load-sensitivity was not accounted for and thus we adapted the equation of Chen et al. [8] according to the group-average value of E_{Nd} reported by Senzaki et al. [5]. The *in silico* validation of their technique revealed an overall accurate performance, yielding good results throughout the physiological and non-physiological range of E_{es} (RMSE=24.4%), with errors which tended to increase for greater E_{es} values.

Lately, more studies on the single-beat estimation of elastance have been published. Notably, Bonnet et al. [7] proposed a method that is able to estimate both E_{es} and V_0 assuming a linear relationship between elastance and time and using the ejection phase of the P-V loop. After approximating the ventricular pressure from carotid tonometry and acquiring detailed data on the intraventricular volume via 3D echocardiography, they obtained both the slope and the intercept of the ESPVR using a nonlinear least-squares fitting. This method was further validated against the experimental data of previous studies and was also found capable of detecting differences in E_{es} between normotensive and hypertensive subjects.

Another interesting approach, suggested by Davidson et al. [27], attempted to derive the time-varying elastance curve beat-by-beat, from measurements of aortic pressure, heart rate and end-diastolic/systolic volumes. Their methodology involves generating the components of the time-varying elastance, i.e. PLV, VLV and V_0 , by following certain assumptions and experimental relations, e.g. reconstruction of diastolic PLV based on aortic pressure. Arguably, the most intriguing aspect of this approach is that the elastance curve is not a priori assumed and thus it is possible to capture and characterize alterations in its shape.

Concurrently, novel techniques are being proposed for monitoring arterial parameters (e.g. EF) and can, subsequently, be further exploited for the extraction of cardiac indices. One method proposed by Pahlevan et al. [28] employs an intrinsic frequency approach to analyze the dynamics of the hemodynamic waveforms in conjunction with the LV contractility. This concept has already been implemented for the noninvasive derivation of EF and could potentially be applied for the estimation of E_{es} . Similarly, Swamy et al. [29] published a method for the derivation of EF and E_{es} using mathematical modeling of the cardiovascular system. This concept uses a 3-element Windkessel and multi-beat recordings of aortic pressure for model parameter fitting. More specifically, the Windkessel time constant is computed based on the exponential decay of the aortic pressure during diastole, whereas the remaining model unknowns, including E_{es} , are tuned according to the systolic ejection phase of the recorded aortic pressure curves. The validation of their EF estimates showed encouraging results, while there is evidence that their technique can capture drug-induced alterations in E_{es} . It should be noted, nevertheless, that this methodology assumes a constant E_{es}/E_{ed} ratio and, therefore, does not allow for an independent estimation of diastolic elastance.

Merits from novel method

The novel method differs from the aforementioned ones in that it gives a broader insight into the LV and arterial interaction as it estimates not only the end-systolic elastance but also the entire P-V loop as well as hemodynamic patterns. In his review, Chirinos [30] stressed that ventricular arterial coupling is a term that cannot be solely characterized in the pressure-volume plane, but should encompass indices of arterial and myocardial load which are indicative of normal physiology or cardiovascular disease. In this sense, he proposed parameters of blood flow pulsatility as additional information, such as characteristic impedance, wave reflection profile and total arterial compliance. The present model is capable of such a broad analysis, since it can additionally compute pressure and flow waveforms throughout the arterial tree.

The present study examined as well the diastolic cardiac function. Contrary to the ESPVR, the end-diastolic pressure volume relation (EDPVR) is inherently nonlinear, which renders its prediction with single beat approach even more challenging [31]. In our work, we evaluated end-diastolic elastance as the lower P-V boundary, defining thus only one point of the EDPV curve. Studies in human, canine, and rat hearts -which have apparently very different sizes- have indicated that EDPV relations can be accurately described as an inverse power relation relating EDP and EDV and that there is surprisingly a common underlying shape of EDPVR [31], [32]. Therefore, there is potential gain from using the E_{ed} value estimated from our algorithm in order to predict the entire EDPV curve [31].

Study limitations

This study is subject to certain limitations which should be acknowledged. The 1D model of the arterial tree was formulated based on a number of assumptions which are thoroughly described in the original publications [9], [10]. As particularly pertinent to this work, it should be mentioned that the model is an open-loop model, thus neglects venous circulation and prescribes a cardiac preload via a constant reservoir pressure.

Cases of aortic valve dysfunction were not considered in the present study. Given the early diagnosis and chronic nature of aortic stenosis, it is, nevertheless, possible to incorporate this data into the algorithm and simulate the effect of valve dysfunction on E_{es} . Apart from being load-sensitive, ESPVR has also demonstrated contractility-dependent curvilinearity [33]–[35], which was initially neglected. Although the concept of a linear ESPVR seems attractive as it allows for full evaluation of ESPVR by its slope and intercept, Sunagawa et al. [35] highlighted the inadequacy of adopting linearity when studying the effects of regional ischemia. Even in cases of homogenous conditions, Burkhoff et al. [33] found *in situ* significant nonlinearity in the end-systolic pressure volume relation at higher contractile states. However, *in vivo* measurements usually detect only insignificant nonlinearities, which do not compromise their results. Kass et al. [36] argued that this is attributed to the fact that only a few P-V loops are recorded over a limited range of load when examining *in vivo* ESPVR, thus nonlinear behaviors become imperceptible.

Computational errors deriving from poor estimation of vessel compliance as well as from not taking into account the load-dependence of ESPV relation were discussed in the present study and are to be examined in our future studies. As already mentioned, the initial concept of a uniform averaged elastance function by Senzaki et al. [29] has been challenged. In fact, their original publication found such a great consistency towards an average curve, that when our method was tested using an elastance curve that differed from the mean by +1SD, the error in E_{es} estimation was small, namely less than 7%. Nevertheless, the cardiac model we used possibly needs to be updated in order to include individual deviations from the group-averaged elastance curve, following the approach of previous investigations [8], [6].

When validating the presented method, changes in the timing of end-systole were not taken into account, although t_{max} has been reported to range from 0.27 to 0.38 sec for individuals aged 36 to 60 years old [18]. Moreover, throughout the study we kept a constant volume axis intercept of the end-systolic pressure volume relation, V_0 , equal to 15 mL. Arguably, this is a limiting assumption, since V_0 can vary in a wide range from -100mL to 300mL, as reported by Senzaki et al. [5] and it is crucial to the accuracy of the elastance estimates (as was depicted in Figure 4.1:2). Prior studies have shown that V_0 correlates poorly with directly measured data [37], whereas others suggest that it can be approximated as a fixed percentage of end-systolic volume [27]. Possibly, we could combine our methodology with other techniques, such as the one proposed by Bonnet et al. [7], in order to additionally estimate dead volume. This potential needs to be further studied.

Clinical implications and future work

The proposed method is based on sound and solid grounds, allowing for the accurate estimation of elastance with only a few easily obtained measurements. Aortic flow and EF can be measured noninvasively using echocardiography, whereas brachial systolic and diastolic pressure can be easily measured with an arm-cuff. In this regard, it is important to consider the method's possible application in the context of clinical routine.

Our present study focused on developing the theoretical background and testing the feasibility of the proposed method in the framework of a computational environment. Future work will be oriented towards two ends: (1) examining the dependence of the normalized elastance curve on load conditions via *in vivo* measurements and (2) validating the E_{es} and E_{ed} estimates against invasive multiple cycle-derived pressure-volume relations in humans.

Conclusion

We developed and validated *in silico* a novel, noninvasive method for estimating end-systolic and end-diastolic elastance from easily obtained data, i.e. aortic flow waveform and brachial pressures. This method proved itself capable of estimating accurately E_{es} and E_{ed} over a wide range of loading conditions when tested *in silico*. Therefore, it offers promising potential for future application in the clinical setting and we will proceed to its experimental validation against *in vivo* multi-beat analysis.

4.1.5 Bibliography

- [1] D. Adler, E. Scott Monrad, E. H. Sonnenblick, O. M. Hess, and H. P. Krayenbuehl, "Time to dp/dt_{max} , a useful index for evaluation of contractility in the catheterization laboratory," *Clin. Cardiol.*, vol. 19, no. 5, pp. 397–403, mai 1996, doi: 10.1002/clc.4960190513.
- [2] H. Suga and K. Sagawa, "Instantaneous pressure-volume relationships and their ratio in the excised, supported canine left ventricle," *Circ. Res.*, vol. 35, no. 1, pp. 117–126, Jul. 1974.
- [3] H. Suga, K. Sagawa, and A. A. Shoukas, "Load Independence of the Instantaneous Pressure-Volume Ratio of the Canine Left Ventricle and Effects of Epinephrine and Heart Rate on the Ratio," *Circ. Res.*, vol. 32, no. 3, pp. 314–322, Mar. 1973, doi: 10.1161/01.RES.32.3.314.
- [4] K. Sagawa, H. Suga, A. A. Shoukas, and K. M. Bakalar, "End-systolic pressure/volume ratio: a new index of ventricular contractility," *Am. J. Cardiol.*, vol. 40, no. 5, pp. 748–753, Nov. 1977.
- [5] H. Senzaki, C. H. Chen, and D. A. Kass, "Single-beat estimation of end-systolic pressure-volume relation in humans. A new method with the potential for noninvasive application," *Circulation*, vol. 94, no. 10, pp. 2497–2506, Nov. 1996.
- [6] T. Shishido, K. Hayashi, K. Shigemitsu, T. Sato, M. Sugimachi, and K. Sunagawa, "Single-Beat Estimation of End-Systolic Elastance Using Bilinearly Approximated Time-Varying Elastance Curve," *Circulation*, vol. 102, no. 16, pp. 1983–1989, Oct. 2000, doi: 10.1161/01.CIR.102.16.1983.
- [7] B. Bonnet, F. Jourdan, G. du Cailar, and P. Fesler, "Noninvasive evaluation of left ventricular elastance according to pressure-volume curves modeling in arterial hypertension," *Am. J. Physiol. Heart Circ. Physiol.*, vol. 313, no. 2, pp. H237–H243, Aug. 2017, doi: 10.1152/ajpheart.00086.2017.
- [8] C.-H. Chen *et al.*, "Noninvasive single-beat determination of left ventricular end-systolic elastance in humans," *J. Am. Coll. Cardiol.*, vol. 38, no. 7, pp. 2028–2034, Dec. 2001, doi: 10.1016/S0735-1097(01)01651-5.
- [9] P. Reymond, Y. Bohraus, F. Perren, F. Lazeyras, and N. Stergiopoulos, "Validation of a patient-specific one-dimensional model of the systemic arterial tree," *Am. J. Physiol. Heart Circ. Physiol.*, vol. 301, no. 3, pp. H1173–H1182, Sep. 2011, doi: 10.1152/ajpheart.00821.2010.
- [10] P. Reymond, F. Merenda, F. Perren, D. Rüfenacht, and N. Stergiopoulos, "Validation of a one-dimensional model of the systemic arterial tree," *Am. J. Physiol. - Heart Circ. Physiol.*, vol. 297, no. 1, pp. H208–H222, Jul. 2009, doi: 10.1152/ajpheart.00037.2009.
- [11] K. Sagawa, "The end-systolic pressure-volume relation of the ventricle: definition, modifications and clinical use," *Circulation*, vol. 63, no. 6, pp. 1223–1227, Jun. 1981.
- [12] R. Holenstein, P. Niederer, and M. Anliker, "A viscoelastic model for use in predicting arterial pulse waves," *J. Biomech. Eng.*, vol. 102, no. 4, pp. 318–325, Nov. 1980.
- [13] Langewouters G. J., "Visco-elasticity of the human aorta in vitro in relation to pressure and age.," PhD Thesis, Free University of Amsterdam, The Netherlands, 1982.
- [14] J. P. Mynard, M. R. Davidson, D. J. Penny, and J. J. Smolich, "A simple, versatile valve model for use in lumped parameter and one-dimensional cardiovascular models," *Int. J. Numer. Methods Biomed. Eng.*, vol. 28, no. 6–7, pp. 626–641, Jun. 2012, doi: 10.1002/cnm.1466.
- [15] C. H. Chen, M. Nakayama, E. Nevo, B. J. Fetters, W. L. Maughan, and D. A. Kass, "Coupled systolic-ventricular and vascular stiffening with age: implications for pressure regulation and cardiac reserve in the elderly," *J. Am. Coll. Cardiol.*, vol. 32, no. 5, pp. 1221–1227, Nov. 1998.
- [16] M. D. Feldman *et al.*, "Acute cardiovascular effects of OPC-18790 in patients with congestive heart failure. Time- and dose-dependence analysis based on pressure-volume relations," *Circulation*, vol. 93, no. 3, pp. 474–483, Feb. 1996.
- [17] P. H. Pak, W. L. Maughan, K. L. Baughman, R. S. Kieval, and D. A. Kass, "Mechanism of acute mechanical benefit from VDD pacing in hypertrophied heart: similarity of responses in hypertrophic cardiomyopathy and hypertensive heart disease," *Circulation*, vol. 98, no. 3, pp. 242–248, Jul. 1998.
- [18] M. R. Starling, R. A. Walsh, L. J. Dell'Italia, G. B. Mancini, J. C. Lasher, and J. L. Lancaster, "The relationship of various measures of end-systole to left ventricular maximum time-varying elastance in man," *Circulation*, vol. 76, no. 1, pp. 32–43, Jul. 1987.
- [19] R. P. Kelly *et al.*, "Effective arterial elastance as index of arterial vascular load in humans," *Circulation*, vol. 86, no. 2, pp. 513–521, Aug. 1992, doi: 10.1161/01.CIR.86.2.513.
- [20] J. M. Bland and D. G. Altman, "Statistical methods for assessing agreement between two methods of clinical measurement," *Lancet Lond. Engl.*, vol. 1, no. 8476, pp. 307–310, Feb. 1986.
- [21] N. Stergiopoulos, J. J. Meister, and N. Westerhof, "Determinants of stroke volume and systolic and diastolic aortic pressure," *Am. J. Physiol.*, vol. 270, no. 6 Pt 2, pp. H2050–H2059, Jun. 1996.

- [22] P. Boutouyrie, S. Laurent, A. Benetos, X. J. Girerd, A. P. Hoeks, and M. E. Safar, "Opposing effects of ageing on distal and proximal large arteries in hypertensives," *J. Hypertens. Suppl. Off. J. Int. Soc. Hypertens.*, vol. 10, no. 6, pp. S87-91, Aug. 1992.
- [23] E. Kimoto *et al.*, "Preferential stiffening of central over peripheral arteries in type 2 diabetes," *Diabetes*, vol. 52, no. 2, pp. 448-452, Feb. 2003.
- [24] M. A. Quiñones, C. M. Otto, M. Stoddard, A. Waggoner, W. A. Zoghbi, and Doppler Quantification Task Force of the Nomenclature and Standards Committee of the American Society of Echocardiography, "Recommendations for quantification of Doppler echocardiography: a report from the Doppler Quantification Task Force of the Nomenclature and Standards Committee of the American Society of Echocardiography," *J. Am. Soc. Echocardiogr. Off. Publ. Am. Soc. Echocardiogr.*, vol. 15, no. 2, pp. 167-184, Feb. 2002.
- [25] J. Baan and E. T. Van der Velde, "Sensitivity of left ventricular end-systolic pressure-volume relation to type of loading intervention in dogs," *Circ. Res.*, vol. 62, no. 6, pp. 1247-1258, Jun. 1988.
- [26] D. Burkhoff, P. P. De Tombe, and W. C. Hunter, "Impact of ejection on magnitude and time course of ventricular pressure-generating capacity," *Am. J. Physiol.*, vol. 265, no. 3 Pt 2, pp. H899-909, Sep. 1993.
- [27] S. Davidson *et al.*, "Minimally invasive, patient specific, beat-by-beat estimation of left ventricular time varying elastance," *Biomed. Eng. OnLine*, vol. 16, Apr. 2017, doi: 10.1186/s12938-017-0338-7.
- [28] N. M. Pahlevan *et al.*, "Noninvasive iPhone Measurement of Left Ventricular Ejection Fraction Using Intrinsic Frequency Methodology," *Crit. Care Med.*, vol. 45, no. 7, pp. 1115-1120, Jul. 2017, doi: 10.1097/CCM.0000000000002459.
- [29] G. Swamy, J. Kuiper, M. S. R. Gudur, N. B. Olivier, and R. Mukkamala, "Continuous left ventricular ejection fraction monitoring by aortic pressure waveform analysis," *Ann. Biomed. Eng.*, vol. 37, no. 6, pp. 1055-1068, Jun. 2009, doi: 10.1007/s10439-009-9675-4.
- [30] J. A. Chirinos, "Ventricular-arterial coupling: Invasive and non-invasive assessment," *Artery Res.*, vol. 7, no. 1, Mar. 2013, doi: 10.1016/j.artres.2012.12.002.
- [31] S. Klotz *et al.*, "Single-beat estimation of end-diastolic pressure-volume relationship: a novel method with potential for noninvasive application," *Am. J. Physiol. Heart Circ. Physiol.*, vol. 291, no. 1, pp. H403-412, Jul. 2006, doi: 10.1152/ajpheart.01240.2005.
- [32] I. Mirsky and W. W. Parmley, "Assessment of passive elastic stiffness for isolated heart muscle and the intact heart," *Circ. Res.*, vol. 33, no. 2, pp. 233-243, Aug. 1973.
- [33] D. Burkhoff, S. Sugiura, D. T. Yue, and K. Sagawa, "Contractility-dependent curvilinearity of end-systolic pressure-volume relations," *Am. J. Physiol.*, vol. 252, no. 6 Pt 2, pp. H1218-1227, Jun. 1987.
- [34] D. A. Kass, R. Beyar, E. Lankford, M. Heard, W. L. Maughan, and K. Sagawa, "Influence of contractile state on curvilinearity of in situ end-systolic pressure-volume relations," *Circulation*, vol. 79, no. 1, pp. 167-178, Jan. 1989.
- [35] K. Sunagawa, W. L. Maughan, and K. Sagawa, "Effect of regional ischemia on the left ventricular end-systolic pressure-volume relationship of isolated canine hearts," *Circ. Res.*, vol. 52, no. 2, pp. 170-178, Feb. 1983.
- [36] D. A. Kass and W. L. Maughan, "From 'Emax' to pressure-volume relations: a broader view," *Circulation*, vol. 77, no. 6, pp. 1203-1212, Jun. 1988, doi: 10.1161/01.CIR.77.6.1203.
- [37] A. Kono, W. L. Maughan, K. Sunagawa, K. Hamilton, K. Sagawa, and M. L. Weisfeldt, "The use of left ventricular end-ejection pressure and peak pressure in the estimation of the end-systolic pressure-volume relationship," *Circulation*, vol. 70, no. 6, pp. 1057-1065, Dec. 1984.

4.2 *In vivo* application and validation of a novel noninvasive method to estimate the end-systolic elastance

Stamatia Pagoulatou ¹, Karl-Philipp Rommel ^{2,3}, Karl-Patrik Kresoja ^{2,3}, Maximilian von Roeder ^{2,3}, Philipp Lurz ^{2,3}, Holger Thiele ^{2,3}, Vasiliki Bikia ¹, Georgios Rovas ¹, Dionysios Adamopoulos ⁴, and Nikolaos Stergiopoulos ¹

¹ Laboratory of Hemodynamics and Cardiovascular Technology (LHTC), Institute of Bioengineering, Ecole Polytechnique Fédérale de Lausanne (EPFL), Lausanne, Switzerland

² Department of Cardiology, Heart Center Leipzig at University of Leipzig, Leipzig, Germany

³ Leipzig Heart Institute, Leipzig, Germany

⁴ Cardiology Department, Geneva University Hospitals (HUG), Geneva, Switzerland

Abstract

Accurate assessment of the left ventricular (LV) systolic function is indispensable in the clinical practice. However, estimation of a precise index of cardiac contractility, i.e., the end-systolic elastance (E_{es}), requires invasive recordings of LV pressure and volume and therefore cannot be established as clinical routine. The objective of this work was to present and validate a methodology that allows for the estimation of E_{es} with simple and readily available noninvasive measurements. The method is based on a validated model of the cardiovascular system and noninvasive data from arm-cuff pressure and routine echocardiography to render the model patient-specific. Briefly, the algorithm first uses the measured aortic flow as model input and optimizes the properties of the arterial system model in order to achieve correct prediction of the patient's peripheral pressure. In a second step, the personalized arterial system is coupled with the cardiac model (time-varying elastance model) and the LV systolic properties, including E_{es} , are tuned to predict accurately the aortic flow waveform. The algorithm was validated against invasive measurements of E_{es} (multiple pressure-volume loop analysis) taken from $n=10$ heart failure patients with preserved ejection fraction and $n=9$ patients without heart failure. Invasive measurements of E_{es} (range [1.0, 5.0] mmHg/mL, average 2.4 ± 0.9 mmHg/mL) agreed well with method predictions (nRMSE=9%, $r=0.92$, bias=-0.1 mmHg/mL and limits of agreement [-0.9, 0.6] mmHg/mL). This is a promising first step towards the development of a valuable tool that can be used by clinicians to assess systolic performance of the LV in the critically ill.

Key words: Left ventricular contractility • Systolic function • Cardiovascular modelling • Inverse methods • Noninvasive tools

Manuscript submitted for publication

4.2.1 Introduction

Left ventricular (LV) contractility is a major determinant of the performance of the cardiovascular system [1]. Its accurate assessment is of vital importance for the hemodynamic evaluation of the critically ill [2]. In clinical practice, LV systolic function is often appreciated through the echocardiographic evaluation of LV volumes and particularly of the ejection fraction (EF), defined as the ratio of stroke volume (SV) over the end-diastolic volume (EDV). Despite its popularity, EF is in fact limited in offering a complete characterization of the cardiac inotropic state [3]; it cannot (and should not) be interpreted without knowledge of preload and afterload. Additionally, it confounds information on the cardiac structure (EDV), changes in which do not necessarily reflect on the level of contractility.

The gold standard method for assessing LV systolic function to date is the invasive measurement of LV pressure-volume (P-V) loops under varying load conditions from which the end-systolic pressure-volume relation (ESPVR) is extracted [4], [5]. The ESPVR as described by its slope, i.e., the end-systolic elastance E_{es} , and its volume axis intercept, i.e., the dead volume V_d , has been proven less load sensitive than other indices of ventricular contractility [6]. For an increased E_{es} , the ventricle is able to eject more blood volume against the same afterload, which is indicative of increased contractility [5]. The bedside use of E_{es} in the clinic is not, however, established due to the invasive and expensive nature of the P-V loop measurement. There is, therefore, a clear need of a method that will allow for the derivation of E_{es} from simple and readily available noninvasive measurements, such as echocardiography.

Recently, we proposed a noninvasive method to estimate E_{es} based on measurements of aortic flow, peripheral pressure and EF [7]. The method leverages a validated, one-dimensional (1D) model of the systemic circulation [8] and works in an inverse problem-solving manner to derive an accurate description of the patient's arterial and cardiac properties. It was previously tested on a database of 50 virtual patients, yielding promising results [7].

Naturally, our next step is the *in vivo* validation of the noninvasive method's accuracy against invasively acquired E_{es} measures. To this aim, this paper presents an improved version of the original methodology. Subsequently, we demonstrate the performance of the updated noninvasive method against invasive P-V loop measurements acquired on a registry of patients with and without heart failure (HF).

4.2.2 Methods

Description of the model of the cardiovascular system

The method uses a complete 1D model of the arterial tree, comprising 103 arterial segments, whereby the Navier-Stokes equations are solved at each segment combined with a constitutive law for the wall elasticity [8]. For a complete description of the mathematical model the reader is referred to the original publication by Reymond et al. [8]. Each terminal arterial segment is coupled with a 3-element Windkessel model which accounts for the resistance and compliance of the terminal beds. As proximal boundary condition, the model can receive two possible inputs: either we prescribe a measured aortic flow waveform (typically acquired via echocardiography or cardiac magnetic resonance imaging (CMR)) or the arterial tree is coupled with a varying elastance model describing the pumping function of the left ventricle.

Originally, the cardiac model consisted of a time-varying elastance function which assumes a linear LV P-V ratio at each time point. Recently, we updated the instantaneous LV P-V relation to include the non-linearity of the end-diastolic pressure-volume relation (EDPVR). The P-V relation is now described as follows:

$$P_{LV}(V_{LV}) = \epsilon(t) * ESPVR + (1 - \epsilon(t)) * EDPVR$$

Equation 4.2:1 – Updated LV pressure-volume relation accounting for the non-linear LV diastolic properties

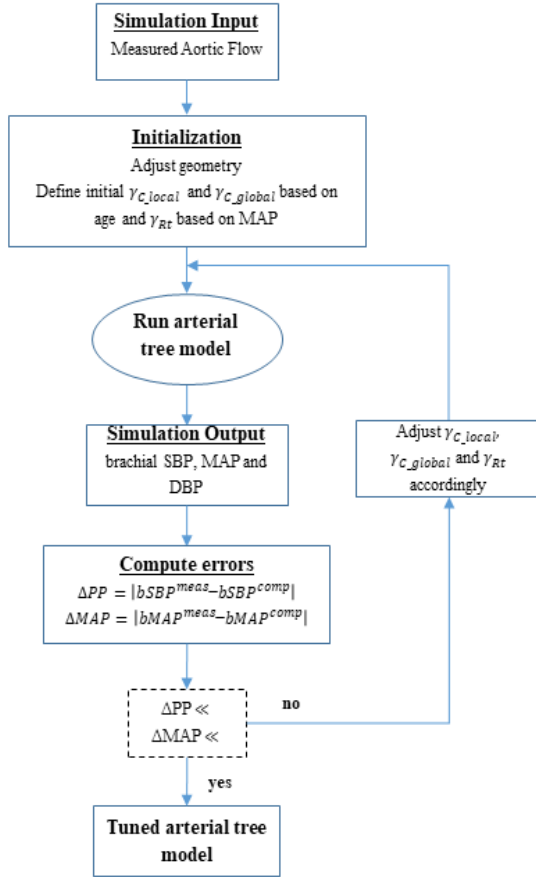
Where $\epsilon(t)$ is an activation function varying from 0 to 1, ESPVR is equal to $E_{es} * (V_{LV} - V_d)$, and EDPVR is equal to $P_0 * \exp(\beta * V_{LV})$, with P_0 being the dead pressure and β a diastolic stiffness parameter.

Description of the noninvasive method to derive E_{es}

The noninvasive method to estimate E_{es} and V_d employs a reverse-engineering approach and works in two steps (Figure 4.2:1). In a first step, it optimizes the properties of the arterial tree according to the patient's age, height, heart rate, arm-cuff brachial systolic (bSBP) and diastolic (bDBP) pressure, echocardiographic aortic flow (LVOT) and diameter (Figure 4.2:1 A). This optimization technique was recently published [9] and was validated against *in vivo* data in terms of predicting the central pulse wave velocity and the central pressure. Briefly, we first adjust the geometry of the arterial tree by multiplying the diameter of each segment by a common factor γ_{geo} (equal to the ratio between the measured and model default aortic root diameter). Subsequently, we prescribe as input the echocardiography-derived proximal aortic flow waveform and tune the remaining model parameters, i.e., the compliance of each systemic artery, and the resistance and compliance of the terminal Windkessel models. The tuning of the arterial compliance curve is done in order to achieve the measured brachial pulse pressure. During this process, we account for the preferential stiffening of the proximal aorta with ageing and, therefore, enforce increased proximal stiffness for older subjects [9]. This entails the use of two stiffening factors, one local (proximal aortic) γ_{local} and one global γ_{global} [9]. The latter factor is also used for the adjustment of the compliance of the terminal Windkessel models. The terminal resistance γ_{Rt} of the Windkessel models is tuned uniformly to achieve the measured mean pressure. At the end of each simulation we compare the model-predicted brachial SBP and DBP to the measured values and correct the factors γ_{local} , γ_{global} and γ_{Rt} , accordingly. The optimization yields an arterial tree that represents the patient's arterial load.

The second step uses the tuned arterial tree model and computes the patient's ESPVR. Figure 4.2:1 B contains a schematic representation of this methodological step, which requires the additional echocardiographic measurement of the mitral valve inflow (namely E-wave and A-wave), septal and lateral mitral annulus velocities (e'), LV end-diastolic (EDV) and end-systolic (ESV) volumes. The model input this time is the measured mitral flow waveform, which is calibrated to produce the measured stroke volume. To set up the simulation, we initially need to define the LV diastolic properties. To this aim, we approximate the end-diastolic pressure (EDP) based on literature expressions relating it with the echocardiographic average E/e' ratio [10], and then calculate the parameters of the exponential EDPVR, i.e. P_0 and β , following the single-beat method proposed by Klotz et al. [11] (the reader is referred to original publication for methodological details). The only parameters remaining to be adjusted are the LV systolic properties, i.e. E_{es} and V_d . The simulation is launched first with arbitrary E_{es} and V_d and yields a prediction of the LV P-V loop and the flow at the proximal aorta. For a specific E_{es} , changes in V_d transpose the P-V loop horizontally (Figure 4.2:2). Therefore, if the computed EDV does not correspond to the measured value, V_d is adjusted iteratively until convergence to the correct EDV (Figures 4.2:1 B & 4.2:2). When the intraventricular volumes are accurately predicted, the aortic flow waveform is compared to the measured LVOT flow curve. E_{es} is then changed in an external optimization loop until the LVOT flow waveform is accurately predicted (Figures 4.2:1 B & 4.2:2). The accuracy level for the EDV is set at $\pm 1\text{mL}$ compared to the measurement, and for the aortic flow waveform, the area between the measured and model-derived curves is minimized until the error becomes smaller than 4% of the stroke volume.

Step 1 Tuning of arterial model parameters



Step 2 Prediction of ESPVR

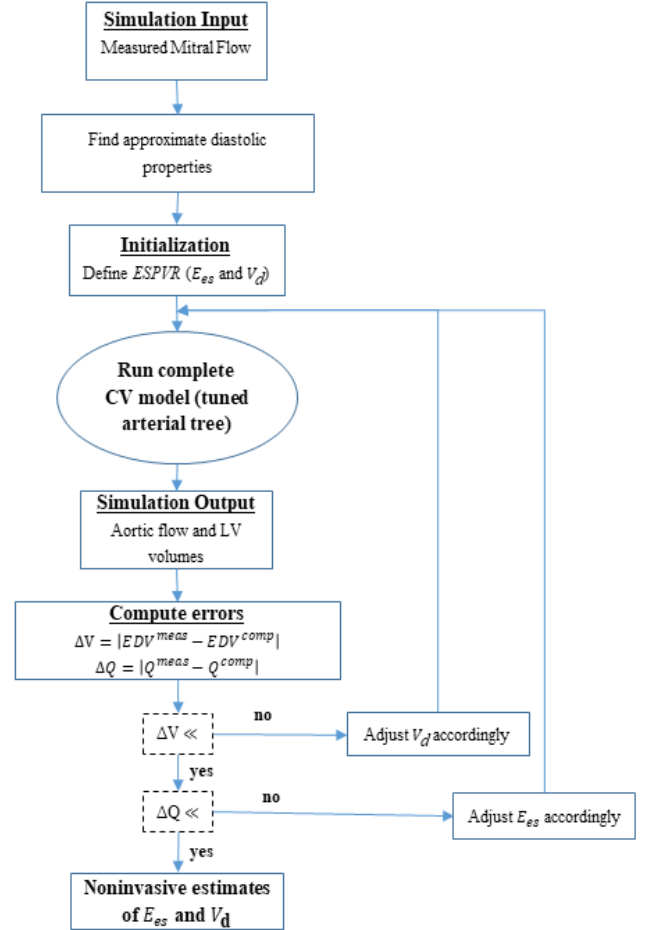


Figure 4.2:1 Two-step optimization algorithm to compute the ESPVR.

***In vivo* data**

Study population. The method was validated against invasive data acquired on patients at the Heart Center, Leipzig University, Germany in the context of a previous study [12], [13]. The study population included a total of $n=19$ patients, among which $n=10$ had clinical and echocardiographic evidence for heart failure with preserved EF (HFpEF group) as well as $n=9$ had no HF symptoms (non-HF group). The latter group was referred for invasive coronary angiography, but was free of any relevant coronary artery disease (CAD) ($LVEF > 50\%$ and $E/e' < 8$). HFpEF patients were identified according to the guidelines of [14], using the following criteria: i) $LVEF \geq 50\%$, ii) New York Heart Association functional class $\geq II$, and iii) $E/e' \geq 15$ or $E/e' 8$ to 15 combined with elevated NT-pro-B-type natriuretic peptide ($> 220\text{ng/l}$). Exclusion criteria included more than moderate valvular diseases or persistent atrial fibrillation. Further details on the study population can be found in [12], [13].

Magnetic Resonance. CMR was performed right before the invasive catheterization on an Intera 1.5-T scanner (Koninklijke Philips N.V., Amsterdam, the Netherlands). Patients were in supine position and imaging was gated by ECG. Contiguous short-axis steady-state free precession sequences (SSFP) were obtained in 2- and 4-chamber views as well as a short-axis cine stack from the mitral valve annulus to the LV apex ($TR=3.8\text{msec}$, $TE=1.6\text{msec}$, 30 phases/cardiac cycle, 10-mm slice thickness). Image analysis was performed offline using a commercially available software (cmr42, Circle Cardiovascular Imaging Inc., Calgary, Alberta, Canada). LV volumes were computed after manually tracing the endocardial contours [12], [13]. Stroke volume was calculated as the difference between the CMR-derived EDV and ESV, and EF was the ratio of the respective SV to EDV.

Cardiac catheterization protocol. The detailed catheterization protocol is available in the original publications by Rommel et al. [12], [13]. After exclusion of significant CAD, a 7F conductance catheter (CD Leycom, Zoetermeer, Netherlands) was introduced into the LV via right femoral artery access to record simultaneous LV P-V data. Subsequently, multiple LV P-V loops were recorded during reduction of the preload via transient occlusion of the inferior vena cava (inflation of an Amplatzer sizing balloon, St. Jude Medical, St. Paul, Minnesota). Volume calibration was achieved by using the LV volumetric data from the CMR scan. The LV E_{es} was determined as the linear slope of the ESPVR and the V_d as its volume axis intercept. These measurements constitute the reference values. Similarly, the parameters of the exponential EDPVR were computed. The computations were performed by an experienced operator who was blinded to other test results (K.-P.R.).

Arm-cuff pressure. Sphygmomanometric arm-cuff pressures were measured at rest at the mid brachial artery and baseline systolic (bSBP) and diastolic (bDBP) pressures were recorded.

Echocardiography. Echocardiographic exams were performed on a Vivid 9 system (General Electric Healthcare, Chalfont St. Giles, Great Britain). LVOT flow velocity was recorded with pulsed wave Doppler in the apical 5-chamber-view. The LVOT flow waveforms were then calibrated in order to produce the stroke volume measured with CMR (also used for calibration of invasive data). This was done due to lack of high quality echocardiographic LV volume data. Aortic root diameter was captured in the parasternal long axis view of the heart. Subsequently, mitral inflow pattern (E-wave and A-wave) were recorded in an apical 4-chamber view along with the septal and lateral mitral valve annular velocities (e'). The average E/e' ratio was automatically computed. The mitral flow waveform was calibrated to produce the same measured stroke volume.

Method implementation and validation

The proposed methodology was implemented on the *in vivo* data of the $n=19$ patients following the algorithm presented in Figure 4.2:1. The model predictions for E_{es} and V_d were compared to the invasively acquired values. Since V_d is a measure of volume at a theoretical non-physiological pressure, we also derived a characteristic LV end-systolic volume (V_{100}) at a given systolic pressure of 100 mmHg, as previously proposed in the literature [15]. This volume index incorporates information on both E_{es} and V_d and is calculated as $V_{100} = \frac{100}{E_{es}} + V_d$. Model-predicted V_{100} values were also compared to the measurements.

Method sensitivity to LV diastolic properties

The methodology requires an approximation of the LV diastolic properties, namely of the EDP and the parameters of the EDPVR (P_0 and β). As this can be a potential source of inaccuracy, we performed two analyses to understand how errors in the approximation of the EDP (and, consequently, in the LV diastolic properties P_0 and β) might undermine the method precision. In the first analysis, we investigated how E_{es} , V_d and V_{100} predictions would be altered for a specific patient if EDP was under- and overestimated. Concretely, for this patient the original approximation of EDP was 21 mmHg according to the measured E/e' ratio. We varied EDP at five levels, i.e., 5, 10, 15, 25 and 30mmHg [16], and estimated the patient's systolic properties anew. In the second analysis, we assessed how E_{es} , V_d and V_{100} predictions would change if we assumed a fixed EDP value of 15 mmHg for all study patients and repeated the optimization process. In this analysis, the respective P_0 and β parameters were set at physiological values in order to achieve the target EDP value.

Statistics

Continuous variables are presented as mean \pm standard deviation (SD) and categorical parameters as percentage. The correlation, accuracy and bias between the model-predicted and invasive measurements of E_{es} , V_d and V_{100} were evaluated by using Pearson's correlation coefficient (r), the root mean squared error normalized for the range (nRMSE), and Bland-Altman analysis (mean difference \bar{d} , SD of differences, and limits of agreement $LoA = \bar{d} \pm 2SD$). Statistical differences between the HFpEF and non-HF patient groups were evaluated via unpaired t-tests. Statistical significance was set for p-values lower than 0.05.

4.2.3 Results

Table 4.2:1 summarizes the demographic and clinical characteristics of the 19 patients included in this study, i.e. 10 HFpEF patients and 9 patients without HF symptoms. Overall, the study population comprised older individuals (age: 61 ± 11 years) as a result of the clinical indication for cardiac catheterization due to suspected critical cardiovascular diseases. The analysis included an equal number of women and men in total (9 vs 10). The majority of patients had arterial hypertension (aHT) (68%) and normal EF ($61 \pm 9\%$).

Table 4.2:1 Descriptive and clinical characteristics of study population (n=19).

| Parameter | Total sample (n=19) | HFpEF group (n=10) | non-HF group (n=9) | p-value |
|---|------------------------|-----------------------|-----------------------|---------|
| Age (years old) | 61 (\pm 12) | 64 (\pm 11) | 57 (\pm 12) | 0.20 |
| Gender (males/females) | 10/9 | 2/8 | 8/1 | 0.001* |
| Height (cm) | 170 (\pm 11) | 165 (\pm 11) | 176 (\pm 10) | 0.034* |
| Weight (kg) | 84 (\pm 14) | 83 (\pm 17) | 84 (\pm 11) | 0.86 |
| Body Mass Index, BMI (kg/m ²) | 28.9 (\pm 4.0) | 30.4 (\pm 4.8) | 27.2 (\pm 2.1) | 0.076 |
| Body Surface Area, BSA (m ²) | 1.98 (\pm 0.21) | 1.95 (\pm 0.24) | 2.03 (\pm 0.18) | 0.43 |
| Ejection Fraction, EF | 61% (\pm 9%) | 62% (\pm 10%) | 59% (\pm 9%) | 0.58 |
| Brachial Systolic Blood Pressure, SBP (mmHg) | 151 (\pm 17) | 152 (\pm 15) | 149 (\pm 19) | 0.61 |
| Mean Arterial Pressure, MAP (mmHg) | 104 (\pm 9) | 106 (\pm 7) | 102 (\pm 12) | 0.47 |
| Brachial Diastolic Blood Pressure, DBP (mmHg) | 80 (\pm 9) | 82 (\pm 7) | 79 (\pm 10) | 0.47 |
| End-Diastolic Volume, EDV (mL) | 136 (\pm 31) | 137 (\pm 40) | 135 (\pm 18) | 0.88 |
| End-Systolic Elastance, E_{es} (mL) | 2.4 (\pm 0.9) | 1.9 (\pm 0.6) | 3.0 (\pm 0.9) | 0.006* |
| Dead Volume, V_d (mL) | -13 (\pm 28) | -30 (\pm 25) | 6 (\pm 16) | 0.002* |
| End-Systolic Volume @ 100mmHg, V_{100} (mL) | 34 (\pm 23) | 27 (\pm 25) | 42 (\pm 18) | 0.18 |
| End-Diastolic Pressure, EDP (mmHg) | 15.4 (\pm 4.2) | 17.9 (\pm 4.0) | 12.6 (\pm 1.9) | 0.002* |
| Heart Rate, HR (bpm) | 72 (\pm 8) | 70 (\pm 7) | 74 (\pm 10) | 0.40 |
| Arterial Hypertension, aHT | 68% | 80% | 55% | 0.28 |

The * denotes statistically significant differences between the two groups as assessed via unpaired t-test.

Method convergence

Figure 4.2:2 demonstrates how the second step of the methodology (presented in Figure 4.2:1) converges to the E_{es} and V_d estimates for a specific HFpEF patient. In the first iteration, E_{es} and V_d are initialized and the respective LV P-V loop and aortic flow waveform are computed (Figure 4.2:2 A1). In an internal optimization loop, V_d is adjusted so that the simulation yields the measured EDV (Figure 4.2:2 A2). After adjusting V_d , the model-predicted aortic flow wave shape still differs from the measured one; it has a higher maximal flow value and a steeper upstroke at early systole (Figure 4.2:2 A2). This discrepancy is due to the erroneous initialization of E_{es} . Subsequently, the aortic flow error is assessed and E_{es} is updated. After 8 iterations, the algorithm converges to a solution for E_{es} and V_d , that is, when LV volumes and aortic flow waveform are accurately predicted (Figure 4.2:2 B2). For each case, convergence of the second methodological step was reached within 15 iterations on average.

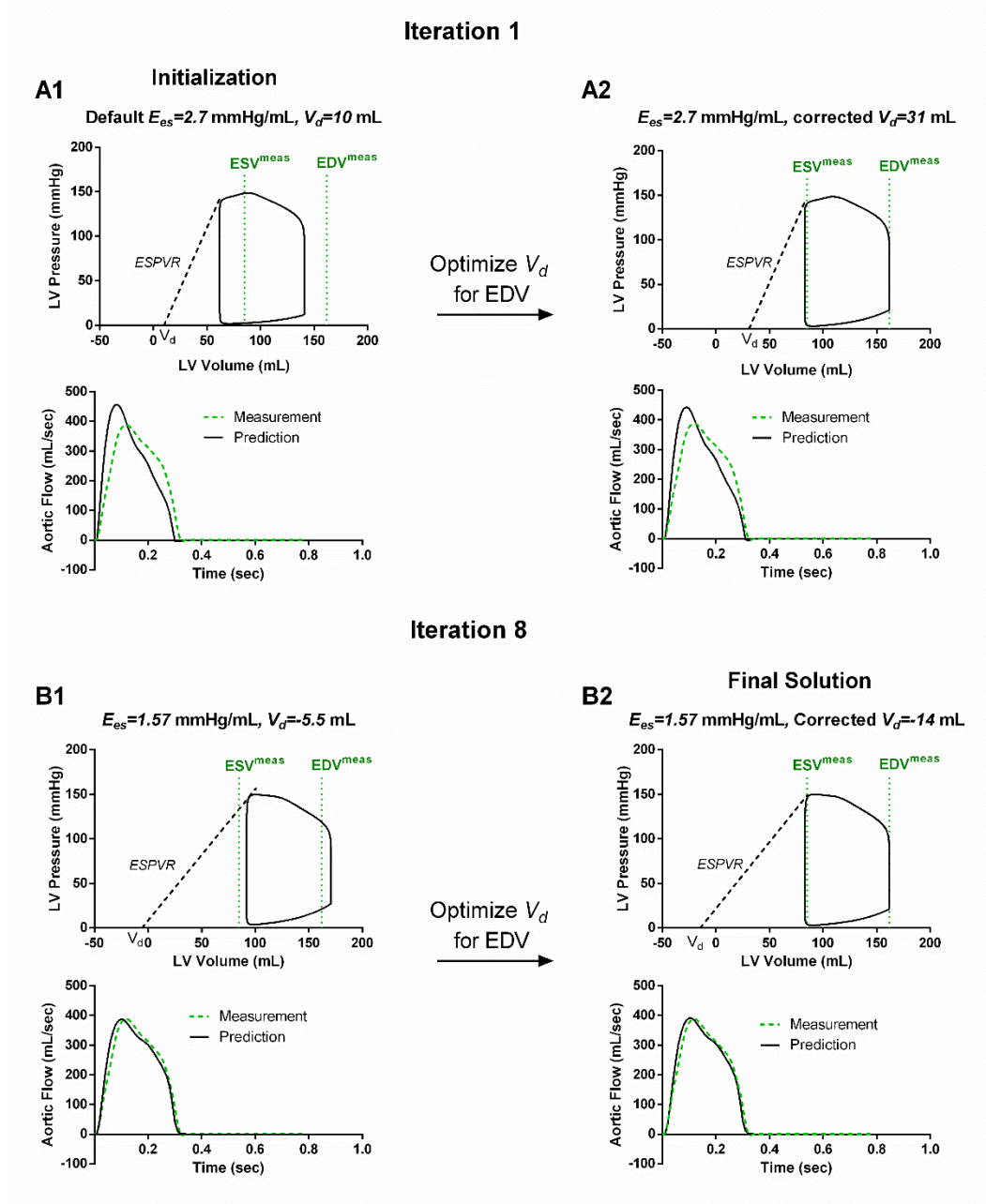


Figure 4.2:2 Example of the optimization process of the ESPVR for a specific HFpEF patient. (A1) Initialization of E_{es} and V_d . (A2) Optimization of V_d based on the measured EDV and update of the E_{es} based on the discrepancy of the model-derived and measured aortic flow. (B2) Convergence to a set of E_{es} and V_d after 8 iterations.

In vivo validation

In Figure 4.2:3, we compare the method predictions for E_{es} , V_d and V_{100} against the invasive measurements. There was a high correlation between the estimated values and invasive measurements, r was 0.92, 0.84 and 0.92 for E_{es} , V_d and V_{100} , respectively. In terms of accuracy, the proposed algorithm was able to predict all E_{es} , V_d and V_{100} well, nRMSE was 9%, 13% and 12%, respectively. For these indices, prediction had low bias (\bar{d}) and narrow limits of agreement, i.e., for E_{es} , $\bar{d} = -0.13$ mmHg/mL with SD = 0.37 mmHg/mL; for V_d , $\bar{d} = -4$ mL with SD = 15 mL; and for V_{100} , $\bar{d} = -4$ mL with SD = 9 mL. We did not notice a statistically significant difference in the performance of the method between the HFpEF and the non-HF groups (for E_{es} , $\bar{d} = -0.04$ mmHg/mL with SD = 0.36 mmHg/mL for the HFpEF group and $\bar{d} = -0.23$ mmHg/mL with SD = 0.33 mmHg/mL for the non-HF group, $p=0.26$).

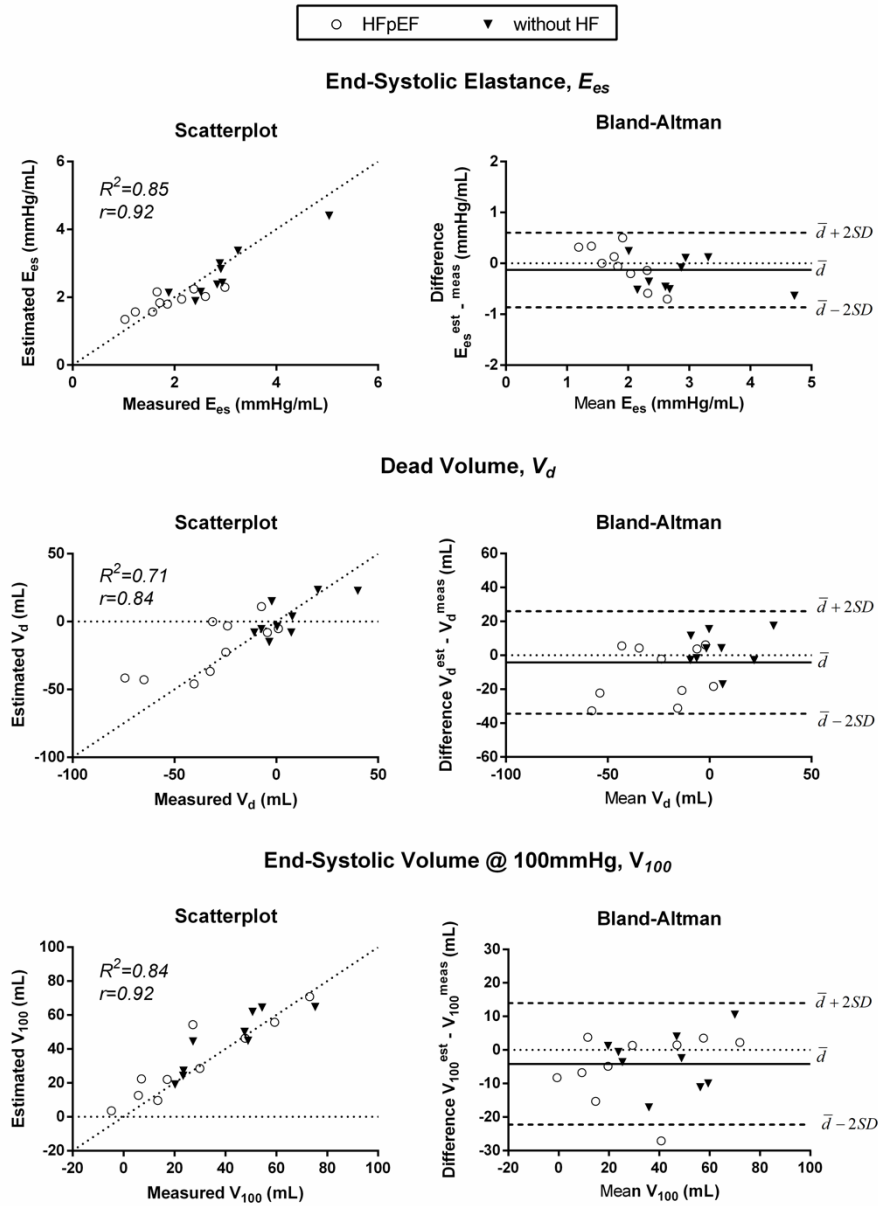


Figure 4.2:3 Scatterplots (left) and Bland-Altman plots (right) for E_{es} (top), V_d (middle) and V_{100} (bottom) as predicted by the method against invasive measurements.

Sensitivity to LV diastolic properties

Figure 4.2:4 demonstrates the accuracy of the estimation of EDP from the echocardiographic E/e' as previously proposed [10]. Interestingly, we observe that E/e' is only fairly a reliable measure of EDP in this pressure range of [10, 24] mmHg. The overall correlation was poor, $r=0.4$, nRMSE was 32% and bias was 2.5 mmHg (LoA = $[-6.1, 11.1]$ mmHg). The experimental relation between EDP and E/e' seemed to work better for the non-HF than the HFpEF group (Figure 4.2:4).

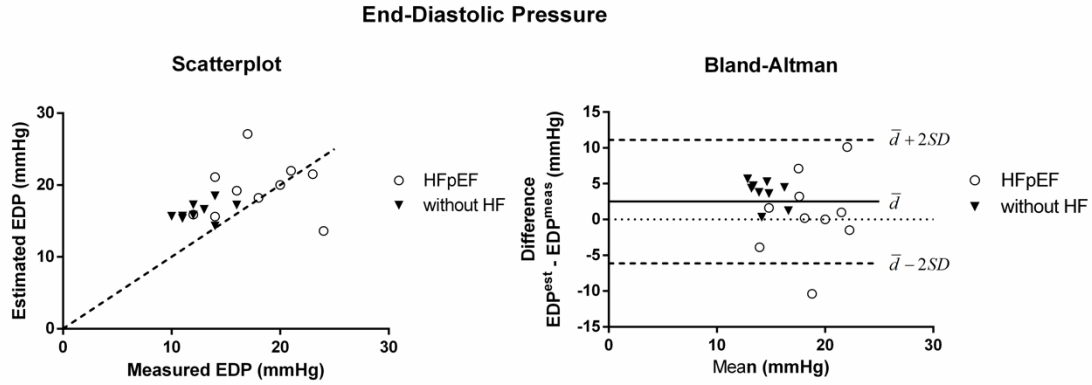


Figure 4.2:4 Scatterplot (left) and Bland-Altman plot (right) for the EDP approximated using its experimental correlation with E/e' [10] against invasive measurements.

To assess whether this level of accuracy in the EDP prediction is sufficient for the needs of our method, we conducted two analyses to appreciate its effect on the E_{es} , V_d and V_{100} predictions. Figure 4.2:5 and Table 4.2:2 contain the results of the first analysis, in which we demonstrate how for a specific HFpEF an over- and underestimation of EDP affect the method predictions. Originally, the EDP was estimated at 21 mmHg according to the echocardiographic measurement of E/e' and the model predicted the patient's P-V loop and aortic flow shown in Figure 4.2:5 (with continuous lines). Then EDP was varied at five discrete levels in the range [5, 30] mmHg. Figure 4.2:5 (bottom) shows the respective changes in the model-predicted aortic flow (dashed and dotted lines) for the two extreme EDP values, i.e., for EDP=5 mmHg and EDP=30 mmHg. We observe that the aortic flow waveform is only minimally affected by these drastic changes in EDP. Accordingly, the method-derived E_{es} , V_d and V_{100} were minimally altered as shown in Table 4.2:2.

Table 4.2:2 Method sensitivity to the approximation of the end-diastolic pressure (EDP). The results pertain to a specific HFpEF case.

| | End-systolic elastance, E_{es} (mmHg/mL) | Dead volume, V_d (mL) | End-systolic volume @ 100mmHg, V_{100} (mL) |
|--|---|----------------------------|--|
| Measurement | 1.57 | -4 | 59 |
| Original estimation, EDP = 21 mmHg | 1.56 | -8 | 56 |
| <i>Estimation for different EDP levels</i> | | | |
| EDP = 30 mmHg | 1.65 (+6.0%) | -4 | 57 (+0.9%) |
| EDP = 25 mmHg | 1.59 (+1.7%) | -8 | 55 (-2.2%) |
| EDP = 15 mmHg | 1.37 (-12.1%) | -22 | 51 (-9.1%) |
| EDP = 10 mmHg | 1.29 (-17.2%) | -29 | 49 (-13.5%) |
| EDP = 5 mmHg | 1.13 (-27.6%) | -45 | 43 (-22.5%) |

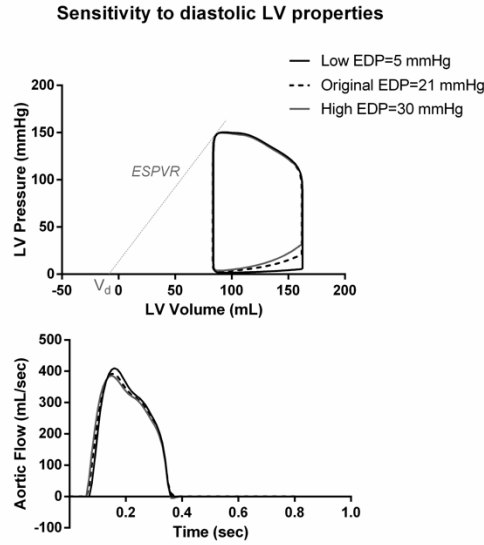


Figure 4.2:5 Method sensitivity to the estimated diastolic LV properties. (top) LV P-V loops. (bottom) Aortic flow.

In the second analysis, we supposed that EDP was equal to 15 mmHg for all patients and run the algorithm anew. This caused only a minor increase in the nRMSE for the E_{es} prediction, namely from 9% to 11%. Bias changed from -0.13 mmHg/mL to -0.18 mmHg/mL and the respective SD of differences from 0.37 mmHg/mL to 0.41 mmHg/mL. This manipulation did not have any significant effect on the estimation of V_d or V_{100} either.

4.2.4 Discussion

In this work, we present and validate a noninvasive method to estimate the LV ESPVR based on echocardiographic and sphygmomanometric measurements. The basic concept relies on the fine tuning of the properties of a generic, validated cardiovascular model to patient-specific standards. An original version of this methodology was previously described [7], where the proof of concept was demonstrated *in silico*. Since its original publication, the method has been upgraded to i) incorporate mechanisms of ageing, according to the insights we have acquired from previous works [9], [17], and ii) allow for the inclusion of different pathologies, such as diastolic dysfunction and hypertension.

Accordingly, we validated the presented method for patients with a critical cardiovascular disease, i.e. HFpEF, as well as for patients without HF symptoms. Overall, the method performed well when compared with *in vivo* acquired invasive data, achieving low bias and narrow limits of agreement. The errors were small for all ESPVR metrics, i.e. E_{es} , V_d and V_{100} , and the predictions were equally precise for HFpEF and non-HF patients.

The success of the proposed method is largely due to the strong coupling between the measured quantities (brachial pressure and echocardiographic indices) and the functional properties of the heart and the arterial tree. In a previous computational study on the ventricular-arterial coupling (pending review), we showed that changes in cardiac contractility have a direct and pronounced effect on central and peripheral hemodynamics even for an unchanged arterial load and cardiac output. Particularly, we reported that when LV contractility increases, the aortic flow wave shape changes, its upstroke becomes steeper and its peak value increases, even if the stroke volume might be maintained. It is exactly this mechanism that we capture with the proposed algorithm, as shown in Figure 4.2:2. In other words, the method is able to predict E_{es} accurately, because this information is contained in the measured aortic flow waveform that drives the optimization of the LV systolic properties. Consequently, accurate measurement of the aortic flow wave shape is vital to the method's accuracy.

A potential source of error is the definition of the LV diastolic properties in our simulations, which was based on the echocardiographic measurement of the E/e' ratio [10] and a previously developed methodology [11]. Of course, the experimental relation relating EDP and E/e' has certain limitations [18] (as also highlighted in Figure 4.2:4) and the overall technique might fail to yield accurate

estimates of the EDPVR parameters. However, we demonstrated that this is not reflected in the accuracy of the E_{es} and V_d estimation; the method is not particularly sensitive to either EDP or parameters P_0 and β (Figures 4.2:4 and 4.2:5, Table 4.2:2).

An important point is that we chose to change the original model for the EDPVR from linear to exponential. This was done in order to achieve a more comprehensive description of the LV diastolic properties. In fact, if we had described the EDPVR with just a constant slope, the method accuracy would not have been undermined (for E_{es} , $nRMSE = 14\%$ and $\bar{d} = -0.34$ mmHg/mL). Overall, we chose to use an exponential model here as we envisage to extend the presented methodology to allow for the additional prediction of LV diastolic properties. This is an ambitious plan to develop a tool that will receive multiple inputs from noninvasive measures and will integrate this information to reverse-engineer the parameters of both the ESPVR and the EDPVR. Such a tool would be most valuable in the clinic, particularly for the diagnosis of diseases of the diastolic relaxation of the LV. Our future works will be oriented towards this direction.

Clinical Perspective

There are important implications to the application of this noninvasive methodology in the clinic. First, this tool can be implemented for the assessment of critically ill patients and for the prediction of personalized interventions in the ICU [13], [19], [20]. A number of other clinical scenarios also could make use of our algorithm to accurately estimate the end-systolic elastance, such cardiac devices, or even coronary interventions [21].

An important point to consider is that the presented methodology does not characterize systolic function (i.e., E_{es}) alone, but also offers a detailed representation of the afterload. This goes beyond the traditional description of the ventricular-arterial coupling as the ratio of end-systolic elastance over an effective arterial elastance E_{es}/E_a . Besides, this concept has been previously seriously challenged [22]. Conversely, the presented methodology might allow for a more sophisticated analysis to characterize the ventricular-arterial coupling [22].

Therefore, there is potential in applying the presented tool for effectively monitoring treatment effects in stable patients as well; particularly, in patients who have altered ventricular-arterial coupling with heightened afterload sensitivity, e.g. aHT or HFpEF patients. This is of essence if we consider recent findings suggesting that hypercontractile phenotypes of aHT and HFpEF patients are linked with adverse prognosis [23]. Our methodology could be used to expose pathological ventricular-arterial coupling and predominantly hypercontractile pathomechanisms, and thereby help identify such individuals and test targeted therapies. On that note, our recent study [24] demonstrated that the effective antihypertensive therapy by renal sympathetic modulation is achieved via reduction in stroke volume, therefore potentially addressing the issue of an "overcompensated" ventricular-arterial coupling state. We plan to investigate this paradigm using the presented methodology in our future work.

Limitations and future steps

A limitation of this work is that the LV volumes used for validation were taken from CMR measurements, although the method has been designed to use only echocardiographic volumes. This was done due to lack of high-quality echocardiographic data of EDV and ESV. Previous studies suggest that EDV and ESV measured with non-contrast and contrast 2D and 3D echocardiography tend to be smaller and show greater variability than those measured with CMR [25]. Therefore, there might be a non-negligible bias when echocardiographic volumes are used instead. We acknowledge this limitation and plan to validate the method with echocardiographic data alone in the future.

It should be noted that the activation function used to describe the LV P-V relation might vary among different individuals, which could have an important impact on the results. This point will be further investigated in the future. Other model-related limitations are acknowledged in our previous publication [8].

The proposed algorithm cannot be applied to any patient without prior knowledge of the condition of his/her aortic valve. Strategically in this study we chose to conduct the validation on patients free from any severe valve diseases. In the presence of severe aortic valve stenosis, aortic hemodynamics and particularly aortic flow wave shape are altered as we previously demonstrated (pending review). Therefore, if we do not integrate an existing valvular pathology into the model, the method will fail to correctly predict the LV ESPVR. Accordingly, significant valvular diseases should be introduced into the simulation in advance. Given that during echocardiographic examination clinicians usually assess valve condition, we assume that such information would be in general available. We plan to investigate the method accuracy in patients with valvular diseases, namely aortic stenosis and regurgitation.

In addition, the model was developed and validated for a healthy young adult [8], [26] and has been adapted to include the effects of normal ageing [17]. Consequently, the method has been developed to adjust the model parameters according to average trends expected in adults, without comprising effects of certain diseases, such as CAD. It would be meaningful to investigate different pathologies in order to have a better understanding of their modeling implications and ultimately achieve a more faithful representation of the cardiovascular properties of each patient. It would also be beneficial to assess the method's ability to capture expected changes in E_{es} due to inotropic drugs or differences between patient groups, such as systolic HF patients, dilated or hypertrophic cardiomyopathy patients, etc. Further studies will be undertaken towards this direction.

Conclusions

In this study, we described and validated a method that allows for the noninvasive estimation of the ESPVR in patients based on a few measurements that are usually conducted in routine cardiology, i.e. echocardiography and sphygmomanometry. This was motivated by the obvious fact that such a method would be a most valuable tool for clinicians in order to achieve accurate cardiac monitoring and optimize patient management. The validation of the proposed algorithm against invasive measurements of P-V loops demonstrated its accuracy and robustness. We concluded that the method performance depends mostly on the precision of the echocardiographic flow data. We plan to further investigate the method accuracy under different settings and for various diseases.

4.2.5 Bibliography

- [1] M. Cecconi *et al.*, "Consensus on circulatory shock and hemodynamic monitoring. Task force of the European Society of Intensive Care Medicine," *Intensive Care Med.*, vol. 40, no. 12, pp. 1795–1815, Dec. 2014, doi: 10.1007/s00134-014-3525-z.
- [2] A. Ochagavía, L. Zapata, A. Carrillo, A. Rodríguez, M. Guerrero, and J. M. Ayuela, "Evaluation of contractility and postloading in the intensive care unit," *Med. Intensiva Engl. Ed.*, vol. 36, no. 5, pp. 365–374, Jun. 2012, doi: 10.1016/j.medine.2012.07.007.
- [3] M. A. Konstam and F. M. Abboud, "Ejection Fraction: Misunderstood and Over-rated (Changing the Paradigm in Categorizing Heart Failure)," *Circulation*, vol. 135, no. 8, pp. 717–719, Feb. 2017, doi: 10.1161/CIRCULATIONAHA.116.025795.
- [4] K. Sagawa, H. Suga, A. A. Shoukas, and K. M. Bakalar, "End-systolic pressure/volume ratio: a new index of ventricular contractility," *Am. J. Cardiol.*, vol. 40, no. 5, pp. 748–753, Nov. 1977.
- [5] H. Suga and K. Sagawa, "Instantaneous pressure-volume relationships and their ratio in the excised, supported canine left ventricle," *Circ. Res.*, vol. 35, no. 1, pp. 117–126, Jul. 1974.
- [6] H. W. Paley, I. G. McDonald, J. Blumenthal, and J. Mailhot, "The effects of posture and isoproterenol on the velocity of left ventricular contraction in man. The reciprocal relationship between left ventricular volume and myocardial wall force during ejection on mean rate of circumferential shortening," *J. Clin. Invest.*, vol. 50, no. 11, pp. 2283–2294, Nov. 1971, doi: 10.1172/JCI106726.
- [7] S. Z. Pagoulatou and N. Stergiopoulos, "Estimating Left Ventricular Elastance from Aortic Flow Waveform, Ventricular Ejection Fraction, and Brachial Pressure: An In Silico Study," *Ann. Biomed. Eng.*, vol. 46, no. 11, pp. 1722–1735, Nov. 2018, doi: 10.1007/s10439-018-2072-0.
- [8] P. Reymond, F. Merenda, F. Perren, D. Rüfenacht, and N. Stergiopoulos, "Validation of a one-dimensional model of the systemic arterial tree," *Am. J. Physiol. - Heart Circ. Physiol.*, vol. 297, no. 1, pp. H208–H222, Jul. 2009, doi: 10.1152/ajpheart.00037.2009.
- [9] S. Z. Pagoulatou, V. Bikia, B. Trachet, T. G. Papaioannou, A. D. Protogerou, and N. Stergiopoulos, "On the importance of the nonuniform aortic stiffening in the hemodynamics of physiological aging," *Am. J. Physiol.-Heart Circ. Physiol.*, vol. 317, no. 5, pp. H1125–H1133, Sep. 2019, doi: 10.1152/ajpheart.00193.2019.
- [10] S. R. Ommen *et al.*, "Clinical utility of Doppler echocardiography and tissue Doppler imaging in the estimation of left ventricular filling pressures: A comparative simultaneous Doppler-catheterization study," *Circulation*, vol. 102, no. 15, pp. 1788–1794, Oct. 2000, doi: 10.1161/01.cir.102.15.1788.
- [11] S. Klotz *et al.*, "Single-beat estimation of end-diastolic pressure-volume relationship: a novel method with potential for noninvasive application," *Am. J. Physiol. Heart Circ. Physiol.*, vol. 291, no. 1, pp. H403–412, Jul. 2006, doi: 10.1152/ajpheart.01240.2005.
- [12] Rommel Karl-Philipp *et al.*, "Load-Independent Systolic and Diastolic Right Ventricular Function in Heart Failure With Preserved Ejection Fraction as Assessed by Resting and Handgrip Exercise Pressure–Volume Loops," *Circ. Heart Fail.*, vol. 11, no. 2, p. e004121, Feb. 2018, doi: 10.1161/CIRCHEARTFAILURE.117.004121.

- [13] K.-P. Rommel *et al.*, “Extracellular Volume Fraction for Characterization of Patients With Heart Failure and Preserved Ejection Fraction,” *J. Am. Coll. Cardiol.*, vol. 67, no. 15, pp. 1815–1825, Apr. 2016, doi: 10.1016/j.jacc.2016.02.018.
- [14] W. J. Paulus *et al.*, “How to diagnose diastolic heart failure: a consensus statement on the diagnosis of heart failure with normal left ventricular ejection fraction by the Heart Failure and Echocardiography Associations of the European Society of Cardiology,” *Eur. Heart J.*, vol. 28, no. 20, pp. 2539–2550, Oct. 2007, doi: 10.1093/eurheartj/ehm037.
- [15] B. Ky *et al.*, “Ventricular-arterial coupling, remodeling, and prognosis in chronic heart failure,” *J. Am. Coll. Cardiol.*, vol. 62, no. 13, pp. 1165–1172, Sep. 2013, doi: 10.1016/j.jacc.2013.03.085.
- [16] E. A. ten Brinke *et al.*, “Noninvasive estimation of left ventricular filling pressures in patients with heart failure after surgical ventricular restoration and restrictive mitral annuloplasty,” *J. Thorac. Cardiovasc. Surg.*, vol. 140, no. 4, pp. 807–815, Oct. 2010, doi: 10.1016/j.jtcvs.2009.11.039.
- [17] S. Pagouladou and N. Stergiopulos, “Evolution of aortic pressure during normal ageing: A model-based study,” *PloS One*, vol. 12, no. 7, p. e0182173, 2017, doi: 10.1371/journal.pone.0182173.
- [18] M. Previtali, E. Chieffo, M. Ferrario, and C. Klersy, “Is mitral E/E’ ratio a reliable predictor of left ventricular diastolic pressures in patients without heart failure?,” *Eur. J. Echocardiogr.*, vol. 13, no. 7, pp. 588–595, Jul. 2012, doi: 10.1093/ejehocardiography/erj286.
- [19] Kawaguchi Miho, Hay Ilan, Fetis Barry, and Kass David A., “Combined Ventricular Systolic and Arterial Stiffening in Patients With Heart Failure and Preserved Ejection Fraction,” *Circulation*, vol. 107, no. 5, pp. 714–720, Feb. 2003, doi: 10.1161/01.CIR.0000048123.22359.A0.
- [20] B. A. Borlaug and W. J. Paulus, “Heart failure with preserved ejection fraction: pathophysiology, diagnosis, and treatment,” *Eur. Heart J.*, vol. 32, no. 6, pp. 670–679, Mar. 2011, doi: 10.1093/eurheartj/ehq426.
- [21] M. B. Bastos *et al.*, “Invasive left ventricle pressure–volume analysis: overview and practical clinical implications,” *Eur. Heart J.*, vol. 41, no. 12, pp. 1286–1297, Mar. 2020, doi: 10.1093/eurheartj/ehz552.
- [22] J. A. Chirinos, “Ventricular-arterial coupling: Invasive and non-invasive assessment,” *Artery Res.*, vol. 7, no. 1, Mar. 2013, doi: 10.1016/j.artres.2012.12.002.
- [23] G. J. Wehner *et al.*, “Routinely reported ejection fraction and mortality in clinical practice: where does the nadir of risk lie?,” *Eur. Heart J.*, vol. 41, no. 12, pp. 1249–1257, Mar. 2020, doi: 10.1093/eurheartj/ehz550.
- [24] Lurz Philip *et al.*, “Changes in Stroke Volume After Renal Denervation,” *Hypertension*, vol. 75, no. 3, pp. 707–713, Mar. 2020, doi: 10.1161/HYPERTENSIONAHA.119.14310.
- [25] P. W. Wood, J. B. Choy, N. C. Nanda, and H. Becher, “Left Ventricular Ejection Fraction and Volumes: It Depends on the Imaging Method,” *Echocardiogr. Mt. Kisco N*, vol. 31, no. 1, pp. 87–100, Jan. 2014, doi: 10.1111/echo.12331.
- [26] P. Reymond, Y. Bohraus, F. Perren, F. Lazeyras, and N. Stergiopulos, “Validation of a patient-specific one-dimensional model of the systemic arterial tree,” *Am. J. Physiol. Heart Circ. Physiol.*, vol. 301, no. 3, pp. H1173–1182, Sep. 2011, doi: 10.1152/ajpheart.00821.2010.

Chapter 5 Methods for Assessing Bio-mechanical Properties of the Aorta

5.1 The effect of the elongation of the proximal aorta on the estimation of the aortic wall distensibility

Stamatia Pagoulatou ¹, Mauro Ferraro ¹, Bram Trachet ^{1,2}, Vasiliki Bikia ¹, Georgios Rovas ¹, Lindsey A Crowe ³, Jean-Paul Vallée ³, Dionysios Adamopoulos ⁴, and Nikolaos Stergiopoulos ¹

¹ Laboratory of Hemodynamics and Cardiovascular Technology (LHTC), Institute of Bioengineering, Ecole Polytechnique Fédérale de Lausanne (EPFL), Lausanne, Switzerland

² Biofluid, Tissue and Solid Mechanics for Medical Applications (BIOMMEDA), Institute of Biomedical Technology, Ghent University, Ghent, Belgium

³ Department of Radiology and Medical Informatics, Hôpitaux Universitaires de Genève (HUG), Geneva, Switzerland

⁴ Department of Cardiology, Hôpitaux Universitaires de Genève (HUG), Geneva, Switzerland

Abstract

The compliance of the proximal aortic wall is a major determinant of cardiac afterload. Aortic compliance is often estimated based on cross-sectional area changes over the pulse pressure, under the assumption of a negligible longitudinal stretch during the pulse. However, the proximal aorta is subjected to significant axial stretch during cardiac contraction. In the present study, we sought to evaluate the importance of axial stretch on compliance estimation by undertaking both an in silico and an in vivo approach. In the computational analysis, we developed a 3D Finite Element Model of the proximal aorta and investigated the discrepancy between the actual wall compliance to the value estimated after neglecting the longitudinal stretch of the aorta. A parameter sensitivity analysis was further conducted to show how increased material stiffness and increased aortic root motion might amplify the estimation errors (discrepancies between actual and estimated distensibility ranging from -20% to -62%). Axial and circumferential aortic deformation during ventricular contraction was also evaluated in vivo based on MR images of the aorta of 3 healthy young volunteers. The in vivo results were in good qualitative agreement with the computational analysis (underestimation errors ranging from -26% to -44%, with increased errors reflecting higher aortic root displacement). Both the in silico and in vivo findings suggest that neglecting the longitudinal strain during contraction might lead to severe underestimation of local aortic compliance, particularly in the case of women who tend to have higher aortic root motion or in subjects with stiff aortas.

Key words: Cross-sectional area compliance • Axial stretch • Proximal aorta • Finite element analysis

Published in Biomechanics and Modeling in Mechanobiology (2020)

5.1.1 Introduction

Arterial compliance is a major determinant of the cardiac afterload and, in consequence, of the pressure and flow resulting from the interaction of the heart with the arterial system. Approximately half of the total arterial compliance resides in the proximal aorta [1]. The ability of the aortic wall to distend during systole serves as a powerful mechanism to limit the increase in blood pressure and to reduce the cardiac afterload [2]. Consequently, a decrease in aortic compliance, as a result of ageing or pathology, plays an important role in the development of hypertension and is a strong predictor of all-cause mortality [3]. In this context, accurate estimation of the aortic compliance might become important in the future for correct risk stratification and optimized patient management.

Volume compliance (C_v) is defined as the change in lumen volume over a change in distending pressure, $C_v = dV/dP$. However, direct measurement of regional blood volume during the cardiac cycle is challenging. The common clinical practice is to derive aortic compliance from cine Magnetic Resonance (MR) images taken perpendicular to the aortic centerline, whereby the maximal and minimal lumen cross-sectional areas are calculated. This measure is referred to as the local or cross-sectional area compliance (C_A), $C_A = dA/dP$, and has been extensively used in the past [4]–[9].

Area compliance is often used to derive volume compliance. The derivation is based on the assumption that the deformation of the vessel takes place primarily in the radial direction and that there is no significant longitudinal stretch during the cardiac cycle. To illustrate this point, we may consider a non-tapered arterial segment. Any change in its volume (V) can be expressed as a function of changes in the corresponding area (A) and centerline length (L) as follows:

$$\delta V = \delta(A * L) = L * \delta A + A * \delta L \cong L * \delta A$$

Equation 5.1:1 – Volumetric changes expressed as changes in area and centerline length

In this equation, the assumption that the aorta does not change its length during the cardiac cycle is equivalent to assuming that $\delta L \cong 0$. However, previous studies [10], [11] have questioned this simplification, particularly for the case of the proximal aorta. It has been demonstrated that during systole the heart pulls the proximal aorta towards the left ventricular apex, which stays practically in place. Plonek et al. [10] studied the axial motion of the aortic annulus in a population comprising both young and old individuals ($n=73$) and reported significant longitudinal displacement values from diastole to systole, with an average of 11.6 ± 2.9 mm.

These findings inevitably lead to the following question: How important is the contribution of axial elongation to the volume compliance of the proximal aorta? In order to answer this question, one should quantify the elongation of the aortic root during systole and calculate the errors in the estimation of aortic compliance when axial elongation is neglected. To this aim, we adopted both an *in silico* (Part I) and an *in vivo* (Part II) approach. The *in silico* approach involved the development of a computational framework to simulate the three-dimensional (3D) aortic wall deformation during the cardiac cycle and to compare the actual wall distensibility (imposed as a model input) to the distensibility estimated after neglecting the longitudinal stretch of the aorta during contraction. In Part II, we validated the *in silico* results *in vivo*. More specifically, we collected MR data of the proximal aorta of three healthy young adults during diastole and peak systole and examined the axial and circumferential aortic deformation during LV contraction and the impact of neglected axial stretch on the estimated compliance.

5.1.2 Methods

Part I. *In silico* investigation

Image data

To build the Finite Element Model (FEM) of the aorta, we used the images of the aortic geometry of a healthy 30-year-old male volunteer (height 183 cm, weight 90 kg) acquired with Magnetic Resonance Imaging (MRI) in the context of a previous study [12] (Figure 5.1:1 A). The MR Angiography (Time of flight – ToF, non ECG-gated) measurement was carried out on a 3T scanner (Siemens Trio-Tim 3T, Germany). The volunteer's heart rate during this acquisition was 61 bpm. Informed consent was obtained from the subject prior to the scan. Details on the protocol can be found in the original publication by Reymond et al. [12].

Segmentation and mesh generation

As described in [12], the segmentation of the aortic geometry was performed from the MR magnitude data following an edge detection method according to the contrast intensity gradient (ITK Snap Software) (Figure 5.1:1 B). The final 3D geometry was cropped to isolate the proximal domain, i.e. starting from the level of the right pulmonary artery and extending down to the celiac trunk (Figure 5.1:1 C). The 3D centerline of this aortic segment was extracted using the open source software Vascular Modelling ToolKit (VMTK) [13].

Subsequently, an unstructured hexahedral mesh was created using the semi-automated algorithm developed by Bols et al. [14]. More specifically, a preliminary multi-block structure was first generated following the branching topology and was then refined. The multi-block structure was projected onto the input surface geometry and a body-fitted grid was obtained. From the hex core, the boundary layer grid was computed. We assumed that the wall thickness varied along the structure and was 10% of the local lumen diameter. This assumption is often adopted in the literature when no ex vivo data is available [15]. The resulting mesh was composed of 172533 nodes and 114568 hybrid hexahedral elements (type C3D8H), with two layers of elements across the vessel wall thickness.

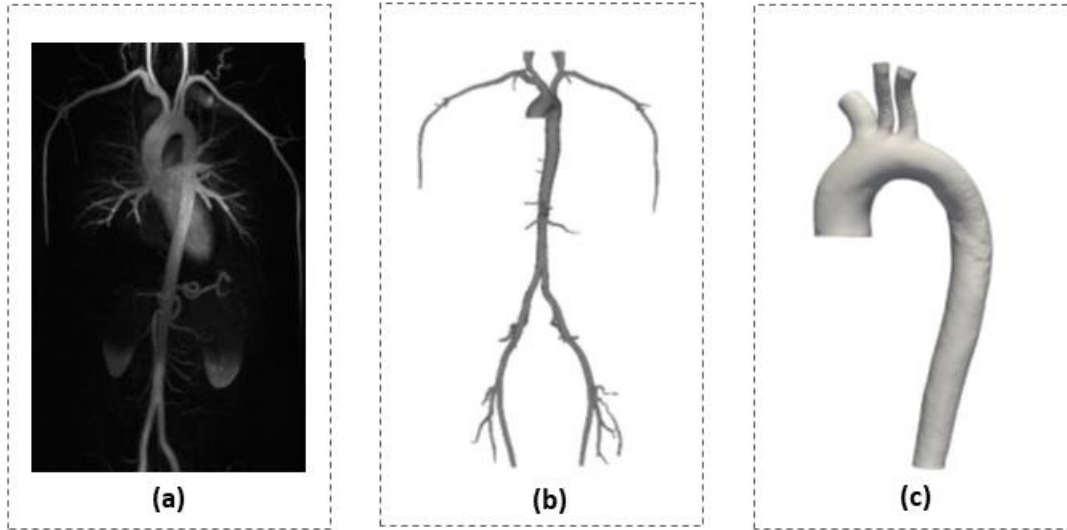


Figure 5.1:1 (a) Raw MR data of the aorta and its main branches acquired with ToF MR Angiography on a healthy young male [12] (b) Reconstruction of the 3D geometry (c) Cropping of the aorta at the main supra-aortic branches and above the celiac trunk

Constitutive material model

The constitutive model for the arterial wall was based on Holzapfel et al. [16] with the extension of Gasser et al. [17]. Hereafter, we will refer to this model as the ‘Holzapfel-Gasser-Ogden’ (HGO) model. The HGO model is a built-in constitutive model in Abaqus. It assumes that the material is incompressible and consists of an isotropic matrix, wherein N families of collagen fibres are embedded and dispersed around a mean orientation. In this work, we assumed that the material contains $N = 2$ families of fibres, as often assumed in the literature [18].

The constitutive model is described by a strain-energy function, U , which relates the energy per unit reference volume to strain and stress. The strain-energy function may then be decomposed into a volumetric response, an isochoric isotropic and an isochoric anisotropic response as follows:

$$U = U_{vol} + U_{iso} + U_{aniso} = \frac{1}{D} \left(\frac{(J^{el})^2 - 1}{2} - \ln J^{el} \right) + C_{10}(\bar{I}_1 - 3) + \frac{k_1}{2k_2} \sum_{a=1}^{N=2} \{ \exp[k_2 \langle \bar{E}_a \rangle^2] - 1 \}$$

Equation 5.1:2 – The strain-energy function according to the HGO model

With

$$\bar{E}_1 = \kappa(\bar{I}_1 - 3) + (1 - 3\kappa)(\bar{I}_{4a} - 1) \text{ and } \bar{E}_2 = \kappa(\bar{I}_1 - 3) + (1 - 3\kappa)(\bar{I}_{6a} - 1)$$

Equation 5.1:3 – Stain-like quantities \bar{E}_1 and \bar{E}_2 that characterize the deformation of the two families of fibres

To approximate the physiological vascular wall response, we chose the material properties according to the population-averaged values proposed in the literature for young male adults. Parameter D was set at 10-6 kPa, as recommended to ensure incompressibility [18]. The two families of fibres were assumed symmetrically oriented, making an angle $\alpha = 55^\circ$ with respect to the circumferential direction. This value was chosen based on physiological data [19], [20]. The dispersion coefficient κ was set to a high value, $\kappa = 0.315$, similarly to [18].

The remaining material parameters, C_{10} , k_1 and k_2 , were approximated according to two criteria: first, the values should be in the physiological range proposed in the literature [16], [19], [21], [22], and, second, the deformation of the aortic wall under the pressure load should reflect the expected elasticity of the aortic wall. From uniaxial tension tests, the three parameters are known to be in the following range: $C_{10} \in [1, 240]$ kPa, $k_1 \in [1, 410]$ kPa, $k_2 \in [2.5, 72]$. The elasticity of the aortic wall was estimated according to the Bramwell-Hill equation using the aortic pulse wave velocity (PWV) measured in the original study by Reymond et al. [12], $PWV = 4.8$ m/s. To match the measured PWV and the aforementioned literature guidelines, the final material parameters were set to the physiological values $C_{10} = 42$ kPa, $k_1 = 290$ kPa and $k_2 = 12.6$.

Optimization of fibre orientation

When defining the mean direction of the different families of fibres, one needs to account for the tortuosity of the aortic geometry. In order to define the mean angle direction in a consistent manner throughout the aortic domain, we need to consider a local coordinate system for each finite element. To do so, we developed a Matlab code in which we adapted the orientation of the collagen fibres following the lumen centerline, similarly to Roy et al. [18].

Zero-Pressure Geometry

At the time of the scan, the aorta is deformed under physiological pressure. This means that the aortic geometry we obtain after segmentation corresponds to the loaded state. To perform the FEM analysis we need to define the unloaded configuration. A number of studies in the literature propose inverse problem-solving techniques, whereby the unloaded configuration is calculated from the known *in vivo* measured geometry and the measured distending pressure. In this work particularly, we follow the fixed-point optimization approach of Bols et al. [23]. The zero-pressure configuration was restored by iteratively updating the coordinates of the unloaded geometry until the deformed geometry at physiological pressure matched closely the *in vivo* measured configuration. This optimization code was written in Matlab and at each optimization cycle the updated mesh coordinates were communicated to the finite element solver (Abaqus). For the restoration of the zero-pressure configuration, we assumed that the distending pressure at the time of the measurement was equal to the measured diastolic pressure.

Load and boundary conditions

Pressure Load. The time-varying pressure load acting on the inner aortic wall was assumed equal to the pressure curve measured at the right common carotid artery of the subject the same day as the scan. Carotid pressure waveform was acquired over 10 heart cycles with applanation tonometry (Millar Instruments, SPT 301, Houston, TX, USA) and was calibrated according to the measured mean and diastolic brachial pressures. The systolic (SBP) and diastolic (DBP) blood pressure were 110 mmHg and 70mmHg, respectively.

Viscoelastic external tissue support. When applying boundary conditions along the aortic wall, one needs to consider the external support provided by the surrounding tissues. Interestingly, this support is exerted non-uniformly throughout the domain. The spine significantly tethers a part of the descending thoracic aorta, whereas the remaining wall is less constrained. The majority of approaches in the literature neglect this fact and apply a constant external pressure all along the outer surface. As explained by Moireau et al. [24], this boundary condition results in artificial motion patterns of the arterial wall. Conversely, their work [24] included the viscoelastic, non-uniform support provided by the extremal tissues. In the present study, we therefore adopt their

approach. More specifically, we applied along the outer aortic wall the extended Robin boundary condition proposed in [24], which models an elastic and a viscoelastic response of the external tissue. W:

$$\sigma \cdot \underline{n} = -k\underline{y} - c\underline{u} - p_o \cdot \underline{n}$$

Equation 5.1:4 – Boundary condition applied along the outer aortic wall comprising an elastic and a viscoelastic response

Where σ is the Cauchy stress tensor, the terms $k\underline{y}$ and $c\underline{u}$ represent the elastic and viscoelastic responses, respectively, and p_o is the intrathoracic pressure. The pressure p_o can be neglected in our case as the scan was performed during breath hold. We imposed this condition perpendicular to the outer aortic wall by connecting each node of the outer surface of the mesh to a spring of stiffness k and a dashpot of damping coefficient c . The values of k and c varied according to the position of the node relatively to the spine. To achieve this, we divided the solid mesh into 3 regions: a) a region in direct contact with spine, b) in the spine vicinity and c) opposite to the spine. The region in contact with the spine was identified by locating the intercostal arteries. A schematic representation of these three regions is shown in Figure 5.1:2. For the different regions, the parameters k and c were chosen according to the values provided by [24] for a young adult. Time-varying effects were neglected. The same Robin boundary condition was used for the outlets, with the parameters k and c assumed equal to the reported values in [24] (Figure 5.1:2).

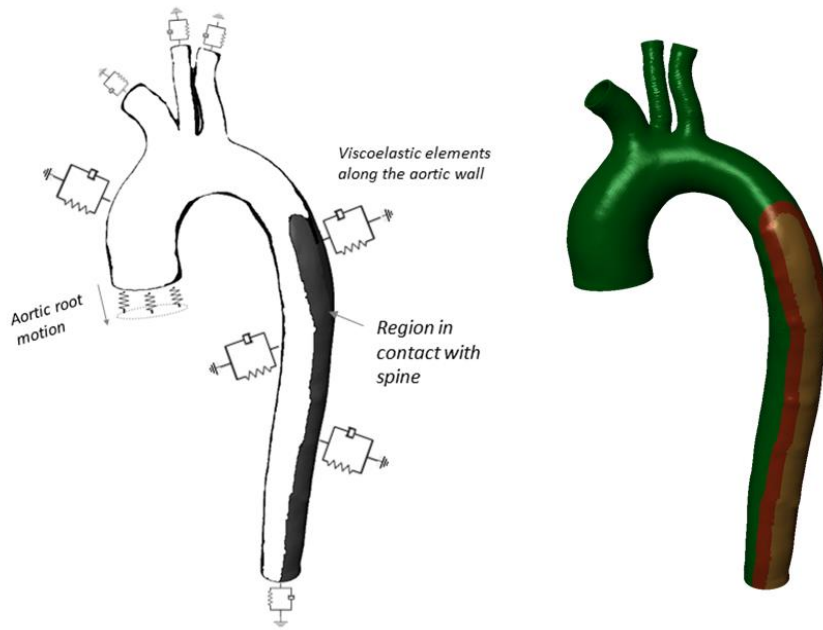


Figure 5.1:2 Boundary conditions (left) Schematic representation of the viscoelastic boundary conditions applied along the vessel wall to mimic the support provided by the external tissues and organs. The measured aortic root displacement is prescribed at the proximal end via stiff springs. Adapted from Moireau et al. (2012). (right) Different regions of the wall domain considered for assigning viscoelastic boundary properties. These regions were identified according to the position of the aorta relative to the spine. The orange region is in contact with the spine, the red region is in the spine vicinity and the green region is less constrained by the surrounding tissues.

Heart motion. To account for the aortic root motion, we prescribed a measured displacement field y_b on the nodes of the proximal boundary of the aortic wall (Figure 5.1:2). This coupling was achieved indirectly by imposing the displacement y_b on reference points connected to the proximal boundary via stiff springs, as in Moireau et al. [24]. The use of springs was necessary in order to allow for the radial expansion of the aorta at the inlet. Additionally, high quality data of the complex heart motion that would justify the direct enforcement of the displacement y_b were not available. The imposed displacement y_b was measured from dynamic MR images of the aortic root collected on a different 28-year-old male subject (height 184 cm, weight 79 kg). The MR examination was carried out on a 3T clinical MRI scanner (MAGNETOM Trio, Siemens AG, Healthcare Sector, Erlangen, Germany) in the context of our ongoing research study (Project ID CER-VD 2017-00954). Approval from the local ethical committee was obtained and the volunteer gave informed consent prior to inclusion. The measurement was performed under breath hold over 7 heart beats in cine TrueFISP

sequences (TR 29.6 ms, TE 1.3 ms, flip angle 30°, resolution 1.4 mm x 1.4 mm x 8 mm). Average heart rate during this acquisition was 63 bpm. The generalized autocalibrating partially parallel acquisition (GRAPPA 3) reconstruction was used.

From visual inspection, the subject presented significant aortic root displacement during the cardiac cycle, a common observation for a young healthy individual. The displacement was calculated at each timeframe by manually tracking the aortic root motion in two planes. First, the position of the ventriculo-aortic junction (VAJ) was established in the coronal plane. The longitudinal displacement of the aortic annulus in this plane was measured between consecutive images as the distance between the mid-points of the VAJ. The estimated displacement was subsequently projected onto the motion vector in the sagittal plane. The methodology is presented in Figure 5.1:3. To account for intra-observer variability, the calculation of the aortic root displacement was conducted again 1 week after the initial assessment. The systolic aortic root displacement was found equal to 9.5 mm (average of two measurements, 9.8 mm and 9.1 mm).

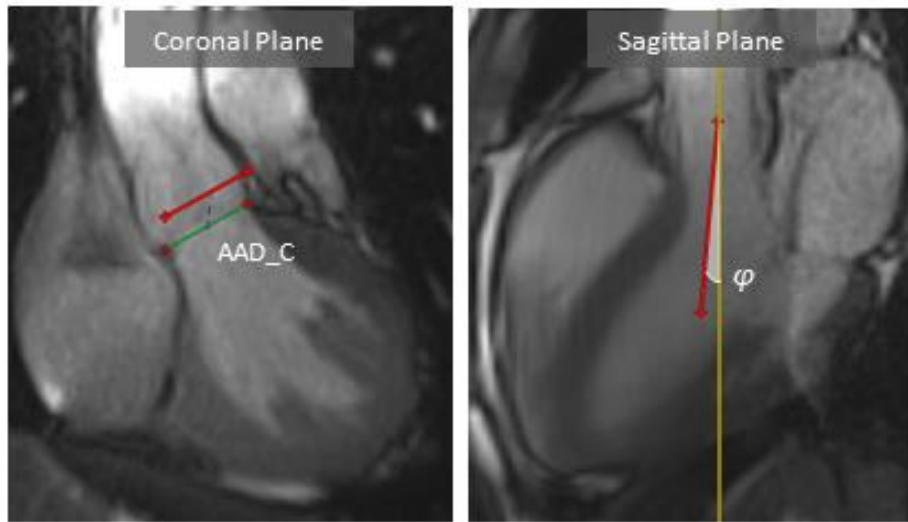


Figure 5.1:3 Motion of the aortic root in 2 planes. (left) Coronal cine-MR images showing the position of the ventriculo-aortic junction (VAJ) in systole (green line) and in diastole (red line). The blue dotted line represents the maximal aortic annulus displacement in the coronal plane (AAD_C) linking the mid-points of the VAJ in systole and diastole. (right) Sagittal cine-MRI images depicting the motion vector in the sagittal plane (red arrow) and the cross-reference line (yellow line). The angle, ϕ , between the red vector and yellow line represents the angle of rotation between the two planes. The total displacement from diastole to systole was calculated as $AAD_C \cdot \cos(\phi)$ and was found equal to 9.5 mm

Effect of elongation on the estimated distensibility

First the fixed-point optimization code was run to restore the unloaded configuration. The unloaded geometry was then imported into Abaqus and inflated to the measured diastolic pressure. Subsequently, we run the complete model with the boundary and loading conditions described above and simulated a full cardiac cycle.

The simulation results were post-processed using VMTK [13], ParaView [25] and in-house codes. More specifically, the dynamic volume of the domain was extracted for each time increment and the peak systolic (V_{max}) and diastolic (V_{min}) values were obtained. The ratio of volume changes over pressure changes was calculated and normalized by the diastolic volume value to yield aortic distensibility, $(V_{max} - V_{min}) / V_{min} / (\text{Pulse Pressure})$. This value served as the reference wall distensibility (imposed by the model properties).

Consequently, seven cross-sections perpendicular to the centerline were tagged along the aorta and were used to calculate the respective area compliances. We then estimated anew the aortic distensibility by integrating the area compliances over the centerline of the aortic segment (computed automatically using VMTK [13]). For the integration, we used the volume formula for a conical cylinder:

$$\text{Volume of conical cylinder} = \frac{\pi L}{12} (D_1^2 + D_1 D_2 + D_2^2)$$

Equation 5.1:5 – Formula for calculation of the volume of a conical cylinder

Where L is the centerline length, D_1 is the diameter of the proximal cross-section and D_2 is the diameter of the distal cross-section. To assess the effect of neglecting the elongation, we assumed that the length of the aortic segment did not vary during the cardiac cycle and remained equal to its diastolic value. This estimate of distensibility was compared to the reference value.

Parametric Analysis

The original model parameters were set according to a) measurements on healthy young adults, b) literature data pertaining to healthy young males. To account for the generic nature of the model, we performed a sensitivity analysis and examined the effect of two key model parameters on the estimation of distensibility. The first parameter that was varied is the aortic wall compliance. The original material parameters corresponded to the highly compliant aorta of a young subject where the pulse wave theoretically propagates with a velocity of 4.8 m/s. Two additional levels of compliance were simulated, a highly stiff and an intermediate level, while the aortic root motion was kept constant at 9.5 mm. As representative of older individuals, the scenario of a stiff aorta was built based on the evolution of the material properties with ageing [19], [20]. For this combination of parameters, the theoretical PWV was 9 m/s. The intermediate level of compliance was simulated also based on [19], [21], corresponding to a theoretical PWV of approximately 7 m/s.

The second parameter that was investigated is the aortic root motion imposed proximally to the domain. The original displacement profile was measured in a healthy young male as a function of time, the maximal displacement being equal to 9.5 mm. Three additional aortic root motion scenarios were considered: a. no systolic displacement during the cardiac cycle, b. a lower systolic displacement of 5 mm, and c. a greater systolic displacement of 15 mm. These values are in the physiological range reported by Plonek et al. [10] (range of 3-19 mm in a population of 73 young and old adults, with an average of 11.2 ± 2.9 mm).

Part II. In vivo investigation**Subjects**

For the *in vivo* validation, three healthy young subjects were recruited: one 38-year-old male (height: 172 cm, weight: 62 kg) and two 18-year-old females (height: 167 cm, weight: 50 kg, and height: 176 cm, weight: 67 kg). All three subjects were free of any cardiovascular disease, normotensive and non-smokers. The subjects gave written consent prior to inclusion in the study (Project ID CER-VD 2017-00954) and were instructed not to consume any caffeine or food at least 4 hours before the measurement.

MRI protocol

Non-contrast enhanced MR angiography acquisitions were performed to capture the aortic geometry at diastole and peak systole. The examination was carried out on a 3T clinical MRI scanner (MAGNETOM Trio, Siemens AG, Healthcare Sector, Erlangen, Germany) using spine and body surface coil elements. Oblique sagittal images of the aorta were acquired with 3D gradient echo sequences (TR 158.22 ms, TE 1.33 ms, flip angle 12° , resolution 0.625 mm x 0.625 mm x 2mm (32 slices), generalized autocalibrating partially parallel acquisitions (GRAPPA) acceleration factor 2). The trigger delay was set after acquiring cine 2-chamber cardiac MR images and observing the static point in systole or diastole. The window of acquisition was 102 ms. Respiratory navigation with around 50% acceptance window was used to reduce respiratory motion artifacts. The acquisition time was approximately 3 minutes.

Data processing and analysis

Initially, the systolic longitudinal displacement of the aortic root was estimated in the sagittal plane bytracking the right coronary artery at systole and diastole. Subsequently, for each subject, the proximal aortic geometry was extracted from the MR angiography data in the peak systolic and diastolic timeframes using the open source software 3D Slicer [26]. The final configuration for peak systole and diastole included the vascular lumen of the ascending and descending aorta, extending down to the celiac trunk. The major neck vessels were truncated (Figure 5.1:4). After acquiring the 3D configurations, the volume of the aortic lumen was extracted at peak systole and diastole using VMTK [13]. The reference aortic wall distensibility was calculated as $(V_{\max} - V_{\min}) / V_{\min} / (\text{Pulse Pressure})$.

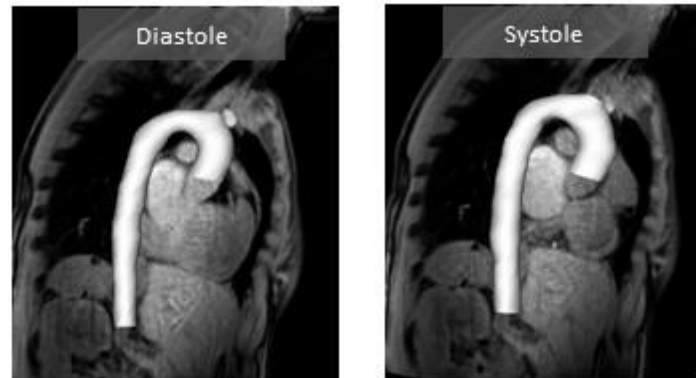


Figure 5.1:4 Imaging of the proximal aorta of the 38-year-old male during diastole (left) and systole (right) in the sagittal plane along with the segmented 3D geometries

Subsequently, eight characteristic cross-sections along the aorta were tagged: the proximal and distal end, before the brachiocephalic artery, before the left common carotid artery, before and after the left subclavian artery and at the level of the 1st and 7th intercostal arteries. The area compliance of these cross-sections was calculated and aortic distensibility was anew estimated by integration over an invariant diastolic centerline length.

5.1.3 Results

Part I. *In silico* Investigation

Zero-pressure configuration

The aortic geometry was brought to its zero-pressure state, assuming that the internal pressure load was 70 mmHg at the moment of the scan (Figure 5.1:5). The optimization algorithm was terminated by the user after 6 cycles, because for a higher number of iterations the structure presented buckling close to the brachiocephalic bifurcation and the algorithm diverged. After 6 simulations, the maximal error was in the order of magnitude of 8% of the local arterial diameter. Figure 5.1:5 also depicts the error map between the measured geometry and the optimized configuration inflated to diastolic pressure.

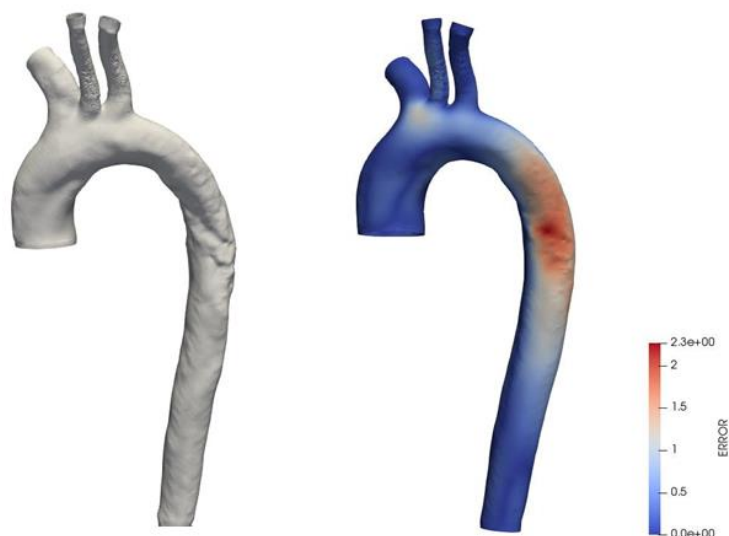


Figure 5.1:5 (left) Unloaded configuration after 6 cycles of the fixed-point optimization algorithm [23]. (right) The corresponding error map between the measured geometry and the configuration inflated to diastolic pressure. Created in ParaView [25]. The error scale is in mm.

Reference distensibility vs distensibility estimate in absence of axial stretch

Generic young model. Figure 5.1:6 shows the model-derived lumen volumetric changes with increasing pressure. The black curve represents the actual volume of the 3D lumen, and the red curve the estimation after neglecting the elongation of the ascending aorta. The volumes are normalized to the volume at diastolic pressure. The slope of each curve represents the aortic distensibility. We clearly note a significant underestimation of the aortic wall distensibility when the longitudinal stretch is not accounted for (error of 30.2%).

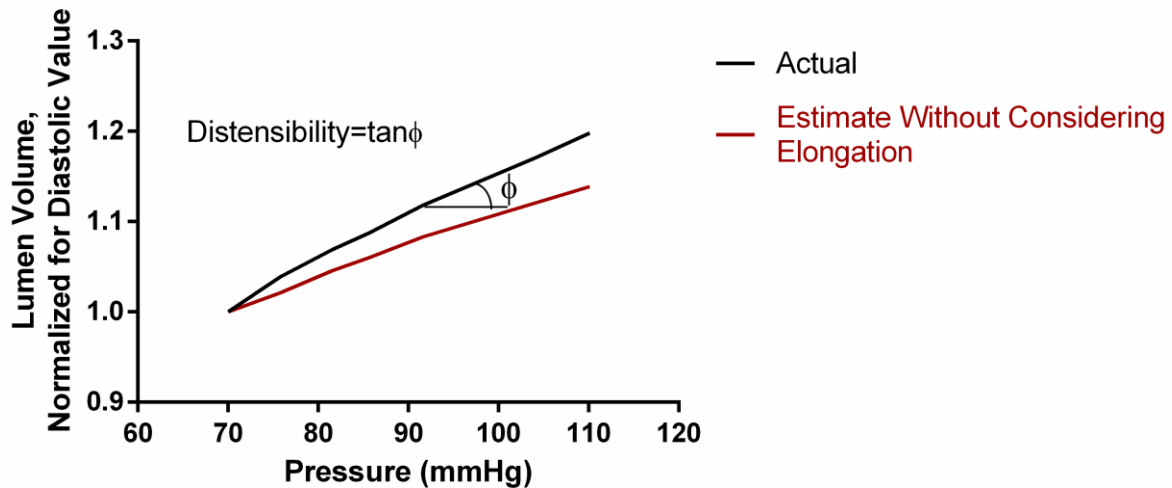


Figure 5.1:6 Generic model results for the lumen volumetric changes with increasing pressure. Comparison between the actual volumes (black line) against the estimates after neglecting (red line) the effect of elongation. The aortic distensibility is equal to the slope of the curve

Sensitivity Analysis. Table 5.1:1 summarizes the simulation results for the generic case as well as after varying two key model parameters, i.e. the wall compliance and the imposed aortic root motion. The table compares the distensibility values as calculated by the actual volume changes (reference) against the estimates after neglecting the longitudinal stretch. Three levels of compliance are examined, from highly compliant to stiff. The corresponding PWVs range from 4.8 m/s to 9 m/s. Note that the same level of aortic root displacement was imposed while varying the wall material properties. We observe that as the stiffness of the wall increases, the underestimation of wall elasticity rises, namely the error doubles from -30.2% in the compliant wall case to -61.9% in the stiff wall case. Furthermore, four levels of aortic root motion are presented. As expected, greater aortic root displacements -and thus elongation- lead to more pronounced underestimation, from -20.5% in the no motion scenario to -36.7% in the significant displacement scenario.

Table 5.1:1 Simulation results after varying key model parameters. The table includes the reference distensibility value along with the estimate without considering elongation. The respective errors are shown.

| | Reference Distensibility (10-3 mmHg-1) | Distensibility estimate without considering elongation (10-3 mmHg-1) | Error |
|--|--|--|---------|
| Generic Young Model (PWV=4.8 m/s and with aortic root displacement of 9.5mm) | 4.94 | 3.45 | -30.2 % |
| Parameter sensitivity | | | |
| Compliance | | | |
| Intermediate level (theoretical PWV=7 m/s) | 3.01 | 1.86 | -41.2% |

| | | | |
|-------------------------------|------|------|--------|
| Stiff (theoretical PWV=9 m/s) | 1.55 | 0.61 | -61.9% |
| Aortic root motion | | | |
| No displacement | 4.45 | 3.59 | -20.5% |
| Displacement of 5 mm | 4.66 | 3.54 | -24.1% |
| Displacement of 15 mm | 5.25 | 3.33 | -36.7% |

Part II. *In vivo* investigation

Table 5.1:2 summarizes the demographic characteristics of the participants as well as the measured aortic root longitudinal displacement. The displacement values were higher for the two young female subjects (15.6 mm and 11.4 mm) when compared to the value for the 38-year-old male subject (8.5 mm). This result is consistent with the literature, which has reported a statistically significant negative correlation between the longitudinal displacement of the aortic annulus and the age of a patient [10]. The table also includes the analysis results on the subjects' distensibility estimation. The estimation errors varied from -26% to -44%. Similarly to the *in silico* results, we observe a tendency for the error to increase with greater aortic root motion. On the other hand, the error is significantly smaller for the older male subject, who has a slightly stiffer aorta. Note that the calculated errors are of comparable magnitude for both the *in vivo* and the *in silico* analyses.

Table 5.1:2 Participant demographic characteristics, measured aortic root displacement and distensibility estimation.

| Subject | Gender | Age | Height (cm), Weight (kg) | Aortic root displacement (mm) | Reference Distensibility (10-3 mmHg-1) | Distensibility without considering elongation (10-3 mmHg-1) | |
|---------|--------|-----|-----------------------------|-------------------------------------|--|--|--------|
| | | | | | | | Error |
| 1 | M | 38 | 172/62 | 8.5 | 6.66 | 4.84 | -25.9% |
| 2 | F | 18 | 168/50 | 11.4 | 7.59 | 5.13 | -32.5% |
| 3 | F | 18 | 176/67 | 15.6 | 6.73 | 3.75 | -44.2% |

5.1.4 Discussion

This study aimed at questioning the established methodology for the estimation of aortic compliance or distensibility from cross-sectional radial deformations. In the past, a plethora of studies has used cross-sectional area measurements in order to provide insights into the effects of ageing [5], [9], training [9] and different pathologies [6]–[9] on the ascending aortic distensibility. A key argument in favor of neglecting the axial vessel stretch is based on the findings of Patel et al. [27]. In their study, Patel et al. [27] analyzed aortic pressure and radius in the living dog and found that the ratio of pressure changes to radius changes along the aorta correlated well with measures of impedance ($r=0.99$). However, it should be stressed that their published data pertains to the descending thoracic aorta, which is not subjected to as significant longitudinal strains when compared to the ascending aorta [28]. An approximation that is sufficient for the study of the elasticity of the descending aorta, does not necessarily apply to the ascending counterpart.

In fact, the presence of significant ascending aortic longitudinal strain has been noted in several previous observations [10], [11]. An *in vivo* study by Bell et al. [11] measured the longitudinal and circumferential strain of the proximal aorta in older adults of both genders and examined the correlation of these values with the measured central pulse wave velocities (which served as the reference for aortic wall elasticity). They found that the central PWV correlated poorly with uncorrected proximal aortic circumferential strain, whereas it was inversely related to longitudinal strain. Longitudinal strain was also associated to other risk factors for higher aortic stiffness such as untreated hypertension. Furthermore, an *ex vivo* study by Bergel [29] showed that longitudinal strain affects the shape and value of the aortic pressure-volume curve and suggested that the longitudinal deformation should be accounted for when measuring arterial compliance *in vivo*.

This work supplements and expands on previous studies by undertaking both a computational and an experimental investigation. Our model-derived results clearly point to a significant underestimation of the aortic wall distensibility when the elongation of the aortic centerline is neglected. Importantly, we observed that the underestimation is not systematically consistent; namely the errors ranged from -20% to -62% according to two key parameters. The first one was the elasticity of the aortic wall. We found that greater stiffness of the aortic wall leads to more pronounced underestimation of the distensibility. This has also been suggested in the past [11] and is likely linked to the smaller circumferential strains of older subjects. In other words, the stiffer the wall is circumferentially, the more its compliance will be affected by axial displacements. Moreover, as can be observed in the second parameter study, the effect of the aortic root displacement is non-negligible. For a higher longitudinal displacement of the aortic annulus, we showed that the errors increase substantially. This finding is rather intuitive: when the aortic root is subjected to a higher displacement due to the cardiac contraction, the aorta is more longitudinally stretched and thus is subjected to a smaller radial extension.

Our *in silico* results compared well with the *in vivo* acquired data. For all three subjects, the underestimation errors were in the anticipated order of magnitude, from 26% to 44%. Despite the small sample size, we were able to observe an interesting difference in the longitudinal aortic root displacement between the male and the female subjects, which is consistent with the literature. Similarly, we noted a higher underestimation of the aortic distensibility for the two female subjects. Bell et al. [11] also reported similar gender patterns, as they showed that longitudinally corrected circumferential strains were greater in women in comparison to men (the female average was 14.4% with a range of [13.6, 15.2]%, while the male average was 13.0% with a range of [12.4, 13.7]%, p -value = 0.01). This is due to the combined effect of a greater aortic root motion and shorter ascending aortas. We expect that the overestimation of aortic stiffness when neglecting the effect of longitudinal strain might therefore be greater in women than in men.

When examining the effect of ageing on the underestimation of local distensibility, one needs to consider two different compensatory mechanisms: older subjects have in general stiffer aortas (which should lead to higher underestimation errors) but also exhibit smaller axial displacements (which should lead to smaller underestimation errors). It is not evident, therefore, which of the two mechanisms dominates in a specific patient. In our future work, we plan to study a larger population in order to propose correction models to disentangle the two effects.

An important implication of our findings is that the longitudinal deformation of the proximal aorta might be a parameter of clinical interest. The inclusion of the aortic root longitudinal strain in risk stratification has also been evoked in the past. A recent study by Guala et al. [30] reported the predictive value of aortic root longitudinal strain for aortic dilation and aortic events in Marfan syndrome patients, while several other studies have demonstrated the potential for aortic longitudinal deformation in the assessment of risk of dissection [31], [32].

Considerations on the analysis: Actual distensibility vs distensibility without considering elongation

In our analysis, we investigated the effect of longitudinal strain by comparing two distensibility values: one obtained from the volumetric deformation of the aorta (reference) and one obtained via integration of the area compliance over an invariant centerline length. Naturally, a part of the comparison errors stems from the integration process itself. That is because the proximal aorta is not a perfectly conical cylinder and therefore the integration of the area compliances over the centerline length using the volume formula for a conical cylinder will involve numerical errors. To quantify these numerical errors, we also integrated the area compliances over a variable centerline length, thus accounting for the effect of elongation. Theoretically, the reference wall distensibility and the estimate after accounting for the elongation should perfectly agree. In all *in silico* and *in vivo* cases, the stiffness underestimation errors were improved by at least 50% after accounting for the elongation. Concretely, the errors due to the integration were non-negligible, but compared to the results obtained without considering elongation at all they were smaller and consistent. This suggests that, even if the reported differences between actual distensibility and estimation without considering elongation may be exaggerated due to numerical errors, they are certainly not an integration artefact.

Limitations of the mathematical model

There are two important points regarding our *in silico* analysis that should be highlighted. Firstly, we adopted a quasi-static approach and hence did not consider wave propagation phenomena. This constitutes a limitation of the study and was done primarily to avoid the expenses of a Fluid-Structure Interaction model. Secondly, the computational model was built from a combination of literature data and *in vivo* measurements on different individuals, thus reflecting only the generic properties of a healthy young aorta. Indeed, the aim of our study was not to build a precise, state-of-the-art patient-specific model of the aortic wall. Our approach was rather to develop a generic model that captures well the physiologic response of the aorta under distending pressure. Accordingly, particular

attention was paid to creating a robust hexahedral mesh and implementing physiologically relevant material behaviors and boundary conditions. The generic nature of the model entails certain limitations, particularly if we consider that the literature on the field provides us with rather scarce reference data. To account for that, we conducted a sensitivity analysis and quantified how variations in the model parameters affected our estimations. The results we obtained were physiological and followed the expected patterns.

The longitudinal displacement of the aortic root was manually tracked, which can be subject to observer-dependent errors. To account for the intra-observer variability, the root displacement was measured twice and the average value was used. Additionally, we implemented a high value of the dispersion parameter κ in accordance with previous literature [18]. For this level of dispersion of the collagen fibres, the material becomes practically isotropic, which might have an impact on the study results. An important parameter that was not examined here is the influence of the geometric configuration, since the entire analysis was performed based on one healthy young aortic geometry. It is known, however, that the aortic geometry differs significantly among individuals of different age, height, gender, etc. The aorta of older subjects is also more tortuous [33], which might affect its compliance. In the future, we plan to include this parameter and develop multiple models of different aortic configurations from young and old subjects of both genders.

In our future work we plan to use gated MR acquisitions, in order to ensure that the *in vivo* measured geometry corresponds indeed to the diastolic configuration; this assumption was made in the present study in order to restore the zero-pressure geometry. The zero-pressure geometry was computed based on the fixed-point optimization method proposed by Bols et al. [23], which is an iterative algorithm. Previous literature [34] suggests that iterative algorithms might lack accuracy and robustness when applied to complex material models, such as the HGO model. This was confirmed by our work, indeed after a few iterations the structure presented buckling at the level of the brachiocephalic bifurcation and the optimization had to be manually terminated. The use of a more sophisticated method to restore the zero-pressure geometry, such as the inverse elastostatics method of Peirlinck et al. [34], might be more appropriate for such a setup. This potential needs further investigation.

Due to the quasi-static nature of the model developed in the present study, the effect of the elongation of the proximal aorta on the regional aortic compliance as assessed via the pulse wave velocity could not be investigated. Aortic PWV is calculated as the time delay between two pressure or flow waveforms in different locations along the aorta. It is therefore expected that the elongation of the aortic root will alter the distance between the measuring locations and potentially affect the PWV. We plan to examine this hypothesis in our future work.

Limitations of the *in vivo* analysis

Although the *in vivo* analysis was conducted on a small number of subjects, the tendencies we observed matched closely what was expected from both the computational model and the literature. A similar analysis in a large cohort study might reveal gender- and age-related differences that cannot be elucidated in the context of the present work.

Furthermore, we need to acknowledge that the absolute values of distensibility presented here are not precise, given that the real aortic pulse pressure was not measured. Indeed, precise measurement of aortic pressure is invasive and practically impossible in the framework of a study on healthy subjects. However, our goal was not to provide the community with reference values of aortic distensibility, an important work that has been undertaken by several studies in the past. Instead, we used the reference pulse pressure values proposed from large cohort studies as representative of each subject's age and gender. This simplification does not affect the generality of our conclusions, given that pulse pressure is cancelled out during the calculation of the underestimation errors.

Conclusion and Future work

Both our computational and experimental findings point to the same direction. We suggest that neglecting the longitudinal strain during contraction might severely hinder the accurate assessment of the distensibility of the proximal aorta. In this context, the established methodology that examines ascending aortic area changes in the cross-sectional plane might lead to severe underestimation of local aortic compliance, particularly in the case of women or older subjects. Following these promising initial results, our future steps will be focused in i) the expansion of the *in silico* study to include multiple aortic geometries from subjects of different ages and gender, ii) the *in vivo* investigation of the correlation between volume compliance and cross-sectional area compliance in a larger cohort study.

5.1.5 Bibliography

- [1] C. V. Ioannou *et al.*, “Hemodynamics induced after acute reduction of proximal thoracic aorta compliance,” *Eur. J. Vasc. Endovasc. Surg.*, vol. 26, no. 2, pp. 195–204, Aug. 2003, doi: 10.1053/ejvs.2002.1917.
- [2] S. S. DeLoach and R. R. Townsend, “Vascular Stiffness: Its Measurement and Significance for Epidemiologic and Outcome Studies,” *Clin. J. Am. Soc. Nephrol.*, vol. 3, no. 1, pp. 184–192, Jan. 2008, doi: 10.2215/CJN.03340807.
- [3] C. Vlachopoulos, K. Aznaouridis, and C. Stefanadis, “Prediction of cardiovascular events and all-cause mortality with arterial stiffness: a systematic review and meta-analysis,” *J. Am. Coll. Cardiol.*, vol. 55, no. 13, pp. 1318–1327, Mar. 2010, doi: 10.1016/j.jacc.2009.10.061.
- [4] S. Vulli  moz, N. Stergiopoulos, and R. Meuli, “Estimation of local aortic elastic properties with MRI: Estimation of Local Aortic Elastic Properties,” *Magn. Reson. Med.*, vol. 47, no. 4, pp. 649–654, Apr. 2002, doi: 10.1002/mrm.10100.
- [5] D. A. Duprez, C. Swingen, R. Sih, T. Lefebvre, D. R. Kaiser, and M. Jerosch-Herold, “Heterogeneous remodelling of the ascending and descending aorta with age,” *J. Hum. Hypertens.*, vol. 21, no. 8, pp. 689–691, Aug. 2007, doi: 10.1038/sj.jhh.1002216.
- [6] Resnick Lawrence M., Militianu Daniela, Cunnings Amy J., Pipe James G., Evelhoch Jeffrey L., and Soulen Renate L., “Direct Magnetic Resonance Determination of Aortic Distensibility in Essential Hypertension,” *Hypertension*, vol. 30, no. 3, pp. 654–659, Sep. 1997, doi: 10.1161/01.HYP.30.3.654.
- [7] A. Lalande *et al.*, “Compliance and pulse wave velocity assessed by MRI detect early aortic impairment in young patients with mutation of the smooth muscle myosin heavy chain,” *J. Magn. Reson. Imaging JMRI*, vol. 28, no. 5, pp. 1180–1187, Nov. 2008, doi: 10.1002/jmri.21565.
- [8] S. Soljanlahti, T. Autti, L. Hyttinen, A. F. Vuorio, P. Keto, and K. Lauerma, “Compliance of the aorta in two diseases affecting vascular elasticity, familial hypercholesterolemia and diabetes: a MRI study,” *Vasc. Health Risk Manag.*, vol. 4, no. 5, pp. 1103–1109, Oct. 2008.
- [9] R. H. Mohiaddin *et al.*, “Regional aortic compliance studied by magnetic resonance imaging: the effects of age, training, and coronary artery disease,” *Heart*, vol. 62, no. 2, pp. 90–96, Aug. 1989, doi: 10.1136/hrt.62.2.90.
- [10] T. Plonek *et al.*, “The evaluation of the aortic annulus displacement during cardiac cycle using magnetic resonance imaging,” *BMC Cardiovasc. Disord.*, vol. 18, no. 1, p. 154, Jul. 2018, doi: 10.1186/s12872-018-0891-4.
- [11] V. Bell *et al.*, “Longitudinal and circumferential strain of the proximal aorta,” *J. Am. Heart Assoc.*, vol. 3, no. 6, p. e001536, Dec. 2014, doi: 10.1161/JAHA.114.001536.
- [12] P. Reymond, Y. Bohraus, F. Perren, F. Lazeyras, and N. Stergiopoulos, “Validation of a patient-specific one-dimensional model of the systemic arterial tree,” *Am. J. Physiol. Heart Circ. Physiol.*, vol. 301, no. 3, pp. H1173–1182, Sep. 2011, doi: 10.1152/ajpheart.00821.2010.
- [13] L. Antiga, M. Piccinelli, L. Botti, B. Ene-Iordache, A. Remuzzi, and D. A. Steinman, “An image-based modeling framework for patient-specific computational hemodynamics,” *Med. Biol. Eng. Comput.*, vol. 46, no. 11, pp. 1097–1112, Nov. 2008, doi: 10.1007/s11517-008-0420-1.
- [14] J. Bols *et al.*, “Unstructured hexahedral mesh generation of complex vascular trees using a multi-block grid-based approach,” *Comput. Methods Biomech. Biomed. Engin.*, vol. 19, no. 6, pp. 663–672, 2016, doi: 10.1080/10255842.2015.1058925.
- [15] J. D. Humphrey, J. F. Eberth, W. W. Dye, and R. L. Gleason, “Fundamental role of axial stress in compensatory adaptations by arteries,” *J. Biomech.*, vol. 42, no. 1, pp. 1–8, Jan. 2009, doi: 10.1016/j.jbiomech.2008.11.011.
- [16] G. A. Holzapfel, T. C. Gasser, and R. W. Ogden, “A New Constitutive Framework for Arterial Wall Mechanics and a Comparative Study of Material Models,” *J. Elast. Phys. Sci. Solids*, vol. 61, no. 1, pp. 1–48, 2000.
- [17] T. C. Gasser, R. W. Ogden, and G. A. Holzapfel, “Hyperelastic modelling of arterial layers with distributed collagen fibre orientations,” *J. R. Soc. Interface*, vol. 3, no. 6, pp. 15–35, Feb. 2006, doi: 10.1098/rsif.2005.0073.
- [18] D. Roy, G. A. Holzapfel, C. Kauffmann, and G. Soulez, “Finite element analysis of abdominal aortic aneurysms: geometrical and structural reconstruction with application of an anisotropic material model,” *IMA J. Appl. Math.*, vol. 79, no. 5, pp. 1011–1026, Oct. 2014, doi: 10.1093/imamat/hxu037.
- [19] H.   strand, “Regulation of aortic wall mechanics and stress : An experimental study in man,” 2008, Accessed: Jan. 28, 2019. [Online]. Available: <http://urn.kb.se/resolve?urn=urn:nbn:se:liu:diva-11556>.
- [20] S. Roccabianca, C. A. Figueroa, G. Tellides, and J. D. Humphrey, “Quantification of regional differences in aortic stiffness in the aging human,” *J. Mech. Behav. Biomed. Mater.*, vol. 29, pp. 618–634, Jan. 2014, doi: 10.1016/j.jmbbm.2013.01.026.
- [21] S. Pasta *et al.*, “Constitutive modeling of ascending thoracic aortic aneurysms using microstructural parameters,” *Med. Eng. Phys.*, vol. 38, no. 2, pp. 121–130, Feb. 2016, doi: 10.1016/j.medengphy.2015.11.001.

- [22] U. Huh, C.-W. Lee, J.-H. You, C.-H. Song, C.-S. Lee, and D.-M. Ryu, "Determination of the Material Parameters in the Holzapfel-Gasser-Ogden Constitutive Model for Simulation of Age-Dependent Material Nonlinear Behavior for Aortic Wall Tissue under Uniaxial Tension," *Appl. Sci.*, vol. 9, no. 14, p. 2851, Jan. 2019, doi: 10.3390/app9142851.
- [23] J. Bols, J. Degroote, B. Trachet, B. Verhegghe, P. Segers, and J. Vierendeels, "A computational method to assess the in vivo stresses and unloaded configuration of patient-specific blood vessels," *J. Comput. Appl. Math.*, vol. 246, pp. 10–17, Jul. 2013, doi: 10.1016/j.cam.2012.10.034.
- [24] P. Moireau *et al.*, "External tissue support and fluid-structure simulation in blood flows," *Biomech. Model. Mechanobiol.*, vol. 11, no. 1–2, pp. 1–18, Jan. 2012, doi: 10.1007/s10237-011-0289-z.
- [25] J. Ahrens, B. Geveci, and C. Law, "ParaView : An End-User Tool for Large Data Visualization," *Energy*, vol. 836, pp. 717–732, 2005.
- [26] R. Kikinis, S. D. Pieper, and K. G. Vosburgh, "3D Slicer: A Platform for Subject-Specific Image Analysis, Visualization, and Clinical Support," in *Intraoperative Imaging and Image-Guided Therapy*, F. A. Jolesz, Ed. New York, NY: Springer, 2014, pp. 277–289.
- [27] D. J. Patel, F. M. De Freitas, J. C. Greenfield, and D. L. Fry, "Relationship of radius to pressure along the aorta in living dogs," *J. Appl. Physiol.*, vol. 18, no. 6, pp. 1111–1117, Nov. 1963, doi: 10.1152/jappl.1963.18.6.1111.
- [28] T. M. Morrison, G. Choi, C. K. Zarins, and C. A. Taylor, "Circumferential and Longitudinal Cyclic Strain of The Human Thoracic Aorta: Age-Related Changes," *J. Vasc. Surg. Off. Publ. Soc. Vasc. Surg. Int. Soc. Cardiovasc. Surg. North Am. Chapter*, vol. 49, no. 4, pp. 1029–1036, Apr. 2009, doi: 10.1016/j.jvs.2008.11.056.
- [29] D. H. Bergel, "The static elastic properties of the arterial wall," *J. Physiol.*, vol. 156, no. 3, pp. 445–457, May 1961, doi: 10.1113/jphysiol.1961.sp006686.
- [30] A. Guala *et al.*, "Proximal aorta longitudinal strain predicts aortic root dilation rate and aortic events in Marfan syndrome," *Eur. Heart J.*, vol. 40, no. 25, pp. 2047–2055, Jul. 2019, doi: 10.1093/eurheartj/ehz191.
- [31] C. J. Beller, M. R. Labrosse, M. J. Thubrikar, and F. Robicsek, "Role of aortic root motion in the pathogenesis of aortic dissection," *Circulation*, vol. 109, no. 6, pp. 763–769, Feb. 2004, doi: 10.1161/01.CIR.0000112569.27151.F7.
- [32] S. D. Singh, X. Y. Xu, J. R. Pepper, C. Izgi, T. Treasure, and R. H. Mohiaddin, "Effects of aortic root motion on wall stress in the Marfan aorta before and after personalised aortic root support (PEARS) surgery," *J. Biomech.*, vol. 49, no. 10, pp. 2076–2084, 05 2016, doi: 10.1016/j.jbiomech.2016.05.011.
- [33] A. Redheuil *et al.*, "Age-Related Changes in Aortic Arch Geometry: Relationship with Proximal Aortic Function and Left Ventricular Mass and Remodeling," *J. Am. Coll. Cardiol.*, vol. 58, no. 12, pp. 1262–1270, Sep. 2011, doi: 10.1016/j.jacc.2011.06.012.
- [34] M. Peirlinck, M. De Beule, P. Segers, and N. Rebelo, "A modular inverse elastostatics approach to resolve the pressure-induced stress state for in vivo imaging based cardiovascular modeling," *J. Mech. Behav. Biomed. Mater.*, vol. 85, pp. 124–133, Sep. 2018, doi: 10.1016/j.jmbbm.2018.05.032.

5.2 Assessing regional aortic Pulse Wave Velocity with compressed-sensing accelerated 4D flow MRI: an *in vivo* comparison with 2D phase contrast MRI

Stamatia Pagoulatou ¹, Dionysios Adamopoulos ², Yanan Niu ¹, Nikolaos Stergiopoulos ¹, Vasiliki Bikia ¹, Georgios Rovas ¹, Ning Jin ⁴, Christoph Forman ⁴, Daniel Giese ⁴, Jean-Paul Vallée ³, Lindsey A Crowe ³

¹ Laboratory of Hemodynamics and Cardiovascular Technology (LHTC), Institute of Bioengineering, Ecole Polytechnique Fédérale de Lausanne (EPFL), Lausanne, Switzerland

² Cardiology Department, Geneva University Hospitals (HUG), Geneva, Switzerland

³ Department of Radiology and Medical Informatics, Geneva University Hospitals (HUG), Geneva, Switzerland

⁴ Siemens Healthineers, USA (NJ) Erlangen Germany (CF, DG)

Abstract

Accurate measurement of the aortic pulse wave velocity (PWV) is of clinical importance. The use of a novel compressed sensing (CS) accelerated 4D Flow MRI sequence might be relevant for the prompt estimation of aortic PWV. The aim of this work is to compare *in vivo* aortic PWV measurements acquired via a novel CS-4D sequence against the clinical standard of 2D phase contrast (PC) MRI. We acquired high temporal resolution 2D PC as well as CS-4D Flow (acceleration factor 7.7) MR data on 21 apparently healthy volunteers. Regional aortic PWV was computed at the aortic arch and the descending aorta. For the calculation of the transit time (PTT), four algorithms were compared: first derivative (FD), tangential (TANGENT), cross-correlation (XCORR) and Fourier (FFT). The capability of CS-4D acquisitions to predict an increase in the proximal aortic PWV with age was investigated. Among the four PTT methods, the FFT was the best performing: it yielded good correlation and agreement for both the aortic arch ($r=0.88$, $\bar{d}\pm SD=-0.24\pm 0.73\text{m/s}$) and descending aortic ($r=0.90$, $\bar{d}\pm SD=-0.27\pm 0.93\text{m/s}$) PWV. The FD method yielded the highest discrepancies between 2D and CS-4D PWV estimates. CS-4D MRI was capable of predicting the expected increase in the aortic stiffness with age, FFT proximal aortic PWV was $3.3\pm 0.8\text{m/s}$ and $5.9\pm 1.9\text{m/s}$ for volunteers under and over 40 years old, respectively. The novel CS-4D Flow MRI sequence with acceleration factor 7.7 can offer a reliable estimate of the regional aortic PWV in under 5 minutes. The most robust PTT algorithm was the FFT.

Key words: 4D Flow MRI • Pulse transit time • Proximal stiffness • Ageing

Manuscript submitted for publication

5.2.1 Introduction

Central arterial stiffness is a major determinant of cardiac afterload [1]. Aortic stiffness has been shown to increase with physiological ageing [2] and is recognized as a key factor contributing to cardiovascular disease, including systolic hypertension [3] and coronary artery disease [4]. Aortic stiffness is commonly assessed via measurement of the aortic pulse wave velocity (PWV), i.e. the velocity with which the pulse wave propagates along the aorta [5]. Accordingly, there is increasing interest in developing and improving techniques to noninvasively evaluate aortic PWV in the clinic.

Aortic PWV measurement requires computation of the time delay, also called the pulse transit time (PTT), between two blood pressure or flow waveforms in different locations inside the aorta. This is usually achieved via the noninvasive measurement of blood flow with Magnetic Resonance Imaging (MRI) [6]. Among the several MRI-based techniques that have been proposed to image blood flow, most studies calculate aortic PWV using two-dimensional (2D) phase contrast (PC) acquisitions with through-plane velocity encoding [7], [8]. 2D PC acquisitions can achieve particularly high temporal and spatial resolution, which is vital for the correct identification of the PTT [9] but have limitations in terms of time-consuming operator-dependent slice positioning and when flow patterns are complex or turbulent.

Alternatively to traditional 2D PC MRI, investigators are currently exploring the possibility of estimating PWV via time-resolved 3D PC MRI, also called 4D Flow MRI [10], [11]. For 4D Flow MRI, images encoded to quantify blood velocity in the three spatial directions as well as an isotropic resolution morphological image allow for the volumetric, functional coverage of the entire aorta and the calculation of any arbitrary direction of flow. Recently, a novel free-breathing 4D Flow technique using compressed sensing (CS) acceleration was proposed [11]–[13]. CS is a framework that allows for the acquisition of only the important coefficients of a signal and the reconstruction of data from an incompletely filled k-space [11]–[13]. Successful application of CS requires that the signal should have a sparse representation in a transform domain, and artifacts caused by the undersampling be incoherent. CS offers an important advantage in speed: compared to previous 4D techniques that last 15–20 minutes, in the CS-4D sequence, the imaging of the thoracic aortic flow is performed with inline image reconstruction on the MRI scanner in under 5 minutes [13]. This technique shows, therefore, promising potential for a fast estimate of aortic PWV. Nevertheless, its reliability has not been demonstrated yet.

Accordingly, the purpose of this work was to evaluate the feasibility of extracting reliable regional aortic PWV values from CS-4D MRI measurements. This was achieved by comparing *in vivo* CS-4D-derived PWV estimates to high temporal resolution 2D PC MRI, which served as reference. Regional aortic PWV was computed and compared at two aortic regions, i.e., the aortic arch and the descending aorta, based on measurements performed on apparently healthy adults. For the calculation of PTT, four previously published algorithms were tested and the agreement between the CS-4D and 2D PWV was examined for each PTT algorithm. The PTT algorithm that yielded the highest agreement between the CS-4D- and 2D-derived PWV was determined. Finally, the capability of the CS-4D MR acquisitions to predict an increase in the proximal aortic PWV with age was investigated.

5.2.2 Methods

Study population

In this prospective study, 21 volunteers without overt cardiovascular disease were enrolled to undergo cardiac MRI. Approval of the local ethical committee was obtained (*CER-VD 2017-00954*) and all study participants provided informed consent. Prior to inclusion in the study, each subject passed a screening examination that comprised a cardiopulmonary physical examination and medical history assessment, 12-lead electrocardiogram at rest, Doppler Ultrasound and echocardiography. During this stage, the absence of atherosclerotic plaques from both the carotid and femoral arteries was verified via the use of Doppler Ultrasound. Subjects with significant heart arrhythmias as assessed by the baseline 12-lead electrocardiogram at rest or significant heart disease, i.e. significant valvular, pericardial disease or ventricular systolic myocardial dysfunction as assessed by echocardiography, were excluded. Additional exclusion criteria were obesity (BMI > 30 kg/m²), smoking and non-eligibility to undergo MRI.

Data acquisition

Cardiac MR images were acquired on a 3T clinical MRI scanner (MAGNETOM Skyra or MAGNETOM PRISMA Fit, Siemens AG, Healthcare Sector, Erlangen, Germany) using the integrated spine coils and body surface coil elements. No contrast agent was used. First, non-contrast MR angiography acquisitions were performed in order to image the aortic geometry. Oblique sagittal images of the aorta were acquired with 3D gradient echo sequences. Typical scan parameters were: echo spacing 3.3 ms, segmented acquisition (32 segments per RR) leading to an acquisition window in diastole of ~104 ms, TE 1.33 ms, flip angle 12°, resolution 0.625 mm x 0.625

mm x 2mm (40 ± 4 slices), generalized autocalibrating partially parallel acquisitions (GRAPPA) acceleration factor 2). Respiratory navigation with around 60% acceptance window (average $58\% \pm 11\%$, range: 35%– 78%) was used to reduce respiratory motion artifacts. The acquisition time was on average 4min 2s ± 56 s (range: 2min 58s – 6min 34s).

Subsequently, a free-breathing 2D gradient echo velocity-encoded PC MR sequence with prospective ECG-gating was applied at four aortic sites for flow quantification. The scanning planes, hereafter called 2D planes, were placed perpendicular to the main flow direction at i) the ascending aorta at the level of the pulmonary artery, ii) the descending aorta at the same level as the ascending counterpart, iii) the descending aorta at the level of the diaphragm, and iv) the abdominal aorta at the level of the renal arteries (Figure 5.2:1). Typical scan parameters for all four planes were: Venc 150 cm/s, TR 27.84 ms, TE 2.47 ms, flip angle 20° , resolution 6 mm x 2 mm x 2 mm, 128 interpolated time frames (average of 4 signals) with temporal resolution of 7 ± 1 ms (range: 5 – 10 ms). Heart rate during these four acquisitions was 64 ± 12 bpm. The overall scan time for the four slices was 4min 39s ± 1 min 40s (range: 2min 54s – 8min 55s).

Finally, for all patients, CS accelerated 4D PC MRI was performed using a Siemens protocol sequence (Siemens WIP 1106) for flow quantification. The acquisition covered the same superior-to-inferior distance as the four 2D planes described above: the sagittal-oblique volume included the entire thoracic aorta extending down to the abdominal aorta at the infra renal level. The net acceleration factor was $R=7.7$. Acquisition parameters were: Venc 150 cm/s, TR 25.04 ms, TE 1.94 ms, flip angle 8° , resolution 2.5 mm x 2.25 mm x 2.25 mm, time frames 31 ± 5 (range: 22 – 43), temporal resolution 30 ± 2 ms (range: 27 – 32 ms). The heart rate during this acquisition was 65 ± 10 bpm (range: 50-90 bpm) and not statistically different than the heart rate during the 2D acquisitions ($p=0.66$). Scan time was on average 5m21s ± 1 m14s (range: 3m21s – 7m43s) with a reconstruction time of under 5 minutes, during which scanning can be continued; of note, however, this sequence was commonly run at the end of the examination. For the reconstruction, the mFISTA algorithm was used with 30 iterations. Figure 5.2:1 contains a schematic description of the 2D PC acquisition strategy as well as a snapshot of the CS-4D data processing. Examples of the acquired flow signals are shown in Figure 5.2:2.

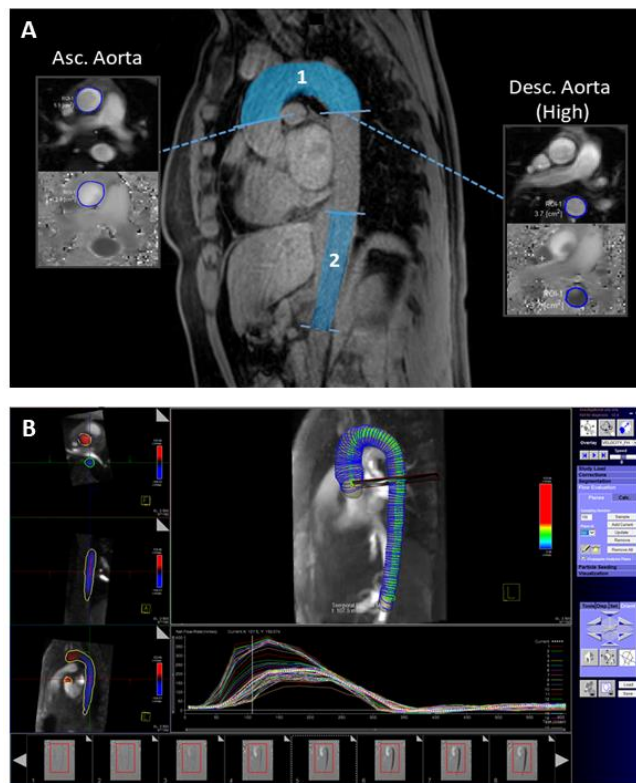


Figure 5.2:1 (A) 2D PC MRI data acquisition strategy. The two aortic regions, i.e. the aortic arch (1) and the descending aorta (2), are highlighted with blue. The corresponding 2D imaging planes are shown. The PC data for the ascending aorta and the descending aorta at the level of the pulmonary artery as processed with the software Segment (Medviso) are depicted. (B) Processing of the CS-4D MRI data using 4D Flow Demonstrator (Free-type Project, Siemens Healthineers, Erlangen, Germany)

Data analysis

The 2D MRI flow data were processed with an open source software (Segment, Medviso) [14]. The regions of interest (ROIs) were interactively drawn within the vessel lumen to measure the flow waveform. It should be noted that for each patient, blood flow at the four 2D planes was not imaged simultaneously, therefore, there was a minor variation in the time period of the measured signals (average variation of ± 2 bpm, maximum variation of ± 5 bpm, $p = \text{NS}$). To account for this, the diastolic part of the 2D-derived flow curves of each volunteer was truncated so that all signals had the same time period. The truncated flow curves were, subsequently, upsampled to a time step of 1 ms using spline interpolation.

The processed 2D flow curves were used to calculate the regional PWV at two aortic segments (Figure 5.2:1, shaded areas). The first region that was examined was the aortic arch, defined as the segment between the 2D planes at the level of the pulmonary artery. Accordingly, the aortic flow measurements at the level of the diaphragm and at the renal arteries were used to define a distal aortic segment, hereafter called descending aorta.

The calculation of PWV for these two aortic regions required the derivation of two quantities: the time delay between the flow signals, i.e., the PTT, and the distance between the respective measuring planes. We detail on the algorithms to derive the PTT in the next section. With respect to the distance between the 2D planes, we performed manual tracking of the aortic centerline on the 3D aortic images obtained with 3D gradient echo sequences. More specifically, to compute the centerline of the two aortic segments, we placed a series of points in the approximate center of the vessel along the aortic axis (approximately one point was placed every 5 mm of centerline length). The centerline was then calculated by creating a spline interpolation of the center points placed. The intersection of the centerline with each individual 2D plane was used to define the final distance.

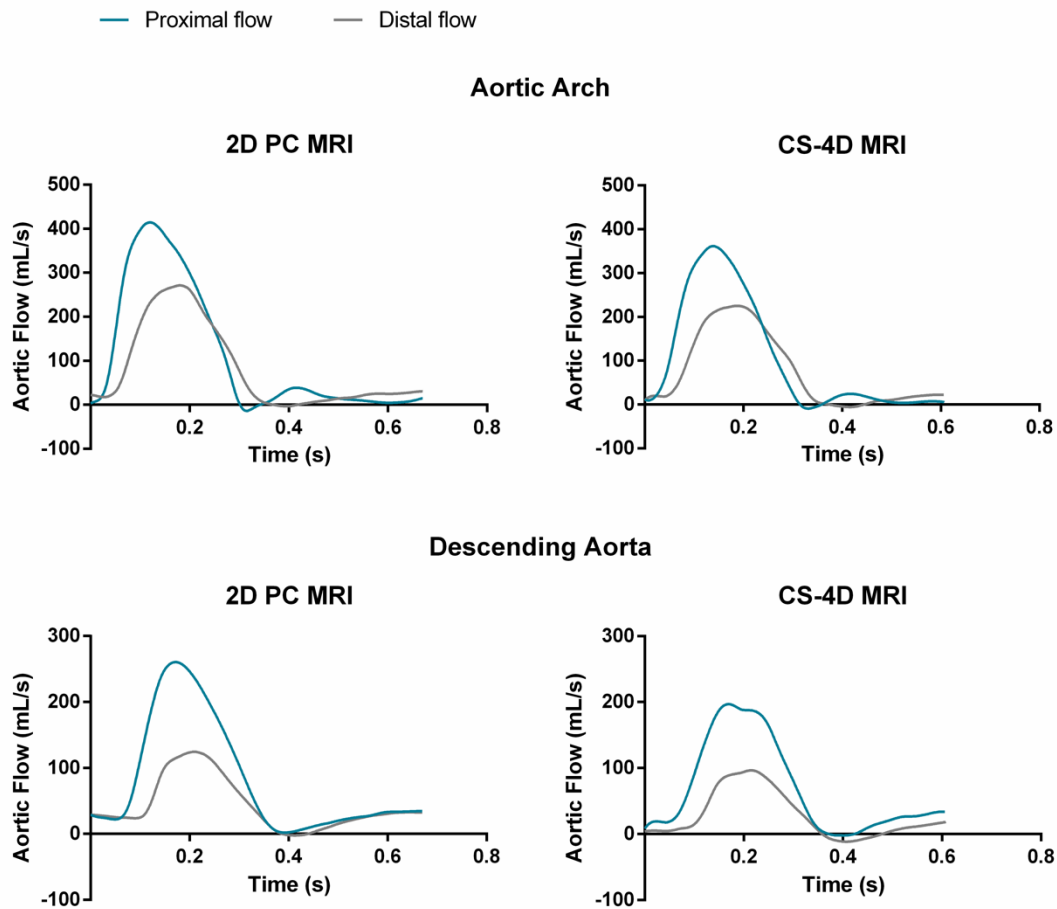


Figure 5.2:2 Examples of flow signals acquired with 2D MRI (left) and the corresponding CS-4D flows (right) for one young volunteer.

The CS-4D data were analyzed using the software 4D Flow Demonstrator (Free-type Project, Siemens Healthineers, Erlangen, Germany) [15]. The software allows for the automatic correction of eddy currents and phase wrapping, as previously described [15]. The CS-4D modulus and velocity images were combined to compute the 3D angiogram through averaging over the time phases around the systolic peak. The centerline of the segmented aortic angiogram was automatically computed by the same software [15]. Approximately 100 equally-spaced points were selected along the centerline between the aortic root and the distal abdominal aorta. Average distance between consecutive centerline points was 3 mm. The flow of the 100 respective cross-sections (hereafter called CS-4D planes) was automatically computed (4D Flow Demonstrator, Siemens Healthineers, Erlangen, Germany) and each flow curve was upsampled to a time step of 1ms via spline interpolation.

Subsequently, we developed a custom Matlab code, which among the 100 selected CS-4D planes identified the ones that matched the coordinates of the four 2D planes. This was achieved by first identifying the 2D planes on the 3D gradient echo angiogram and extracting the corresponding centerline coordinates. Subsequently, the 2D center point coordinates were extrapolated onto the CS-4D volume after calculating the corresponding transformation matrix. The center point of all CS-4D planes was automatically computed (4D Flow Demonstrator, Siemens Healthineers, Erlangen, Germany) and was compared to the extrapolated 2D center points. All CS-4D data were then discarded, except for the data of the four matched CS-4D planes. The flow curves of these four CS-4D planes were used for the estimation of the respective CS-4D PWV at the two aortic regions, i.e. the aortic arch and descending aorta, according to the PTT algorithms presented below. The corresponding distances for the two aortic regions were automatically derived.

Pulse transit time calculation

For both 2D and CS-4D flow signals, the PTT was calculated using four previously proposed algorithms. Concretely, we tested the first derivative (FD), tangential (TANGENT), cross-correlation (XCORR) [16], and Fourier (FFT) [17] algorithms. Technical details regarding these algorithms are provided in the following paragraphs as well as in Figure 5.2:3.

PTT algorithms using a characteristic point (FD and TANGENT). The first two techniques compute the PTT after identifying a characteristic point on the flow waveforms. For the FD algorithm, the PTT is calculated using the timing of the maximal slope points on the two flow waves (Figure 5.2:3a). Here, the first derivative of each flow wave was computed by a five-point central difference scheme in a region extending from the flow minimum to the peak value (Figure 5.2:3a). For the TANGENT algorithm, the calculation of PTT uses as characteristic point the intersection of two tangents on the flow waveform. The first tangent passes from the maximal first derivative point, calculated as explained above. The second tangent passes from the minimum point and is parallel to the time axis (Figure 5.2:3a).

Cross-correlation PTT. For the XCORR algorithm published by Fielden et al. [16], the flow signals are first normalized. The normalized distal flow signal is then shifted in time relatively to the normalized proximal signal. This produces a correlation plot, as shown in Figure 5.2:3b. The PTT is calculated as the time shift that maximizes the correlation between the two signals, i.e. the maximum of the correlation plot. For this analysis, we considered only the systolic upstroke of the flow waveform rather than the entire heart cycle, as previously proposed [18].

Fourier PTT. The FFT algorithm, proposed by Meloni et al. [17], operates in the frequency domain. It defines the transfer function, H , that receives as input the Fourier transformed proximal flow waveform, $X(f)$, and produces the Fourier transformed distal flow wave, $Y(f)$, i.e., $H(f) = Y(f)/X(f)$. The group delay (GD) of the filter represents the average time delay across individual frequency bands of the input. The PTT is set equal to the group delay weighted by the harmonics of the input signal (Figure 5.2:3c). For this frequency domain-based PTT algorithm, normalized flow waves were used and the systolic upslope rather than the entire time interval was considered [18].

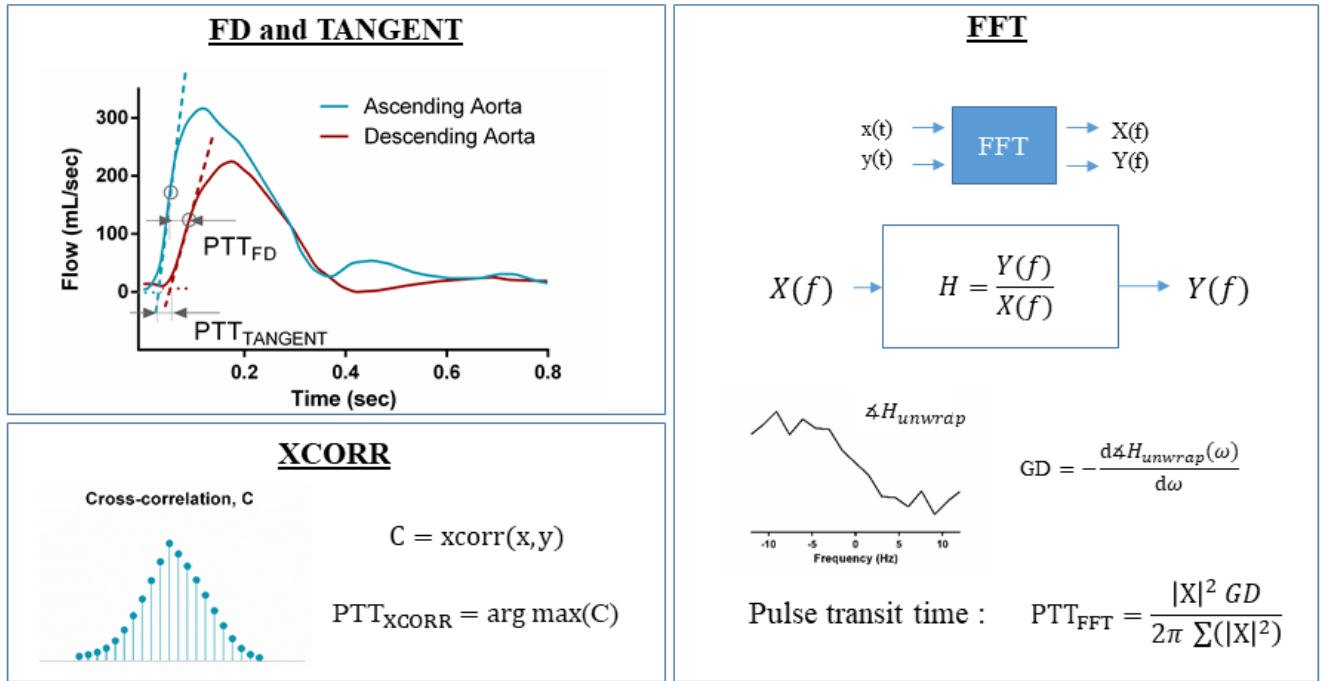


Figure 5.2:3 Schematic representation of the four previously proposed algorithms to calculate PTT. (a) PTT algorithms that use a characteristic time point, i.e. the first derivative (FD) and tangential (TANGENT) algorithms. (b) The cross-correlation (XCORR) algorithm. (c) The Fourier (FFT) algorithm.

Intra- and inter-observer reproducibility

One important source of variability in our calculations could be the extraction of the flow signal from the 2D PC MR data, given that the regions of interest are user-defined in the processing software (Segment, Medviso). To account for the intra- and inter-observer variability, a subset of 8 subjects was randomly selected three months after initial analysis. Their 2D PC MR data were processed anew by the same observer as well as a second experienced software user, and the PWV analysis was repeated.

Additionally, we examined the reproducibility of the length measurements. Concretely, we investigated differences in the 2D plane distance estimated by manually tracking the aortic centerline on the 3D gradient echo angiogram, and the distance between the corresponding CS-4D planes, which was automatically derived by the 4D Flow Demonstrator software [15].

Statistical analysis

Continuous variables are presented as mean \pm standard deviation (SD) and categorical parameters as percentage. Correlation between the 2D and CS-4D PWV values was evaluated using Pearson's correlation coefficient (r). Bland-Altman analyses were performed in order to compare the estimated aortic arch and descending aortic PWV values for the two MRI methods and for each PTT algorithm. The bias (\bar{d}), the SD of differences, and the limits of agreements (LA), defined as the mean bias \pm 2 SD of differences, were reported for all Bland-Altman analyses. Differences between the 2D and CS-4D PWV estimates for each PTT algorithm were also examined using paired t-test. A result was reported as significant if $p < 0.05$. Intra- and inter-observer variability was assessed on a subset of 8 volunteers using the intraclass correlation coefficient (ICC) as well as Bland-Altman analysis. Statistical analyses were performed in Matlab (Mathworks, Natick, Massachusetts, USA).

5.2.3 Results

All 21 volunteers were included in the study, their demographic and clinical characteristics are presented in Table 5.2:1. The subjects' ages ranged from 22 to 57 years with an average of 32 ± 11 years. There was an equal distribution between males and females (10/11).

Table 5.2:1 Demographic and clinical characteristics of study volunteers.

| | <i>n</i> = 21 |
|------------------------|---------------|
| Age, years | 32 ± 11 |
| Males/Females | 10/11 |
| BMI, kg/m ² | 22.0 ± 2.6 |
| BSA, m ² | 1.78 ± 0.19 |
| Heart rate, bpm | 62 ± 11 |
| Cardiac output, L/min | 5.1 ± 1.2 |
| brachial SBP, mmHg | 117 ± 9 |
| brachial DBP, mmHg | 68 ± 6 |
| brachial MAP, mmHg | 85 ± 6 |
| brachial PP, mmHg | 50 ± 8 |

BMI: body mass index, BSA: body surface area, HR: heart rate, SBP: systolic blood pressure, DBP: diastolic blood pressure, MAP: mean arterial pressure, PP: pulse pressure. Mean values ± SD are presented.

Figure 5.2:4 contains box plots of the PWV estimates for the 2D and CS-4D MR techniques. The results are presented for the two aortic regions, i.e. the aortic arch and descending aorta, as calculated using the four PTT algorithms. Overall, the first derivative algorithm showed the highest degree of variability for the CS-4D PWV estimation (Figure 5.2:4). The remaining PTT algorithms resulted in PWV estimates of similar magnitude and variability for the 2D and CS-4D data.

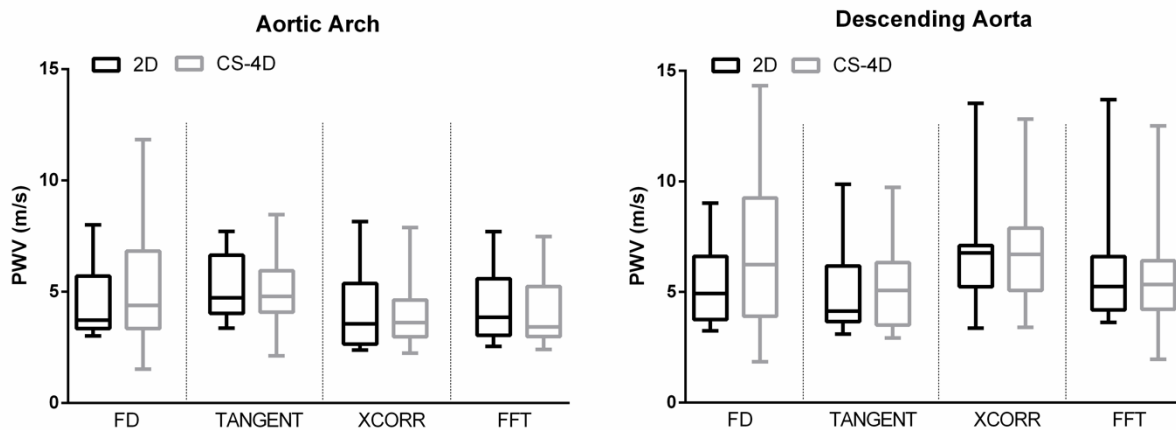


Figure 5.2:4 Box plots of the 2D and CS-4D PWV calculated at the aortic arch (left) and descending aorta (right), using four previously proposed algorithms: FD: first derivative algorithm, TANGENT: tangential algorithm, XCORR: cross-correlation algorithm, FFT: Fourier algorithm. Note the high variability in the PWV estimates when the FD algorithm was used.

Correlation coefficients and results of agreement assessed via Bland-Altman analysis are summarized in Table 5.2:2 for each PTT algorithm. There was significant correlation ($p < 0.001$) between the 2D and CS-4D PWV estimates for all PTT methods, but the FD algorithm ($r = 0.41$ for the aortic arch PWV and $r = 0.27$ for the descending aortic PWV). FD had the poorest performance overall, with the highest bias and widest limits of agreement for both aortic segments ($\bar{d} = 0.58$ m/s with SD of differences 2.51 m/s for the aortic arch PWV and $\bar{d} = 1.51$ m/s with SD of differences 3.25 m/s for the descending aortic PWV). Particularly when applied to the

descending aorta, it resulted in a statistically significant difference between the 2D and CS-4D PWV predictions ($p=0.045$) (Table 5.2:2). Therefore, FD was deemed inappropriate for the extraction of the CS-4D PWV and was excluded from the subsequent analysis.

Among the three remaining PTT algorithms (i.e., TANGENT, XCORR, FFT), the FFT was the best performing. It yielded the highest correlation coefficients ($r=0.88$ for the aortic arch PWV and $r=0.90$ for the descending aortic PWV), had low bias ($\bar{d}=-0.24$ m/s for the aortic arch and $\bar{d}=-0.27$ m/s for the descending aorta) and the narrowest limits of agreement (SD of differences 0.73 m/s for the aortic arch PWV and 0.93 m/s for the descending aortic PWV) (Table 5.2:2). There was no tendency for the estimation error to increase for higher PWV values. Of note, the accuracy of the FFT PWV predictions was consistent for both aortic regions. This did not hold true for the TANGENT and XCORR algorithms: when the latter algorithms were applied to the descending aorta, there was a tendency for higher discrepancies between the 2D and CS-4D PWV estimates. This is evidenced by the poorer correlation, higher bias values and the wider limits of agreement (for TANGENT, $\bar{d}=-0.24$ m/s with SD=1.21 m/s for the ascending aortic PWV versus $\bar{d}=0.39$ m/s with SD=1.42 m/s for the descending aortic PWV, and for XCORR, $\bar{d}=-0.21$ m/s with SD=0.97 m/s versus $\bar{d}=0.25$ m/s with SD=1.53 m/s, respectively) (Table 5.2:2). Scatterplots and Bland-Altman plots for the predictions of the best performing technique, i.e., the FFT algorithm, are provided in Figure 5.2:5.

Table 5.2:2 Indices of correlation, accuracy and agreement between the 2D and CS-4D measurements of PWV as evaluated via four PTT algorithms. The results for both the aortic arch and the descending aorta are provided.

| | Algorithm | 2D | CS-4D | Correlation | R2 | Bias (m/s) | SD of | SEM | 95% CI (m/s) | 2D vs. |
|------------------|-----------|------------------------|------------------------|-------------|------|---------------|----------------------|-------|---------------|------------------|
| | | Mean \pm SD (m/s) | Mean \pm SD (m/s) | | | | differences (m/s) | (m/s) | | CS-4D p-value |
| Aortic Arch | FD | 4.55 \pm 1.52 | 5.14 \pm 2.72 | 0.41 | 0.17 | 0.59 | 2.51 | 0.55 | [-0.56, 1.73] | NS |
| | TANGENT | 5.27 \pm 1.48 | 5.03 \pm 1.58 | 0.69 *** | 0.47 | -0.24 | 1.21 | 0.26 | [-0.79, 0.31] | NS |
| | XCORR | 4.18 \pm 1.73 | 3.97 \pm 1.37 | 0.83 *** | 0.68 | -0.21 | 0.97 | 0.21 | [-0.65, 0.23] | NS |
| | FFT | 4.30 \pm 1.54 | 4.06 \pm 1.50 | 0.88 *** | 0.78 | -0.24 | 0.73 | 0.16 | [-0.58, 0.09] | NS |
| Descending Aorta | FD | 5.23 \pm 1.68 | 6.74 \pm 3.26 | 0.27 | 0.07 | 1.51 | 3.25 | 0.71 | [0.04, 2.99] | 0.045 |
| | TANGENT | 4.88 \pm 1.64 | 5.27 \pm 1.83 | 0.67 *** | 0.45 | 0.39 | 1.42 | 0.31 | [-0.25, 1.04] | NS |
| | XCORR | 6.48 \pm 2.16 | 6.72 \pm 2.12 | 0.74 *** | 0.55 | 0.24 | 1.53 | 0.33 | [-0.45, 0.94] | NS |
| | FFT | 5.77 \pm 2.25 | 5.50 \pm 2.23 | 0.90 *** | 0.83 | -0.27 | 0.93 | 0.20 | [-0.69, 0.16] | NS |

SD: standard deviation, SEM: standard error of mean, CI: confidence interval

FD: first derivative method, TANGENT: tangential method, XCORR: cross-correlation method, FFT: Fourier method.

*** denotes correlation of p -value<0.001 as assessed via paired t-test

NS: not significant

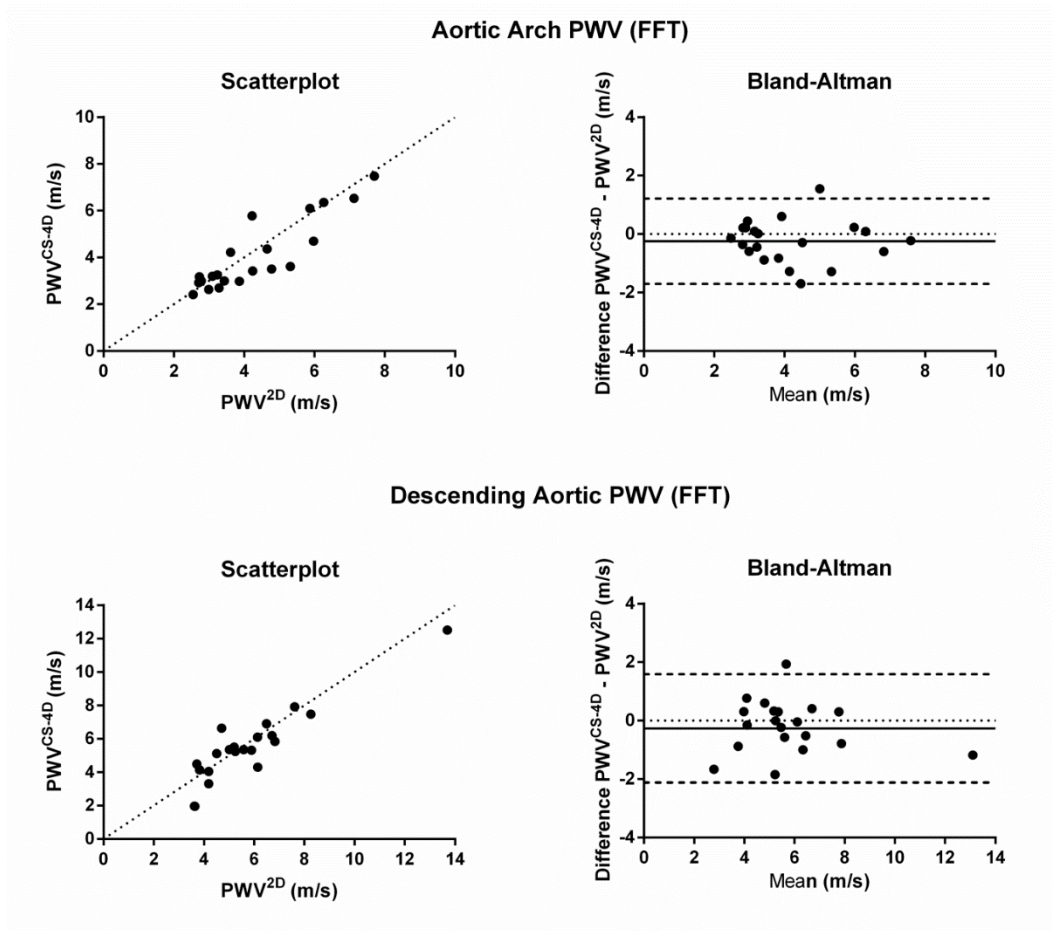


Figure 5.2:5 Scatterplots and Bland-Altman plots of the PWV estimated from the 2D and the CS-4D data using the FFT algorithm. The top panel corresponds to the aortic arch PWV and the lower panel to the descending aortic PWV.

Intra- and inter-observer reproducibility

The results of the intra- and inter-observer reproducibility analysis for the 2D flow extraction are summarized in Table 5.2:3. The FD method was the most susceptible to variability, suggesting that small changes in the flow signal might have an important effect on the method accuracy. This is evidenced by the overall lower ICCs (range: [0.74, 0.93]) and the high values of SD of differences (range: [0.64, 0.98] m/s). Bland-Altman analysis showed small bias between the two observers as well as for the repeated flow measurements when the TANGENT, XCORR, and FFT methods were used (bias range: [-0.01, 0.31] m/s, SD range: [0.31, 0.65] m/s), all differences lied within the limits of agreement. For these three methods, intraclass correlation coefficients were high (range: [0.85, 0.99]).

The reliability of the 2D plane distances, which were manually extracted from the non-contrast MR angiography, was good when compared to the automatically calculated CS-4D plane distances. The average aortic arch distances calculated were 108 ± 20 mm for the 2D planes and 106 ± 19 mm for the CS-4D planes, while the descending aortic distances were 125 ± 36 mm for the 2D planes and 125 ± 34 mm for the CS-4D planes. For both the aortic arch and the descending aorta, there was high correlation between the two length estimation techniques, $r=0.89$ and $r=0.97$, respectively. The bias was close to zero with SD of differences of approximately 10 mm for both aortic regions. There was no statistically significant difference between the 2D and CS-4D plane distance calculations ($p>0.9$).

Table 5.2:3 Intra- and inter-observer variability of 2D PWV estimation.

| | Algorithm | Intra-observer variability | | | | Inter-observer variability | | | |
|------------------|-----------|----------------------------|-------------------|---------|------|----------------------------|-------------------|---------|------|
| | | Bias (m/s) | SD of diff. (m/s) | p-value | ICC | Bias (m/s) | SD of diff. (m/s) | p-value | ICC |
| Aortic Arch | FD | -0.19 | 0.64 | 0.45 | 0.93 | 0.07 | 0.98 | 0.85 | 0.80 |
| | TANGENT | 0.31 | 0.55 | 0.18 | 0.90 | 0.17 | 0.48 | 0.38 | 0.95 |
| | XCORR | 0.04 | 0.26 | 0.68 | 0.99 | 0.04 | 0.44 | 0.82 | 0.97 |
| | FFT | 0.06 | 0.34 | 0.67 | 0.98 | 0.02 | 0.33 | 0.88 | 0.98 |
| Descending Aorta | FD | 0.46 | 0.86 | 0.20 | 0.74 | 0.21 | 0.75 | 0.47 | 0.81 |
| | TANGENT | 0.01 | 0.31 | 0.94 | 0.96 | 0.16 | 0.44 | 0.36 | 0.91 |
| | XCORR | 0.21 | 0.50 | 0.31 | 0.89 | 0.16 | 0.65 | 0.53 | 0.85 |
| | FFT | -0.01 | 0.40 | 0.93 | 0.96 | 0.01 | 0.47 | 0.96 | 0.95 |

SD: standard deviation, ICC: intraclass correlation coefficient

FD: first derivative method, TANGENT: tangential method, XCORR: cross-correlation method, FFT: Fourier method.

Association between CS-4D PWV and age

For the three most reliable PTT algorithms, i.e., the TANGENT, XCORR, FFT, the CS-4D PWV estimates at the aortic arch were significantly correlated with age ($p < 0.01$). As shown in the linear regression plots in Figure 5.2:6, all three PTT algorithms predicted an increase in aortic arch PWV with advancing age. The highest correlation coefficients were found when the FFT and XCORR algorithms were used : $r=0.79$, 0.78 , 0.62 and $R^2=0.62$, 0.60 , 0.40 for the FFT, XCORR and TANGENT, respectively. Correlation was significant for all three algorithms, $p<0.003$. There was no significant difference between the three models, $p>0.3$.

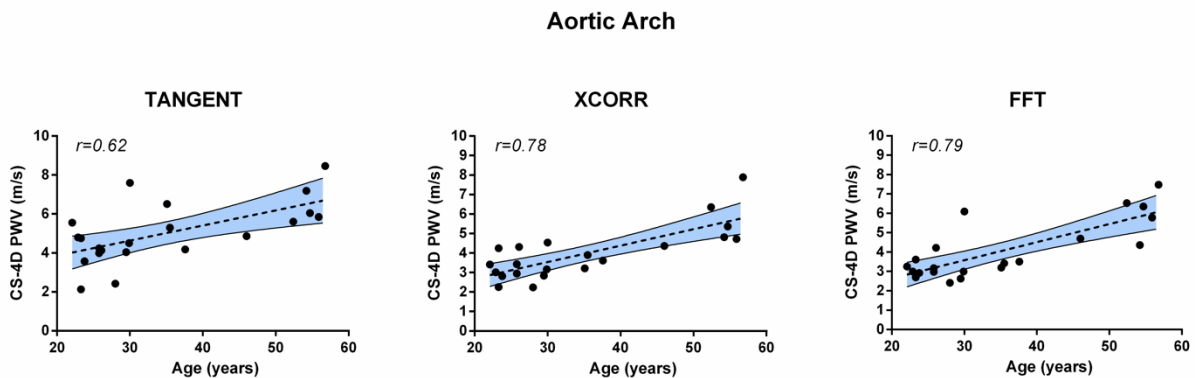


Figure 5.2:6 Association between age and the CS-4D aortic arch PWV estimated using three PTT algorithms. TANGENT:tangential, XCORR:cross-correlation, FFT: Fourier.

5.2.4 Discussion

In this study, we demonstrated the feasibility of using compressed-sensing accelerated 4D flow MRI to evaluate aortic PWV. To the best of our knowledge, this is the first study to compare regional aortic PWV measured via the novel CS-4D MRI sequence using an acceleration factor of 7.7 with the current clinical standard of 2D PC MRI measurements.

Regional PWV was examined *in vivo* at the proximal and distal aorta using four previously developed PTT algorithms. Two were point-based, i.e., the first derivative and tangential techniques, and two were wave-based, i.e., the cross-correlation and Fourier

techniques. Our choice for the implemented PTT methods was driven by the fact that these techniques are widely used in previous literature on 2D PC and 4D MRI [6], [16], [18]–[22]. The tangential and first derivative algorithms are also integrated into commercial devices to measure PWV (the SphygmoCor system and the Complior system, respectively).

Point-based methods are considered reliable for the calculation of PTT when applied to pressure waveforms. However, it has been suggested that they might perform poorer on MR blood flow signals, due to low velocity to noise ratios[22], [23]. This observation was corroborated by our findings. Especially the FD algorithm yielded PWV estimates of high variance, had a tendency to overestimate the CS-4D PWV when compared to the 2D data and was particularly inconsistent when applied to the descending aorta. Therefore, the FD algorithm was deemed inappropriate for such an application. The second point-based algorithm, i.e., the tangential method, showed better correlation and agreement between the two PWV estimates than the FD method. This is in line with previous findings [6].

Both point-based algorithms were, nevertheless, inferior to the wave-based algorithms. Indeed, previous literature has also shown that frequency and time-frequency domain methods for PTT calculation are more reproducible and reliable when implemented on 2D PC MR or 4D MR data [16], [20], [24]. This can be attributed to the fact that wave-based techniques are in general less sensitive to low temporal resolution, which is a known limitation of CS-4D acquisitions[20], [21]. Of note, the precision and reproducibility of these wave-based methods might be compromised when they are applied to the entire cardiac cycle[18], due to the effect of wave reflections on the morphology of the pressure and flow signals. Such an effect might be amplified in the elderly[21]. Accordingly, in the present study, we restricted the analysis only to the systolic upslope of the flow waves, as also previously proposed[18].

Among all PTT techniques implemented, the FFT was deemed the most appropriate. When the FFT method was used, there was high correlation between the 2D and CS-4D PWV estimates, the bias was small with narrow limits of agreement (Table 5.2:2). The FFT CS-4D PWV was 4.1 ± 1.5 m/s in the proximal aorta and 5.5 ± 2.2 m/s in the descending aorta, which is in accordance with the physiological values reported in the literature for healthy adults[25]–[27]. There was no tendency for the estimation errors to increase for higher PWV values.

It should be highlighted that for all PTT algorithms but the FFT, the 2D and CS-4D PWV values were in better agreement for the proximal aorta rather than its descending counterpart. Given that the CS-4D acquisitions were centered approximately on the apex of the left ventricle, the distal descending aorta is the furthest from the iso-center, which might cause an increase in the phase errors. Correction is included in the analysis software, but it could still account for the discrepancy at the extreme locations. This might justify the inconsistencies in the distal descending aortic PWV estimation. One previous publication[28] also reported higher correlation between 2D and CS-4D net flow measurements in the ascending aorta compared to the descending aorta.

CS-4D PWV and age

The reliability of the CS-4D proximal aortic PWV estimation was also corroborated by its positive association with age. It is widely acknowledged that normal ageing induces stiffening of the arterial tree[2]. In young subjects, the proximal aorta is highly compliant and the arterial stiffness gradually increases in the distal aorta and the more peripheral muscular arteries[2]. This results in low aortic PWV values, typically around 4 ± 1 m/s for healthy subjects under 30 years old [25], [27]. With increasing age, the arterial tree stiffens in a non-uniform way, the proximal aorta loses its elasticity more markedly than its distal counterpart [25], [26]. This entails an increase in the proximal aortic PWV, which might rise to 6 ± 2 m/s for 40-60 year-old adults[25]. In the present study, we demonstrated that CS-4D MRI was capable of predicting the expected increase in the aortic stiffness with age. For subjects under 40 years old, the proximal aortic PWV calculated with the FFT method was 3.3 ± 0.9 m/s, while for volunteers over 40 years old, it was 5.9 ± 1.2 m/s ($p < 0.001$). The highest correlation between CS-4D aortic arch PWV and age was found when the FFT and XCORR algorithms were used.

Previous literature on 4D MRI

Previous literature has also explored the potential of using 4D MRI to calculate global and regional aortic PWV. One previous study by Wentland et al.[6] undertook the comparison of 4D Flow MRI-based PWV with high temporal resolution 2D PC measurements. They performed 2D and 4D (PC with vastly undersampled isotropic projection reconstruction, scan time ~11min) MR measurements on 14 volunteers (age 38 ± 15 years) and tested several PTT methods, including the cross-correlation and tangential techniques. They found that 4D PWV measurements were in the physiologically expected range (3.8-4.8) m/s, while both XCORR and TANGENT algorithms gave similar and reliable results.

Harloff et al. [29] successfully applied 4D flow MRI with parallel imaging and acceleration (PEAK-GRAPPA with an acceleration factor $R=5$) to calculate global aortic PWV in a cohort of 126 subjects aged from 20 to 80 years old. They found that 4D PWV was higher for subjects over 70 years old (8.0 ± 1.0 m/s) compared to young subjects under 30 years old (4.9 ± 0.5 m/s). Additionally, 4D PWV was significantly associated with increased blood pressure and correlated well with 2D measurements of aortic wall distensibility. Finally, one previous study by Dyverfeldt et al. [18] used 4D Flow MRI (parallel imaging reduction factor SENSE = 2) to estimate regional PWV and compare two age groups (8 healthy young subjects aged 23 ± 2 years and 8 older normal volunteers aged 58 ± 2 years). Similarly to our results, they found a significant correlation between age and the proximal aortic PWV (4.3 ± 0.8 m/s for the young group versus 8.8 ± 1.6 m/s for the older group).

Clinical relevance

The possibility of using CS-4D MRI to derive aortic PWV is of clinical importance, particularly if we consider that CS-4D MRI can overcome methodological limitations of conventional MR techniques. With respect to 2D PC MRI, placement of the scanning planes can be tedious and time-consuming. For example, in the specific study, the 2D flow imaging for the four slices lasted more than 10 minutes for each volunteer, if we consider scan time (~ 5 min in total), slice placement time (~ 1 min per slice) and the additional time due to the need of repeating scans in case of artifacts or slice misplacement. This also means that a poorly positioned slice that is not identified at the time would be lost from the analysis. The CS-4D, however, allows retrospective positioning of any slice at the time of analysis. Additionally, there are often reproducibility issues, given that slice placement is user-dependent and, therefore, prone to errors that may compromise the accuracy of the PWV measurement. This concern is especially applicable to older subjects, whose aortas tend to be more tortuous. Finally, in addition to flow imaging, the measurement of PWV requires imaging of the vessel geometry. For CS-4D MRI, the 3D lumen is readily available after scan, whereas in the case of 2D PC flow measurements, an additional 3D angiography needs to be performed, which significantly increases the scan time (by approximately 5 min).

The major advantage of this novel CS-4D MRI approach over 2D PC and other 4D MRI sequences is that it provides the opportunity to derive a plethora of hemodynamic indices in under 5 minutes. Such indices include the volumetric flow along the aortic centerline [11], [12], wall shear stress [11]–[13], and pressure gradients for evaluation of aortic valve stenosis [30]. Importantly, the CS-4D MRI allows for the simultaneous measurement of these characteristics and is not subject to heart rate variations, which can be an important concern for measurement in children [31]. In this study, we demonstrate that measurement of the accurate regional aortic PWV is also possible. This may have important clinical implications, given that the aortic PWV is a biomarker linked to cardiovascular disease and can possibly be taken into consideration for patient management in the future.

Of note, the acceleration factor of the CS-4D MRI in our study was limited to 7.7. A previous work by Peper et al. [32] demonstrated that CS-4D Flow MR of the carotid arteries with high acceleration factors ($R=10-30$) is feasible *in vivo* and yields consistent data quality that can be used for lumen centerline reconstruction, calculation of flow waves as well as WSS estimation. The ability to further accelerate the acquisition of CS-4D MRI of the aorta is intriguing and remains to be further studied.

Study considerations and limitations

It should be highlighted that 2D PC MRI was used here as reference for measurement of PWV. Certainly, the established gold standard method for deriving PWV is catheterization; however, performing invasive measurement of PWV in normal volunteers was not feasible. The chosen 2D PC MR technique represents a widely accepted clinical practice that has shown good agreement with invasive measurements [33]–[35]. Accordingly, in our analysis we could only demonstrate the agreement between the two MR techniques. Future work should be undertaken to validate the CS-4D PWV estimates with invasive measurements.

Additionally, the study comprised an apparently healthy population, including both young and older adults. For subjects older than 60 years or patients with cardiovascular diseases, such as hypertension, PWV might reach values higher than 10 m/s. Such ranges were not investigated in the present work and are left to future studies.

The reproducibility of the MR flow data acquisition was not investigated as it is already known to be high [36]. The reproducibility of PWV measurements depends on several other factors, including the user-dependency of slice placement and data processing. However, the scanning planes were placed by an experienced MR user after careful inspection of the aortic configuration. With respect to data processing, the reproducibility of the 2D flow analysis was demonstrated. We reported low intra- and inter-observer variability for the 2D approach, which further reinforces our choice of 2D measurements as reference for the PWV estimation. The CS-4D data were automatically processed.

The distances used for the 2D PWV calculation were obtained by manually tracing the center point of the aortic cross-section on the 3D gradient echo-derived angiography. Note that this technique has been also used in the past and has been shown to perform better than length estimations from measurements of the 2D oblique-sagittal plane[37]. We found no significant difference between the distance measurements derived from the 2D and CS-4D planes. Additionally, for each volunteer we reported no significant variation in heart rate during the MR acquisitions.

Conclusions

In this study, we demonstrated that CS-4D MRI can be successfully used for the reliable estimation of regional aortic PWV. Among four PTT algorithms tested, the FFT was deemed the most robust method to derive the CS-4D PWV. For this technique, there was high correlation and good agreement between the CS-4D and 2D PWV estimated at the aortic arch and at the descending aorta. CS-4D MRI was also able to capture the anticipated increase in proximal aortic PWV with age.

5.2.5 Bibliography

- [1] W. W. Nichols, S. J. Denardo, I. B. Wilkinson, C. M. McEniery, J. Cockcroft, and M. F. O'Rourke, "Effects of arterial stiffness, pulse wave velocity, and wave reflections on the central aortic pressure waveform," *J. Clin. Hypertens. Greenwich Conn*, vol. 10, no. 4, pp. 295–303, Apr. 2008, doi: 10.1111/j.1751-7176.2008.04746.x.
- [2] C. M. McEniery *et al.*, "Normal vascular aging: differential effects on wave reflection and aortic pulse wave velocity: the Anglo-Cardiff Collaborative Trial (ACCT)," *J. Am. Coll. Cardiol.*, vol. 46, no. 9, pp. 1753–1760, Nov. 2005, doi: 10.1016/j.jacc.2005.07.037.
- [3] S. S. Franklin *et al.*, "Hemodynamic patterns of age-related changes in blood pressure. The Framingham Heart Study," *Circulation*, vol. 96, no. 1, pp. 308–315, Jul. 1997.
- [4] K. Sutton-Tyrrell *et al.*, "Elevated aortic pulse wave velocity, a marker of arterial stiffness, predicts cardiovascular events in well-functioning older adults," *Circulation*, vol. 111, no. 25, pp. 3384–3390, Jun. 2005, doi: 10.1161/CIRCULATIONAHA.104.483628.
- [5] M. F. O'Rourke, J. A. Staessen, C. Vlachopoulos, D. Duprez, and G. E. Plante, "Clinical applications of arterial stiffness; definitions and reference values," *Am. J. Hypertens.*, vol. 15, no. 5, pp. 426–444, May 2002, doi: 10.1016/s0895-7061(01)02319-6.
- [6] A. L. Wentland *et al.*, "Aortic pulse wave velocity measurements with undersampled 4D flow-sensitive MRI: comparison with 2D and algorithm determination," *J. Magn. Reson. Imaging JMRI*, vol. 37, no. 4, pp. 853–859, Apr. 2013, doi: 10.1002/jmri.23877.
- [7] R. H. Mohiaddin *et al.*, "Regional aortic compliance studied by magnetic resonance imaging: the effects of age, training, and coronary artery disease," *Heart*, vol. 62, no. 2, pp. 90–96, Aug. 1989, doi: 10.1136/hrt.62.2.90.
- [8] J. M. Boese, M. Bock, S. O. Schoenberg, and L. R. Schad, "Estimation of aortic compliance using magnetic resonance pulse wave velocity measurement," *Phys. Med. Biol.*, vol. 45, no. 6, pp. 1703–1713, Jun. 2000, doi: 10.1088/0031-9155/45/6/320.
- [9] B. D. Bolster, E. Atalar, C. J. Hardy, and E. R. McVeigh, "Accuracy of Arterial Pulse-Wave Velocity Measurement Using MR," *J. Magn. Reson. Imaging JMRI*, vol. 8, no. 4, pp. 878–888, 1998.
- [10] Z. Stankovic, B. D. Allen, J. Garcia, K. B. Jarvis, and M. Markl, "4D flow imaging with MRI," *Cardiovasc. Diagn. Ther.*, vol. 4, no. 2, pp. 173–192, Apr. 2014, doi: 10.3978/j.issn.2223-3652.2014.01.02.
- [11] P. Dyverfeldt *et al.*, "4D flow cardiovascular magnetic resonance consensus statement," *J. Cardiovasc. Magn. Reson. Off. J. Soc. Cardiovasc. Magn. Reson.*, vol. 17, p. 72, Aug. 2015, doi: 10.1186/s12968-015-0174-5.
- [12] M. Markl *et al.*, "Advanced flow MRI: emerging techniques and applications," *Clin. Radiol.*, vol. 71, no. 8, pp. 779–795, Aug. 2016, doi: 10.1016/j.crad.2016.01.011.
- [13] E. Neuhaus, K. Weiss, R. Bastkowski, J. Koopmann, D. Maintz, and D. Giese, "Accelerated aortic 4D flow cardiovascular magnetic resonance using compressed sensing: applicability, validation and clinical integration," *J. Cardiovasc. Magn. Reson.*, vol. 21, no. 1, p. 65, Oct. 2019, doi: 10.1186/s12968-019-0573-0.
- [14] E. Heiberg, J. Sjögren, M. Ugander, M. Carlsson, H. Engblom, and H. Arheden, "Design and validation of Segment - freely available software for cardiovascular image analysis," *BMC Med. Imaging*, vol. 10, no. 1, p. 1, Dec. 2010, doi: 10.1186/1471-2342-10-1.
- [15] Siemens Healthineers, *4D Flow Demonstrator (Free-type Project)*. Erlangen, Germany.

- [16] S. W. Fielden, B. K. Fornwalt, M. Jerosch-Herold, R. L. Eisner, A. E. Stillman, and J. N. Oshinski, "A new method for the determination of aortic pulse wave velocity using cross-correlation on 2D PCMR velocity data," *J. Magn. Reson. Imaging JMRI*, vol. 27, no. 6, pp. 1382–1387, Jun. 2008, doi: 10.1002/jmri.21387.
- [17] A. Meloni, H. Zymeski, A. Pepe, M. Lombardi, and J. C. Wood, "Robust estimation of pulse wave transit time using group delay," *J. Magn. Reson. Imaging*, vol. 39, no. 3, pp. 550–558, Mar. 2014, doi: 10.1002/jmri.24207.
- [18] P. Dyverfeldt, T. Ebberts, and T. Länne, "Pulse wave velocity with 4D flow MRI: systematic differences and age-related regional vascular stiffness," *Magn. Reson. Imaging*, vol. 32, no. 10, pp. 1266–1271, Dec. 2014, doi: 10.1016/j.mri.2014.08.021.
- [19] S. Houriez-Gombaudo-Saintonge *et al.*, "Comparison of different methods for the estimation of aortic pulse wave velocity from 4D flow cardiovascular magnetic resonance," *J. Cardiovasc. Magn. Reson.*, vol. 21, no. 1, p. 75, Dec. 2019, doi: 10.1186/s12968-019-0584-x.
- [20] A. Meloni, H. Zymeski, A. Pepe, M. Lombardi, and J. C. Wood, "Robust estimation of pulse wave transit time using group delay," *J. Magn. Reson. Imaging JMRI*, vol. 39, no. 3, pp. 550–558, Mar. 2014, doi: 10.1002/jmri.24207.
- [21] A. Dogui *et al.*, "Measurement of aortic arch pulse wave velocity in cardiovascular MR: comparison of transit time estimators and description of a new approach," *J. Magn. Reson. Imaging JMRI*, vol. 33, no. 6, pp. 1321–1329, Jun. 2011, doi: 10.1002/jmri.22570.
- [22] M. Markl, W. Wallis, S. Brendecke, J. Simon, A. Frydrychowicz, and A. Harloff, "Estimation of global aortic pulse wave velocity by flow-sensitive 4D MRI," *Magn. Reson. Med.*, vol. 63, no. 6, pp. 1575–1582, Jun. 2010, doi: 10.1002/mrm.22353.
- [23] A. Dogui *et al.*, "Consistency of aortic distensibility and pulse wave velocity estimates with respect to the Bramwell-Hill theoretical model: a cardiovascular magnetic resonance study," *J. Cardiovasc. Magn. Reson.*, vol. 13, no. 1, p. 11, Jan. 2011, doi: 10.1186/1532-429X-13-11.
- [24] I. Bargiotas *et al.*, "Estimation of aortic pulse wave transit time in cardiovascular magnetic resonance using complex wavelet cross-spectrum analysis," *J. Cardiovasc. Magn. Reson.*, vol. 17, no. 1, Jul. 2015, doi: 10.1186/s12968-015-0164-7.
- [25] V. Taviani *et al.*, "Age-related changes of regional pulse wave velocity in the descending aorta using Fourier velocity encoded M-mode," *Magn. Reson. Med.*, vol. 65, no. 1, pp. 261–268, 2011, doi: 10.1002/mrm.22590.
- [26] E. Kimoto *et al.*, "Preferential stiffening of central over peripheral arteries in type 2 diabetes," *Diabetes*, vol. 52, no. 2, pp. 448–452, Feb. 2003.
- [27] S. S. Hickson *et al.*, "The relationship of age with regional aortic stiffness and diameter," *JACC Cardiovasc. Imaging*, vol. 3, no. 12, pp. 1247–1255, Dec. 2010, doi: 10.1016/j.jcmg.2010.09.016.
- [28] S. Ebel *et al.*, "Comparison of two accelerated 4D-flow sequences for aortic flow quantification," *Sci. Rep.*, vol. 9, no. 1, Art. no. 1, Jun. 2019, doi: 10.1038/s41598-019-45196-x.
- [29] A. Harloff *et al.*, "Determination of aortic stiffness using 4D flow cardiovascular magnetic resonance - a population-based study," *J. Cardiovasc. Magn. Reson.*, vol. 20, no. 1, Art. no. 1, Dec. 2018, doi: 10.1186/s12968-018-0461-z.
- [30] B. P. Adriaans *et al.*, "Clinical assessment of aortic valve stenosis: Comparison between 4D flow MRI and transthoracic echocardiography," *J. Magn. Reson. Imaging*, vol. 51, no. 2, pp. 472–480, 2020, doi: 10.1002/jmri.26847.
- [31] J. P. Finley and S. T. Nugent, "Heart rate variability in infants, children and young adults," *J. Auton. Nerv. Syst.*, vol. 51, no. 2, pp. 103–108, Feb. 1995, doi: 10.1016/0165-1838(94)00117-3.
- [32] E. S. Peper *et al.*, "Highly accelerated 4D flow cardiovascular magnetic resonance using a pseudo-spiral Cartesian acquisition and compressed sensing reconstruction for carotid flow and wall shear stress," *J. Cardiovasc. Magn. Reson.*, vol. 22, no. 1, p. 7, Jan. 2020, doi: 10.1186/s12968-019-0582-z.
- [33] P. D. Gatehouse *et al.*, "Applications of phase-contrast flow and velocity imaging in cardiovascular MRI," *Eur. Radiol.*, vol. 15, no. 10, pp. 2172–2184, Oct. 2005, doi: 10.1007/s00330-005-2829-3.
- [34] M. Hoppe, J. T. Heverhagen, J. J. Froelich, M. Kunisch-Hoppe, K. J. Klose, and H. J. Wagner, "Correlation of flow velocity measurements by magnetic resonance phase contrast imaging and intravascular Doppler ultrasound," *Invest. Radiol.*, vol. 33, no. 8, pp. 427–432, Aug. 1998, doi: 10.1097/00004424-199808000-00001.
- [35] H. Machida *et al.*, "Accurate measurement of pulsatile flow velocity in a small tube phantom: comparison of phase-contrast cine magnetic resonance imaging and intraluminal Doppler guidewire," *Jpn. J. Radiol.*, vol. 28, no. 8, pp. 571–577, Oct. 2010, doi: 10.1007/s11604-010-0472-7.
- [36] M. Markl, W. Wallis, and A. Harloff, "Reproducibility of flow and wall shear stress analysis using flow-sensitive four-dimensional MRI," *J. Magn. Reson. Imaging JMRI*, vol. 33, no. 4, pp. 988–994, Apr. 2011, doi: 10.1002/jmri.22519.
- [37] A. van Engelen *et al.*, "Aortic length measurements for pulse wave velocity calculation: manual 2D vs automated 3D centreline extraction," *J. Cardiovasc. Magn. Reson.*, vol. 19, no. 1, p. 32, Mar. 2017, doi: 10.1186/s12968-017-0341-y.

Chapter 6 Conclusions

6.1 Summary of results

Profound understanding of the effects of ageing on the performance of the cardiovascular system is a major milestone that needs to be reached before we can decipher the link between age and disease. With CVD being a major concern for public health, accurate and noninvasive assessment of cardiovascular performance becomes of outmost importance. Accordingly, the presented body of research focused on four major axes, which aimed at providing novel insights into the physiology of the ventricular-arterial interaction and the evolution of hemodynamics with ageing, as well as at evaluating existing and novel techniques to derive biomarkers of importance.

The first part of this thesis (**Chapter 2**) aimed at the investigation of age-induced alterations in hemodynamics. We first developed a 1D model of the ageing cardiovascular system (*Paper I*), which was found highly consistent with published data from large-scale studies in terms of pressure evolution, wave shape and reflection indices. Examination of the wave reflection profile revealed an increase in the forward wave amplitude over time, which might constitute the major determinant of the age-induced increase in systolic pressure. In an additional analysis (*Paper II*), we demonstrated the importance of considering the heterogeneous effects of ageing on the arterial distensibility when adapting the properties of the arterial tree model. We showed that if we differentiate between young and old subjects and accordingly employ different mechanisms of arterial stiffening we are able to capture the expected increase in the carotid-to-femoral PWV with age and correctly predict central pressures. Accordingly, we proposed and tested *in vivo* a technique for effectively tuning the parameters of the 1D arterial model using noninvasive measurements of peripheral pressure and aortic flow.

In the second part of this thesis (**Chapter 3**), we studied the importance of the cardiac systolic function on arterial hemodynamics. In a computational study (*Paper III*), we demonstrated that a physiological increase in cardiac contractility leads to a steeper forward pressure wave pumped by the LV, which, subsequently, drastically alters central and peripheral pressure and flow waves. A major finding was that the characteristic *Type A* and *Type C* aortic pressure phenotypes, which are commonly associated with arterial stiffness, are also highly dependent on LV contractility. Enhanced contractility also augments the amplification of the pulse pressure from the central aorta to the periphery, which implies that caution should be exerted when using peripheral measurements as surrogate for aortic pressure. The effect of contractility on central flow and pressure phenotypes as predicted by the mathematical model was also confirmed by our subsequent *in vivo* analysis in the setting of Transcatheter Aortic Valve Replacement (*Paper IV*). Our findings support the development of systolic hypertension shortly after TAVR, which is likely driven by the enhancement of the forward wave pumped by the heart. Similarly to our model predictions, the AIx was markedly decreased after TAVR; a decrease which was not associated with any significant change in the stiffness of the vascular system or the wave reflection coefficient. This supports our modelling finding, that is AIx and pressure wave shape are not dictated solely by vascular properties but are also determined by the heart.

The third part (**Chapter 4**) was devoted to the design, development, testing and validation of a noninvasive inverse method to monitor cardiac systolic performance. Initially (*Paper V*), we developed the theoretical background and a prototype algorithm for estimating the end-systolic elastance after personalization of the cardiovascular model according to a few noninvasive measurements. We evaluated the algorithm's performance on a database of virtual patients, achieving promising results. The method was later improved (*Paper VI*) in order to allow for the noninvasive derivation of the entire ESPVR of a patient based on measurements that are usually conducted in routine cardiology, i.e., echocardiography and sphygmomanometry. The improved algorithm was tested against invasive LV P-V loops acquired under varying loading conditions from 19 patients and the validation process demonstrated high method accuracy and robustness.

Lastly, the fourth part of this thesis (**Chapter 5**) focused on the examination of existing and novel methods for the assessment of aortic biomechanical properties. The first analysis (*Paper VII*) was devoted to local indices of aortic wall elasticity. Concretely, we examined whether lumen area changes over pulse pressure, i.e., local area compliance, is an appropriate measure of total volume compliance when applied to the proximal aorta. We found both *in silico* and *in vivo* that neglecting the longitudinal strain during contraction might lead to severe underestimation of the proximal aortic distensibility. Importantly, this underestimation could be inconsistent among different populations and patient groups. In the second analysis (*Paper VIII*), we focused our attention on measures of regional aortic compliance and more specifically, on the potential of using compressed-sensing 4D Flow MRI to reliably estimate aortic PWV. There was high correlation and good agreement between the CS-4D and high-resolution 2D PWV estimates at the proximal and distal aorta. CS-4D MRI was also able to capture the anticipated increase in proximal aortic PWV with age.

6.2 Perspectives and future work

Our initial work on the development of an age-adjusted cardiovascular model gave some interesting insights into the mechanisms of age-induced hypertension and lays the ground for further investigation of the hemodynamics of old age, e.g. changes in the pulsatility transmitted to target organs. The presented work was based on fragmental literature data on the age-related changes in the structure and function of the cardiovascular system. However, extensive literature search reveals a lack of a complete and consistent set of data depicting how ageing affects aortic biomechanical properties, aortic hemodynamics and structure, and ventricular function in a holistic manner. Future work will be oriented towards acquiring such a database in order to develop anew an age-adjustable 1D model of the systemic circulation and validate on a person-specific basis. Future models should also incorporate gender-related differences in cardiovascular ageing, given that gender seems to be an important determinant of incidence and prognosis of cardiovascular disease [1]. An age-tunable and gender-specific 1D model would be a most valuable tool for further analyzing and understanding the effects of old age on aortic hemodynamics and the ventricular-arterial coupling. Additionally, it could provide the basis for the development and testing of new methods for the estimation of central hemodynamic or cardiac properties, likely improving the precision of the monitoring techniques that were proposed in the context of this dissertation.

The examination of the alterations in the ventricular-arterial coupling with ageing and disease can yield mechanistic insights into the pathophysiology of these conditions and increase the effectiveness of current therapeutic interventions [2]. In the context of this thesis, we showed that changes in the interaction between the two systems has important implications for the evolution of hemodynamics in certain patient populations. For example, in patients with severe aortic valve stenosis, an enhancement of the forward wave pumped by the heart might be expected after the TAVR procedure. The prognostic significance of the resulting systolic hypertension observed post-TAVR needs further investigation.

A major outcome of this thesis is the development and implementation of model-based, inverse methods for cardiac and hemodynamic monitoring. This piece of work was motivated by the obvious fact that such software would be a most valuable tool for clinicians in order to assess cardiovascular health and improve the current strategies for diagnosis and treatment of cardiac diseases. Particularly, our novel noninvasive tool for the estimation of E_{es} based on standard echocardiography and sphygmomanometry was proven accurate and robust. Further investigation needs to be undertaken in order to improve the techniques for the personalization of the cardiovascular model and integrate the effects of various pathologies, such as valvular dysfunction. Particularly with respect to the cardiac model, improvements should be made in order to keep up with the latest state-of-the-art. More specifically, the implemented cardiac model relies on the assumption that the normalized elastance, $E_N(t)$, shares a uniform shape among different individuals [3]. This view has been challenged as previous studies showed a significant variation of $E_N(t)$ according to afterload and introduced correction models [4]. This feature is not yet included in our simulations, but will be incorporated in our future studies. Additionally, more advanced finite-element models exist [5], [6] that couple cavity mechanics with sarcomere mechanics, the use of which might be more relevant.

As we move towards novel monitoring tools and treatment strategies that require high-fidelity patient-specific data inputs, accurate estimation of aortic biomechanical properties becomes a topic of interest. Aortic PWV is a biomarker linked to cardiovascular disease and might be taken into consideration for patient management in the future. In the presented work, we raised questions regarding the accuracy of an established method for acquiring the local proximal aortic compliance and suggested that the elongation of the ascending aorta might be a parameter of clinical interest. The inclusion of the aortic root longitudinal strain in risk stratification is increasingly being recognized and might offer predictive value for aortic disease [7], [8], [9]. Future work should be undertaken in order to offer guidance as to how the elongation of the aortic root should be incorporated into the estimation of aortic compliance

and propose correction models. Finally, we demonstrated that CS-4D Flow MRI is a promising technique for evaluating regional aortic PWV. This has important implications, particularly if we consider that CS-4D MRI can overcome methodological limitations of conventional MR techniques, such time efficiency and user-dependence, and can offer estimates of a plethora of hemodynamic indices in a brief amount of time, e.g. volumetric flow [10], [11], wall shear stress [10]–[12], and pressure gradients for patients with aortic valve stenosis [13]. Future work should be undertaken to investigate the potential of using higher acceleration factors of CS-4D to further truncate scan time.

6.3 Bibliography

- [1] L. Mosca, E. Barrett-Connor, and N. K. Wenger, “Sex/Gender Differences in Cardiovascular Disease Prevention What a Difference a Decade Makes,” *Circulation*, vol. 124, no. 19, pp. 2145–2154, Nov. 2011, doi: 10.1161/CIRCULATIONAHA.110.968792.
- [2] I. Ikonidis *et al.*, “The role of ventricular–arterial coupling in cardiac disease and heart failure: assessment, clinical implications and therapeutic interventions. A consensus document of the European Society of Cardiology Working Group on Aorta & Peripheral Vascular Diseases, European Association of Cardiovascular Imaging, and Heart Failure Association,” *Eur. J. Heart Fail.*, vol. 21, no. 4, pp. 402–424, 2019, doi: 10.1002/ehf.1436.
- [3] K. Sagawa, H. Suga, A. A. Shoukas, and K. M. Bakalar, “End-systolic pressure/volume ratio: a new index of ventricular contractility,” *Am. J. Cardiol.*, vol. 40, no. 5, pp. 748–753, Nov. 1977.
- [4] T. Shishido, K. Hayashi, K. Shigemitsu, T. Sato, M. Sugimachi, and K. Sunagawa, “Single-Beat Estimation of End-Systolic Elastance Using Bilinearly Approximated Time-Varying Elastance Curve,” *Circulation*, vol. 102, no. 16, pp. 1983–1989, Oct. 2000, doi: 10.1161/01.CIR.102.16.1983.
- [5] J. Lumens, T. Delhaas, B. Kirn, and T. Arts, “Three-wall segment (TriSeg) model describing mechanics and hemodynamics of ventricular interaction,” *Ann. Biomed. Eng.*, vol. 37, no. 11, pp. 2234–2255, Nov. 2009, doi: 10.1007/s10439-009-9774-2.
- [6] R. C. P. Kerckhoffs, M. L. Neal, Q. Gu, J. B. Bassingthwaite, J. H. Omens, and A. D. McCulloch, “Coupling of a 3D Finite Element Model of Cardiac Ventricular Mechanics to Lumped Systems Models of the Systemic and Pulmonic Circulation,” *Ann. Biomed. Eng.*, vol. 35, no. 1, pp. 1–18, Jan. 2007, doi: 10.1007/s10439-006-9212-7.
- [7] A. Guala *et al.*, “Proximal aorta longitudinal strain predicts aortic root dilation rate and aortic events in Marfan syndrome,” *Eur. Heart J.*, vol. 40, no. 25, pp. 2047–2055, Jul. 2019, doi: 10.1093/eurheartj/ehz191.
- [8] C. J. Beller, M. R. Labrosse, M. J. Thubrikar, and F. Robicsek, “Role of aortic root motion in the pathogenesis of aortic dissection,” *Circulation*, vol. 109, no. 6, pp. 763–769, Feb. 2004, doi: 10.1161/01.CIR.0000112569.27151.F7.
- [9] S. D. Singh, X. Y. Xu, J. R. Pepper, C. Izgi, T. Treasure, and R. H. Mohiaddin, “Effects of aortic root motion on wall stress in the Marfan aorta before and after personalised aortic root support (PEARS) surgery,” *J. Biomech.*, vol. 49, no. 10, pp. 2076–2084, 05 2016, doi: 10.1016/j.jbiomech.2016.05.011.
- [10] P. Dyverfeldt *et al.*, “4D flow cardiovascular magnetic resonance consensus statement,” *J. Cardiovasc. Magn. Reson. Off. J. Soc. Cardiovasc. Magn. Reson.*, vol. 17, p. 72, Aug. 2015, doi: 10.1186/s12968-015-0174-5.
- [11] M. Markl *et al.*, “Advanced flow MRI: emerging techniques and applications,” *Clin. Radiol.*, vol. 71, no. 8, pp. 779–795, Aug. 2016, doi: 10.1016/j.crad.2016.01.011.
- [12] E. Neuhaus, K. Weiss, R. Bastkowski, J. Koopmann, D. Maintz, and D. Giese, “Accelerated aortic 4D flow cardiovascular magnetic resonance using compressed sensing: applicability, validation and clinical integration,” *J. Cardiovasc. Magn. Reson.*, vol. 21, no. 1, p. 65, Oct. 2019, doi: 10.1186/s12968-019-0573-0.
- [13] B. P. Adriaans *et al.*, “Clinical assessment of aortic valve stenosis: Comparison between 4D flow MRI and transthoracic echocardiography,” *J. Magn. Reson. Imaging*, vol. 51, no. 2, pp. 472–480, 2020, doi: 10.1002/jmri.26847.

Publications

1. [S. Pagoulatou](#), N. Stergiopoulos. ***“Evolution of aortic pressure during normal ageing: A model-based study”*** (2017), PLoS One.
2. [S. Pagoulatou](#), V. Bikia, B. Trachet, G. Papaioannou, A. Protogerou, N. Stergiopoulos. ***“On the importance of the nonuniform aortic stiffening in the hemodynamics of physiological aging”*** (2019), American Journal of Physiology - Heart and Circulatory Physiology.
3. [S. Pagoulatou](#), D. Adamopoulos, V. Bikia, G. Rovas, N. Stergiopoulos. ***“Effect of changes in left ventricular contractility on arterial hemodynamics: a modelling investigation”*** (2020), Submitted for publication.
4. [S. Pagoulatou](#), N. Stergiopoulos, V. Bikia, G. Rovas, M.J. Licker, H. Müller, S. Noble, D. Adamopoulos. ***“Acute effects of Transcatheter Aortic Valve Replacement on the ventricular-aortic interaction”*** (2020), Submitted for publication.
5. [S. Pagoulatou](#), N. Stergiopoulos. ***“Estimating Left Ventricular Elastance from Aortic Flow Waveform, Ventricular Ejection Fraction, and Brachial Pressure: An In Silico Study”*** (2018), Annals of Biomedical Engineering.
6. [S. Pagoulatou](#), KP. Rommel, P. Lurz, V. Bikia, G. Rovas, D. Adamopoulos, N. Stergiopoulos. ***“In vivo application and validation of noninvasive method to estimate end-systolic elastance”*** (2020), Submitted for publication.
7. [S. Pagoulatou](#), M. Ferraro, B. Trachet, V. Bikia, G. Rovas, L. Crowe, J.P. Vallée, D. Adamopoulos, N. Stergiopoulos. ***“The Effect of the Elongation of the Proximal Aorta on the Estimation of the Aortic Wall Distensibility”*** (2020), Biomechanics and Modeling in Mechanobiology.
8. [S. Pagoulatou](#), D. Adamopoulos, Y. Niu, N. Stergiopoulos, V. Bikia, G. Rovas, N. Jin, C. Forman, D. Giese, J.P. Vallée, L.A. Crowe. ***“Assessing regional aortic Pulse Wave Velocity with compressed-sensing accelerated 4D Flow MRI: an in vivo comparison with 2D phase contrast MRI”*** (2020), Submitted for publication.
9. V. Bikia, [S. Pagoulatou](#), B. Trachet, D. Soulis, A. D Protogerou, T. G Papaioannou, N. Stergiopoulos. ***“Noninvasive Cardiac Output and Central Systolic Pressure From Cuff-Pressure and Pulse Wave Velocity”*** (2019), IEEE Journal of Biomedical and Health Informatics.
10. K. Kadry, [S. Pagoulatou](#), Q. Mercier, G. Rovas, V. Bikia, H. Muller, D. Adamopoulos, N. Stergiopoulos. ***“Biomechanics of diastolic dysfunction: a 1D computational modeling approach”*** (2020), American Journal of Physiology - Heart and Circulatory Physiology.

Curriculum Vitae

Stamatia Zoi Pagoulatou

Address : Avenue Mont d'Or 59, 1007 Lausanne, Switzerland
Email : m.pagoulatou@hotmail.com
Telephone : +41 (0)78 634 51 90



EDUCATION

PhD in Biotechnology and Bioengineering, (4-year program) 2016 –2020
École Polytechnique Fédérale de Lausanne (EPFL), Switzerland
Doctoral thesis at the Laboratory of Hemodynamics and Cardiovascular Technology (LHTC) entitled “Hemodynamics of ageing, ventricular-arterial coupling and noninvasive assessment of key hemodynamical and cardiac quantities”

BSc & MSc in Mechanical Engineering, (5-year joint degree; 300 ECTS) 2011 –2016
National Technical University of Athens (NTUA), Greece
Grade: 9.29/10, “Excellent”

WORK EXPERIENCE

Doctoral researcher in the Laboratory of Hemodynamics and Cardiovascular Technology 2016 –2020
École Polytechnique Fédérale de Lausanne (EPFL), Switzerland

- Research on monitoring cardiovascular biomarkers and hemodynamics
- Supervision of 12 MSc semester projects and 3 MSc theses
- Teaching courses on Fluid Mechanics (BSc) and Biomechanics of the Cardiovascular System (MSc) for 4 years

Internship at Daikin Air Conditioning Hellas S.A., Greece 2015
Department of Maintenance and Operation (3 months)

TRAINING

Online Specialization on Engineering Project Management, (4-month program) 2020 – now
Rice University, USA

Online Specialization on Project Management Principles and Practices, (5-month program) 2020
University of California, Irvine, USA

Online Course on Machine learning, (60-hour course) 2020
Stanford University, USA

PATENTS

Systems and Methods for Real Time Noninvasive Estimation of Cardiovascular Parameters, Serial No. [PCT/IB2020/057656](https://patents.google.com/patent/PCT/IB2020/057656), filed on 14/08/2020 by Stamatia Pagoulatou, Vasiliki Bikia, Nikolaos Stergiopoulos (equal contribution)

SKILLS

| | |
|-------------------------|--|
| Technical Skills | Development and validation of clinical tools for hemodynamic monitoring Organization and execution of biomedical/clinical studies Programming languages/environments: Matlab, Python, C, Visual Basic, Mathematica Simulations: FEA (Abaqus), CFD (Ansys Fluent, Comsol), Paraview, Vascular Modeling Toolkit, CAD (SolidWorks) |
| Soft Skills | Strong organization and management skills Innovation enthusiast Strong communication skills Self-driven and disciplined Team player |
| Languages | Greek (native) English (full professional proficiency, speaking/writing) French (professional working proficiency – C2, speaking/writing) German (limited working proficiency – B2, speaking/writing) Spanish (limited working proficiency – B2, speaking/writing) |

CURRENT RESEARCH FOCUS

Noninvasive cardiovascular monitoring, wearable devices, TAVR

SCIENTIFIC DISTINCTIONS

| | |
|--|------------|
| Award for excellence during undergraduate studies, Technical Chamber of Greece, | 2017 |
| Scholarship for excellence during undergraduate studies, State Scholarship Foundation, | 2012 –2013 |

INTERESTS

Jogging, Dancing, Pilates, Hiking, Traveling, Cooking

